Synthesis and Structure Determination
of New Pharmaceutical Cocrystals

By

Anas Mouayed Al-Abachi

Under the supervision of Dr.Maryjane Tremayne

A thesis submitted to

The University of Birmingham

for the degree of

MASTER OF PHILOSOPHY

School of Chemistry

University of Birmingham   September 2015

Abstract

Pharmaceutical cocrystals have an important and influential role in the pharmaceutical industry through the formation of substitutional crystalline material to obtain the optimum physical properties of an active pharmaceutical ingredient (API) without changing its chemical properties. Pyrazinamide is anti-bacterial drug which is used to treat tuberculosis that infects the lung tissues. In this thesis, the ability of pyrazinamide to form co-crystals with different di-carboxylic acids through the formation of strong hydrogen bonds to form motifs is investigated.

Pyrazinamide cocrystals were synthesised through different methods using a variety of different solvents and different starting stoichiometric ratios. New cocrystals were formed between pyrazinamide and glutaric acid (1:1), pyrazinamide and adipic acid (4:1), pyrazinamide and pimelic acid (1:1), and pyrazinamide and sebacic acid (2:1). In all cases, X-ray powder diffraction and NMR were used to characterise the new material formed with the crystal structures of these materials determined through single crystal X-ray diffraction. The crystal structure of a polymorph of azelaic acid was also determined through single crystal X-ray diffraction analysis following attempted synthesis of a pyrazinamide:azelaic acid cocrystal.

Other new products were characterised through X-ray powder diffraction, although further structural analysis was not carried out. These include adducts based on pyrazinamide:oxalic acid, pyrazinamide:malonic acid, pyrazinamide:maleic acid, pyrazinamide:isonicotinamide, nicotinamide:isonicotinamide and isonicotinamide:fumaric acid. Attempts to prepare adducts between pyrazinamide with histidine and nicotinamide only resulted in a mixture, as did the combination of L-dopamaine with succinic acid.

Acknowledgements

First of all, I would like to express my deep thanks and gratitude to my supervisor Dr. Maryjane Tremayne for her guidance, support and encouragement during this research study. Thanks are also due to Dr. Louise Male for providing me all the single crystal X-ray measurements of all the samples.

A special debt of gratitude is given to my parents for their continuance support and encouragement during the preparation of my thesis. Finally I would like to thank everyone assisted me.

Contents

List of Figures

List of tables

1. Introduction

1.1 <u>Solid state chemistry</u>

The molecular crystalline solid state is a branch of materials chemistry with a wide range of applications that are often combined with crystal and crystallographic sciences[1]. The molecular solid state is the study of structure, synthesis and the physical properties of solid materials, with a focus on producing new materials based on a knowledge of structure and finding improved methods of characterisation[2,3,4]. The structure of a crystalline molecular material is important in the determination and understanding of physical properties and the role of elemental units or molecules in these materials[5,6]. This branch of chemistry has witnessed dramatic developments over the last few decades due to the increased impact on industry in the production of new products for larger markets such as pharmaceuticals, electronics, ceramics and dyes[6].

A crystal material is a solid body in which the atoms, molecules or ions are arranged in a regular manner such that a repeat unit runs in three-dimensional space[3,7]. Crystallisation is a process of formation of these crystals often from solution or a melt form[8]. A crystalline structure then enables diffraction to occur and hence the structure and properties of the material can be investigated using a crystallographic approach[9]. An amorphous material is a solid in which the atoms are not distributed or arranged in a regular distribution network with the atoms being arranged randomly without any crystallographic symmetry[3,10,11]. Non-crystalline materials include glasses, gels, thin films and nanostructured materials[12]. These materials often display very different properties when compared to crystalline materials and hence can be used in different ways.

In the field of organic solid state materials, crystalline entities can take various solid forms based around the compound of interest. These different forms can normally be categorised as crystalline or amorphous and whether they are polymorphs, solvates, hydrates, salts or cocrystals[3,10,13] (figure 1.1).
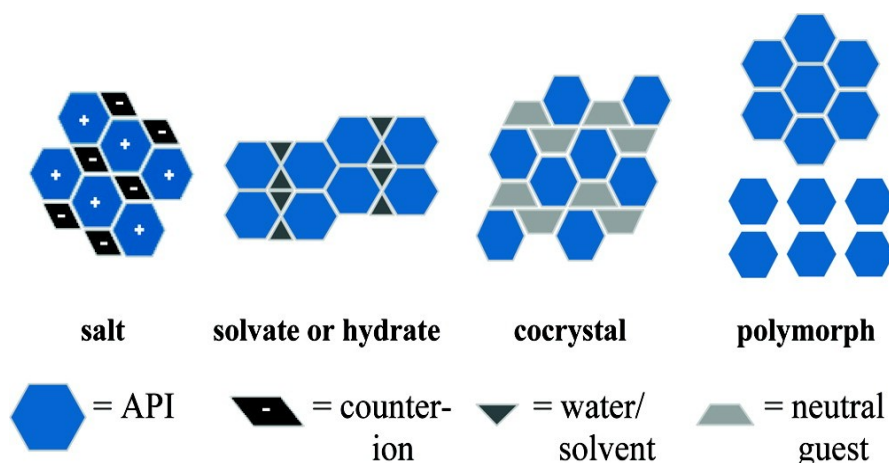
Figure 1.1: Classification of organic solid state materials and their components (Taken from ref.3).

In terms of crystalline materials, there are number of possible forms. Polymorphism is the ability of a solid crystalline material to display more than one crystalline structure or form [3,14,15]. Despite being of the same chemical composition, polymorphic materials often have different physical properties such as solubility, melting point and bioavailability[5,13,16]. This means that polymorphism can provide additional opportunities for the application of a material, whilst also providing problems in terms of purity control[16].

Other forms of organic solid materials such as salts, hydrates, solvates and cocrystals are all multicomponent crystalline materials[6]. A solvate is a crystalline material that contains solvent of crystallisation whilst a hydrate contains water as the solvent of crystallisation within the crystal structure framework. These are then also distinct in terms of physical properties from the pure anhydrous material. A cocrystal, or salt, also incorporates an additional component in the crystal structure and will be discussed in detail later[6].

1.1.2 <u>Crystal and the pharmaceutical solid state</u>

One of the largest areas of interest for organic materials is in the drug development and solid form selection. Organic solid state chemistry plays an important role in this as crystalline molecular forms with therapeutic effect are considered an important formulation class of solid pharmaceutical materials[4,6,16]. The solid form chosen for an active pharmaceutical ingredient (API) affects the therapeutic activity and hence the value of many drugs on the market through the differences that formulation can make change to many physical properties such as solubility, dissolution, melting point and bioavailability[1-9]. APIs can be classed using the

Biopharmaceutical Classification System (BCS)[17] depending on the solubility and permeability of the drug substance. The classification has four areas: (I) high solubility + high permeability; (II) low solubility + high permeability; (III) high solubility + low permeability; (IV) low solubility + low permeability[17].

The preferable area for most APIs is class (I) where the drug substance has high solubility and high permeability; i.e when the highest dose of the drug is highly soluble in 250 ml of water and therefore the bioavailability will be high. In addition, these substances have high level of permeability and their absorption rate is usually higher than excretion, for example paracetamol, metoprolol. A drug substance is considered to have a poor solubility and permeability in class (IV) when more than 85% of drug substance is insoluble in 250 ml of water, is therefore also has poor bioavailability and usually is not well absorbed in the tissue, for example bifonazole. There are many physicochemical factors which are affect drug absorption including pKa, solubility, stability, particle size, polar-non polar surface area and crystal form; physiological factors include the absorption mechanism, gastric empty and intestinal transit time[17].

The Biopharmaceutical Classification System (BCS)[17] acts as a tool to improve, simplify and speed up the drug development process and allows the prediction of the rate limit in the intestinal absorption process after oral administration. BCS can be used to characterise the drugs for which a drug product may be eligible for bioequivalence studies. The classification itself can be used to expand the regulatory application of the BCS and drug discovery and recommend methods for classifying drugs[17]. Overall, the BSC is also considered useful in saving costs within the drug development procedure.

The solid state form of an active pharmaceutical ingredient (API) can be used to optimise the physical properties of the drug product without changing the chemical composition or affecting the pharmacological properties[2,6]. Physical properties often depend on amorphous form or polymorphic structure[7] or on the salt/cocrystal form, all of which lead to different structures and hence different physical properties to improve the drugs activity[9,18]. New pharmaceutical cocrystal preparations provide a potential route to the development of innovative drugs from existing API products, and hence the interest in cocrystal research has been increased in the last decade due to pharmaceutical applications[2,4,18].

The pharmaceutical ingredients with active coccrystals have different pharmaceutical properties and that depending on the second component in the cocrystal. Some of the cocrystals exhibit lower or higher melting point with comparison to their pure original components for example: The melting points of succinic acid and urea are 135.5 ^{o}C and 188.9 ^{o}C respectively while the melting point of the cocrystal of succinic acid-urea is 149.9 ^{o}C[15]. Such a cocrystal would then display the active chemical properties of succinic acid and urea individually in solution but in combination with display distinct cocrystal physical properties in the solid state[6,18].

1.2 Cocrystals and salts

The definition of a cocrystal has been the subject of debate in the scientific literature to reach the accepted form of definition[7,10,13,19]. According to Aakeroy, a cocrystal is structural crystalline solid material that consists of two or more equal constructing blocks (organic molecules that are solid at ambient temperature) that are in stoichiometric amounts[19,20]. Cocrystals are already used in many applications including pharmaceuticals, pigments, dyes, chemical processing and superconductors. However, one of the most potentially significant impacts will be through the increased options for optimum solid form in the pharmaceutical industry where formulations are currently limited to salt form only[6,20].

Cocrystals and salts are both ordered crystalline materials but differ in terms of proton transfer between the two molecular components[3,21,22]. Figure 1.2 shows the possibility of cocrystal and salt formation between pyrazinamide and a carboxylic acid. If there is no proton transfer between the two components, the material formed will be a cocrystal (1) whereas proton transfer from the acid to the amide would result in a salt (2) (figure 1.2.).

(1)   (2)
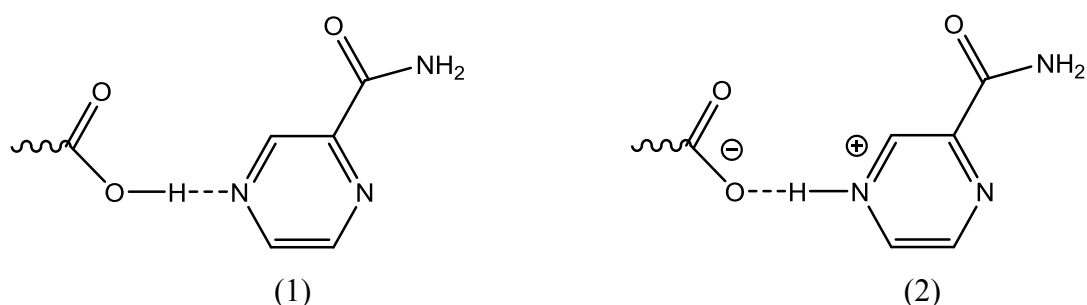
Figure 1.2: Schematic example of an organic cocrystal pyrazinamide:carboxylic acid (1) or a salt (2).

Many crystalline materials are found in salt form in the pharmaceutical industry and these are considered as an alternative to cocrystals when the product has easily ionisable positions in the active pharmaceutical ingredients[7,23]. Conversely, cocrystals are often considered a vital option when no ionisable groups are present. Both cocrystals and salts are important in pharmaceutical development as both of them can give the advantages found in multicomponent structures[6]. There are many drugs on the market in the crystalline salt form of an API, such as hydrochloride salts and these are used to optimize the crystallinity, solubility and stability of the active pharmaceutical component[6,23].

The probability of forming a cocrystal or salt depends on the difference in pKa values of the components which indicate if proton transfer is likely between the acid and base coformers[11]. If ΔpKa = pKa (base) – pKa (acid) is greater than 2 or 3 in general a salt will be formed, whereas if ΔpKa is less than 0 the product is often predicted to be a cocrystal (figure 1.3). The prediction of a cocrystal or salt form based on ΔpKa is unreliable if ΔpKa lies between 0 and 3 [23,24,25]. It is why when ΔpKa is sufficiently large that salt formation is highly likely[24].

$$\Delta pKa = pKa\ (base) - pKa\ (acid)$$
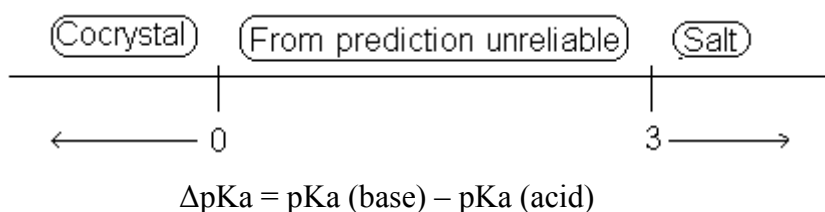
Figure 1.3: The effect of ΔpKa values on cocrystal or salt formation[25,26,27].

The value of pKa (base) depends on the dissociation of the base and is constant for a particular species as defined as below[28]:

$$BOH\ (base) \rightleftharpoons B^+ + OH^-(salt),\ Ka\ (base) = [B^+] * [OH^-] / [BOH];$$
$$pKa\ (base) = -\log_{10} Ka\ (base)$$
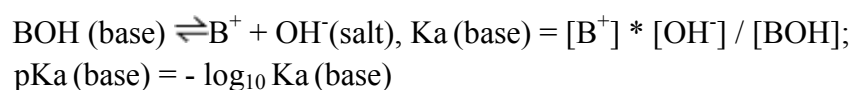
The value of pKa (acid) depends on the dissociation of the acid and is constant for particular species as defined as below[28]:

$$HA\ (acid) \rightleftharpoons H^+ + A^-\ (salt),\ Ka = [H^+] * [A^-] / [HA];$$
$$pKa = -\log_{10} Ka\ (acid)$$
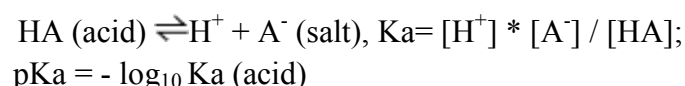
This is a property of an acid or base in solution and describes the behaviour of a molecule in the medium. Hence, the extension to solid state is not always reliable, although there is a potential link through the nucleation phase and other limitations of some species of a mixed

salt and cocrystal when the hydrogen proton be shared between the base and acid or partially occupied two sites[25,27]. There are some factors which are affecting on the formation of salt-cocrystal continuum such as solvent, stoichiometric ratio of coformers and temperature [28,29,30].

The proton location is not always a clear indicator of salt or cocrystal form as the proton can be shared across the two sites, not clearly bonded to either the acid or the base. Temperature can have an effect on the cocrystal-salt continuum as in the example of pentachlorophenol:4-methylpyridine[25]. The position of the proton in pentachlorophenol:4-methylpyridine changes with temperature; the complex becomes more like a cocrystal at higher temperature as the proton moves closer to the oxygen of pentachlorophenol[25]. Neutron diffraction was used to locate the position of the hydrogen in between the donor and acceptor. At 20K the N-H and O-H distances were 1.208 Å and 1.309 Å respectively showing that the proton had migrated away from the phenol and towards the pyridine N, forming a salt. The complex showed a higher cocrystal nature at 200K where the N-H and O-H distances were 1.306 Å and 1.228 Å, respectively[25,26]. This proton migration was shown to be a gradual process with the proton being almost central within interaction at a temperature of 80K[25].

The choice of solvent during synthesis can also have an effect on the proton transfer and whether the product forms as either a salt or cocrystal. Different forms can also be produced using the same molecular coformers but variation of the stoichiometric ratio of the starting materials. In salt-cocrystal the hydrogen proton can partially occupy two sites and the physical effects: solvent, temperature and stoichiometric are also have effect for example: pentachlorophenol:4-methylpyridine[25]. 2,3-lutidine:fumaric acid is an example of a combination that can form cocrystal or salt forms through different stoichiometric amounts of starting materials[30]. A starting ratio of 1:1 coformers produces a 1:2 salt complex while a 2:1 cocrystal form is obtained from a 2:1 ratio of starting materials[29,30].

The formation of a cocrystal or salt is depends on the hydrogen proton position between the acid and base which affects the physical properties of the crystal, Aakeroy[21,30] has shown during investigations to materials structural determination of more than 80 crystalline materials produced from equal stoichiometric amounts of carboxylic acid and N-heterocycles shows that 45% form a salt which is a result of hydrogen proton transfer from the acid to base with unexpected stoichiometry compound or solvate included, while 5% form a cocrystal, which is result of no hydrogen proton transfer from the acid[21]. The result of 5% cocrystal in

the comparison to 45% salt shown positive advantages in structural prediction of cocrystal which is much easier than structural prediction of salt through converting carboxylic acid into carboxylic anion and that will provide more chances in producing new types of solid forms which have significant effect in developing of drugs and the possibility of design prediction in the pharmaceutical industry[21,30].

The first cocrystal to be reported and studied was quinhydrone in 1844 by Friedrich Wohler [2,19]. The quinhydrone cocrystal consists of the two organic components, quinone and hydroquinone. Wohler synthesised this material whilst studying quinine, after mixing quinine and hydroquinone to produce a new cocrystal material which was synthesised by grinding a 1:1 stoichiometric ratio of coformers[19,31]. Quinhydrone has been characterised and analysed through various methods during the last decades[19,31]. At the end of the 1800s and early in the 1900s a variety of cocrystal materials were discovered, but in the absence of modern analytical and crystallographic techniques were described as organic molecular compounds. More detailed structural information on cocrystals was absent until the 1960s when a group began the study of cocrystal formation of 9-methyladenine with 1-methylthymine[32]. In 2009 the Cambridge structural database (CSD) announced that cocrystals only account for 0.5 % of the crystal structure archive[33]. In 2014 the CSD web site published statistical figure shows that cocrystals account for more than 0.7 % of the cocrystal structure, so there significant potential for many more cocrystals to be discovered[34].

1.3 <u>Cocrystal design</u>

Cocrystals are often discovered by using screening techniques or by cocrystallisation from solution containing the coformer components[33]. The components in cocrystal structures normally interact through hydrogen bonding[32], as formation of strong intermolecular interactions between the different molecules enables the production of a multicomponent system rather than recrystallisation of individual components[4,9]. The additional interactions between the coformer molecules will produce cocrystal structures with specific physical and chemical properties which differ from that of the single components[14,33].

An example of a cocrystal based on a strong molecular synthon is shown below (figure 1.4). Succinic acid and urea form a strong hydrogen bond to produce a cocrystal structure of succinic acid: urea in a 1:1 ratio[6]. The carboxylic acid group forms a preferential interaction

with the amide group in the urea molecule to form an alternative heteromolecular $R_2^2(8)$ ring as shown in (figure 1.4)[6]. This heterosynthon is formed in preference to the combination of acid-acid and amide-amide rings that would be produced if the components were recrystallized as separate components.
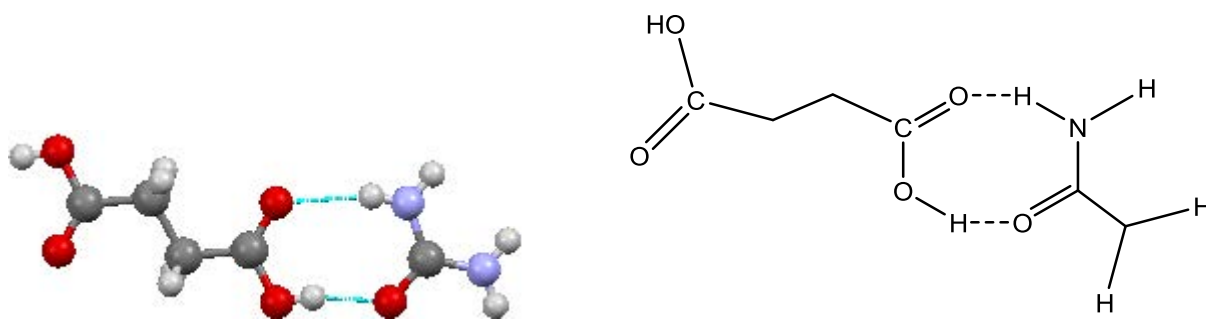
Figure 1.4: Cocrystal structure of succinic acid-urea[6].

In most cases the combination of two components will not result in the formation of a cocrystal and hence the synthon approach is used in the design process to generate new cocrystal materials[35]. A synthon is a supramolecular building unit made of multiple molecules interacting through a strong and reliable hydrogen bond network[4-6]. The example of the succinic acid-urea cocrystal above displays the hydrogen bond synthon commonly found in acid-amide cocrystals (figure 1.4)[6,35].

As mentioned previously, cocrystal synthesis depends on the preferential formation of these supramolecular synthons rather than the formation of crystals by the interactions between molecules of the individual components. The synthons involved in cocrystal formation of acid-amide cocrystals are often based on acid-pyridine (I) (figure 1.5) in combination with amide-amide (II), acid-amide (III) or amide-pyridine (IV) depending on the stoichiometry of the components. The examples given in Figure 1.5 represent the behaviour that is commonly expected in isonicotinamide or nicotinamide with alkanedicarboxylic acid cocrystals[36].

(I)

(II)

(III)

(IV)
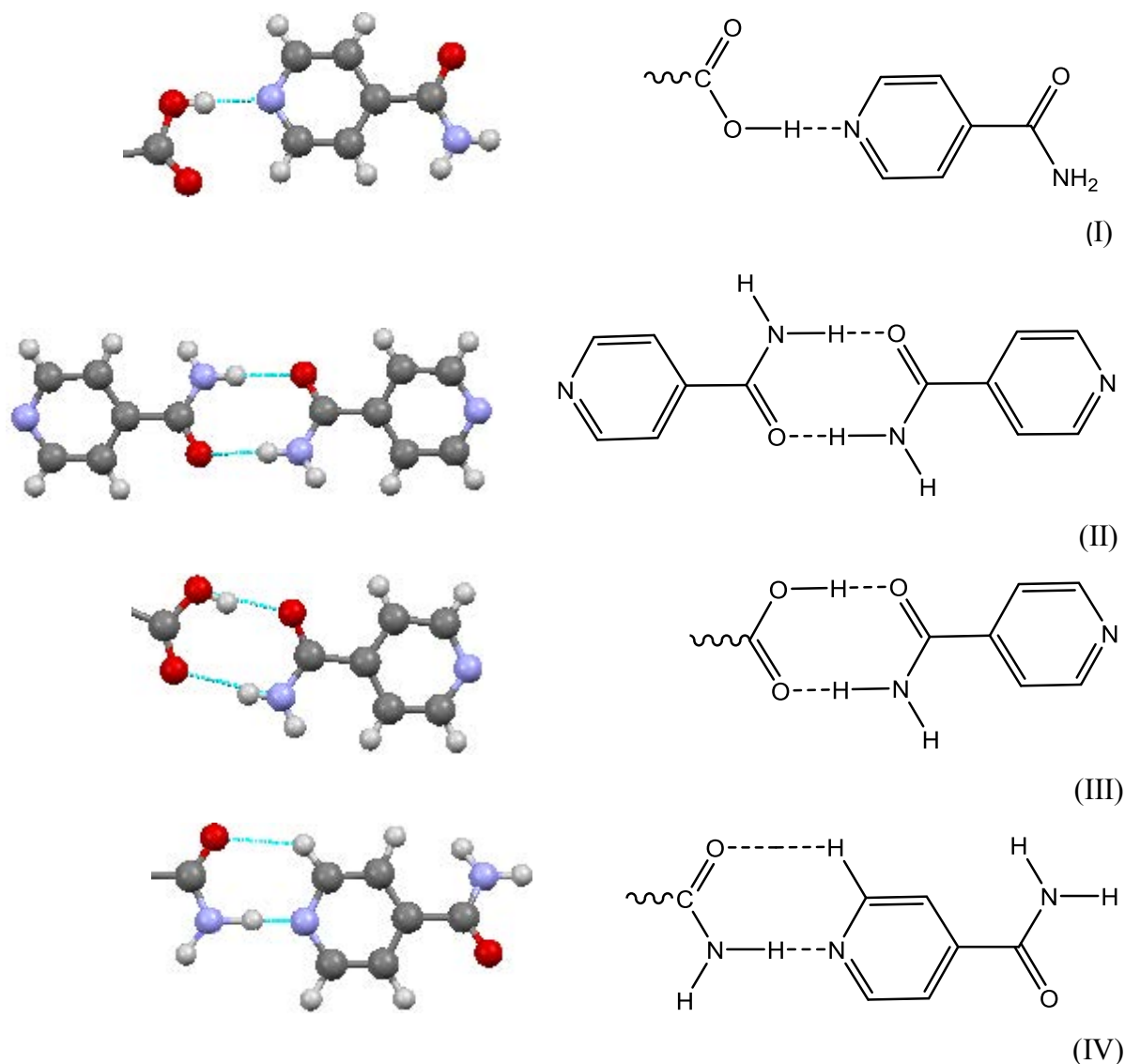
Figure 1.5: The hydrogen bonding synthons commonly found in acid-amide cocrystals formed between isonicotinamide and alkanedicarboxylic acids[36].

1.4 Cocrystal synthesis and characterisation

There are a variety of methods employed for the synthesis of cocrystals although in many cases, the need for single crystal X-ray diffraction means that full cocrystal analysis requires formation by using slow solvent evaporation. This is the traditional method of synthesis and is based on slow evaporation from solution containing stoichiometric amounts of the components or cocrystal formers required[4,6].

Although this is the most common synthetic approach, cocrystallisation through solvent evaporation often requires the starting materials to have a similar solubility to prevent the

recrystallisation of the cocrystal coformers before the crystallisation process[4]. Complete dissolution of all starting materials is also needed to enable possible crystallisation of the cocrystal. The diagram below (figure 1.6) illustrates the coformer solubility effect on cocrystal formation through a ternary phase diagram[9,37]. In figure 1.6, A shows similar solubility between the coformers related area A,B and D,E to produce cocrystal C in presence the solvent F while ternary phase diagram B shows different solubility between the coformers related area A,B and D,E and the production of cocrystal C reduce significantly due to the difference in the solubility of coformers of A,B and D,E in presence the solvent F [9].

(A)   (B)
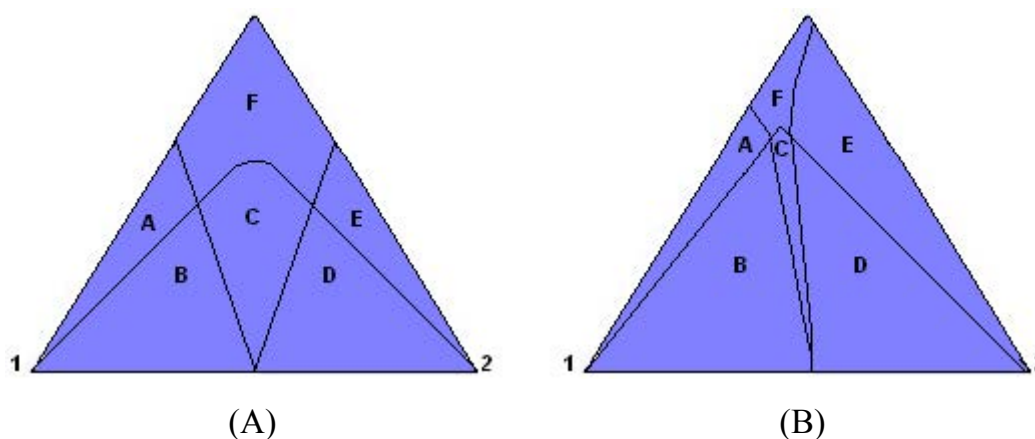
Figure 1.6: The crystallisation through solvent evaporation. Diagram (A) shows similar solubility between two coformers to form cocrystal, while Diagram (B) shows the different solubility between two coformers and the effect on the cocrystal formation. Area A acts as coformer 1 with the solvent, area B acts as coformer 1 with cocrystal, area C acts as cocrystal, area D acts as coformer 2 with cocrystal, area E acts as coformer 2 with the solvent, area F represents the solvent (Adapted from ref.9).

The cocrystallisation is consider to be another method to synthesis cocrystals, the solvent is important in any kind of crystallisation, the intermolecular interaction is change by changing solvent then change the solubility profile of components[6]. The crystallisation, by adding excess amount of one cocrystal to the former, may lead to the production of cocrystal[38,39].

1.4.1   Alternative synthesis methods

Grinding[40] is a common method for cocrystal synthesis and this method does not require the need for solvent[40]. Grinding can take the form of either dry or liquid assisted grinding and both these techniques have been used in producing cocrystals[41]. In dry grinding the motor and pestle are used and the cocrystal formers are mixed together manually inside the motor[37,42]. In

liquid assisted grinding (or solvent drop grinding) a small amount of the liquid (solvent) is used and added to the components mixture. The technique includes grinding stoichiometric amounts of components in presence of small amount of solvent to give more kinetic to the molecules of components and increase the control. Example of solvent drop grinding with different stoichiometries includes the synthesis of Meloxicam cocrystals through grinding meloxicam with naphthoic acid (1:1) in presences some drops of tetrahydrofuran. Meloxicam also form cocrystal with glutaric acid (1:1) and cocrystals of Meloxicam with fumaric acid (2:1) through solvent drop grinding synthesis[37,43]. The dry grinding which is without solvent with different stoichiometries such as nicotinamide with 2-Chloro 4-nitrobenzoic acid (1:1) and the cocrystal formed is more stable than the pure compound of nicotinamide[44]. The advantages of the solvent drop grinding method are to increase the yield, control the formation of polymorphs and improve product crystallinity[37]. Melting is another method to produce cocrystal and this method is based on melting two components of cocrystal formers together and after that cooling them at room temperature, the cocrystal may be produced by melting such as the cocrystal of carbamazepine with nictotinamide[45].

Supercritical fluid technology[46] is consider alternative method of synthesis can be used to generate pharmaceutical single pure cocrystals and that can be achieved by using different properties of supercritical fluids and that technique can be used to design and screening of cocrystals and can be used to produce cocrystal from materials that have thermal sensitivity and or an instable structure[47,48,49]. The Supercritical fluid technology is used in crystal engineering to produce new cocrystal with different API to increase the rate of cocrystal formation such as producing pharmaceutical cocrystals of indomethacin with saccharine[48].

The slurry method is also used as a method of crystallisation and depends on the removal of the excess amount of solvent normally required for crystallisation, hence reducing the limitations encountered when the coformers have a big difference in solubility. The method includes isolation of the coformers in a small quantity of solvent such as the cocrystal of stanolone with L-tartaric acid[50,51].

1.4.2 **Methods of characterisation**

The structure of cocrystals can be characterised and analysed by many kinds of methods. The common method which was used to characterise cocrystal structure was by powder X-ray diffraction[52]. X-ray diffraction was used to detect the new cocrystals formed and if they were

cocrystal or not and to compare the new cocrystal formed with the original component pattern[53]. Single crystal X-ray diffraction was used to characterise single cocrystal and to obtain the cocrystal structure, but it may be difficult to use single crystal X-ray diffraction on some cocrystals which were formed from dry grinding[37].

NMR spectroscopy was used to characterise the new cocrystal formed and it has advantages in distinguishing the new cocrystal structures in comparison with similar structures[54]. From the NMR chart it was also possible to know the stoichiometric ratio of cocrystal molecule formed. Raman and FT-IR spectroscopy were considered spectroscopic methods that were commonly used to characterise a new cocrystal material formed through comparing known cocrystal formers so as to find the match cocrystal peak[53].

The physical properties of cocrystals can be determined by using Thermogravimetric Analysis (TGA) and Differential Scanning Calorimetry (DSC) which are physical methods that were commonly used to characterise and measure the physical properties of crystalline materials such as: melting point and enthalpy factors of cocrystals[53,55].

1.5 Pharmaceutical cocrystals

The chemical and physical properties of drug can be optimized in pharmaceutical cocrystals. A pharmaceutical cocrystal is define as a single organic crystal in solid state that integrates two equal molecules one of them an active pharmaceutical ingredient (API) and the other a cocrystal former and the two molecules interact together through non-covalent interactions by hydrogen bonding[2,4,56]. The physical properties are dependent on the structure of the pharmaceutical cocrystal and its structure design which is important for new solid materials with specified chemical and physical properties. In the pharmaceutical industry cocrystal composition is used to create products with specific physiochemical properties such as solubility, stability and bioavailability without influencing the pharmacological properties. Pharmaceutical cocrystal technology was used to characterize and improve new forms of drugs and increase the number of API[2,4,56]. The scientists have proven that pharmaceutical cocrystals can improve the quality and performance of drugs that have poor solubility, on the other hand some pharmaceuticals do not show maximum activity due to poor physiochemical properties which are specified by unconditioned polymorphic or amorphous occurrence. Pharmaceutical cocrystals have been used in many drug applications such as aspirin,

paracetamol, isonicotinamide, carbamazepine, diclofenac, meloxicam and dopamine. The fundamental aim of a pharmaceutical cocrystal is to generate a cocrystal with specific physical properties that are very different from the active pharmaceutical ingredient by changing or breaking covalent bonds[2]. It is also important to consider the condition of a safe coformer with API. The Food and Drug Administration (FDA) classifies pharmaceutical cocrystals as ''API-excipient''[57]. Generally Recognized As Safe (GRAS)[58] is an FDA designation and distinguishes that a chemical or substance added to food or drug should be considered as safe by experts[58]. Examples include saccharin, nicotinamide and acetic acid, therefore it is possible to use citric acid as a safe coformer with pyrazinamide to form pharmaceutical cocrystals while benzoic acid would be considered unsafe and not suitable to use in combination with an API in a pharmaceutical product.

The melting point is important and affects the solubility and stability of a cocrystal. The melting point of a new cocrystal is often very different than that compared with the coformers. If the melting point of the cocrystal is higher than the coformers, then it will also be more stable and less soluble[3,9,44]. The dicarboxylic acids exhibit different melting point values due to effect of chain length and different number of carbon atoms[36]. The melting point of a pharmaceutical product can be designed to improve the activity of an API by selection of coformers with a desired different range of melting point[13]. The melting point of isonicotinamide:pimelic acid (1:1) cocrystal is higher than the melting point of pure pimelic acid and this (1:1) cocrystal has melting point lower than the melting point of isonicotinamide:azelaic acid (2:1), therefore both isonicotinamide cocrystals (2:1) and (1:1) have melting points which are higher than the melting points of component dicarboxylic acids and that is due to strong interactions bonds that formed between the molecules of isonicotinamide with dicarboxylic acids[36].

In the 1950s Higuchi and Kuramotor[59] studied the complex composition of pharmaceutical cocrystals between pharmaceutical and macromolecules such as the complex of polyvinylpyrrolione (PVP) with a series of molecules such as sulfathiazole, procaine, sodium salicylate, benzyl penicillin, and caffeine[59].

1.5.1 **Pharmaceutical cocrystal applications**

Cocrystals have attractive interest in pharmaceutical research and development with different applications:

A) Pharmaceutical cocrystals of Carbamazepine (Tegretol):

Carbamazepine (with the commercial name Tegretol) is a drug which is used as an anticonvulsant via oral administration. The drug has a low solubility and a low dissolution bioavailability therefore the drug is required at a high dosage, more than (100mg/day) for therapeutic effect. The active ingredient is also detrimentally affected by polymorphism and uncontrolled hydration[60].

The pharmaceutical cocrystal of carbamazepine:saccharin consists of carbamazepine and saccharin in a 1:1 stoichiometric ratio. The stability and solubility of the API increases in the saccharin1:1 cocrystal, significantly improving the bioavailability and solubility of the carbamazepine drug. Carbamazepine is a good example that can be used to explain how the active pharmaceutical ingredient can be incorporated into a pharmaceutical cocrystal and provide a more stable and soluble crystalline drug that does not form the hydrate. The molecules in the carbamazepine:saccharin cocrystal combining together through hydrogen bonding synthon between the molecules as shown in (figure 1.7)[61]. The cocrystal structure was obtained through single crystal X-ray diffraction.
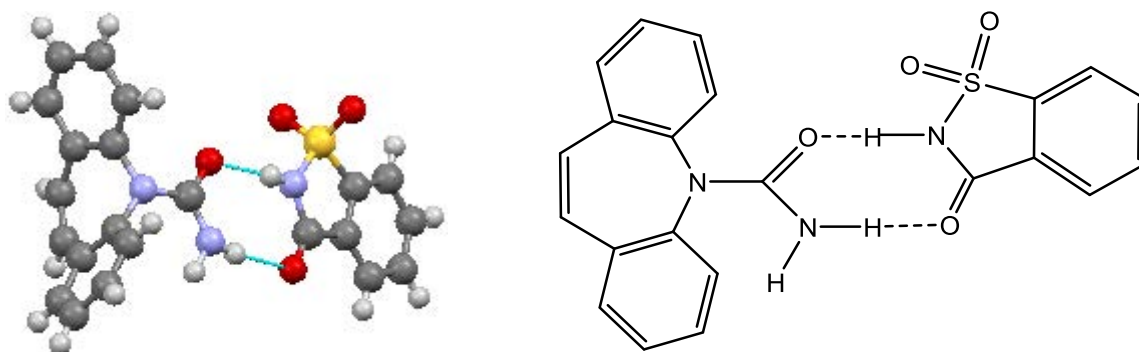
Figure 1.7: Cocrystal structure of carbamazepine:saccharin 1:1 cocrystal through hydrogen bonding synthon[61]

B) Pharmaceutical cocrystals of fluoxetine hydrochloride (Prozac):

Fluoxetine is antidepressant drug and was used in the market in the last decade; it is commercially available as a tablet, capsules and solution. The active ingredient in Prozac is fluoxetine HCl which is available in a salt crystalline solid form. However this form has poor solubility. The active ingredient can be cocrystallised so as to modify the physical properties with keeping the hydrochloride salt of the API. Cocrystals of fluoxetine HCl can be produced

by cocrystallisation with a series of chemical organic compounds such as benzoic acid (1:1), fumaric acid (2:1), succinic acid (2:1) through the evaporation techniques. It was found in the fluoxetine hydrochloride cocrystals that the carboxylic acid group in succinic acid is bonded with the chloride ion in fluoxetine hydrochloride and the two molecules of fluoxetine hydrochloride are bonded with succinic acid through hydrogen bonding (figure 1.8). The fluoxetine HCl: succinic acid cocrystal shows an increase in the solubility compared with the crystalline form of the drug while fluoxetine HCl:benzoic acid has shown a decrease in aqueous solubility. Powder X-ray diffraction and infra-red spectroscopy have been used to confirm the formation of this cocrystal[62].
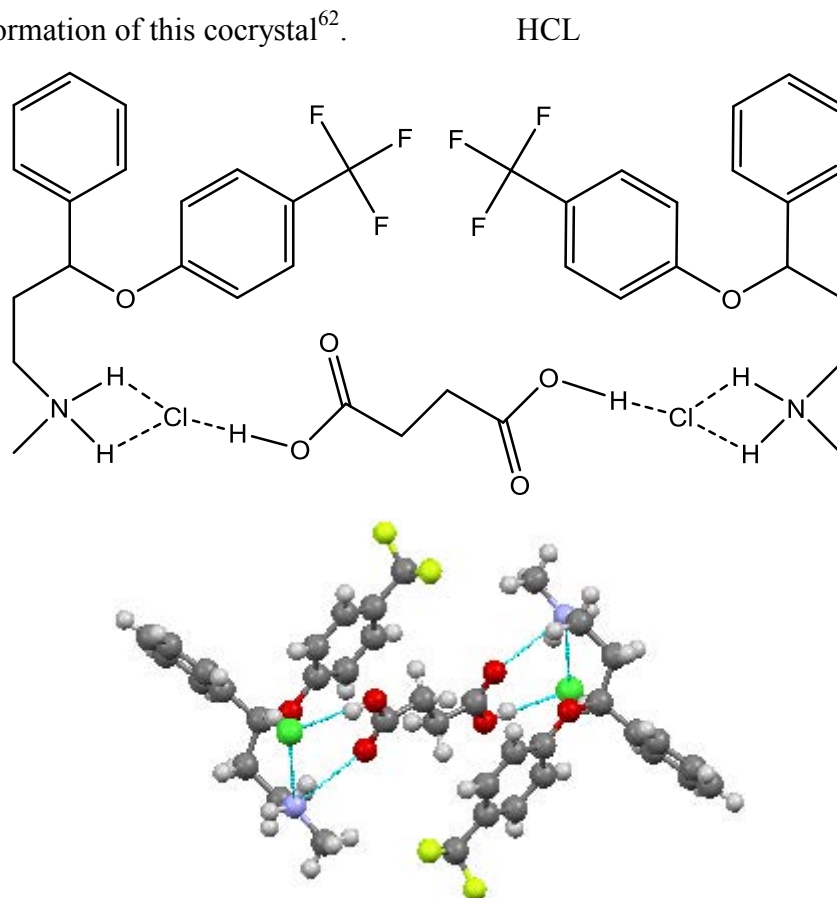
Figure 1.8: Cocrystal structure of fluoxetine:succinic acid (2:1)[62].

C)   Pharmaceutical cocrystals of meloxicam:

Meloxicam is an anti-inflammatory drug which is poorly soluble in water and in organic solvents. Meloxicam (figure 1.9) forms cocrystals with succinic acid (2:1), fumaric acid (2:1) and maleic acid (1:1) produced by solvent drop grinding. These materials were analysed using X-ray powder, single crystal X-ray diffraction and IR spectroscopy to confirm the new cocrystal structure formation. These cocrystals show improvement in solubility and an increase in the bioavailability[43,63].
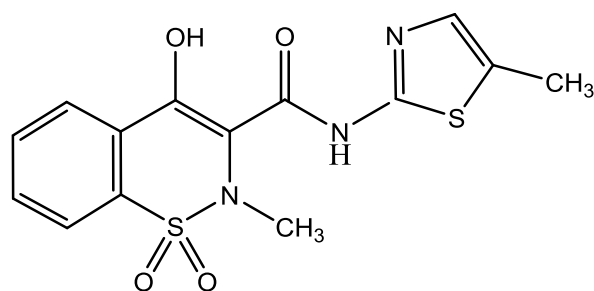
Figure 1.9: Chemical structure of meloxicam[43,63].

D) Pharmaceutical cocrystals of diclofenac:

Diclofenac is an anti-inflammatory analgesic drug and is extremely poorly soluble in water. It has the ability to form cocrytstals with three hydrogen bond acceptors and two hydrogen bond donors. Diclofenac produces cocrystals with aromatic compounds containing nitrogen such as 2-aminopyrimidine and 2-amino-4, 6-dimethylpyrimidine[64]. These diclofenac cocrystals were obtained by solvent drop grinding of diclofenac with 2-aminopyrimidine and 2-amino-4, 6-dimethylpyrimidine in a stoichiometric ratio of 1:1. X-ray powder diffraction and IR were used to analyse and confirm the cocrystal structure (figure 1.10)[64]. The cocrystal combination through hydrogen bonds synthon in diclofenac:2-amino pyrimidine.
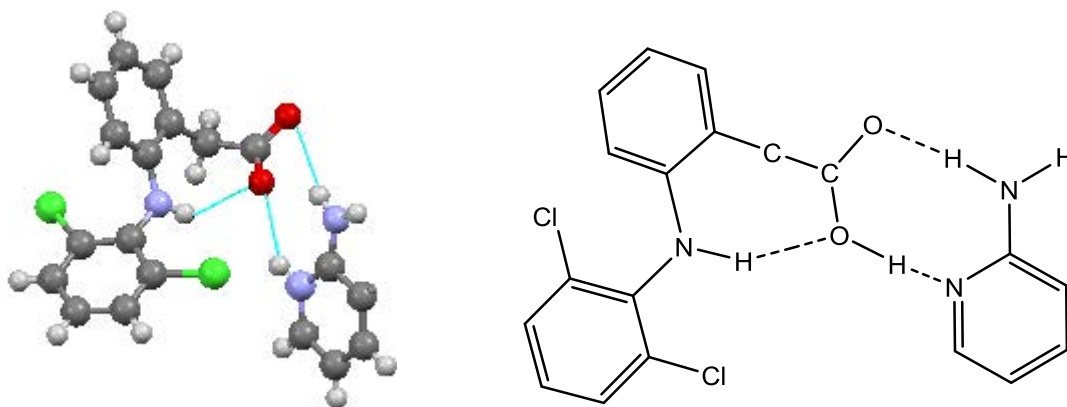
Figure 1.10: Cocrystal structure of diclofenac:2-aminopyrimidine (1:1) connecting through three hydrogen bond synthons[64].

E) Pharmaceutical cocrystals of acetazolamide:

Acetazolamide (figure 1.11) is an antiepileptic drug which is used for glaucoma treatment. This drug has the commercial name (Diamox). Acetazolamide has a low solubility in water and has a number of polymorphic forms. Solvent drop grinding and slow solvent evaporation were used to synthesise acetazolamide cocrystals with nicotinamide and 4-hydroxybenzoic

acid[65]. X-ray powder diffraction and IR-spectroscopy were used to characterise the cocrystals and Differential Scanning Calorimetry (DSC) and Thermogravimetric Analysis TGA were used for melting point measurements.
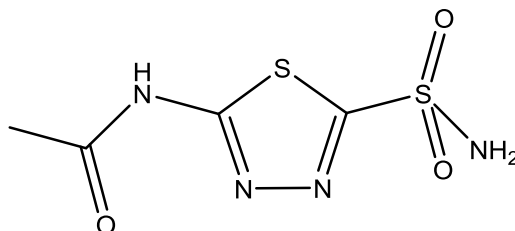
Figure 1.11: The chemical structure of acetazolamide[65].

F) <u>Pharmaceutical cocrystal of 2-chloro 4-nitrobenzoic acid:</u>

2-chloro 4-nitrobenzoic acid can be used for treatment of immunodeficiency diseases[44,66], viral infection and anti-cancer[44]. The active pharmaceutical ingredient 2-chloro 4-nitrobenzoic acid forms cocrystal with nicotinamide in a stoichiometric ratio 1:1. The cocrystals were synthesised by slow solvent evaporation and solvent drop grinding. The cocrystal was characterised by using X-ray powder diffraction and the cocrystal structure was determined through single crystal X-ray diffraction. The cocrystal structure formed through hydrogen bonding of acid-pyridine between the two molecules (figure 1.12)[44,66]. It was found that the cocrystal has melting point higher than the melting point of the pure components and that confirming that the pharmaceutical cocrystal has more stability than that of the pure pharmaceutical components[44].
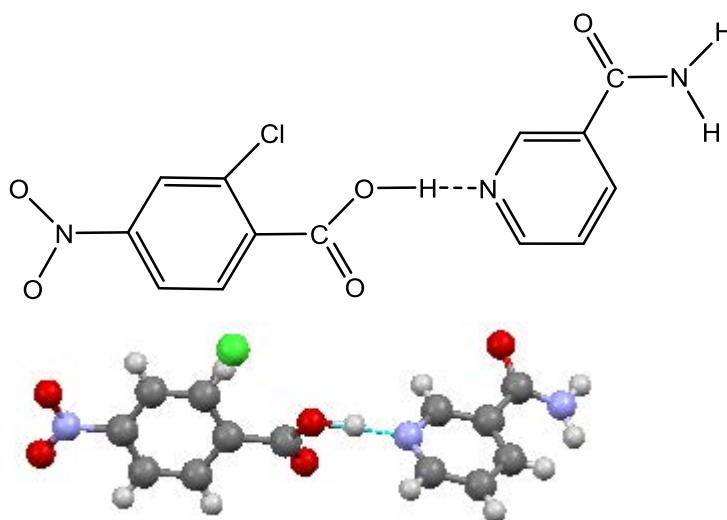
Figure 1.12: Cocrystal structure of 2-chloro 4-nitrobenzoic acid:nicotinamide (1:1) [44,66].

G) Pharmaceutical cocrystal of dopamine:

Dopamine is a drug which is used to treat Parkinson's disease. The Dopamine drug is available in salt form as dopamine hydrochloride or dopamine hydrobromide. Dopamine hydrobromide forms a cocrystal with 3,5-dinitrobenzoic acid in a stoichiometric ratio 1:1 (figure 1.13). The cocrystal was synthesised by slow solution evaporation[67]. The cocrystal was characterised by using X-ray powder diffraction and the melting point determined by using Thermogravimetric Analysis (TGA) and Differential Scanning Calorimetry (DSC).
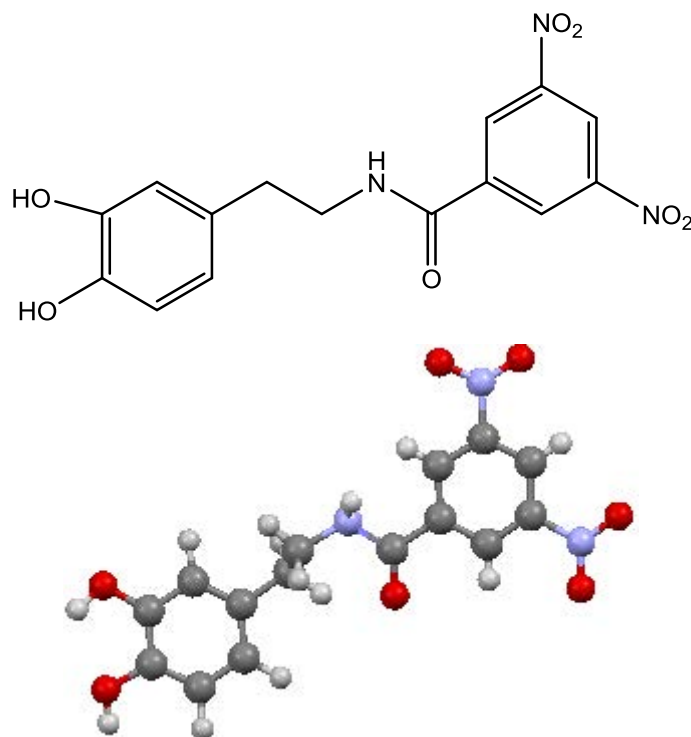
Figure 1.13: Cocrystal structure of dopamine:3,5-dinitrobenzoic acid (1:1)[67].

H) Pharmaceutical cocrystal of nicotinamide and isonicotinamide:

Nicotinamide can be used for anti-inflammatory skin. Nicotinamide forms cocrystal with fumaric acid in a stoichiometric ratio 1:1[68]. Slow solvent evaporation method was used for synthesis and the cocrystal structure was characterised through powder X-ray diffraction and the cocrystal structure was determined through single crystal X-ray diffraction[68]. This structure includes one molecule nicotinamide and one molecule fumaric acid linked through acid-pyridine hydrogen bond (figure 1.14).
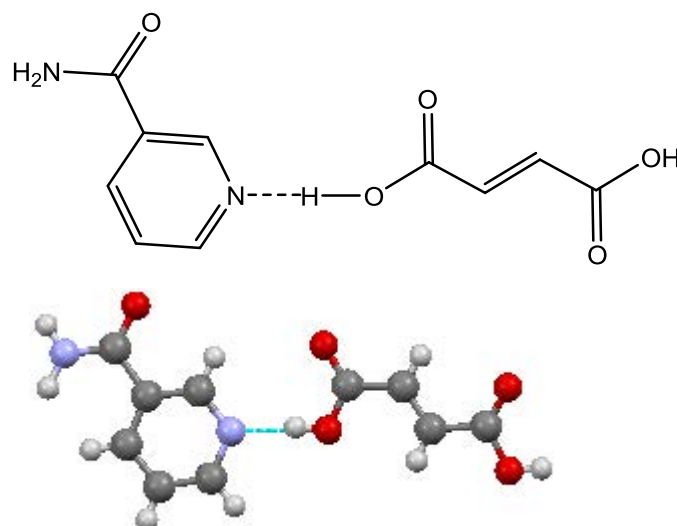
Figure 1.14: Cocrystal structure of nicotinamide:fumaric acid (1:1)[68] .

Isonicotinamide form cocrystals with carboxylic acids (Pimelic acid, subaric acid, azelaic acid and benzoic acid) in a stoichiometric ratio 1:1[36,69]. The cocrystals were synthesised by slow solution evaporation and methanol was used as solvent. All the cocrystals formed were characterised by using powder X-ray diffraction and the cocrystal structures were obtained through single crystal X-ray diffraction. The cocrystal structure of isoniotinamide:pimelic acid includes one molecule isonicotinamide and one molecule pimelic acid linked through acid-amide hydrogen bonds (figure 1.15).
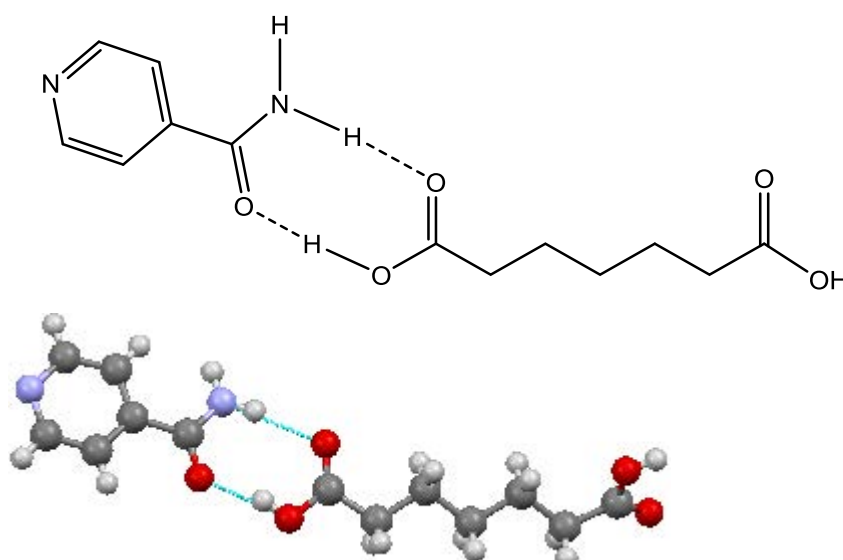
Figure 1.15: Cocrystal structure of isonicotinamide:pimalic acid (1:1) [36,69].

1.6 <u>**Pharmaceutical polymorphism**</u>

"Polymorph" is a word which is derived from two Greek words: "Polus" which means many and "morphs" which means shape[70]. Polymorph is a word that is used in crystallography and biology to describe the behaviour of a natural solid material and can occur in different forms. More specifically, it is the ability of a solid chemical compound to crystallise in more than one crystal arrangement with a different physical properties but with same chemical properties [6,15,71]. This means that two polymorphic forms of a compound can display two distinct behaviours in terms of solid state based properties.

The first discovery of polymorphism in organic solid materials was by Friedrich Wohler and Justus von Liebig when they discovered polymorphs of benzamide in 1832, during their experiments on a boiling solution of benzamide. After cooling the solution analysis of the resulting crystalline material identified three polymorphs of benzamide[72,73].

The polymorph phenomenon is not always clear to understand. In 2006 a new polymorph of maleic acid was discovered which was first crystallised and studied 124 years earlier[74,75]. Maleic acid is a solid organic chemical compound which is widely used in the chemical industry. The new polymorph of maleic acid was found when caffeine and maleic acid (2:1) were dissolved in chloroform and the solvent evaporated slowly from the solution[74].

Polymorphs have different stabilities and can be changed from stable to unstable forms at a specific temperature. These differing stabilities can also affect the solubility and dissolution rate of the drug and hence the bioavailability in the body[76]. Conditions which can determine which polymorph is present in the crystal solid material include: solvent effects, crystallisation temperature and stirring conditions[6,77]. Pharmaceutical polymorphs have different solubility and that affecting on the drug therapeutic activity and one polymorph may be more active than the other polymorph of the same drug.

Polymorphs play a big role in the pharmaceutical industry and in developing active drug ingredients[6,77]. Drugs can usually be taken orally in crystalline solid form and the drug dissolution rate depends on the crystal form of the polymorph. It has been found that paracetamol (acetaminophen) exhibits polymorphism[78] and has three forms; polymorph I (stable), polymorph II (metastable) and polymorph III (unstable)[79]. Polymorph I is

thermodynamically more stable than polymorph II at room temperature which in turn displays more favourable compression properties than polymorph I[77]. This is an important consideration as polymorph I is difficult to make into tablets and most of the paracetamol drug products on the market contain polymorph I mixed with agents to improve the compression properties[77,79]. Polymorph II however is costly in the crystallisation process during production [80].

1.7 <u>Pyrazinamide</u>

Pyrazinamide is an anti-tuberculosis[81] drug which is used in combination with other drugs to kill the bacteria that cause tuberculosis[82]. It is white crystalline powder soluble in water 50 mg/ml and methanol 13.8 mg/ml and ethanol 5.7 mg/ml and stable at room temperature with a melting point at 190 $^{\circ}$C. Pyrazinamide (figure 1.16) contains an amide group and two heterocyclic (N) groups thus containing both strong hydrogen bond donors and acceptors. Those groups provide good potential for pyrazinamide to form cocrystals with dicarboxylic acids through acid-amide hydrogen bonds; N-H$^{....}$O=C in which the amide NH_2 acts as a donor to the carboxyl C=O and OH$^{...}$O=C in which the carboxyl OH acts as a donor. There is also opportunity for pyrazinamide to interact with carboxylic acids through the formation of strong acid-pyridine O-H$^{...}$N (heterocyclic) hydrogen bonds in which the carboxyl OH acts as a donor to pyridine nitrogen which is acting as an acceptor. There is also the possibility for the formation of intramolecular hydrogen bonds between the amide and the neighbouring pyridine group forming a five-membered ring through strong N-H$^{....}$N (heterocyclic) interactions or the formation of a C-H$^{...}$O=C hydrogen bond also generating a five-membered intramolecular ring on the opposite side of the molecule. These interactions act to stabilize the planarity and conformation of the pyrazinamide molecule.
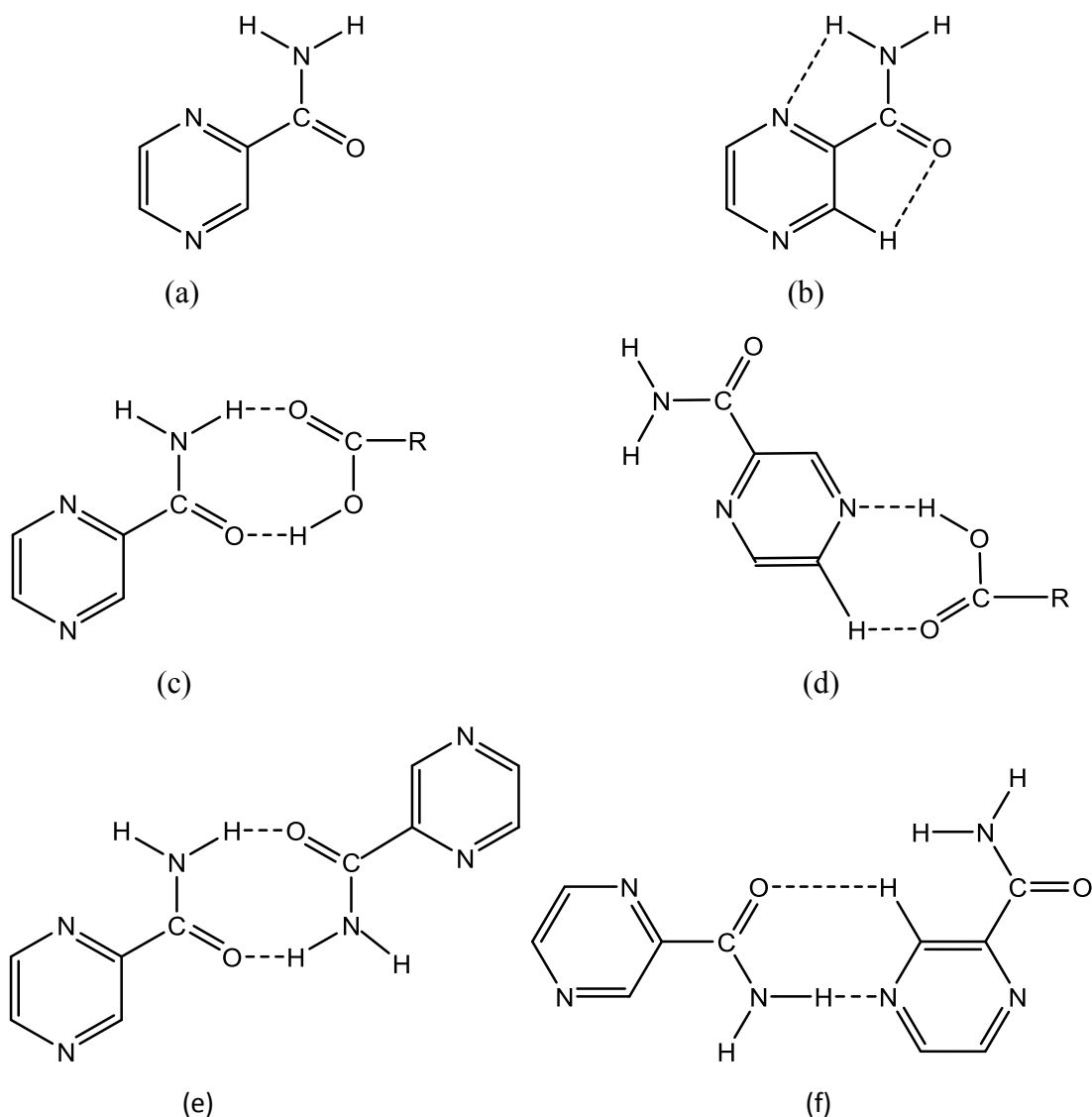
Figure 1.16: Chemical structure of (a) Pyrazinamide showing, (b) possible intramolecular hydrogen bonds, (c, d) possible intermolecular interactions in formation of a crystal, (e, f) possible intermolecular interactions with pyrazinamide in formation of a crystal.

1.8 Polymorphism of pyrazinamide

A number of pyrazinamide polymorphs have been reported in the literature[76,83,84,85], many of these papers report the study of similar forms or investigation of these forms at different temperatures[76]. Analysis of these literature sources reveals that pyrazinamide has four distinct polymorphic forms (α[86], β[87], δ[88] and γ[89]). These forms have been synthesised using a variety of methods including solvents drop grinding and solution crystallisation through solvent

evaporation from different solvents with varying polarity and hydrogen bonding. The literature shows that the α polymorph is the most stable commercial form[76].

The polymorphic behaviour of pyrazinamide (α[86], β[87], δ[88], and γ[89]) has been studied using a variety of characterisation techniques including infrared spectroscopy, powder X-ray diffraction, Differential Scanning Calorimetry (DSC) and polarized light thermal microscopy. The IR spectra alone exhibit two main profiles in the N-H stretching vibration region that can be used to identify the polymorphs α, β and δ whose crystalline structures have pyrazinamide dimers where the dimer does not exist with the γ form[76]. However the most detailed information regarding these polymorphs can be obtained through X-ray diffraction study. The structures of all four polymorphs have been determined by single crystal X-ray diffraction and the hydrogen-bond networks and packing features are discussed below.

Crystallization of the α form[83,86] (figure 1.17) takes place within the P2$_1$/n monoclinic space group with pyrazinamide dimers formed through complementary amide-amide hydrogen bonds. Hence the structure forms the expected centrosymmetric $R_2^2(8)$ dimer formed by classical complementary N–H$\cdots$O=C interactions. The dimers are then held together in a ladder-type arrangement by the formation of complementary N–H$\cdots$N (heterocyclic) interactions forming an $R_2^2(10)$ ring motif. This network is reinforced by formation of C-H$\cdots$O interactions such that the carbonyl oxygen acts as a double acceptor. The second heterocyclic N forms a further weak intramolecular hydrogen bond with neighbouring pyrazinamide dimers through a C-H$\cdots$N (heterocyclic) interaction that links the ladders together. This structure (figure 1.17) highlights the formation of the interactions predicted in Figure 1.16 motif *e*.
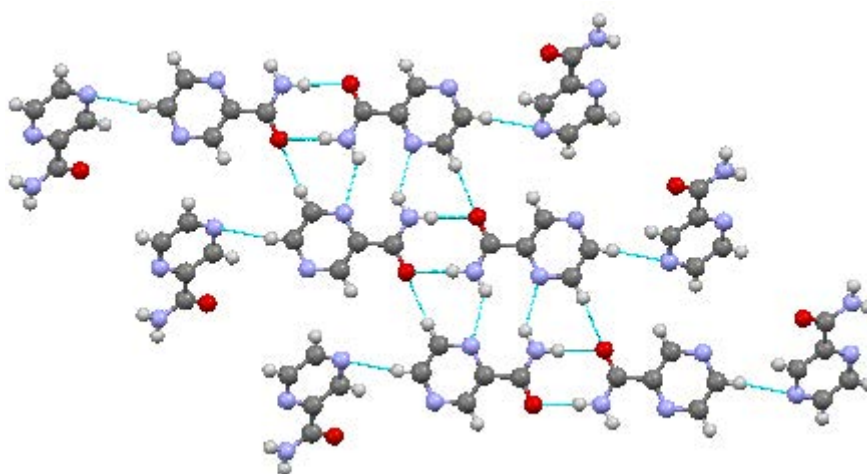
Figure 1.17: A view of the crystal structure of pyrazinamide α form.

The β form[83,87] (figure 1.18) of pyrazinamide also crystallises in the P2$_1$/c monoclinic space group. The structure of this form also contains the expected amide dimer through amide-amid hydrogen bonds, forming the standard $R_2^2(8)$ motif through complementary N-H$^{....}$O=C interactions. The dimers are then held together through a ladder-type arrangement by the complementary C-H$^{....}$N (heterocyclic) interactions forming $R_2^2(10)$ ring motif, the ring is reinforced by formation other N-H$^{....}$O=C. The second heterocyclic N forms a further weak intramolecular hydrogen bond with neighbouring rotated pyrazinamide dimers through a C-H$^{....}$N (heterocyclic) interaction that links the ladders together. This structure (figure 1.18) highlights the formation of the interactions predicted in Figure 1.16 motif *e*.
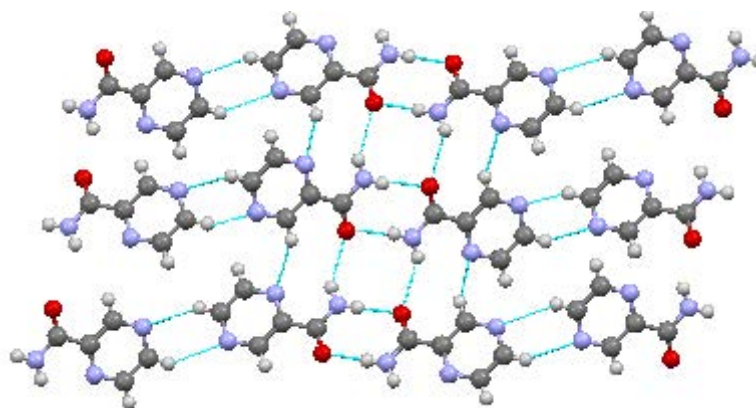
Figure 1.18: A view of crystal structure of pyrazinamide β form.

The δ form[83,88] of pyrazinamide (figure 1.19) crystallises in the P-1 triclinic space group and forms one of the most simple packing diagrams. The centrosymmetric amide dimer is also present in this structure giving the expected $R_2^2(8)$ motif through complementary N-H$^{....}$O=C interactions. The dimers are then held together in a ladder-type arrangement by the formation of complementary C-H$^{....}$N (hetero) interactions between neighbouring dimers forming an R_2^2 (6) motif. These ladders are then linked to adjacent ones by further C-H$^{....}$N interactions forming another set of $R_2^2(6)$ motifs. This structure (figure 1.19) highlights the formation of the interactions predicted in Figure 1.16 motif *e*.
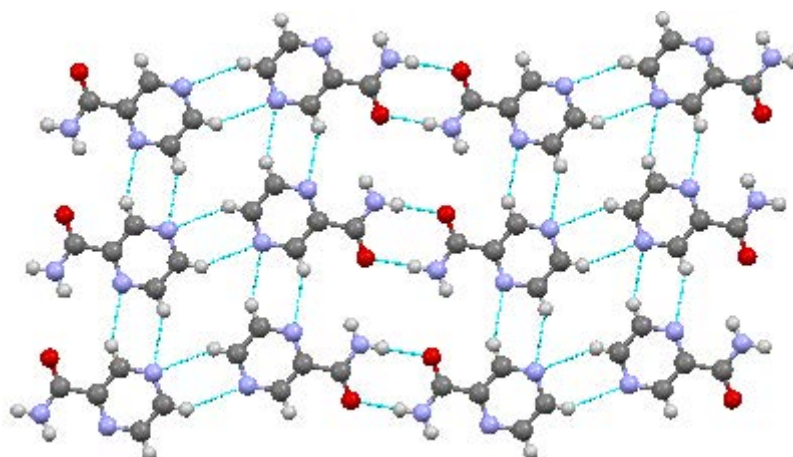
Figure 1.19: A view of crystal structure of pyrazinamide δ form.

The γ form[83,89] of pyrazinamide (figure 1.20) crystallises in the Pc monoclinic group space but unlike the other polymorphs there are no amide dimers present. The NH_2 group is involved in interactions with two different adjacent molecules; one through formation of a N-H$\cdots$O=C hydrogen bond linking together molecules in a vertical chain, the other through N-H$\cdots$N (heterocyclic) interaction forming an infinite chain in a horizontal direction. The other hydrogen bond C-H$\cdots$N forming spiral interaction. This structure (figure 1.20) highlights the formation of the interactions predicted in Figure 1.16 motif *f*.
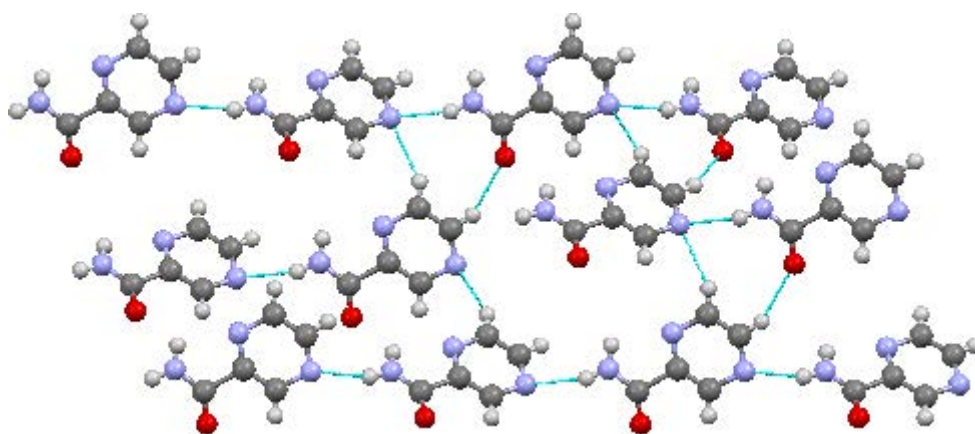
Figure 1.20: A view of crystal structure of pyrazinamide γ form.

1.8.1 Crystal thermal stability of pyrazinamide polymorphs

Thermal analysis has demonstrated that the α, β and δ forms give rise to the γ form on heating and that in the endothermic transition some super-heating is observed[76] (the DSC peaks display irregular shape)[76,83]. The thermal analysis showed (figure 1.21) that form β changes to form polymorph γ when heated at 95 °C, whilst polymorph α and polymorph δ undergo

transitions to form polymorph γ at higher temperatures, 145 ^{o}C and 135 ^{o}C respectively. The other additional phase transition from form δ to form α on heating at 120 ^{o}C. The relative stability of the four pyrazinamide polymorphs γ> α> δ> β at 145 ^{o}C were derived from the experimental observations and polymorph γ is more stable and preferential formation structure without dimer at temperature values higher than 145 ^{o}C[76] and the stability of the four polymorphs were α> δ> β > γ at 25 ^{o}C while the stability of the four polymorphs were δ > α> β > γ at zero temperature[76,83]. It was noticed that the stability of the four pyrazinamide polymorphs depends on the changing in the temperature degree and the most stable polymorph form of pyrazinamide is α at room temperature. The thermal analysis study of pyrazinamide polymorphs helps to find out the relative stability of pyrazinamide polymorphs forms.
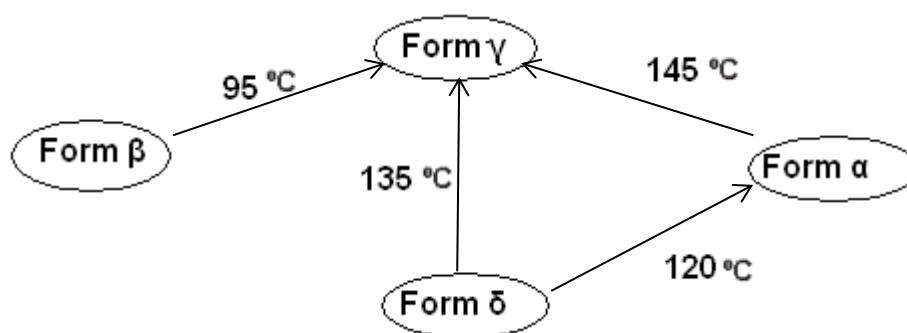
Figure 1.21: Thermal analysis of the pyrazinamide polymorphs[83].

1.9 Pharmaceutical cocrystals of pyrazinamide

Pyrazinamide forms cocrystals with a number of molecular coformers including fumaric acid succinic acid, benzoic acid, malonic acid and glutaric acid. These structures contain a variety of structural motifs.

A) Pyrazinamide:fumaric acid and pyrazinamide:succinic acid

Pyrazinamide forms cocrystals with fumaric[82] and succinic acid[90] both in a stoichiometric ratio 2:1. Both cocrystals were synthesised by slow solvent evaporation from methanol and the structures characterised by using single crystal X-ray diffraction. The cocrystal structures contain pyrazinamide dimers linked through N-H⋯O=C hydrogen bonds. The cocrystals with

fumaric acid (A) and succinic acid (B) are formed through acid-pyridine hydrogen bonds (figure 1.22). Both cocrystal structures include one pyrazinamide per one half molecule acid linked through acid-pyridine strong hydrogen bonds while the pyrazinamide molecule is linked to another pyrazinamide molecule through amide-amide hydrogen bonds forming an $R_2^2(8)$ pyrazinamide dimer.

(A)

(B)
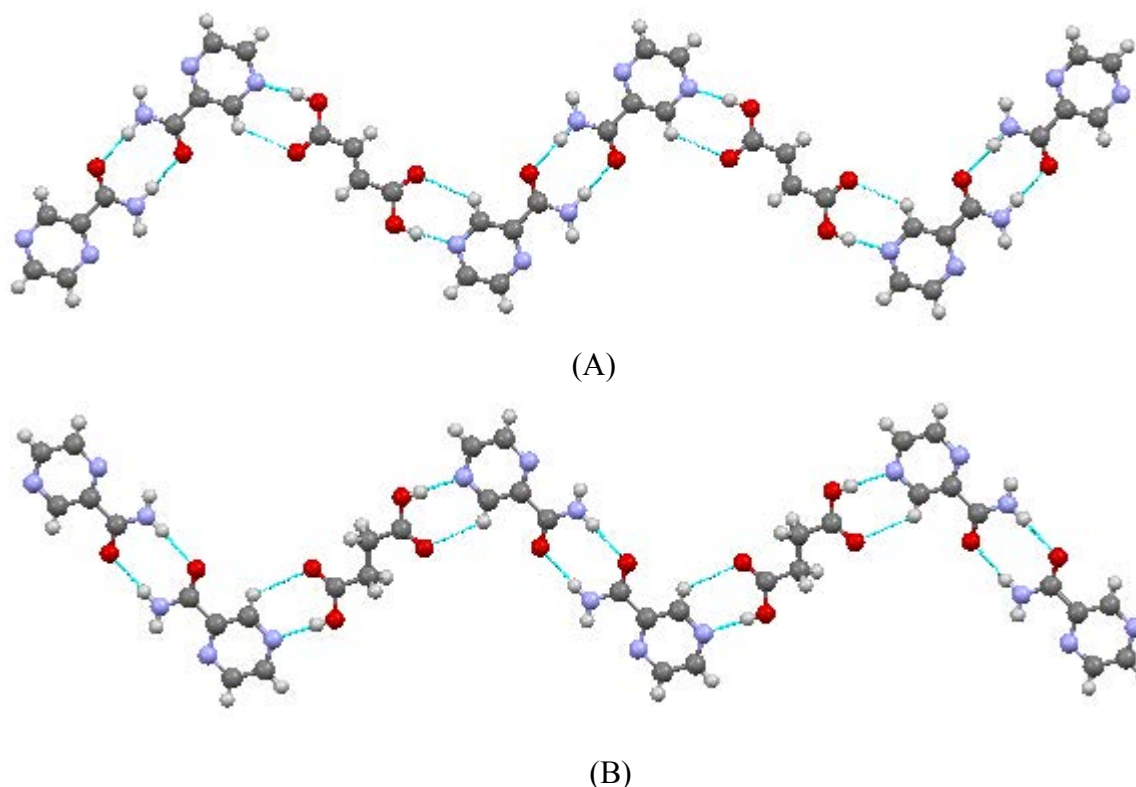
Figure 1.22: A view of the cocrystal structures of (A) pyrazinamide:fumaric acid 2:1 and (B) pyrazinamide:succinic acid (2:1) showing the hydrogen bonded structural motifs.

B) <u>Pyrazinamide:isoniazid dual drug</u>

Pyrazinamide forms cocrystal with isoniazed drug (1:1)[82] dual drug cocrystal and synthesis by solvent drop grinding and characterised by powder X-ray diffraction.

It was found that the combination of multi drugs of pyrazinamide and isoniazed with succinic acid acids or fumaric acid forms adduct cocrystal structures and characterised by powder X-ray diffraction and single crystal X-ray diffraction (figure 1.23)

The melting point of product obtained showed increase in the drug solubility and that will improve the drug activity.

Pyrazinamide   Succinic acid   Isoniazed
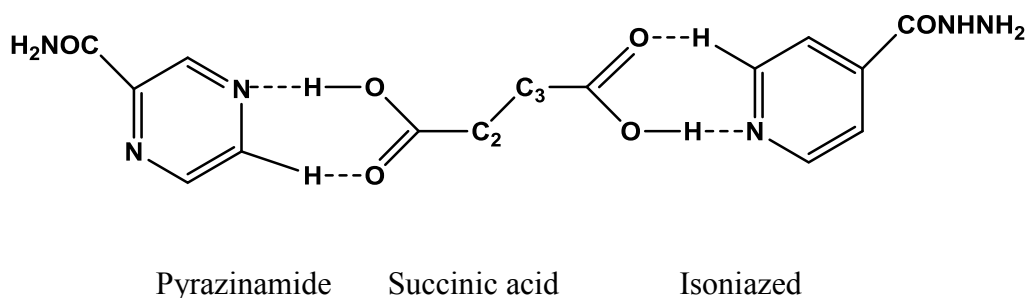
Figure 1.23: A view of the crystal structure proposed of drug-drug adduct of
pyrazinamide:succinic acid:isoniazed linked through acid-pyridine hydrogen bonds

C) <u>Pyrazinamide:2,5-dihydrobenzoic acid</u>

Pyrazinamide forms cocrystal with 2,5-dihydroxy benzoic acid[91] in a stoichiometric ratio 1:1. The cocrystal was synthesised by solvent drop grinding and characterised by X-ray powder diffraction analysis. This structure was obtained through single crystal X-ray diffraction. The cocrystal structure contains acid-amide and acid-pyridine hydrogen bonds forming an $R_2^2(8)$ ring (figure 1.24).
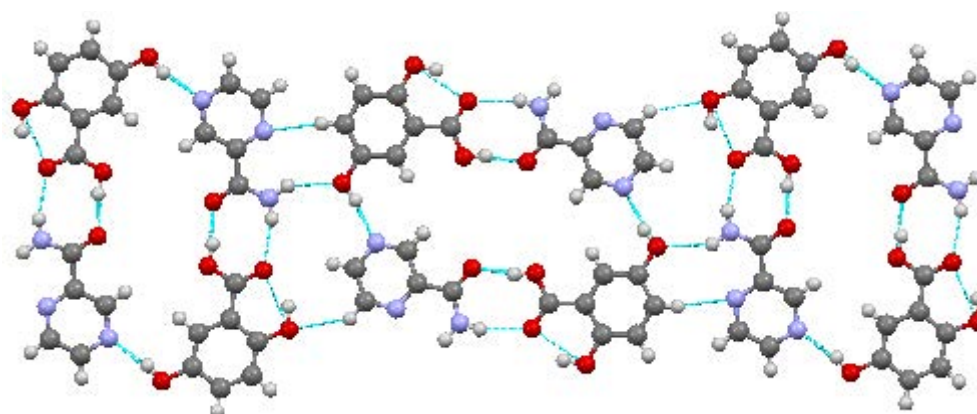
Figure 1.24: A view of the cocrystal structure of pyrazinamide:2,5-dihydroxy benzoic acid
(1:1) in chain showing the hydrogen bonded structural motifs.

D) <u>Pyrazinamide:malonic acid</u>

Pyrazinamide forms cocrystal with malonic acid 1:1[90].The cocrystal was synthesised through slow solvent evaporation from methanol and characterised by X-ray powder diffraction analysis. This structure was obtained through single crystal X-ray diffraction (figure 1.25). The cocrystal structure contains acid-pyridine and acid-amide hydrogen bonds and forms an acid-amide dimer $R_2^2(8)$.
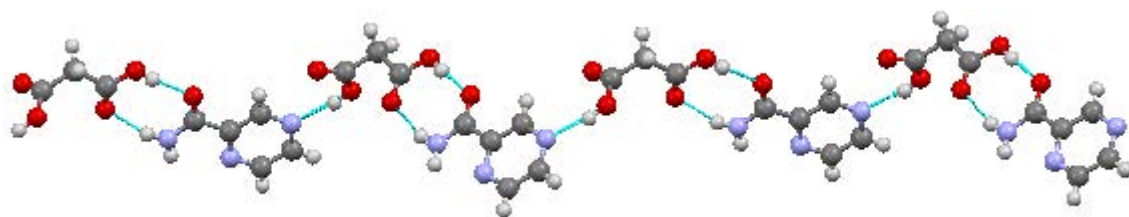
Figure 1.25: A view of the cocrystal structure of pyrazinamide:malonic acid 1:1 showing the hydrogen bonded structural motifs.

E) Pyrazinamide:glutaric acid

Pyrazinamide form cocrystal with glutaric acid $(1:1)^{90}$ through acid-amide dimer and acid-pyridine in pyrazine. The cocrystal of pyrazinamide-fumaric acid was synthesised though slow solvent evaporation and characterised through powder X-ray diffraction and the cocrystal structure was obtained through single crystal X-ray diffraction (figure 1.26). The cocrystal structure includes acid-amide and acid-pyridine hydrogen bonds; together these hydrogen bonds forming an $R_2^2(8)$ and $R_2^2(7)$ rings between pyrazinamide and glutaric acid molecules.
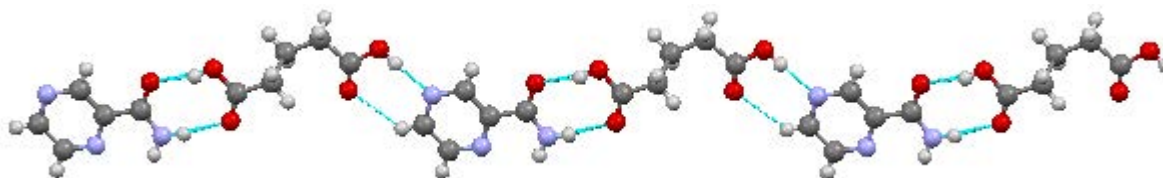
Figure 1.26: A view of the cocrystal structure of pyrazinamide:glutaric acid showing the hydrogen bonded structural motifs.

1.10 <u>Aims and objectives</u>

The aim of the present work focuses on the following objective:

1- Synthesis and determination of new binary cocrystals using solvent evaporation crystallization and solvent drop grinding methods using different solvents (methanol and ethanol) and different stoichiometric ratios.

2- Attempt to synthesis new cocrystals from combination of pyrazinamide with a series of selected dicarboxylic acid such as: oxalic acid, oxamic, malonic acid, malieic acid, fumaric acid, succinic acid, glutaric acid, adipic acid, pimelic acid, subaric acid, azelaic acid, sebacic acid and with other molecules such as histidine, nicotinamide and isonictotinamide.

The former molecules chosen for the above study have complementary donor and acceptor functional groups that can form potential supra-molecular bonds in the crystallisation   process. Pyridine ring and amide functional groups on pyrazinamide can form hydrogen bonds with carboxylic acid functional groups on dicarboxylic acid producing cocrystals or salts.

3- Characterisation using powder X-ray diffraction data to confirm the formation of new material.

4- Using NMR to identify the stoichiometric ratio of the new cocrystal material formed.

6- Crystal structure determination using single crystal X-ray powder diffraction and powder X-ray diffraction methods.

7- Discussion and analysis of new structures relative to each other and with other previously published work.

2 . Experimental

2.1 Synthesis by solvent evaporation crystallization

0.1g of pyrazinamide and equivalent stoichiometric molar ratio of dicarboxylic acid were dissolved separately in two conical flasks in 20 ml solvent at room temperature. The solutions were heated and stirred until all the starting materials were totally resolved. The solutions were hot filtered in another conical flask to remove any undissolved starting materials. The filtered solutions were combined in a further conical flask and left on the bench for crystallization at room temperature for up to two weeks. The material obtained from crystallization was filtered and dried by suction for half an hour. The experiments were repeated using a variety of different solvents (methanol, ethanol and ethyl acetate) and different stoichiometric ratios (1:1, 1:2 and 2:1). The time required for crystallization varied from one to two weeks depending on the length of the chain of acid coformer.

This experimental procedure was used in the synthesis of all conformer combinations. The method was used also to cover other unsuccessful other combinations such as dopamine, histidine with dicarboxylic acids.

2.2 Synthesis by solvent drop grinding

0.1g of pyrazinamide was ground with the equivalent stoichiometric molar ratio of dicarboxylic acid with a few drops of solvent (methanol, ethanol or ethyl acetate) added .The mixture was ground in a mortar and pestle for 30 minutes at room temperature.

2.3 Powder X-ray diffraction data

All data were collected at room temperature using a Bruker D8 high resolution X-ray powder diffractometer in transmission mode. The crystalline samples were ground and placed in a flat disc of approximately 10mm diameter between transparent polyethylene tape. The wavelength used was $\lambda= 1.5406$ Å generated by the selected tube X-ray source (CuKα_1). Powder X-ray diffraction data were recorded between either $5^o \leq 2\theta \leq 60^o$ or $5^o \leq 2\theta \leq 90^o$ for 30 minutes. The X-ray powder diffraction patterns data were collected in the form of a RAW file and that file converted to a UXD file for additional analysis. The UXD file was after that converted into XY format file through using Perl software for additional analysis through using the Microsoft office Excel software.

2.4   <u>Single crystal X-ray diffraction data</u>

Single X-ray diffraction data of **Pyrazinamide:PimelicAcid 1:1** was collected and recorded by using diffractometer equipment and the data was collected by the EPSRC UK National Crystallography Service[92] on a Rigaku AFC12 goniometer equipped with an enhanced sensitivity (HG) Saturn724+ detector mounted at the window of an FR-E+ Super Bright molybdenum rotating anode generator with HF Varimax optics. The data collection was driven and processed and an absorption correction was applied using CrystalClear-SM Expert[93]. The remaining datasets were measured on an Agilent Super Nova diffractometer using an Atlas detector and the data collections were driven and processed and absorption corrections were applied using CrysAlisPro[94]. All five structures were solved using ShelXS4 and refined by a full-matrix least-squares procedure on F2 in ShelXL[95]. All non-hydrogen atoms were refined with anisotropic displacement parameters. In **Pyrazinamide:AdipicAcid** the hydrogen atoms bonded to N(7A), N(7B) and O(8), and in **Pyrazinamide:SebacicAcid** the hydrogen atoms bonded to N(7) and O(8) were located in the electron density and their positions refined freely, with their isotropic thermal parameters based on the equivalent isotropic thermal parameter of the parent atom (Uiso(H) = 1.2(Ueq(N) and Uiso(H) = 1.5(Ueq(O)). In **Azelaic Acid** the hydrogen atoms bonded to O(1) and O(9) were located in the electron density and their positions and isotropic thermal parameters refined freely All other hydrogen atoms in all five structures were added at calculated positions and refined by use of a riding model with isotropic displacement parameters based on the equivalent isotropic displacement parameter (Ueq) of the parent atom.

2.5   <u>¹H NMR spectra</u>

 0.05g of a crystalline sample was dissolved in 2ml of dimethyl sulfoxide-d6 (DMSO) solvent in a 5mm diameter quad probe (NMR tube). The NMR data were recorded at 300.15 MHz by using Bruker AVIII300 spectrometer equipment. The data were analysed using the Mestrenova software[96].

2.6   <u>**Crystallographic Data**</u>

Crystal structure determination of compound **Pyrazinamide:PimelicAcid 1:1**: $C_5H_5N_3O:C_7H_{12}O_4$, M_r = 283.29, crystal dimensions: 0.42 x 0.16 x 0.02 mm, triclinic, space group: P-1, a = 5.3302(4) Å, b = 8.4201(6) Å, c = 15.5321(11) Å, α = 89.478(7)^o, β = 82.760 (7)^o, γ = 71.840(6)^o, V = 656.75(9) Å^3, Z = 2, ρ_{calcd} = 1.433 Mg/m^3 ,μ = 0.113 mm^{-1}, $\lambda_{Mo-K\alpha}$ = 0.71075Å, T = 100(2) K, $2\theta_{max}$ = 54.96^o, 7308 reflections measured, 2979 independent reflections (R_{int} = 0.0290), R_1 = 0.0350 (observed reflections), wR = 0.1010 (all data), largest diff. peak and hole: 0.404 and -0.207 e.Å^{-3}.

Crystal structure determination of compound **Pyrazinamide:GlutaricAcid 1:1**: $C_5H_5N_3O:C_5H_8O_4$, M_r = 255.23, crystal dimensions: 0.15 x 0.10 x 0.03 mm, monoclinic, space group: P21/c, a = 11.3844(9) Å, b = 4.8251(7) Å, c = 21.9011(16) Å, β = 104.610 (9)^o, V = 1164.1 (2) Å^3, Z = 4, ρcalcd = 1.456 Mg/m^3, μ = 1.012 mm^{-1}, $\lambda_{Cu-K\alpha}$ = 1.5418 Å ,T = 100.00(10) K, $2\theta_{max}$ = 133.16^o, 3397 reflections measured, 3397 independent reflections, R1 = 0.0397 (observed reflections), wR = 0.1076 (all data), largest diff. peak and hole: 0.179 and -0.217 e.Å-3. The crystal was a non-merohedral twin with the domains related by 180° about the direct axis [0 0 1] and the refined percentage domain ratio being 64:36.

Crystal structure determination of compound **Pyrazinamide:AdipicAcid 4:1**: $4(C_5H_5N_3O):C_6H_{10}O_4$, M_r = 638.62, crystal dimensions: 0.20 x 0.09 x 0.06 mm, triclinic, space group: P-1, a = 5.1814(8) Å, b = 11.7163(16) Å, c = 12.2250(14) Å, α = 74.708 (11)^o ,β = 87.314 (11)^o, γ = 85.212 (12)^o, V = 713.13 (17) Å^3, Z = 1, ρ_{calcd} = 1.487 Mg/m^3 , μ = 0.963 mm^{-1}, $\lambda_{Cu-K\alpha}$ = 1.5418 Å, T = 100.00 (10) K, $2\theta_{max}$ = 140.106^o, 4178 reflections measured, 2666 independent reflections (R_{int} = 0.0348), R_1 = 0.0623 (observed reflections), wR = 0.1780 (all data), largest diff. peak and hole: 0.353 and -0.368 e.Å^{-3}.

Crystal structure determination of compound **Pyrazinamide:SebacicAcid 2:1**: $2(C_5H_5N_3O):C_{10}H_{18}O_4$, M_r = 448.48, crystal dimensions: 0.35 x 0.20 x 0.10 mm, triclinic, space group: P-1, a = 5.1790(2) Å, b = 5.4406(2) Å, c = 19.2691(7) Å, α = 94.342 (3)^o, β = 93.910(3)^o, γ = 94.681(3)^o, V = 538.07(3) Å^3, Z = 1, ρ_{calcd} = 1.384 Mg/m^3 ,μ = 0.869 mm^{-1}, $\lambda_{Cu-K\alpha}$ = 1.5418 Å, T = 100.00 (10) K, $2\theta_{max}$ = 140.116^o, 5733 reflections measured, 2026

independent reflections (R_{int} = 0.0159), R_1 = 0.0339 (observed reflections), wR = 0.0911 (all data), largest diff. peak and hole: 0.290 and -0.169 e.$Å^{-3}$.

Crystal structure determination of compound **Azelaic Acid 1:1**: $C_9H_{16}O_4$, M_r = 188.22, crystal dimensions: 0.14 x 0.13 x 0.03 mm, monoclinic, space group: P21/c, a = 5.4938(2) Å, b = 9.4418 (3) Å, c = 18.8258(6) Å, β = 95.673 (3)^o, V = 971.74 (6) $Å^3$, Z = 4 , ρ_{calcd} = 1.287 Mg/m^3, μ = 0.838 mm^{-1}, $\lambda_{Cu-K\alpha}$ = 1.5418 Å, T = 100.00 (10) K, $2\theta_{max}$ = 148.496^o, 3622 reflections measured, 1922 independent reflections (R_{int} = 0.0182), R_1 = 0.0430 (observed reflections), wR = 0.1287 (all data), largest diff. peak and hole: 0.288 and -0.224 e.$Å^{-3}$.

3. <u>Results</u>

Pyrazinamide was used in this investigation as the API for co-crystallisation with a group of alkane dicarboxylic acids (table 3.1). Potential synthesis of cocrystal adducts was carried out with variation of acid chain length to form products using different solvents and different methods of synthesis in combination with different stoichiometric ratios (1:1, 1:2, 2:1). Pyrazinamide shows extensive polymorphic behaviour and has demonstrated the ability to form cocrystals with dicarboxylic acids through strong hydrogen bonds formed with the amide and pyridine groups. This increases the potential to form cocrystals with oxalic acid, oxamic acid, malonic acid, maleic acid, fumaric acid, succinic acid, glutaric acid, adipic acid, pimelic acid, subaric acid, azelaic acid and sebacic acid (as shown in table 3.1). Further investigation was carried out to assess the potential for pyrazinamide to form cocrystals with other amides such as isonicotinamide, nicotinamide and histidine (table 3.2).

Other work was carried out to investigate the adduct formation behaviour of isonicotinamide with nicotinamide to form new products with different stoichiometric ratios (1:1, 1:2, 2:1), and its behaviour in adduct formation with fumaric acid. Additional experiments were carried out to investigate any potential cocrystal formation by the API, L-dopamaine with succinic acid.

X-ray powder diffraction was used as the primary method to confirm the formation of a new material. NMR nuclear magnetic resonance spectroscopy was used to identify the stoichiometric ratio of the cocrystal or adduct formed. Single crystal X-ray diffraction analysis was used to determine the crystal structures of any new material formed. This was carried out in the case of pyrazinamide with glutaric acid, adipic acid, pimelic acid, azelaic acid and sebacic acid.

Table 3.1. Molecular structures of the dicarboxylic acids used in this investigation.
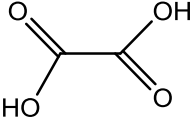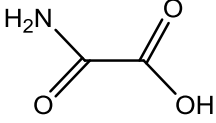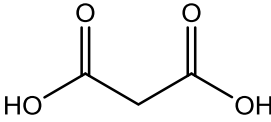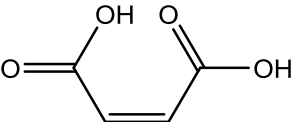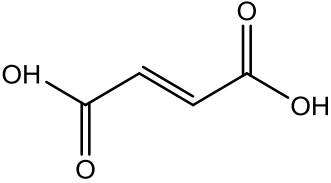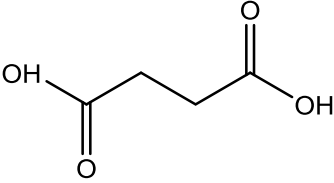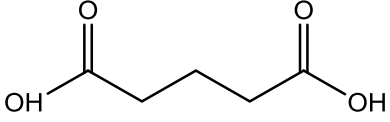
Coformer	Chemical Structure
Oxalic acid	
Oxamic acid	
Malonic acid	
Maleic acid	
Fumaric acid	
Succinic acid	
Glutaric acid	

Table 3.1. Continued molecular structures of the dicarboxylic acids used in this investigation.
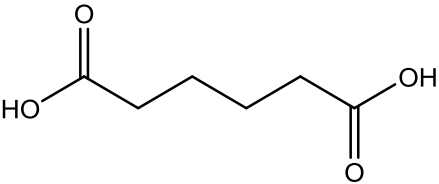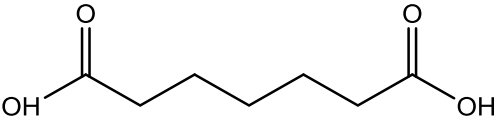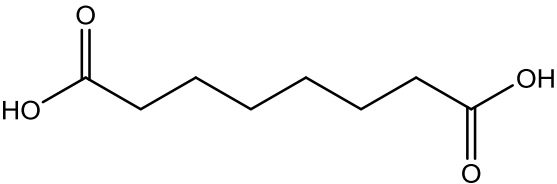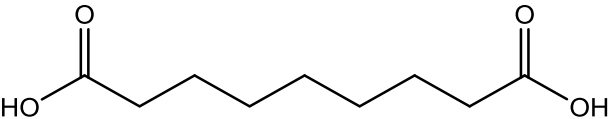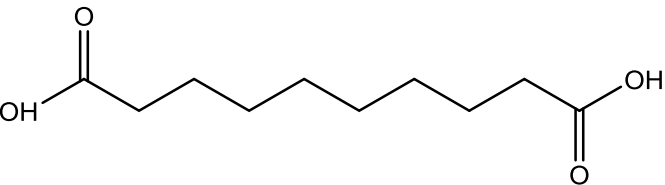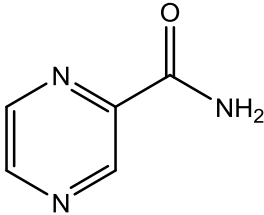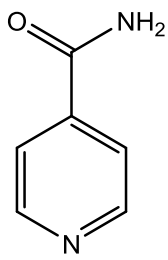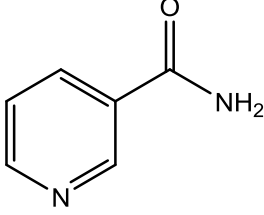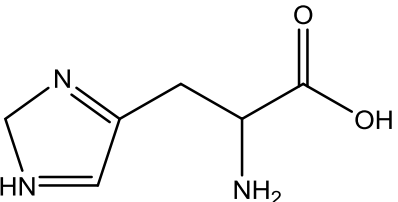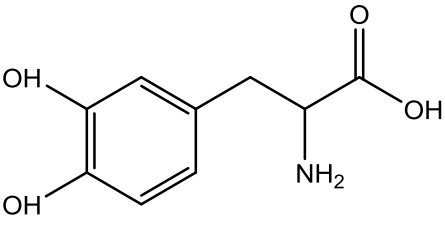
Coformer	Chemical Structure
Adipic acid	
Pimelic acid	
Suberic acid	
Azelaic acid	
Sebacic acid	

Table 3.2   Molecular structures of the amides and APIs used in this investigation.

Coformer	Chemical Structure
Pyrazinamide	
Isonicotinamide	
Nicotinamide	
Histidine	
L-Dopaamine	

3.1 <u>Pyrazinamide and oxalic acid</u>

Pyrazinamide and oxalic acid were dissolved separately in methanol, the solutions combined in a 1:1 stoichiometric ratio and the solvent allowed to evaporate. The product was a white solid crystalline material obtained through the solvent evaporation crystallisation method. The X-ray powder diffraction pattern of the product formed was compared with data of the starting materials and with a number of simulated patterns from previously published pyrazinamide polymorphs[76,83,97,98]. The X-ray powder diffraction pattern of the product confirms that a new material has been formed (figure 3.1). The pattern also indicates that a small amount of oxalic acid starting material may be present (see peaks at 18º, 26º and 29º 2-theta), but there is no indication of the presence of pyrazinamide polymorphs in the product. The crystal quality of this product was insufficient for single crystal X-ray diffraction and hence further structure investigation was not carried out. It is worth nothing that this figure confirms that the pyrazinamide used as a starting material is matches polymorph (α(PYRAZIN15))[97].
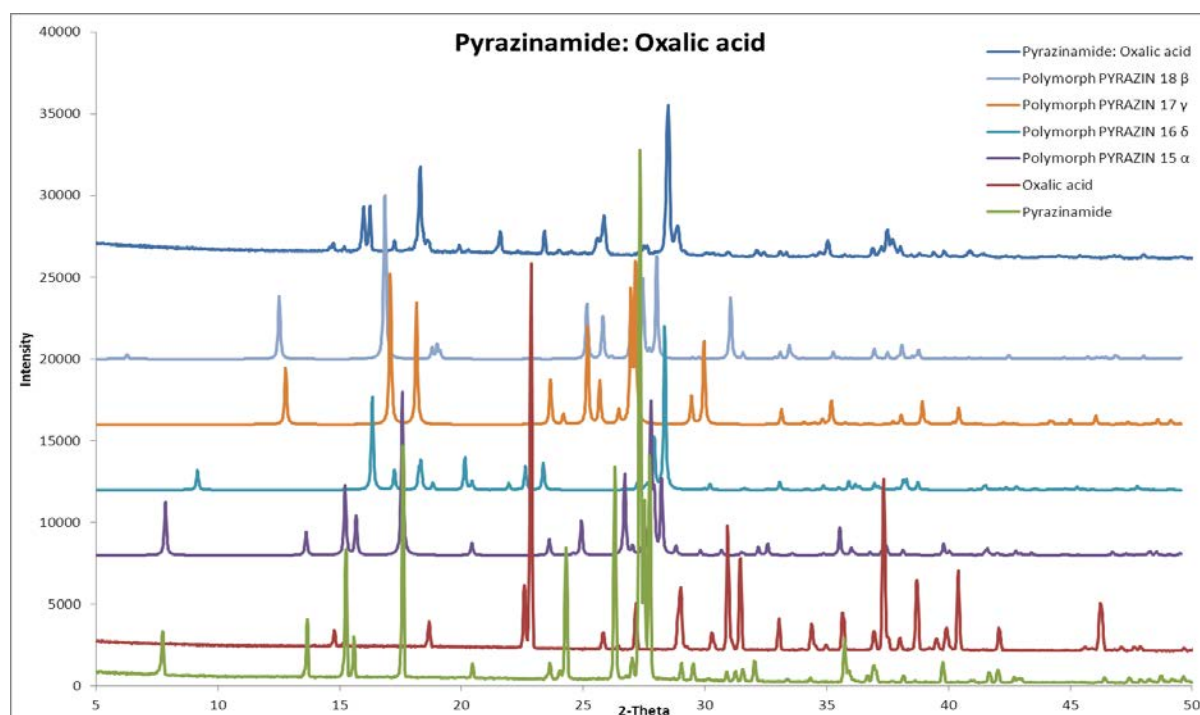
Figure 3.1: X-ray powder diffraction patterns of the product of pyrazinamide and oxalic acid crystallisation from methanol, the starting materials (pyrazinamide, oxalic acid), and common pyrazinamide polymorphs.

^{1}H NMR was unable to identify the presence of oxalic acid in the sample and hence characterisation of this product was not possible.

3.2 Pyrazinamide and oxamic acid

Pyrazinamide was crystallised with oxamic acid (as described in the solution-mediated synthesis method), with methanol used as solvent to dissolve the starting materials in a 1:1 stoichiometric ratio. The solvent evaporation crystallisation method was used for obtain the product which was a white solid. The X-ray powder diffraction pattern of the product formed was compared to the patterns of the starting materials and to a number of simulated patterns from previously published pyrazinamide polymorphs[76,83,97,98]. Figure 3.2 shows that the product formed is indeed a mixture of the oxamic acid starting material with polymorph $(\gamma(PYRAZIN17))$[83]
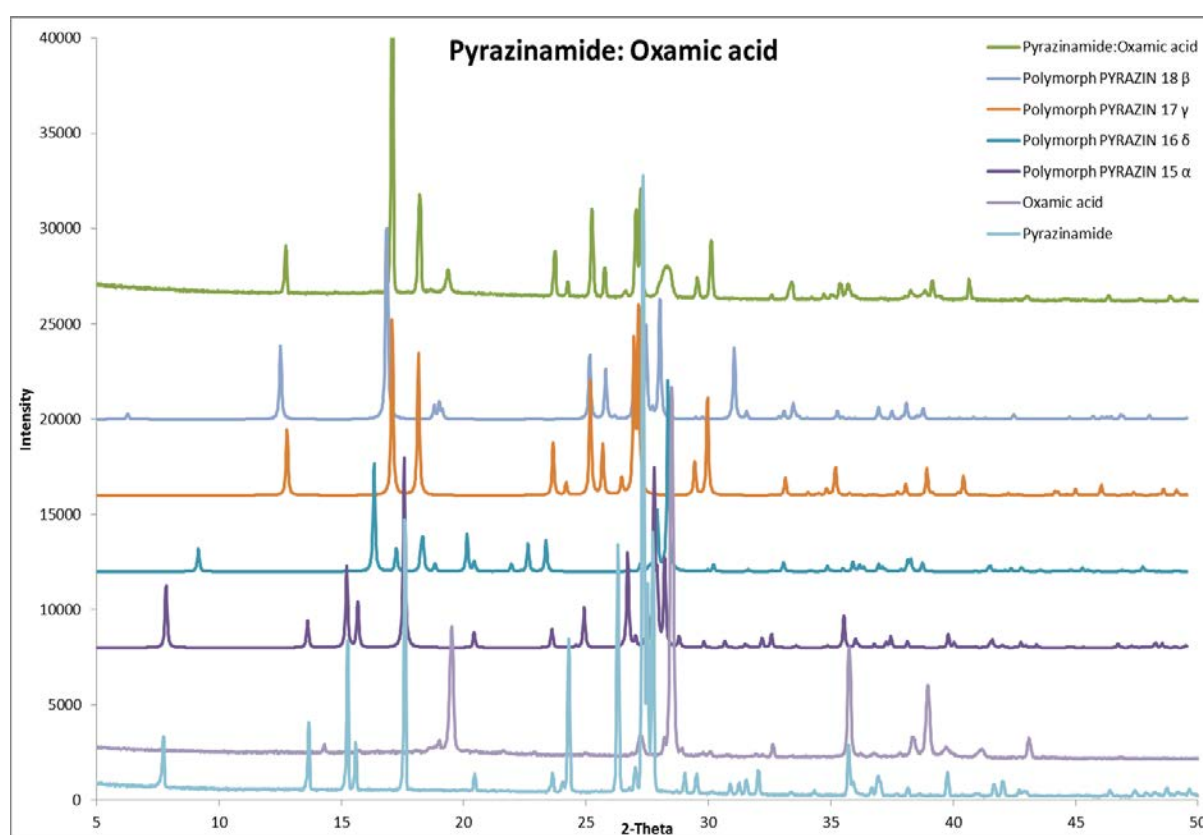
Figure 3.2: X-ray powder diffraction patterns of the product of pyrazinamide and oxamic acid crystallisation from methanol, the starting materials (pyrazinamide, oxamic acid) and common pyrazinamide polymorphs.

The ^{1}H NMR of this product showed the presence of both pyrazinamide and oxamic acid, confirming that the resultant solid was a mixture of the two components in an approximate ratio 1:1 pyrazinamide $(\gamma(PYRAZIN17))$[83] to oxamic acid (figure 3.3).
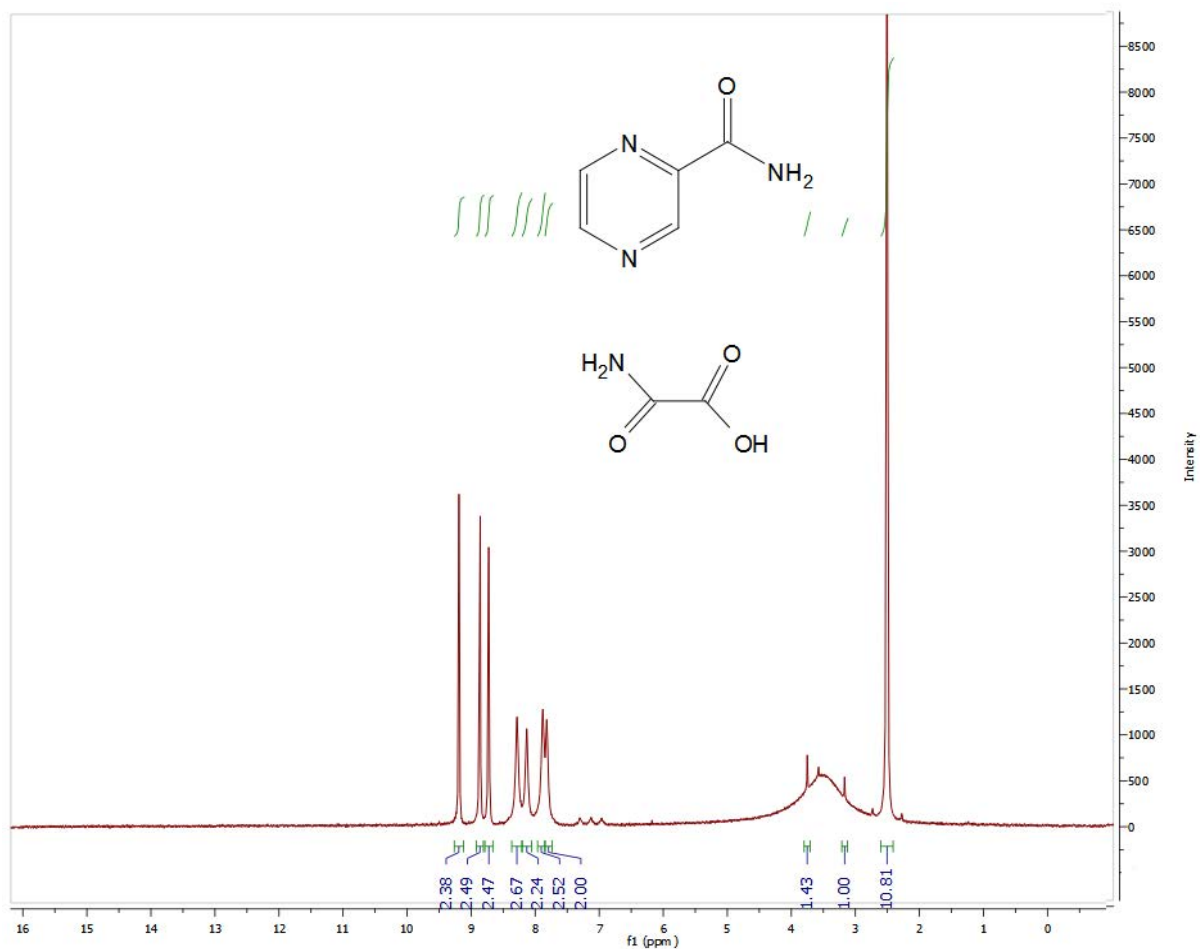
Figure 3.3: ^1H NMR of the product of pyrazinamide and oxamic acid (1:1) starting ratio using DMSO as a solvent. ^1H NMR 300MH$_z$ (DMS0-d$_6$): pyrazinamide 7.87 (1H, s), 8.29 (1H, s), 8.72 (1H, s), 8.86 (1H, s), 9.19 (1H, s): oxamic acid 7.81 (1H, s), 8.13(1H, s).

3.3 Pyrazinamide and malonic acid

Pyrazinamide was combined with malonic acid in a 1:1 stoichiometric ratio using methanol as the solvent of crystallisation. The solvent evaporation crystallisation method was used for cocrystal synthesis and resulted in a new material that formed as a white solid. The X-ray powder diffraction pattern of the product is different to that of the starting materials but was also compared to a number of patterns simulated from previously published pyrazinamide polymorphs[76,83,97,98]. It can be seen from figure 3.4 that the product may contain a mixture of the polymorphs (δ(PYRAZIN16) and γ(PYRAZIN17))[98,83]. The quality of new product was not suitable for single crystal X-ray diffraction analysis and further investigation was not carried out. As the product was clearly a mixture, it was also deemed not suitable for NMR. The cocrystal structure of pyrazinamide:malonic acid (1:1)[90] was published by another research group after this work had been carried out. The X-ray powder diffraction pattern of product formed was compared with the simulated pattern of the pyrazinamide: malonic acid that was published. The patterns displayed no match with the published structure and hence the cocrystallisation in this work was unsuccessful.
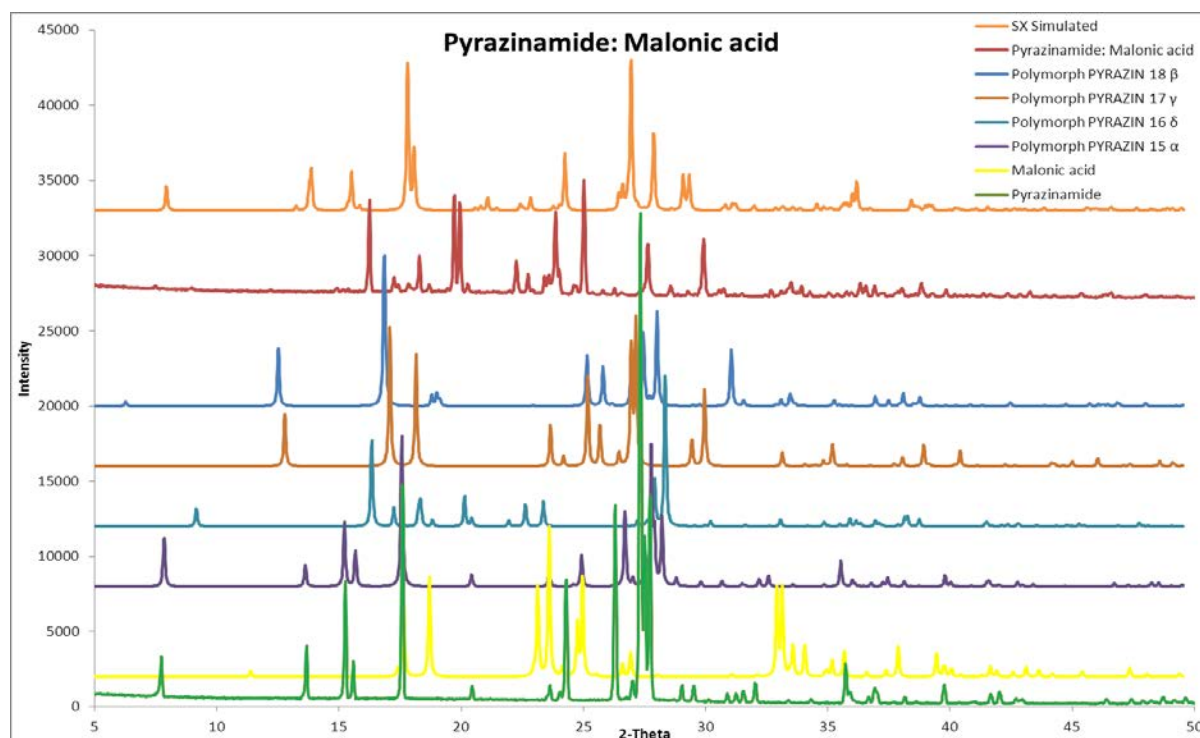
Figure 3.4: X-ray powder diffraction patterns of the product of pyrazinamide and malonic acid crystallisation from methanol, the starting materials (pyrazinamide, malonic acid), common pyrazinamide polymorphs and SX Simulated pattern of published structure of pyrazinamide and malonic acid.

3.4 **Pyrazinamide and maleic acid**

Pyrazinamide was crystallised with maleic acid, using methanol used as solvent in a 1:1 stoichiometric ratio. The product formed as a dark yellow solid using solvent evaporation method for synthesis. The X-ray powder diffraction pattern of the product formed was different to that of the starting materials confirming the formation of new material. The X-ray powder diffraction pattern of the product was also compared with a number of simulated patterns from previously published pyrazinamide polymorphs[76,83,97,98]. Figure 3.5 shows that the product contains some excess maleic acid (see peaks at 17º, 25º and 28º 2-theta) possibly mixed with polymorph (γ(PYRAZIN17))[83] but also with some new unknown product present.
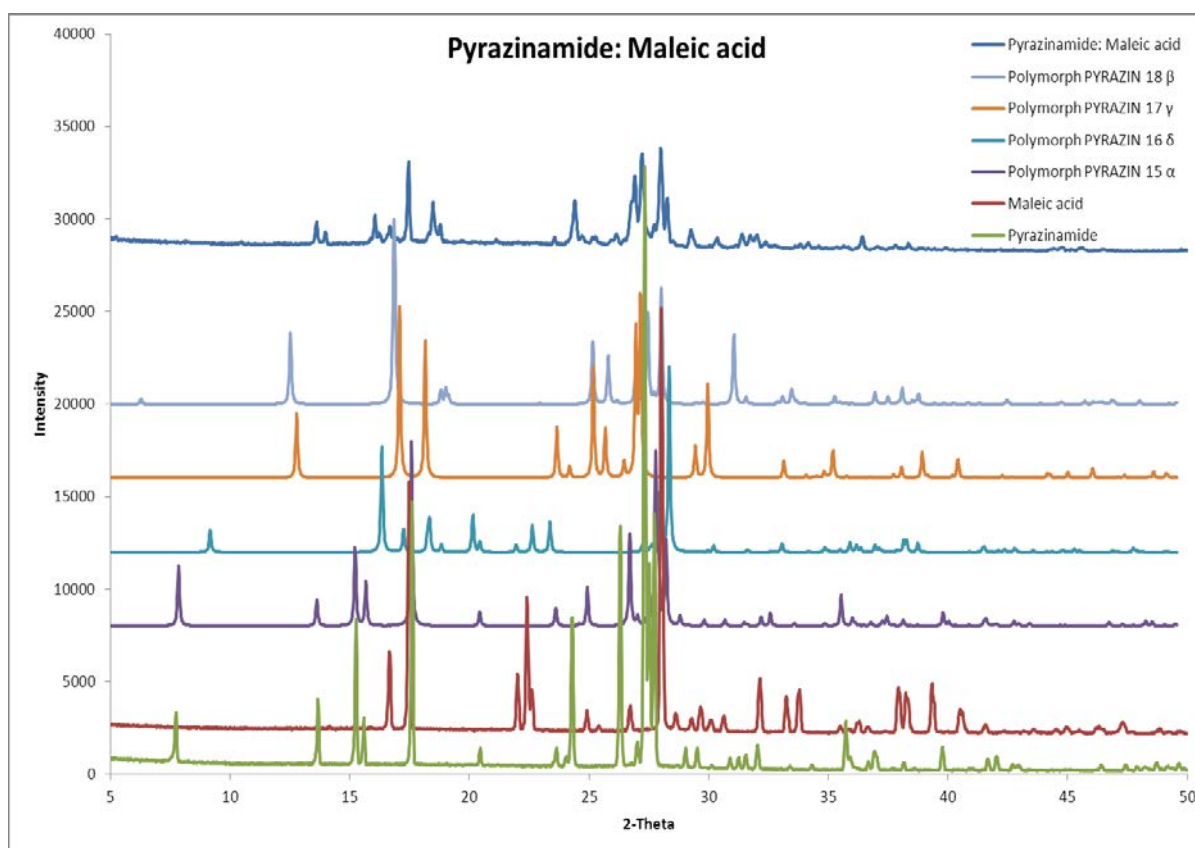
Figure 3.5: X-ray powder diffraction pattern of the product of pyrazinamide and maleic acid crystallisation from methanol, the starting materials (pyrazinamide, maleic acid) and common pyrazinamide polymorphs.

The ^{1}H MNR analysis (appendix a-1) showed a pyrazinamide:maleic acid stoichiometry of 1:1 but this is inconclusive as the product is clearly a mixture of a number of materials.

3.5 <u>Pyrazinamide and fumaric acid</u>

Pyrazinamide and fumaric acid were dissolved in methanol and the solutions combined for cocrystal synthesis as in previous experiments in a 1:1 stoichiometric ratio. The product formed was a white solid, obtained through the solvent evaporation method for crystallisation. The X-ray powder diffraction pattern of the product formed was compared with the starting materials and with the simulated powder pattern of the previously published of pyrazinamide:fumaric acid (2:1)[82] cocrystal structure. This confirmed that the product obtained was identical to the previously published pyrazinamide:fumaric acid cocrystal structure although the sample also contained a small excess of fumaric acid (see peaks at 24º, 26º and 29º 2-theta) (figure 3.6).

Figure 3.6: X-ray powder diffraction patterns of the products of pyrazinamide and fumaric aid crystallisation from methanol, the starting materials (pyrazinamide, fumaric acid), common pyrazinamide polymorphs and SX Simulated pattern of published structure of pyrazinamide and fumaric acid.

Analysis of the ^{1}H NMR showed a pyrazinamide:fumaric acid proportion of 1:1; however this is not agreement with the PXRD result in which a 2:1 stoichiometry is confirmed. This anomaly may however be explained by the presence of excess fumaric acid in the product

that may by coincidence increase the NMR ratio0 of the components from 2:1 to 1:1 (figure 3.7).

Figure 3.7: ^1H NMR of the product of pyrazinamide and fumaric acid (1:1) starting ratio using DMSO as a solvent. ^1H NMR 300MH$_z$ (DMS0-d$_6$): pyrazinamide 7.83 (1H, s), 8.29 (1H, s), 8.72 (1H, t), 8.90 (1H, d), 9.19 (1H, d): fumaric acid 6.65 (2H, s).

3.6 <u>Pyrazinamide and succinic acid</u>

Pyrazinamide and succinic acid were dissolved separately in methanol for crystallisation, the solutions combined in a 1:1 stoichiometric ratio and the solvent allowed to evaporate. The product was a white solid crystalline material obtained through the solvent evaporation crystallisation method. The X-ray powder diffraction pattern of the product formed was compared with starting materials and with the simulated powder pattern of previously published of pyrazinamide:succinic acid cocrystal structures (2:1)[90]. This confirmed that the product formed was mixture and showed no match with the simulated powder pattern of previously published of pyrazinamide:succinic acid cocrystal and the product also contain an excess of succinic acid (figure 3.8).
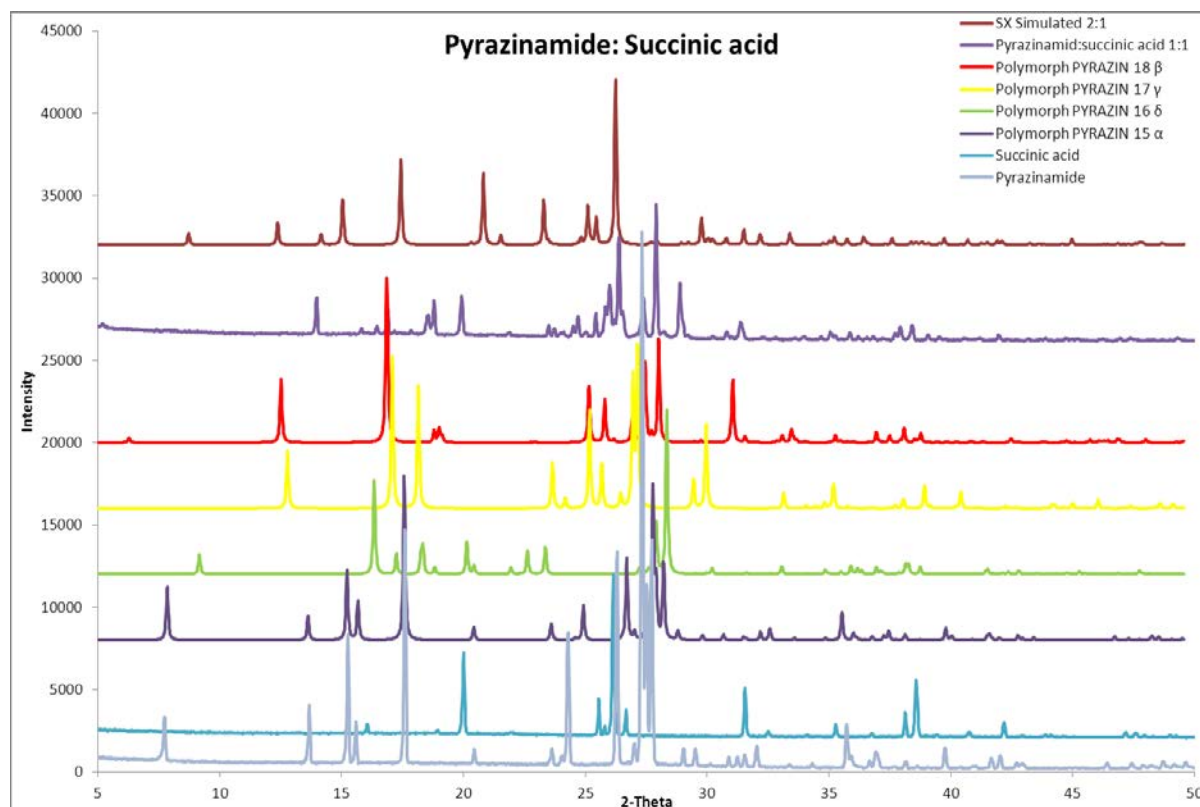
Figure 3.8: X-ray powder diffraction patterns of the products of pyrazinamide and succinic aid crystallisation from methanol, the starting materials (pyrazinamide, succinic acid), common pyrazinamide polymorphs and SX Simulated pattern of published structure of pyrazinamide and succinic acid.

Analysis of the ^{1}H NMR showed a pyrazinamide:succinic acid proportion of 3:2 confirming that the resultant solid was a mixture of the two components (figure 3.9).
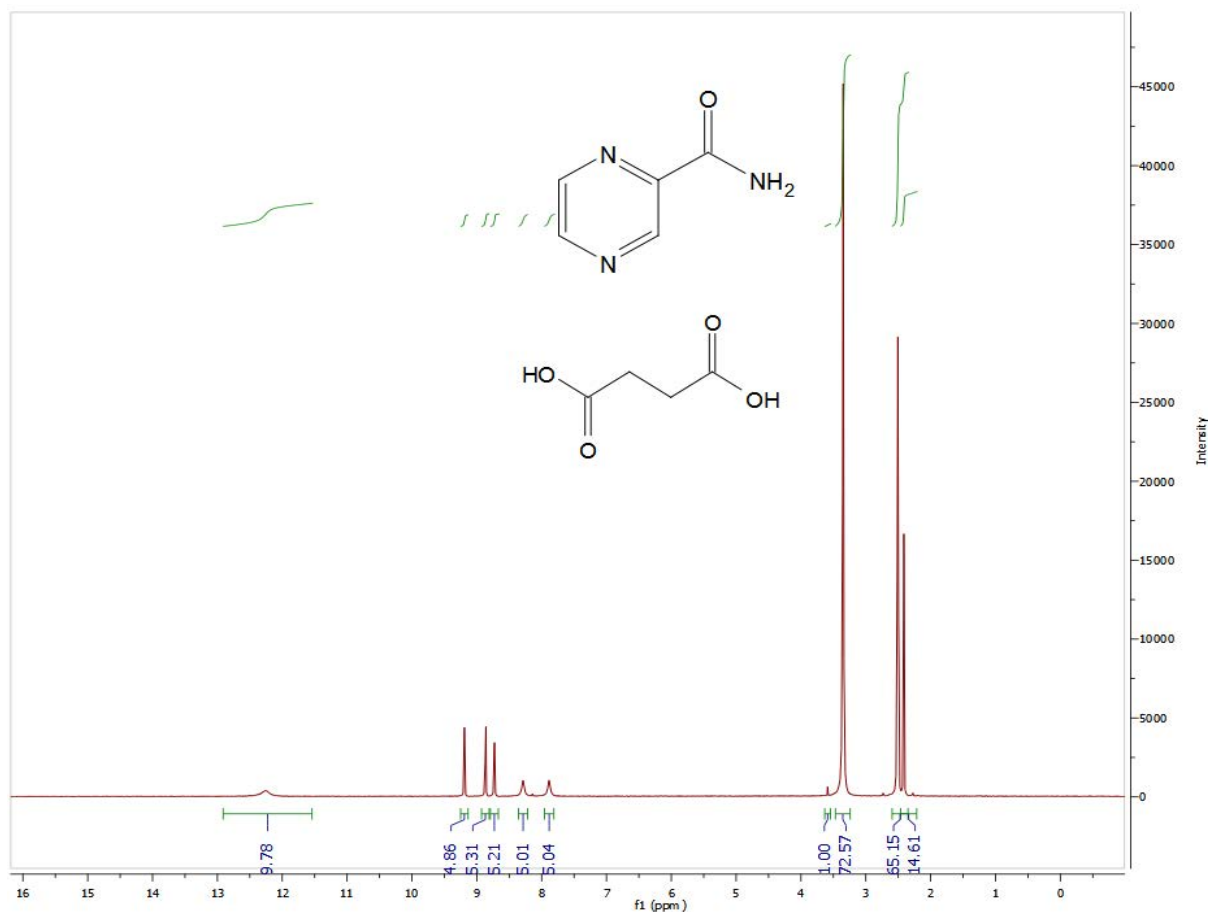
Figure 3.9: ^{1}H NMR of the product of pyrazinamide and succinic acid (1:1) starting ratio using DMSO as a solvent. ^{1}H NMR 300MH$_z$ (DMS0-d$_6$): pyrazinamide 7.83 (1H, s), 8.29 (1H, s), 8.72 (1H, t), 8.90 (1H, d), 9.19 (1H, d):succinic acid 2.40 (3H, s).

3.7 <u>Pyrazinamide and glutaric acid</u>

Pyrazinamide and glutaric acid were dissolved in methanol in the solution combined in a 1:1 stoichiometric ratio and the solvent allowed to evaporate for crystallisation. The product was a white solid. The X-ray powder diffraction pattern of this product was different to that of the starting materials confirming the formation of a new material. The powder diffraction pattern of the product was also compared to a number of simulated patterns from previously published pyrazinamide polymorphs[76,83,97,98]. It can be seen from figure 3.10 that the product does not contain any trace of either of the starting materials but is mixed with a negligible amount of polymorph (γ(PYRAZIN17))[83].
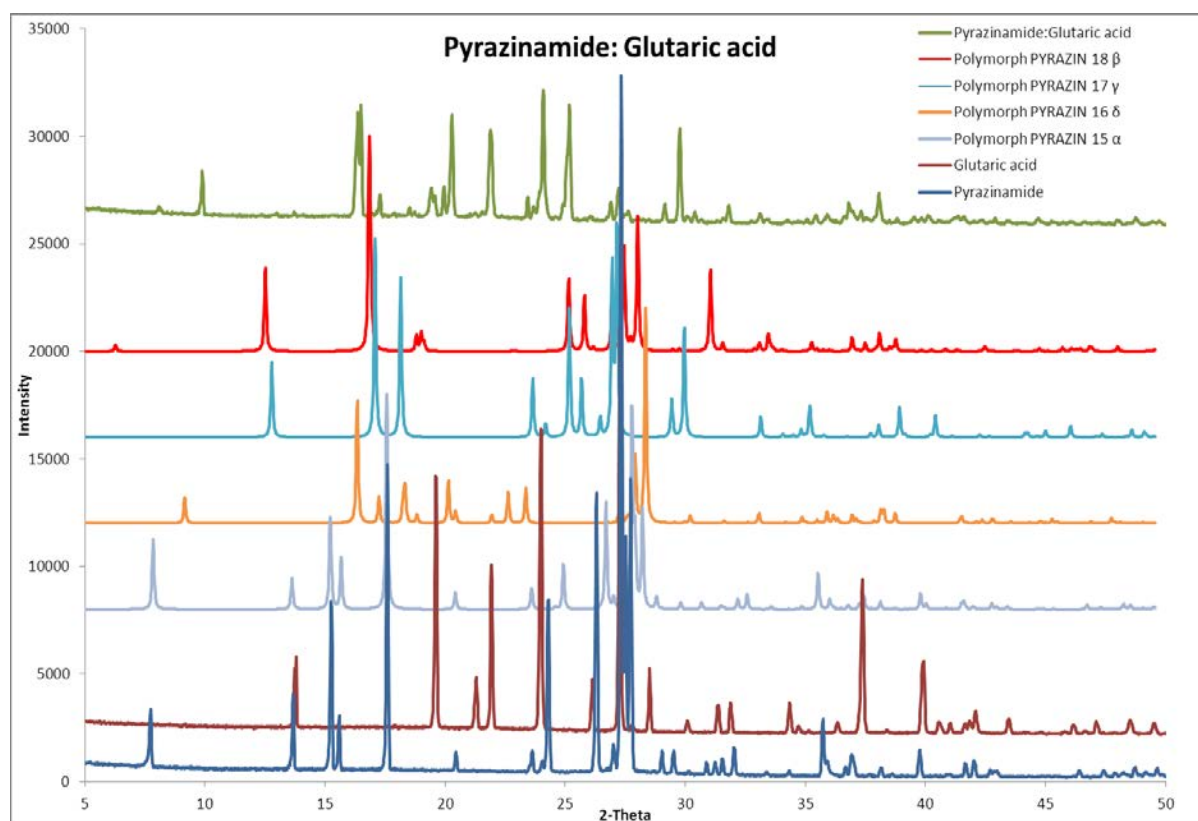
Figure 3.10: X-ray powder diffraction patterns of the product of pyrazinamide and glutaric acid crystallisation form methanol, the starting materials (pyrazinamide, glutaric acid), and common pyrazinamide polymorphs.

^{1}H NMR indicated that the new material prepared from crystallisation of a 1:1 stoichiometric starting ratio also contains the molecular coformers in a 1:1 stoichiometric ratio (figure 3.11).
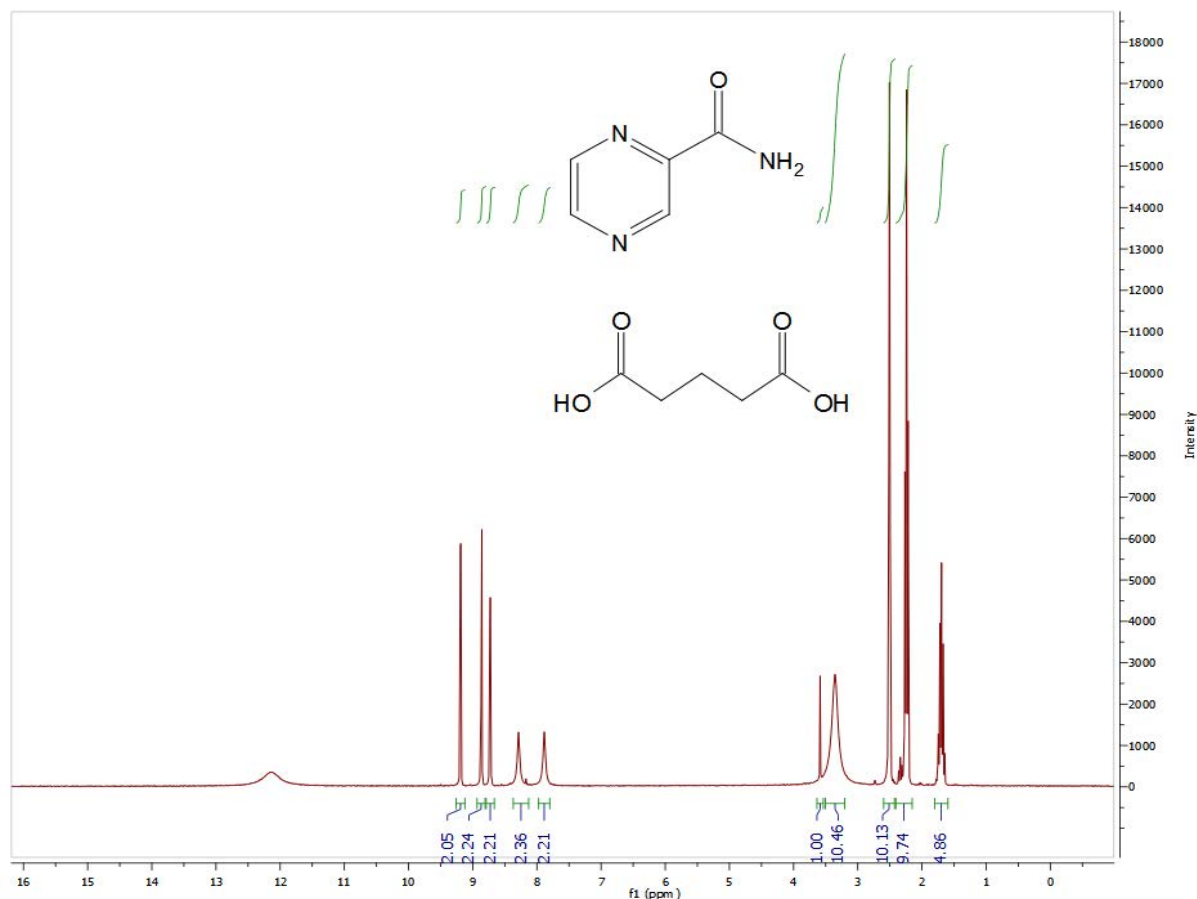
Figure 3.11: ^{1}H NMR of the product of pyrazinamide and glutaric acid (1:1) starting ratio using DMSO as a solvent. ^{1}H NMR 300MH$_z$ (DMS0-d$_6$): pyrazinamide 7.83 (1H, s), 8.29 (1H, s), 8.72 (1H, t), 8.92(1H, d), 9.19(1H, d) : glutaric acid 1.71 (2H, t), 2.26 (4H, q).

3.7.1 Crystal structure determination from single crystal X-ray diffraction data

Once the bulk product was identified as a new solid material with a 1:1 ratio of components, the sample was submitted for single crystal analysis. This crystal structure determination confirmed that the stoichiometric ratio of the pyrazinamide and glutaric acid adduct was indeed 1:1 and that a neutral cocrystal of pyrazinamide:glutaric acid had been formed (no proton transfer had taken place between the components). Further crystallographic details of this structure determination are given in Table 3.3.

Figure 3.12 shows the asymmetric unit of this cocrystal structure containing one glutaric acid molecule and one pyrazinamide molecule linked through two hydrogen bonds. The atom labelling used for subsequent discussion is also shown in the figure.

Table 3.3. Crystal data and structure refinement of pyrazinamide:glutaric acid 1:1.

Identification code	Pyrazinamide_Glutaric Acid	
Empirical formula	$(C_5H_5N_3O)$, (C5H8O4)	
Formula weight	255.23	
Temperature	100.00(10) K	
Wavelength	1.5418 Å	
Crystal system	Monoclinic	
Space group	$P2_1/c$	
Unit cell dimensions	a = 11.3844(9) Å	α= 90.00 °.
	b = 4.8251(7) Å	β= 104.610(9)°.
	c = 21.9011(16) Å	γ = 90.00 °.
Volume	1164.1(2) $Å^3$	
Z	4	
Density (calculated)	1.456 Mg/m^3	
Absorption coefficient	1.012 mm^{-1}	
F(000)	536.0	
Crystal size	0.15 x 0.1 x 0.03 mm^3	
Theta range for data collection	12.98 to 133.16°.	
Index ranges	-13 ≤ h ≤ 13, -5 ≤ k ≤ 5, -22 ≤ l ≤ 26	
Reflections collected	3397	
Independent reflections	3397 [R(int) = 0.0000, R(sigma) = 0.0256]	
Completeness to theta = 67.684°	99.0 %	
Absorption correction	Semi-empirical from equivalents	
Max. and min. transmission	0.970 and 0.859	
Refinement method	Full-matrix least-squares on F^2	
Data / restraints / parameters	3397 / 0 / 166	
Goodness-of-fit on F^2	1.049	
Final R indices [I>2sigma(I)]	R_1 = 0.0397, wR_2 = 0.1037	
R indices (all data)	R_1 = 0.0491, wR_2 = 0.1076	
Extinction coefficient	n/a	
Largest diff. peak and hole	0.18 and -0.022 $e.Å^{-3}$	

Notes: The crystal was a non-merohedral twin with the domains related by 180 degrees about the direct axis [0 0 1] and the refined percentage domain ratio being 64:36.
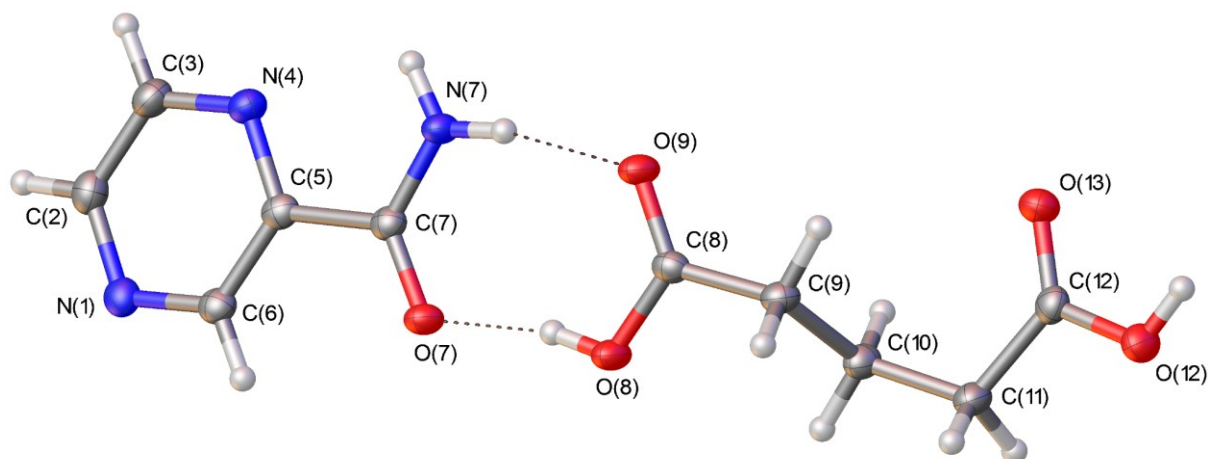
Figure 3.12: The asymmetric unit in the crystal structure of pyrazinamide:glutaric acid (1:1) showing the atom numbering scheme and the strong hydrogen bonds between the two molecular components. Hydrogen bonds are shown as dotted lines.

The basic supramolecular structure motif within the asymmetric unit (figure 3.12) is formed by the pyrazinamide molecule linked to a glutaric acid molecule through two strong hydrogen bonds; N-H⋯O=C in which the amide nitrogen N(7) acts as a donor via H(7A) to the carboxyl oxygen O(9), and O-H⋯O=C in which O(8) acts as a donor via H(8) to the amide oxygen O(7) as acceptor table 2.These combine to form a $R_2^2(8)$ hydrogen bond ring (table 3.4).

The formation of an intramolecular N-H⋯N hydrogen bond within the pyrazinamide molecule in which the amide nitrogen N(7) acts as a donor via H(7B) to N(4) further stabilizes the conformation of the pyrazinamide within the asymmetric unit this intramolecular interaction is not shown in Figure 3.12.

The asymmetric units are linked together into an infinite chain by two further hydrogen bonds; a strong acid-pyridine interaction O-H⋯N in which O(12) acts as a donor via H(12) to the pyridine nitrogen N(1) and a weak C-H⋯O=C interaction in which C(2) in the pyrazinamide acts as a donor via H(2) to the oxygen O(13) in the glutaric acid. Together these hydrogen bonds form a $R_2^2(7)$ ring such that a supramolecular chain of alternating $R_2^2(7)$ and $R_2^2(8)$ rings are generated through alternating acid-amide and acid-pyridine motifs (figure 3.13).

Table 3.4: Intermolecular and intramolecular hydrogen bond distances (Å) and angles (°) within the pyrazinamide:glutaric acid (1:1) cocrystal.

D-H-A	d(D-H)	d(H⋯A)	d(D⋯A)	<(DHA)
N(7)-H(7A)⋯O(9)	0.88	1.98	2.849(16)	168
N(7)-H(7B)⋯N(4)	0.88	2.32	2.701(2)	105
N(7)-H(7B)⋯O(9)^i	0.88	2.17	2.851(16)	133
O(8)-H(8)⋯O(7)	0.84	1.79	2.616(15)	166
O(12)-H(12)⋯N(1)^{ii}	0.84	1.88	2.727(16)	178
C(2)-H(2)⋯O(13)^i	0.95	2.58	3.252(2)	127
C(3)-H(3)⋯O(13)^{iii}	0.94	2.97	3.571(2)	122
C(9)-H(9A)⋯O(8)^i	0.99	2.55	3.382	141
C(11)-H(11A)⋯O(7)^i	0.98	2.825	3.214	104

Symmetry code: i) 1-x,2-y, (ii) x-1,-y, z-1/2; (iii) x+1,-y, z+1/2
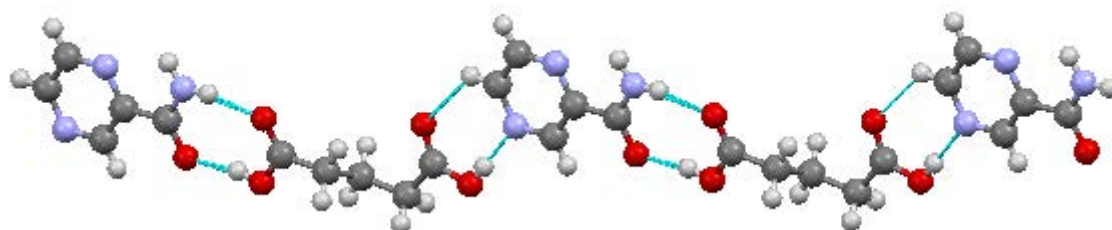
Figure 3.13: A view of the pyrazinamide:glutaric acid (1:1) cocrystal structure showing the alternating acid-amide and acid-pyridine rings in the chain. Hydrogen bonds are shown as thin light blue lines.

Within each of these chains the pyrazinamide molecules adopt the same orientation and face the same direction. These hydrogen bonded chains are then cross-linked to a neighbouring parallel chain via an additional N-H⋯O=C intermolecular hydrogen bond donated by N(7) through H(7B) to O(9) of a glutaric acid on the neighbouring chain. This complementary hydrogen bond interaction results in the formation of an $R_4^2(8)$ ring between the chains which run in opposite but parallel directions (figure 3.14). This is reinforced by a weak hydrogen bond intermolecular hydrogen bond C(3)-H(3)⋯O(13) in which H(3) on the pyrazinamide ring is donated by C(3) to O(13) of the glutaric acid (table 3.4).

Figure 3.14: A view of the pyrazinamide:glutaric acid cocrystal structure (1:1) showing the intermolecular hydrogen bonds between opposing chains.

Each of these ribbons is linked to another by two weak C-H$\cdots$O hydrogen bonds in which C(9) in the glutaric acid molecule acts as a donor via H(9A) to the oxygen O(8) as acceptor in the neighbouring glutaric acid molecule, and secondly in which C(11) in the glutaric acid molecule acts as a donor via H(11A) to the pyrazinamide oxygen O(7) (figure 3.15). All strong hydrogen bonding donor and acceptor sites in both molecules are involved in the hydrogen-bonded network in this structure.
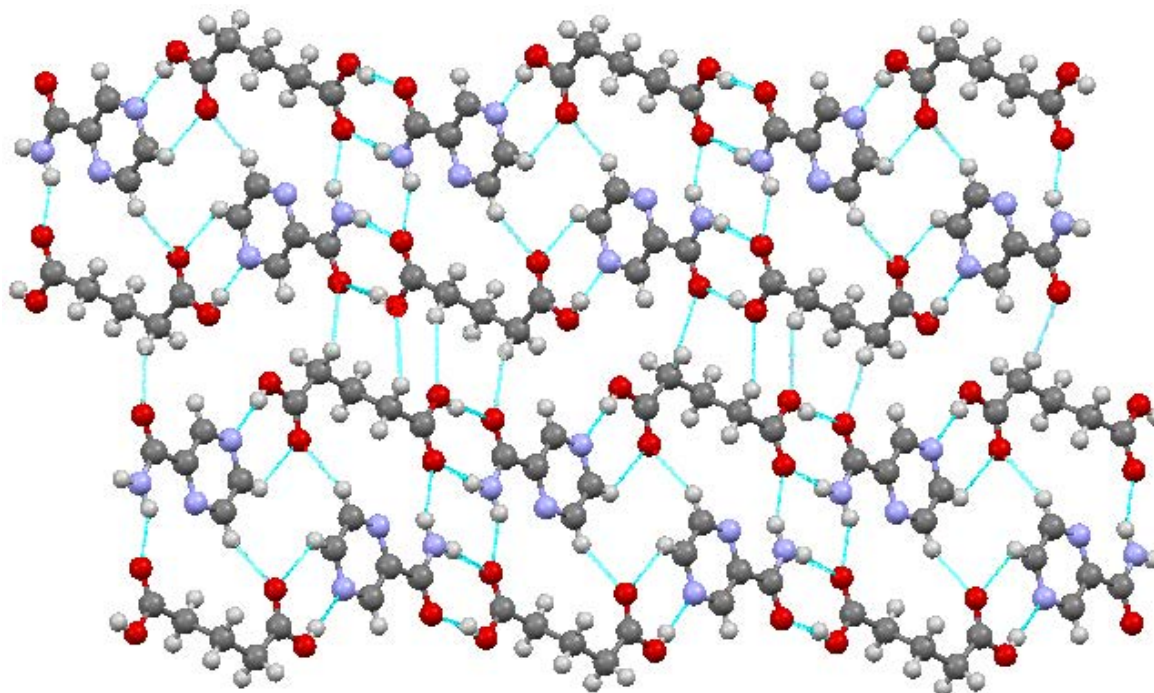
Figure 3.15: Diagram of the pyrazinamide:glutaric acid cocrystal structure (1:1) showing the combination of ribbons linked by C-H$\cdots$O interactions to form an infinite sheet.

Table 3.5 gives information regarding the geometry within the pyrazinamide:glutaric acid molecules. In the pyrazinamide, the bond lengths of C(7)-N(7) and C(7)-O(7) are 1.3192(19)

and 1.488(17) respectively and confirm the orientation of the amide group . In the acid, the bond lengths of C(8)-O(8) and C(8)-O(9) are 1.3221(17) and 1.2227(18); C(12)-O(12) and C(12)-O(13) are 1.3291(18) and 1.214(18) respectively, showing a clear distinction between the C=O and C-O(H) components of the carboxylic acid functional group, hence confirming that there is no proton transfer between the neutral components in this cocrystal structure.

The torsion angles within the pyrazinamide molecule N(4)-C(5)-C(7)-N(7) and C(6)-C(5)-C(7)-N(7) are 2.13(2) and -177.63(13) respectively and show a slight deviation from planarity. The molecule is partially stabilized in this conformation by the intramolecular N-H⋯N which would result a planner conformation, but other intermolecular interactions also effect this geometry and causes slight distortion.

The conformation of the glutaric acid is however far from expected. There is only one of the backbone angles C(8)-C(9)-C(10)-C(11) that is close to planar. All others, including the relationship between the carbon backbone and the carboxylic acid groups is significantly distorted. The result is that the angle between the planes of the two carboxylic groups is -71.04(17) and 153.15(12)°. The orientation of the protonated oxygen on both ends is the same and the molecule then acts as a 'bent' molecule linker in the cocrystal structure. This type of unconventional conformation is not unusual for diacids with odd chain length.

Table 3.5: Selected intramolecular bond lengths and torsion angles within the pyrazinamide: glutaric acid (1:1) cocrystal.

Pyrazinamide Bond Lengths	(Å)	Acid Bond Lengths	(Å)
C(7)-N(7)	1.3192(19)	C(8)-O(8)	1.3221(17)
C(7)-O(7)	1.2488(17)	C(8)-O(9)	1.2227(18)
		C(12)-O(12)	1.3291(18)
		C(12)-O(13)	1.214(18)
Pyrazinamide Torsion Angles	(°)	Acid Torsion Angles	(°)
N(4)-C(5)-C(7)-N(7)	2.13(2)	C(8)-C(9)-C(10)-C(11)	-177.22(12)
N(4)-C(5)-C(7)-O(7)	-178.54(13)	C(9)-C(10)-C(11)-C(12)	-68.44(17)
C(6)-C(5)-C(7)-O(7)	1.70(2)	C(10)-C(11)-C(12)-O(12)	173.80(12)
C(6)-C(5)-C(7)-N(7)	-177.63(13)	O(8)-C(8)-C(9)-C(10)	61.34(16)
		O(8)-C(8)-C(12)-O(12)	-71.04(17)
		O(8)-C(8)-C(12)-O(13)	153.15(12)
		O(9)-C(8)-C(9)-C(10)	-117.84(16)

The synthesis of this pyrazinamide:glutaric acid adduct was also attempted using different methods of synthesis and the resulting X-ray powder diffraction patterns were compared with each other. The X-ray powder data of the material obtained from solvent evaporation matches that of the material obtained through solvent drop grinding with both of these patterns matching that of the simulated powder diffraction pattern from the single crystal structure of pyrazinamide:glutaric acid (1:1) (figure 3.16). Please note that the crystal structure in this work was determined at low temperature (100 k) and hence some peak positions will be shifted.

Following the completion of this work and determination of the pyrazinamide:glutaric acid (1:1) cocrystal structure reported here, a paper was published in the literature by Luo et al[90]. also reporting this crystal structure. It can be seen from Figure 3.16 that the powder diffraction pattern matches the structure in this work. (the differences in peak positions arise from the Luo et al. structure being determined at 293 k.)
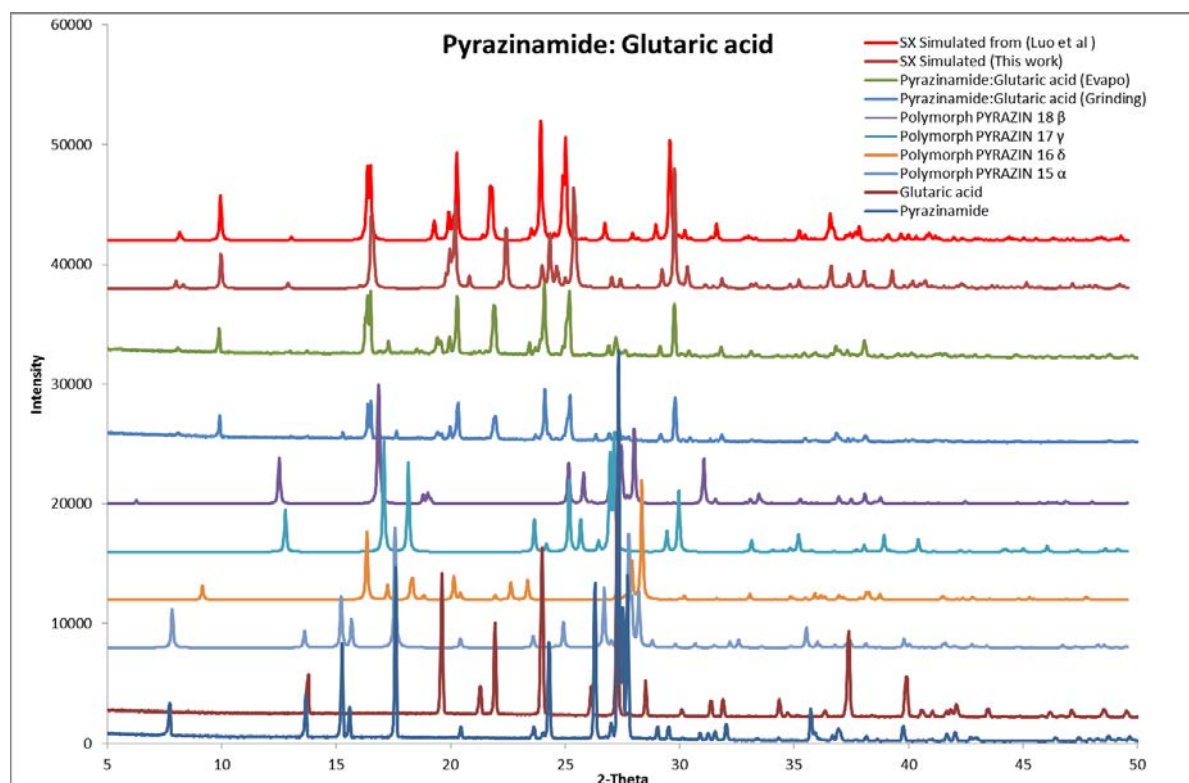
Figure 3.16: X-ray powder diffraction patterns of products obtained through different methods of synthesis and the simulated powder diffraction patterns from the single crystal structure of the pyrazinamide:glutaric acid (1:1) cocrystal. From both this work and published structure.(Luo et al.)[90]

3.8 Pyrazinamide and adipic acid

Pyrazinamide was combined with adipic acid using methanol as a solvent to dissolve the starting materials in a 1:1 stoichiometric molar ratio. The solvent evaporation method was used for crystallisation and the new material formed as a white crystalline solid. The powder diffraction pattern of the product was compared with that of the starting materials and patterns simulated from previously published pyrazinamide polymorphs[76,83,97,98]. The X-ray powder diffraction pattern of the product material confirms the formation of a new material (figure 3.17) but the sample may also contains an excess of adipic acid starting material (see peaks at 21º, 25º and 31º 2-theta) and there may be some pyrazinamide polymorph (β (PYRAZIN18))[76] present.
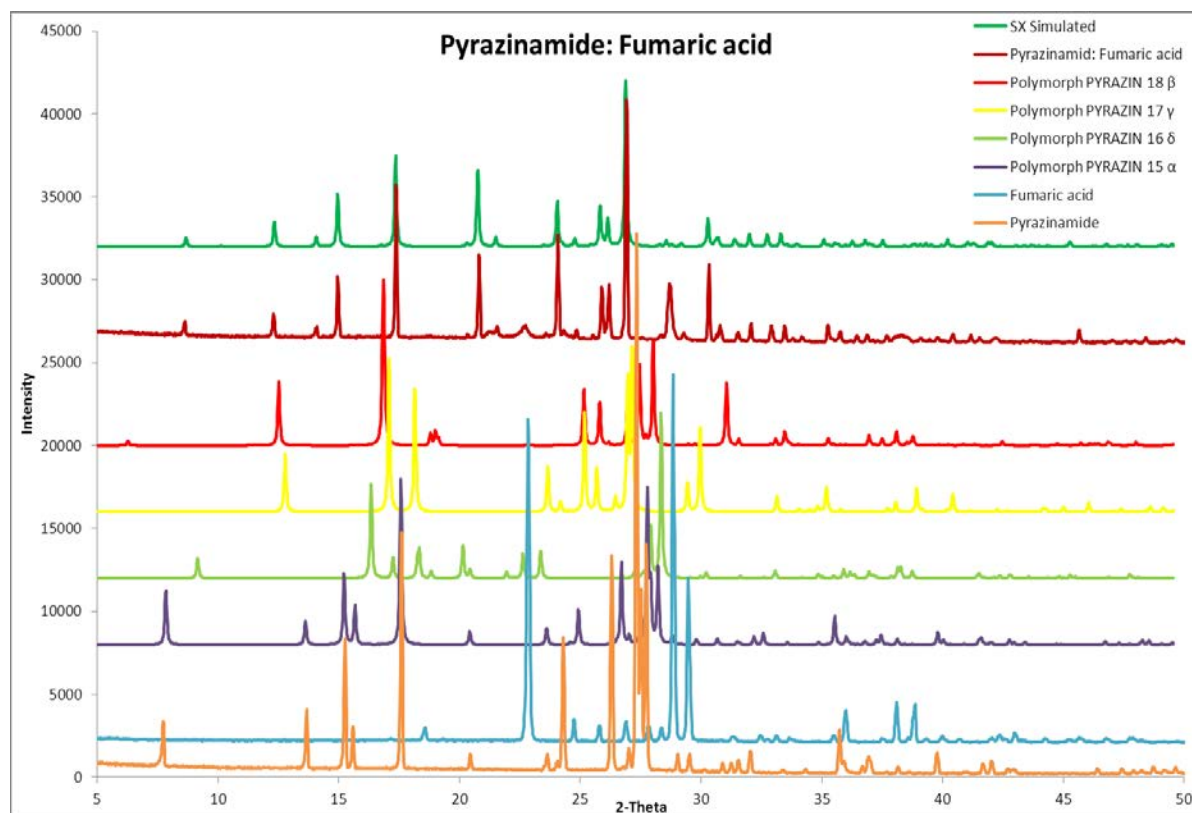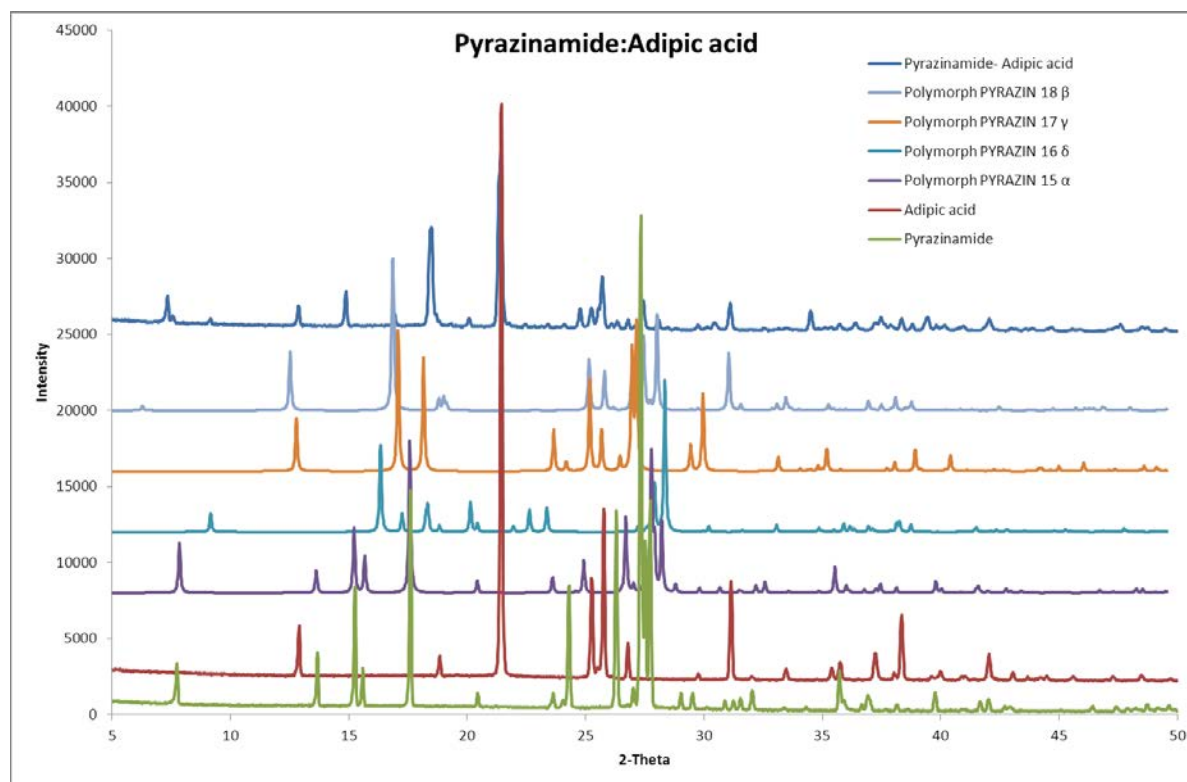

Figure 3.17: X-ray powder diffraction patterns of the product of pyrazinamide and adipic acid crystallisation from methanol, the starting materials (pyrazinamide and adipic acid) and common pyrazinamide polymorphs.

From the powder diffraction data, the bulk material formed is clearly a mixture. ^{1}H NMR of the product formed by crystallisation of 1:1 starting materials shows a resulting 2:3 stoichiometric ratio of pyrazinamide and adipic acid (figure 3.18).
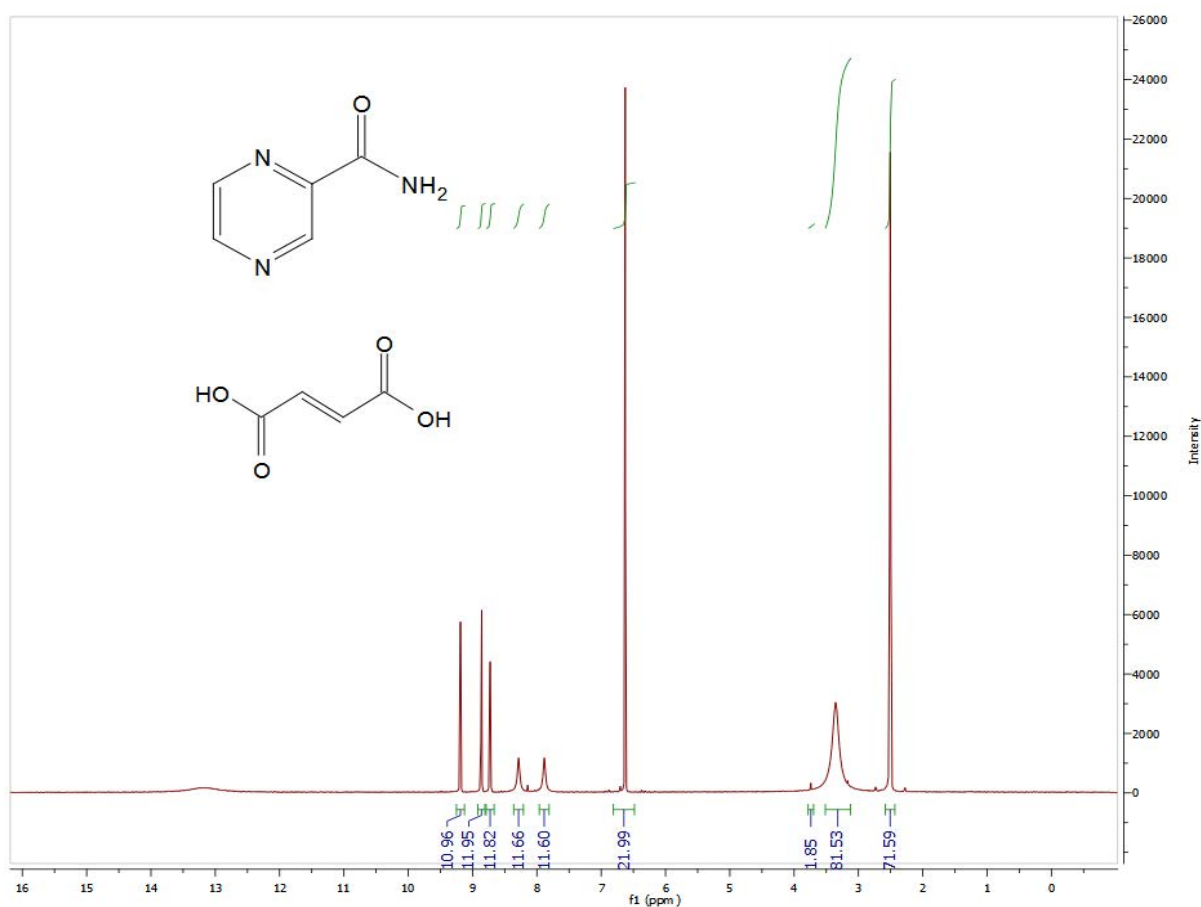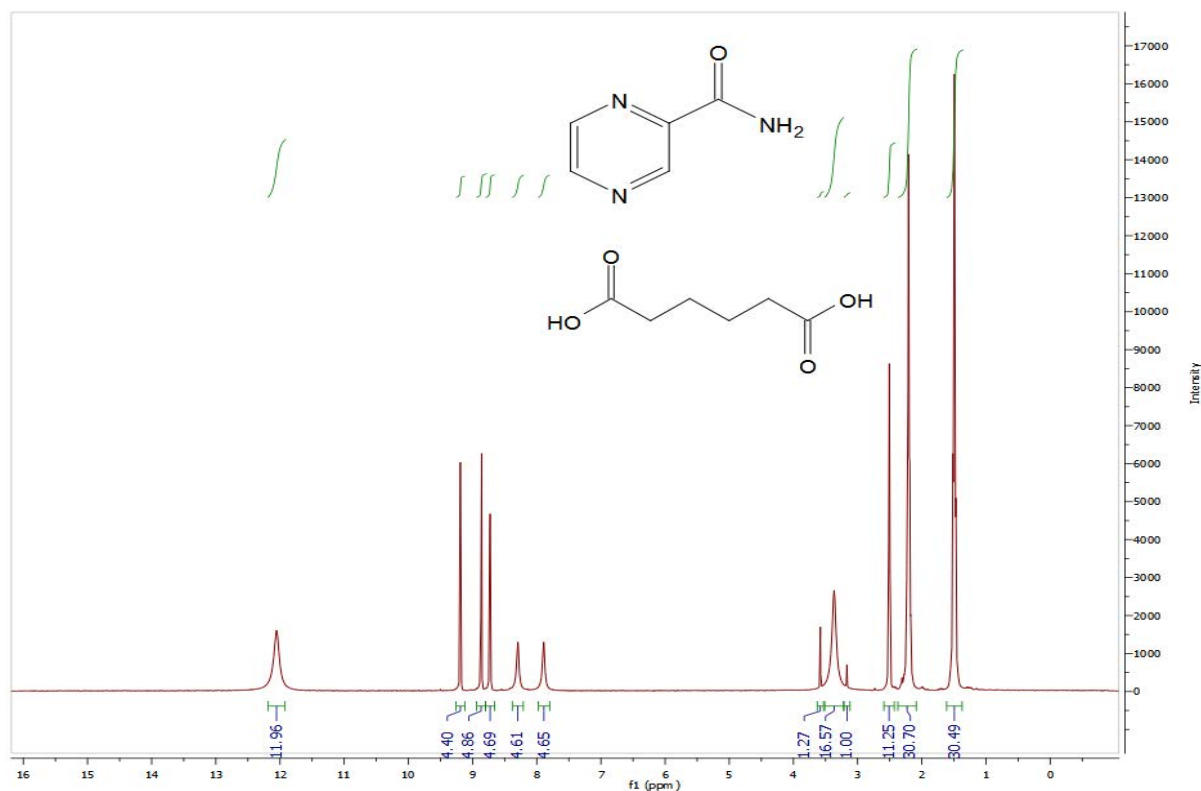
Figure 3.18: ^{1}H NMR of the product of pyrazinamide and adipic acid (1:1) starting ratio using DMSO as a solvent. ^{1}H NMR 300MHz (DMS0-d6): pyrazinamide 7.83 (1H ,s), 8.29 (1H, s), 8.72 (1H, t), 8.92(1H, d), 9.19(1H, d) : adipic acid 1.51(6H, q), 2.22(6H, t), 12.08 (2H, s).

3.8.1 Crystal structure determination from single crystal X-ray diffraction data

A small amount of the product was submitted for single crystal analysis and the crystal structure of a new pyrazinamide: adipic acid cocrystal was determined. The stoichiometric ratio of the pyrazinamide:adipic acid adduct was found to differ significantly from the NMR result above. This crystal structure determination confirmed that the ratio of the conformers within the adduct was indeed 4:1 pyrazinamide: adipic acid. This contradiction between the two techniques is to be expected as PXRD showed the presence of adipic acid in the mixed bulk material hence significantly increasing the proportion of adipc acid with respect to the pure cocrystal structure identified by single crystal diffraction. This crystal structure also confirmed that a neutral cocrystal of pyrazinamide: adipic acid had been formed and that no proton transfer had taken place between the two molecular components. The crystallographic details of this structure are given in Table 3.6.

Table 3.6. Crystal data and structure refinement of pyrazinamide:adipic Acid 4:1.

Identification code	Pyrazinamide_AdipicAcid
Empirical formula	$4(C_5H_5N_3O)$, $C_6H_{10}O_4$
Formula weight	638.62
Temperature	100.00(10) K
Wavelength	1.5418 Å
Crystal system	Triclinic
Space group	P -1
Unit cell dimensions	a = 5.1814(8) Å α= 74.708(11)°.
	b = 11.7163(16) Å β= 87.314(11)°.
	c = 12.2250(14) Å γ = 85.212(12)°.
Volume	713.13(17) Å^3
Z	1
Density (calculated)	1.487 Mg/m^3
Absorption coefficient	0.963 mm^{-1}
F(000)	334
Crystal size	0.200 x 0.090 x 0.060 mm^3
Theta range for data collection	7.516 to 70.053°.
Index ranges	-6<=h<=5, -13<=k<=14, -14<=l<=10
Reflections collected	4178
Independent reflections	2666 [R(int) = 0.0348]
Completeness to theta = 67.684°	99.0 %
Absorption correction	Semi-empirical from equivalents
Max. and min. transmission	0.9445 and 0.8308
Refinement method	Full-matrix least-squares on F^2
Data / restraints / parameters	2666 / 0 / 223
Goodness-of-fit on F^2	1.050
Final R indices [I>2sigma(I)]	R_1 = 0.0623, wR_2 = 0.1642
R indices (all data)	R_1 = 0.0731, wR_2 = 0.1780
Extinction coefficient	n/a
Largest diff. peak and hole	0.353 and -0.368 e.Å^{-3}

Notes: There are four pyrazinamide molecules for every acid. The acid is located on an inversion centre such that only half the molecule is crystallographically unique. The hydrogen atoms bonded to N(7A), N(7B) and O(8) were located in the electron density and their positions refined. The remaining hydrogen atoms were fixed as riding models. The U_{iso} of all hydrogen atoms are based on U_{eq} or the parent atoms.

Figure 3.19 shows the atom labelling and the hydrogen bonds present in the asymmetric unit of this cocrystal structure. It contains two pyrazinamide molecules to one half adipic acid molecule linked through hydrogen bonds.
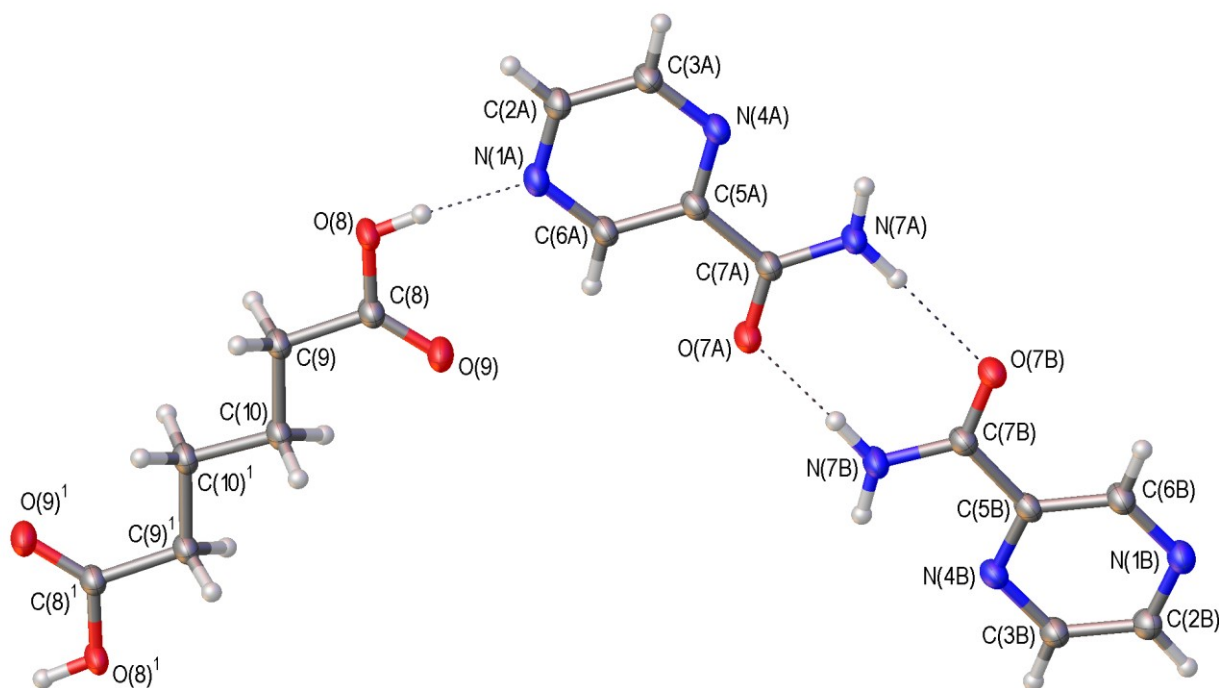
Figure 3.19: The asymmetric unit in the crystal structure of pyrazinamide:adipic acid (4:1) showing the atom numbering scheme. Strong hydrogen bonds are shown as dotted lines. Atom labels with superscript denote the crystallographically equivalent half adipic acid molecule. Atom labels 'A' and 'B' denote the two crystallographically inequivalent pyrazinamide molecules.

The basic supramolecular structure motif within the asymmetric unit (Figure 3.19) is formed by two pyrazinamide molecules and one half adipic acid molecule that is located on an inversion centre to create the complete molecule. There is a strong acid-pyridine interaction O-H···N in which O(8) in the adipic acid acts as a donor via H(8) to the pyridine nitrogen N(1) in the pyrazinamide molecule, this is reinforced by a weak hydrogen bond C-H···O in which C(6A) in pyrazinamide acts as donor via H(6A) to O(9) in adipic acid. These combine to form a $R_2^2(7)$ hydrogen bond ring. The two pyrazinamide molecules are linked to each other through complementary strong hydrogen bonds N-H···O in which the amide nitrogen

N(7A) or N(7B) acts as a donor via H(7A2) or H(7B2) to amide oxygen O(7B) or O(7A) respectively. These combine to form the common $R_2^2(8)$ hydrogen bond ring found in most pyrazinamide structures. There are two N-H···N intra hydrogen bonds in pyrazinamide molecules influences on the planarity of pyrazinamide molecule; N-H···N in which the amide nitrogen N(7A) or N(7B) acts as a donor via H(7A) or H(7B) to the pyridine nitrogen N(4A) or N(4B) respectively table 3.7.

The pyrazinamide dimer within each asymmetric unit is then linked to the adjacent unit via additional three sets of hydrogen bonds. N-H···O in which the amide nitrogen N(7A) acts as a donor via H(7A1) to the amide oxygen O(7B) to form a complementary $R_4^2(8)$ ring. Two distinct C-H···N interactions are formed in which C(3A) acts as a donor via H(3A) to the pyridine nitrogen N(1B) while C(6B) acts as a donor via H(6B) to the other heterocyclic nitrogen N(4A), together forming a $R_2^2(6)$ ring. Finally, these units are linked together into an infinite chain through the adipic acid lying on an inversion centre (figure 3.20).

Table 3.7: Intermolecular hydrogen bond distances (Å) and angles (º) within pyrazinamide: adipic acid

D-H-A	d(D-H)	d(H······A)	d(D······A)	<(DHA)
N(7A)-H(7A1)···O(7B)[ii]	0.89	2.28	3.026(2)	140
N(7A)-H(7A2)···O(7B)	0.92	2.08	2.998(3)	175
N(7A)-H(7A1)···N(4A)	0.89	2.40	2.768(3)	105
N(7B)-H(7B1)···N(4B)	0.91	2.31	2.732(3)	107
N(7B)[1]-H(7B1)···N(4B)iv	0.90	2.55	3.183(3)	126
N(7B)-H(7B1)···O(7A)	0.90	1.87	2.784(3)	176
O(8)-H(8)···N(1A)	0.91	1.83	2.711(3)	173
C(2A)-H(2A)···O(8)	0.89	2.38	3.297(3)	163
C(2B)-H(2B)···O(9)[iii]	0.95	2.43	3.356(3)	165
C(3A)-H(3A)···N(1B)[ii]	0.95	2.63	3.451(3)	144
C(3B)-H(3B)···O(7A)	0.95	2.39	3.325(3)	170
C(6A)-H(6A)···O(9)	0.95	2.53	3.226(3)	130
C(6B)-H(6B)···N(4A)	0.95	2.39	3.269(3)	154

Symmetry code: i) −3+x,1+y,2+z, (ii)3-x,-y,-z, (iii) x,y,1+z,(iv) −x+3,-y,-z+1
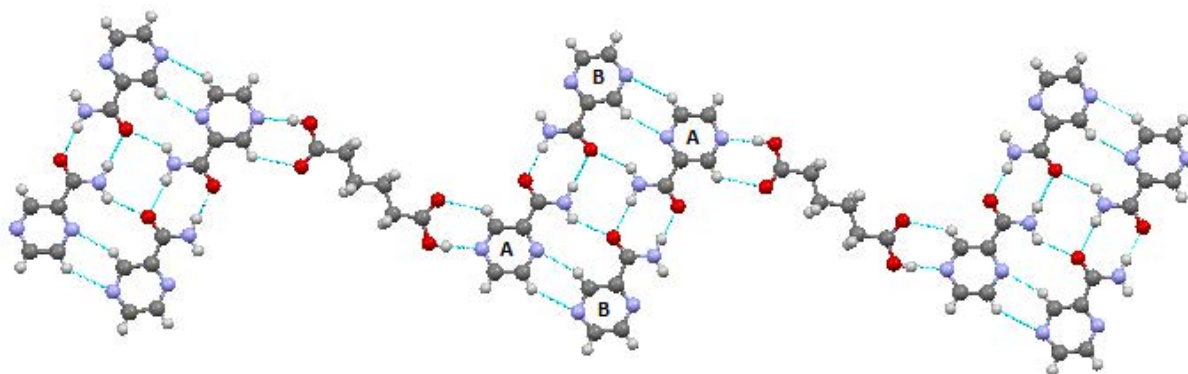
Figure 3.20: A view of the pyrazinamide:adipic acid (4:1) cocrystal structure showing the hydrogen bonded acid-pyridine rings, pyrazinamide dimers and linking hydrogen bonded rings to form an infinite chain. Hydrogen bonds are shown as thin light blue lines. The pyrazinamide molecules A and B are indicated.

These hydrogen bonded chains are then cross-linked to a neighbouring parallel chain via four intermolecular hydrogen bonds on the neighbouring chain; three weak C-H···O in which C(2A) in pyrazinamide acts as a donor through H(2A) to oxygen O(8) in a adipic acid as acceptor; C-H···O in which C(2B) in pyrazinamide acts as a donor through H(2B) to oxygen O(9) in adipic acid as acceptor; C-H···O in which C(3B) in pyrazinamide acts as a donor through H(3B) to oxygen O(7A) in pyrazinamide as acceptor and finally a strong hydrogen bond N-H···N in which the amide nitrogen N(7B) in pyrazinamide acts as a donor through H(7B1) to the pyridine N(4B) in the neighbouring pyrazinamide dimer (figure 3.21).

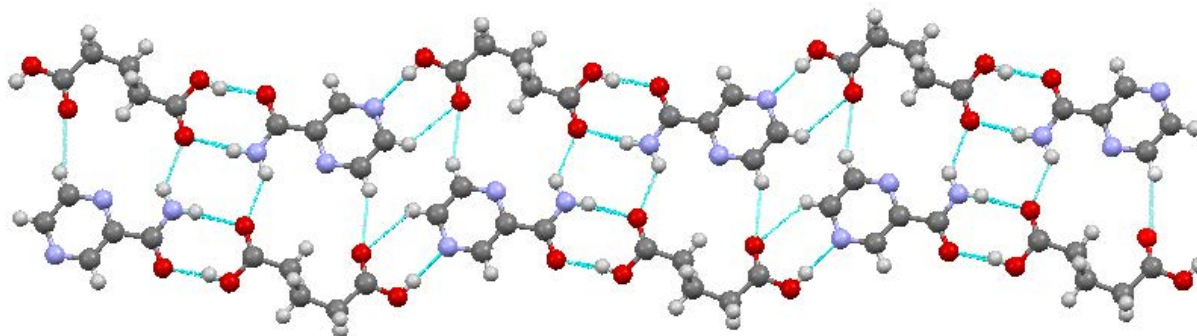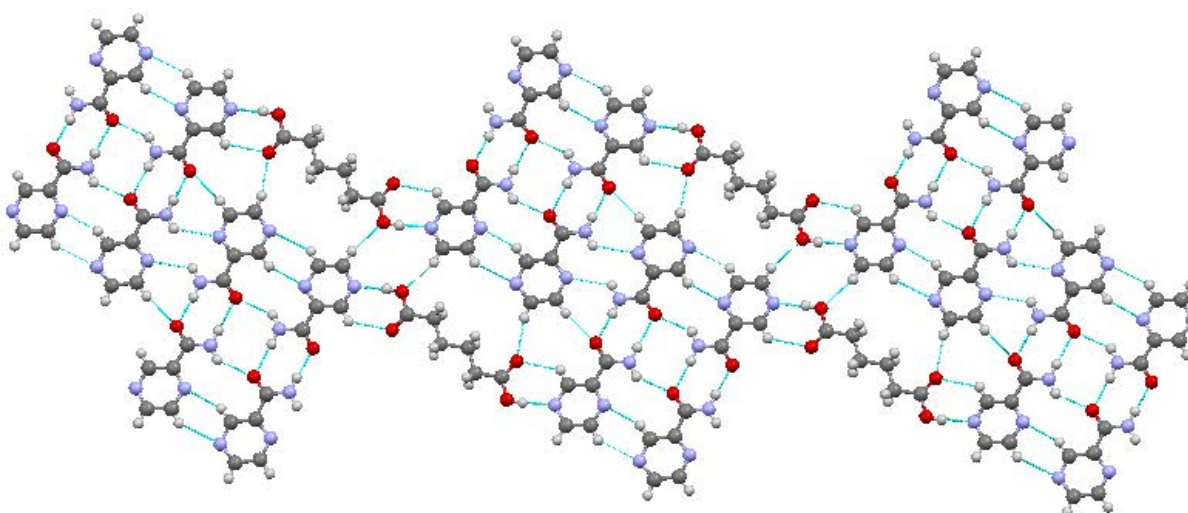*Figure 3.21: A view of the pyrazinamide:adipic acid (4:1) cocrystal structure showing the intermolecular hydrogen bonds between opposing supramolecular chains.*

This results in the formation of an extended hydrogen bonded sheet in which all strong hydrogen bond donors and acceptors are used in the complex hydrogen-bonded network.

The bond lengths and torsion angles within the pyrazinamide:adipic acid cocrystal are given in (table 3.8). The bond lengths in pyrazinamide C(7A)-N(7A) and C(7A)-O(7A) are 1.334(3) and 1.235(2) respectively, confirming the orientation of the amide group. In the acid, the bond lengths C(8)-O(8) and C(8)-O(9), again show a clear distinction between the C=O and C-O(H) components of the carboxylic acid functional group, hence confirming that there is no proton transfer between the components in this cocrystal structure.

The torsion angles within the pyrazinamide molecule (A) [N(4A)-C(5A)-C(7A)-N(7A) and C(6A)-C(5A)-C(7A)-N(7A)] are -0.91(3) and 179.33(2) respectively and show that molecule (A) is planar. However, the torsion angles of molecule (B) [N(4B)-C(5B)-C(7B)-N(7B) and C(6B)-C(5B)-C(7B)-N(7B)] are 9.80(3) and -168.51(2) respectively showing that molecule (B) is slightly distorted in terms of the conformation of the the amide group. Both molecules are stabilised by the intramolecular N-H⋯N interaction, but the amide group in molecular B is also involved in an intermolecular N-H⋯N interaction that may explain the required distortion of this molecular conformation.

The torsion angles within the adipic acid molecule show that overall the molecule is planar as expected in this type of acid with an inversion centre and even chain length.

Table 3.8: Selected intramolecular bond lengths and torsion angles within the pyrazinamide: adipic acid (4:1) cocrystal.

Pyrazinamide Bond Lengths	(Å)	Acid Bond Lengths	(Å)
C(7A)-N(7A)	1.334(3)	C(8)-O(8)	1.324(3)
C(7A)-O(7A)	1.235(2)	C(8)-O(9)	1.209(3)
C(7B)-N(7B)	1.331(3)		
C(7B)-O(7B)	1.240(2)		
Pyrazinamide Torsion Angles	(°)	Acid Torsion Angles	(°)
N(4A)-C(5A)-C(7A)-N(7A)	-0.91(3)	O(8)-C(8)-C(9)-C(10)	-179.39(19)
C(6A)-C(5A)-C(7A)-N(7A)	179.33(2)	O(9)-C(8)-C(9)-C(10)	0.44(3)
N(4B)-C(5B)-C(7B)-N(7B)	9.80(3)	C(8)-C(9)-C(10)-C(10)[1]	-174.20(2)
C(6B)-C(5B)-C(7B)-N(7B)	-168.51(2)	C(9)-C(10)-C(10)[1]-C(9)[1]	180.00
		O(8)-C(8)-C(8)[1]-O(8)[1]	180.00
		O(9)-C(8)-C(8)[1]-O(9)[1]	-180.00

The synthesis of this pyrazinamide: adipic acid adduct was also attempted using different methods of synthesis. The X-ray powder data of the material obtained from solvent evaporation was compared with that obtained through solvent drop grinding and both of these patterns were compared with the simulated powder diffraction pattern from the single crystal structure of pyrazinamide:adipic acid (4:1) (figure 3.22). The (4:1) crystal structure was determined at low temperature and hence some peak positions are shifted relative to room temperature of powder diffraction patterns. As expected, the original pattern from evaporation shows a mixture of adipic acid and the single crystal structure although there is also some preferred orientation distorting the relative intensities. The material obtained by grinding shows a mixture of cocrystal, with both adipic acid and pyrazinamide starting materials.
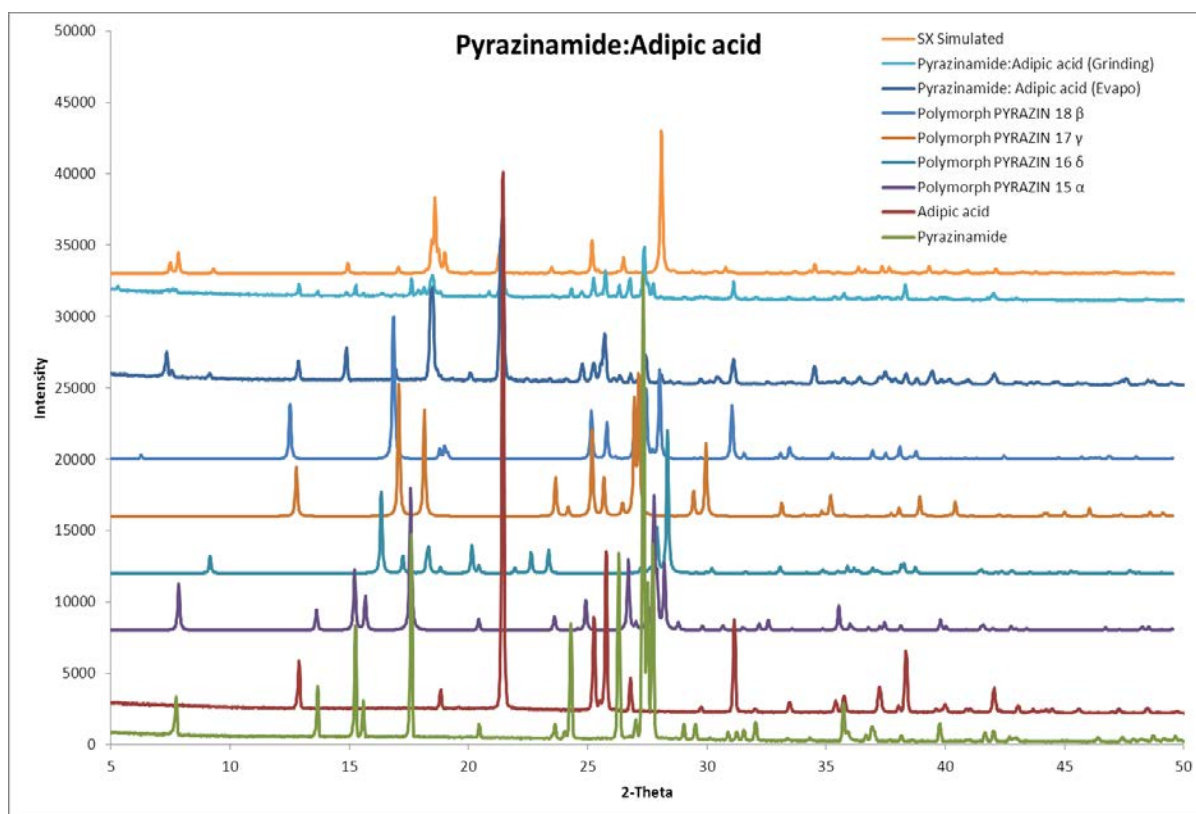
Figure 3.22: X-ray powder diffraction patterns of products obtained through different methods of synthesis and the simulated powder diffraction pattern from the single crystal structure of the pyrazinamide:adipic acid (4:1) cocrystal.

3.9 <u>Pyrazinamide and pimelic acid</u>

Pyrazinamide was crystallised with pimelic acid in this case using a range of different solvents for synthesis (methanol, ethanol, isopropanol and ethyl acetate) in combination with a number of different stoichiometric starting ratios (1:1, 1:2 and 2:1). All products formed as white solids and were obtained through the solvent evaporation crystallisation method. The X-ray powder diffraction patterns of three materials formed were compared with those data from the starting materials and a number of simulated powder patterns from previously published pyrazinamide polymorphs[76,83,97,98]. It can be seen from Figure 3.23 that the powder patterns of all three products are inconclusive except that they contain differing amounts of new product mixed with both pimelic acid (see peaks at 19º, 23º and 27º 2-theta) and pyrazinamide polymorphs (α(PYRAZIN15, δ(PYRAZIN16))[97,98].

The X-ray powder patterns for pyrazinamide:pimelic acid in stoichiometric ratio 1:2 and 2:1 match that of pyrazinamide: pimelic acid (1:1) with excess stating material also present in the mixture.
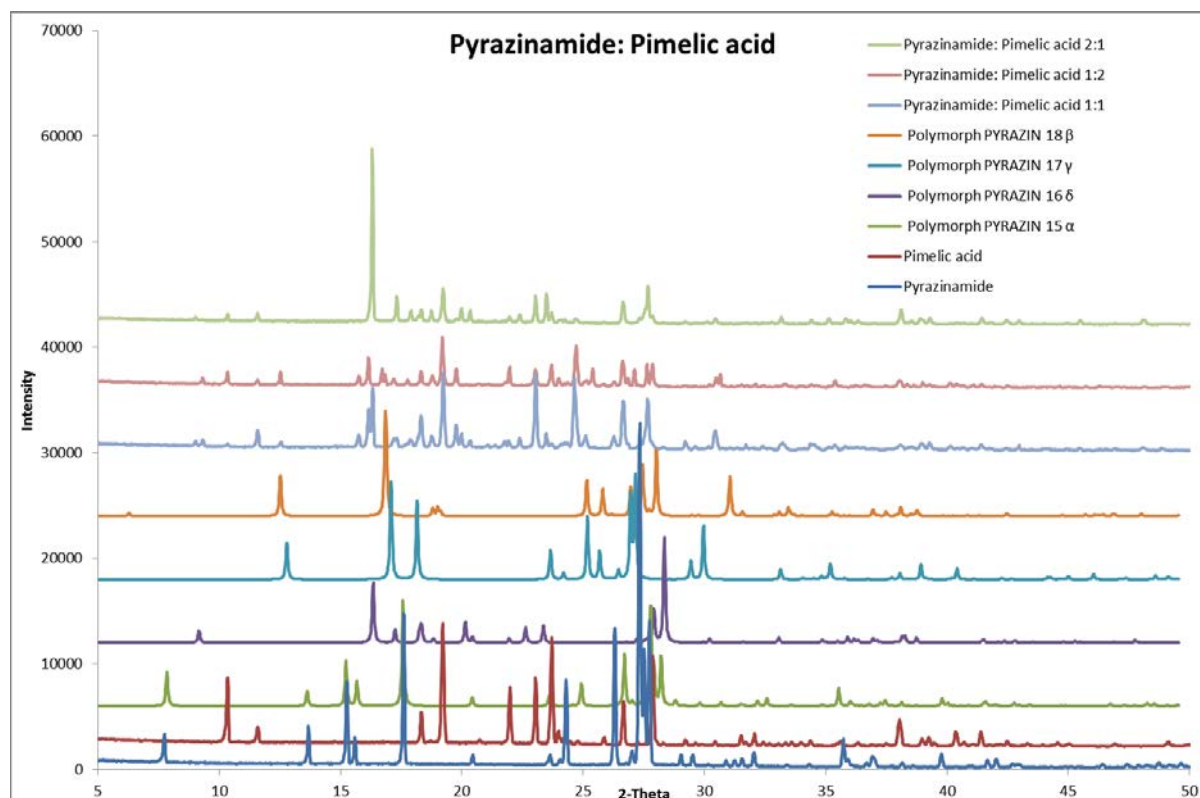
Figure 3.23: X-ray powder diffraction patterns of the products of pyrazinamide and pimelic acid crystallisation from methanol in different stoichiometric ratios (1:1 and 1:2), the starting materials (pyrazinamide, pimelic acid) and other common pyrazinamide polymorphs.

The bulk product is clearly a mixture but ^{1}H NMR indicated that the new material prepared from crystallisation of a 1:1 ratio of starting materials, also contains the molecular coformers in a 1:1 stoichiometric ratio (figure 3.24).

Figure 3.24: ^{1}H NMR of the product of pyrazinamide and pimelic acid (1:1) starting ratio using DMSO as a solvent. ^{1}H NMR 300MH$_z$ (DMS0-d$_6$): pyrazinamide 7.83 (1H, s), 8.29 (1H, s), 8.72 (1H, t), 8.92(1H, d), 9.19(1H, d): pimelic acid 1.25(2H, q), 1.51(4H, q) 2.22(4H, t)

3.9.1 <u>Crystal structure determination from single crystal X-ray diffraction data</u>

Once the bulk product was identified as containing a small amount of new unidentified material, the sample was submitted for single crystal analysis. This crystal structure determination confirmed that the stoichiometric ratio of the pyrazinamide and pimelic acid adduct was indeed 1:1, and that a neutral cocrystal of pyrazinamide:pimelic acid had been formed in which no proton transfer had taken place between the components. Further crystallographic details of this structure determination are given in Table 3.9.

Table 3.9. Crystal data and structure refinement of pyrazinamide:pimelic acid 1:1.

Identification code	Pyrazinamide_Pimelic acid
Empirical formula	$(C_5H_5N_3O)$, $(C7H12O4)$
Formula weight	283.29
Temperature	100.15 K
Wavelength	0.71075 Å
Crystal system	Triclinic
Space group	P-1
Unit cell dimensions	a = 5.3302(4) Å　　　　α= 89.478(7)°.
	b = 8.4201(6) Å　　　　β=82.760(7)°.
	c = 15.5321(11) Å　　　γ =71.840(6)°.
Volume	656.75(9) Å^3
Z	2
Density (calculated)	1.433 Mg/m^3
Absorption coefficient	0.113 mm^{-1}
F(000)	300.0
Crystal size	$0.42 \times 0.16 \times 0.02$ mm^3
Theta range for data collection	7.46 to 54.96 °.
Index ranges	$-6 \leq h \leq 6$, $-10 \leq k \leq 10$, $-20 \leq l \leq 20$
Reflections collected	7308
Independent reflections	2979 [R(int) = 0.0290, R(sigma) = 0.0228]
Completeness to theta = 67.684°	99.0 %
Absorption correction	Semi-empirical from equivalents
Max. and min. transmission	0.998 and 0.954
Refinement method	Full-matrix least-squares on F^2
Data / restraints / parameters	2979 / 0 / 183
Goodness-of-fit on F^2	1.062
Final R indices [I>2sigma(I)]	R_1 = 0.0350, wR_2 = 0.0984
R indices (all data)	R_1 = 0.0381, wR_2 = 0.1010
Extinction coefficient	n/a
Largest diff. peak and hole	0.40 and -0.21 e.Å^{-3}

Figure 3.25 shows the asymmetric unit of this cocrystal structure containing one pyrazinamide molecule and one pimelic acid molecule linked through hydrogen bonds. The atom labelling used for subsequent discussion is also shown below.
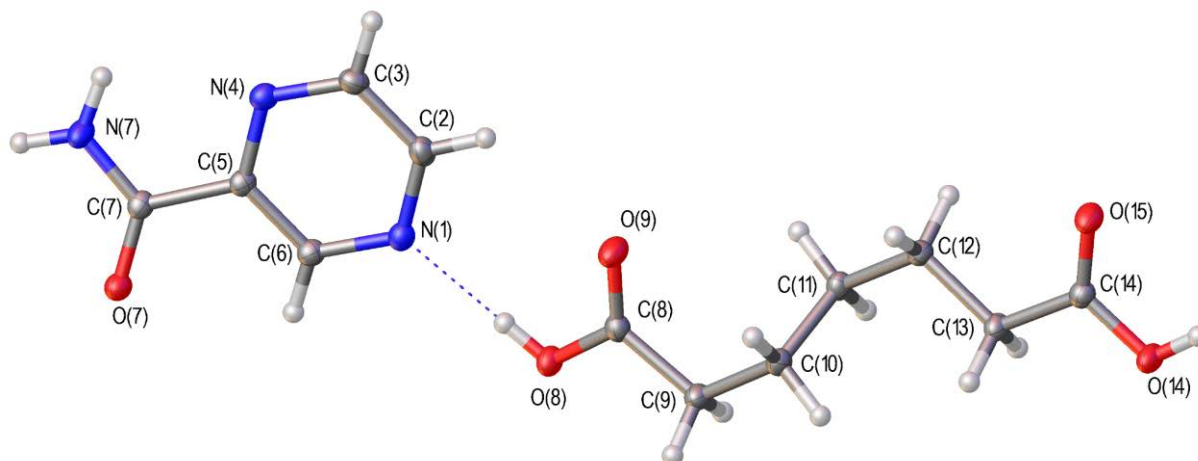
Figure 3.25: The asymmetric unit in the structure of the pyrazinamide:pimelic acid (1:1) showing the atom numbering scheme and the strong hydrogen bond between the two molecular components. Hydrogen bonds are shown as dotted lines.

The basic supramolecular structure motif within the asymmetric unit (figure 3.25) is formed by the pyrazinamide molecule interacting with the pimelic acid molecule through a strong hydrogen bond O-H⋯N in which O(8) in the carboxyl oxygen acts as a donor via H(8) to the pyridine nitrogen N(1). This is reinforced by a weak hydrogen bond C-H⋯O in which C(2) in pyrazinamide acts as donor via H(2) to O(9) in the pimelic acid (table 3.10). As in previous structures, there is an intramolecular hydrogen bond formed between N(7) and N(4) via H(7B) within the pyrazinamide molecule, stabilising the conformation.

Table 3.10: Intermolecular hydrogen bond distances (Å) and angles (^{o}) within the pyrazinamide:pimelic acid (1:1) cocrystal.

D-H-A	d(D-H)	d(H⋯⋯A)	d(D⋯⋯A)	<(DHA)
N(7)-H(7A)⋯O(15)	0.88	2.09	2.938(12)	162
N(7)-H(7B)⋯O(15)[ii]	0.88	2.57	3.011(12)	112
N(7)-H(7B)-N(4)	0.88	2.36	2.727	105
O(8)-H(8)⋯N(1)	0.84	1.91	2.751(12)	178
O(14)-H(14)⋯O(7)[iii]	0.84	1.81	2.643(11)	168
C(12)-H(12B)⋯N(4)	0.99	2.69	3.472	135
C(2)-H(2)⋯O(9)	0.95	2.51	3.187	127
C(3)-H(3)⋯O(9)	0.95	2.55	3.359	142
C(9)-H(9A)⋯O(7)	0.99	2.56	3.367	138

Symmetry code: i) +X,-1+Y,1+Z; (ii) -X,2-Y,-Z; (iii) +X,1+Y,-1+Z

The asymmetric units are linked together into an infinite chain by two further strong hydrogen bonds; a strong acid-amide interaction N-H$\cdots$O=C in which the amide nitrogen N(7) acts as a donor via H(7A) to the carboxyl oxygen O(15) and O-H$\cdots$O=C in which O(14) acts as a donor via H(14) to the amide oxygen O(7) as acceptor. Together these hydrogen bonds form a $R_2^2(7)$ ring such that a supramolecular chain of alternating $R_2^2(7)$ and $R_2^2(8)$ rings are generated through alternating acid-amide and acid-pyridine motifs (figure 3.26). Within each of these chains the pyrazinamide molecules adopt the same orientation and face the same direction.
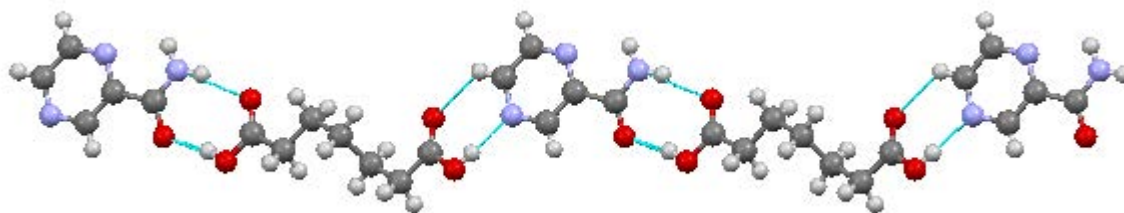
Figure 3.26: A view of the pyrazinamide:pimelic acid (1:1) cocrystal structure showing the alternating acid-amide and acid-pyridine rings.

These hydrogen bonded chains are then cross-linked to a neighbouring parallel chain via three additional hydrogen bonds. One strong hydrogen bond, N-H$\cdots$O=C, is donated by the amide nitrogen N(7) through H(7B) to O(15) on pimelic acid in the neighbouring chain. The complementary nature of this hydrogen bond results in the formation of an $R_4^2(8)$ ring between the chains which run in opposite but parallel directions (figure 3.27). Two weak hydrogen bonds then act to reinforce this structure; C-H$\cdots$N is formed by C(12) via H(12B) from pimelic acid to the heterocyclic N(4) and C-H$\cdots$O by donation of H(3) to the pimelic acid O(9).
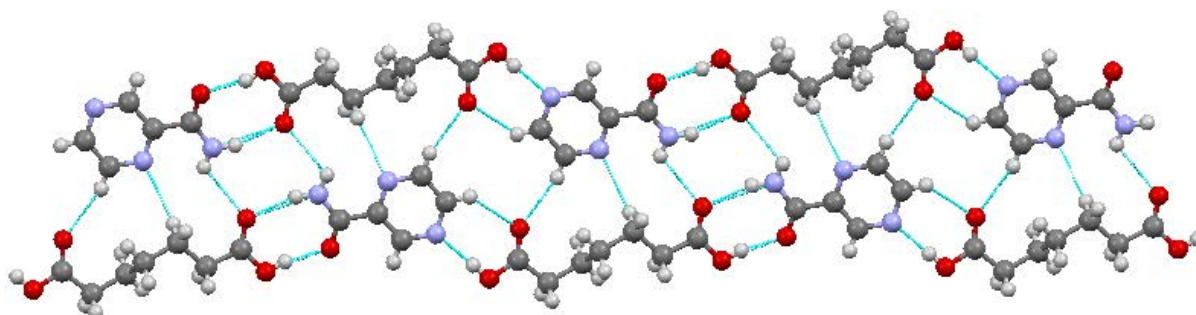
Figure 3.27: Diagram of pyrazinamide:pimelic acid crystal structure (1:1) showing the intermolecular interactions between two adjacent chains.

Each ribbon is linked to another ribbon by a further C-H⸱⸱⸱O hydrogen bond in which C(9) in the pimelic acid molecule acts as a donor via H(9A) to oxygen O(7) in the neighbouring pimelic acid molecule which in this case acts as the acceptor (figure 3.28). This forms an infinite hydrogen bonded sheet of molecules lying parallel to the [0,-1,1] plane.

All strong hydrogen bonding donor and acceptor sites are involved in the hydrogen-bonding network in this structure.
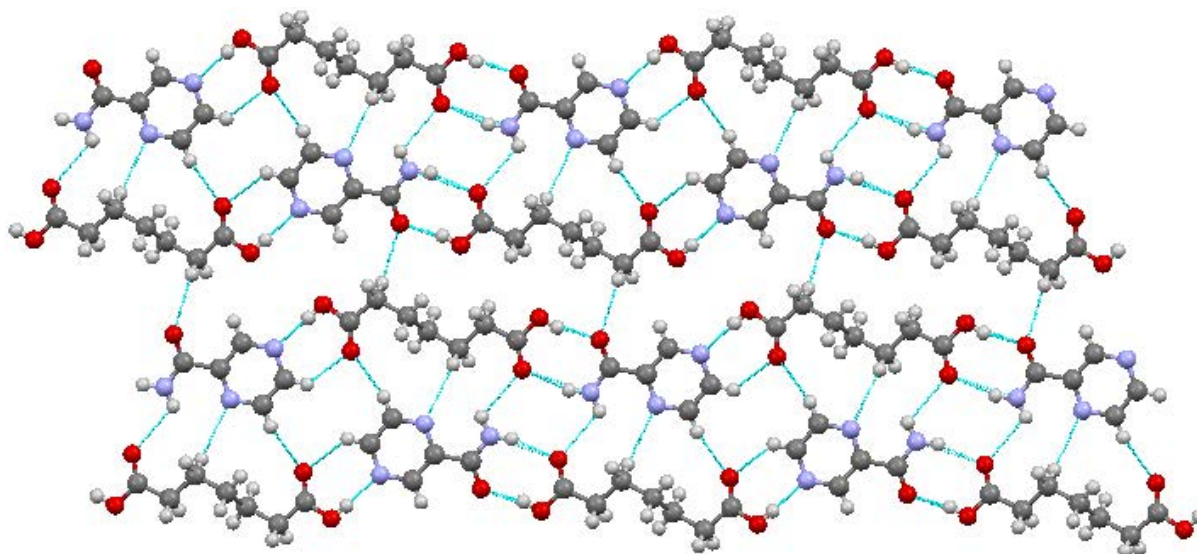
Figure 3.28: *A view of the pyrazinamide:pimelic acid cocrystal structure showing the infinite molecular sheet.*

The bond lengths within the pyrazinamide:pimelic acid cocrystal are given in Table 3.11. The bond lengths of C(7)-N(7) and C(7)-O(7) are 1.326(13) and 1.241(12) respectively and confirm the orientation of the amide group. In the acid, the bond lengths of C(8)-O(8) and C(8)-O(9) are 1.337(12) and 1.211(13); C(14)-O(14) and C(14)-O(15) are 1.325(12) and 1.217(13) respectively showing a clear distinction between the C=O and C-O(H) components of the carboxylic acid functional group, hence confirming that there is no proton transfer between the neutral components in this cocrystal structure.

The torsion angles within the pyrazinamide molecule N(4)-C(5)-C(7)-N(7) and C(6)-C(5)-C(7)-N(7) are 6.77(13) and -175.28(9) respectively show a slight deviation from planarity. The molecule is partially stabilized in this conformation by the intramolecular N-H⸱⸱⸱N, but other intermolecular interactions are likely to effect this conformation.
The torsion angles within the pimelic acid molecule show some distortion from planarity arising again from interactions formed between the components. The torsion angles defining

the acid groups O(8)-C(8)-C(9)-C(10) and C(12)-C(13)-C(14)-O(14) show that this conformation as is expected, as do the components of the carbon backbone C(9)-C(10)-C(11)-C(12) and C(11)-C(12)-C(13)-C(14). The other angles C(8)-C(9)-C(10)-C(11) and C(10)-C(11)-C(12)-C(13) are -72.02(11) and 70.18(11) respectively and result in the overall conformation of the pimelic acid being distorted. The relationship between the two acid groups then differs significantly from planarity, again giving a 'bent' flexible linker within the cocrystal, not uncommon in diacids of odd chain length.

Table 3.11: Intermolecular and intramolecular hydrogen bond distances and torsion angles within the pyrazinamide:pimelic acid cocrystal.

Pyrazinamide Bond Lengths	(Å)	Acid Bond Lengths	(Å)
C(7)-N(7)	1.326(13)	C(8)-O(8)	1.337(12)
C(7)-O(7)	1.241(12)	C(8)-O(9)	1.211(13)
		C(14)-O(14)	1.325(12)
		C(14)-O(15)	1.217(13)
Pyrazinamide Torsion Angles	(^{o})	Acid Torsion Angles	(^{o})
N(4)-C(5)-C(7)-N(7)	6.77(13)	O(8)-C(8)-C(9)-C(10)	178.24(8)
N(4)-C(5)-C(7)-O(7)	-172.48	O(9)-C(8)-C(9)-C(10)	-2.54(15)
C(6)-C(5)-C(7)-O(7)	5.48(14)	O(9)-C(8)-C(14)-O(14)	170.40
C(6)-C(5)-C(7)-N(7)	-175.28(9)	O(8)-C(8)-C(14)-O(15)	154.82
		O(9)-C(8)-C(14)-O(15)	-2.38
		C(8)-C(9)-C(10)-C(11)	-72.02(11)
		C(9)-C(10)-C11)-C(12)	-179.92(8)
		C(10)-C(11)-C(12)-C(13)	70.18(11)
		C(11)-C(12)-C(13)-C(14)	174.49(8)
		C(12)-C(13)-C(14)-O(14)	-174.50(9)
		C(12)-C(13)-C(14)-O(15)	4.55(15)

The X-powder diffraction patterns of the products obtained through different methods of synthesis were compared with the simulated powder pattern from the crystal structure determined by single crystal X-ray diffraction to confirm if this structure is representative of the bulk. Figure 3.29 shows that the bulk material is not a good match with that from the single crystal analysis. This is a similar conclusion to the initial experimental observation that the crystal selected for structure determination was atypical of other parts of the bulk sample. Although there is some similarity between the samples obtained by solvent evaporation and solvent-drop grinding, it is clear that both are mixtures containing different proportions of product, starting materials and polymorphic form.
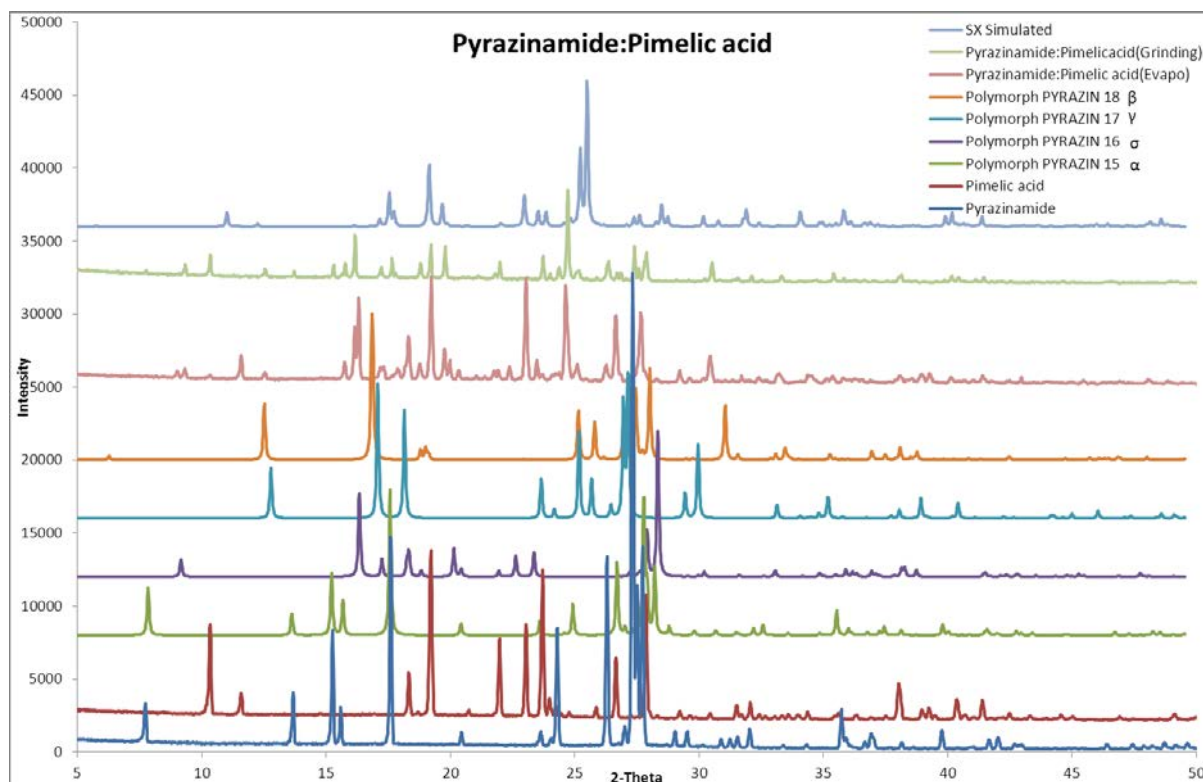
Figure 3.29: X-ray powder diffraction patterns of the products of pyrazinamide and pimelic acid crystallisation from methanol through different method of synthesis, the starting materials (pyrazinamide, pimelic acid), common pyrazinamide polymorphs and the simulated pattern from the single crystal structure.

Different solvents (methanol, ethanol, propanol and ethyl acetate) were also used for attempted synthesis of the cocrystal of pyrazinamide:pimelic acid with the aim of obtaining the pure material Figure 3.30 shows the products obtained by solvent evaporation from different solvents. The results obtained from all solvents are similar, with that from propanol and ethyl acetate being the most similar. None of these have produced the pure bulk cocrystalline material, hence highlighting the difficulties that are encountered with the prolific polymorphic behaviour of pyrazinamide.
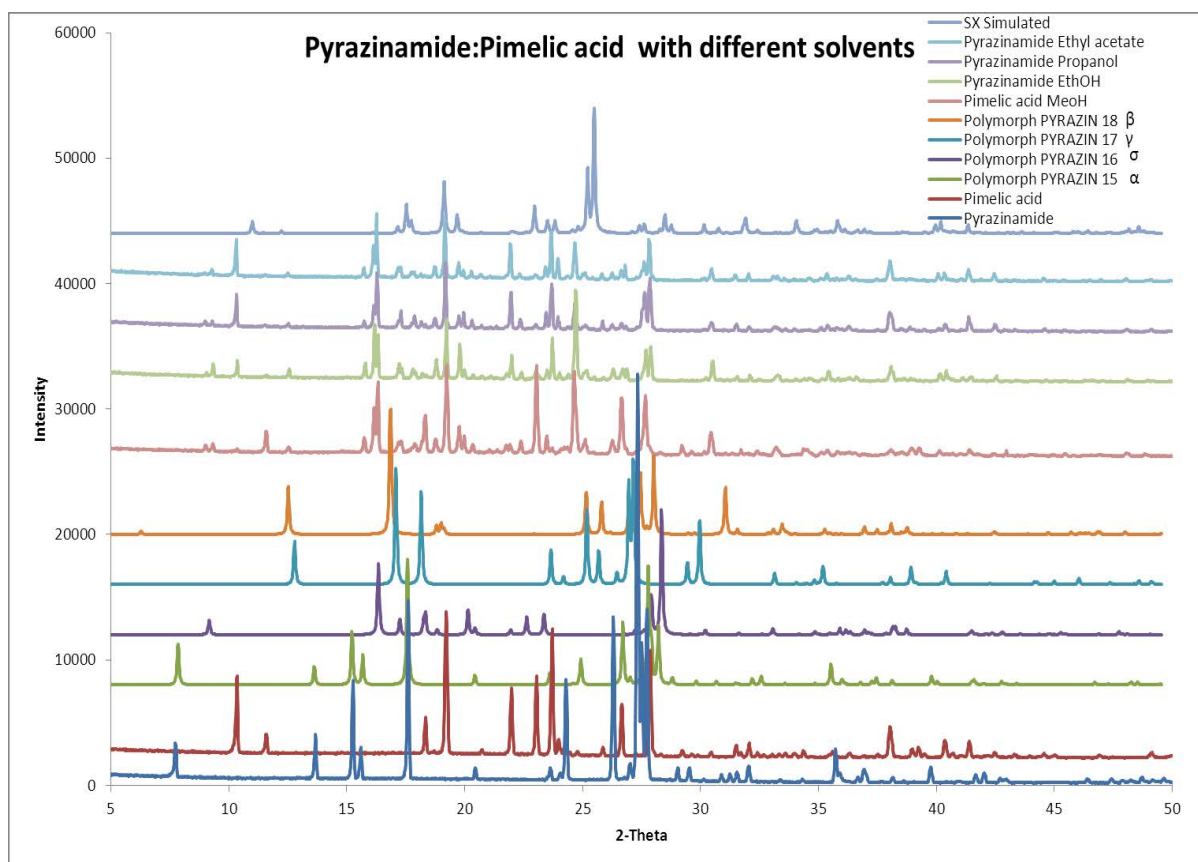
Figure 3.30: X-ray Powder diffraction patterns and single x-ray powder diffraction pattern of the products of pyrazinamide and pimelic acid from different solvents, the starting materials (pyrazinamide, pimelic acid) and common pyrazinamide polymorphs.

3.10 Pyrazinamide and subaric acid

Pyrazinamide and subaric acid were dissolved in methanol in a 1:1 stoichiometric starting ratio and the solvent evaporation method was used for crystallisation. The product formed was a white solid. The X-ray powder diffraction pattern of product formed is clearly a match to a combination of the patterns of the starting materials, confirming that this is a mixture of the starting materials and there is no new material has been formed (figure 3.31).
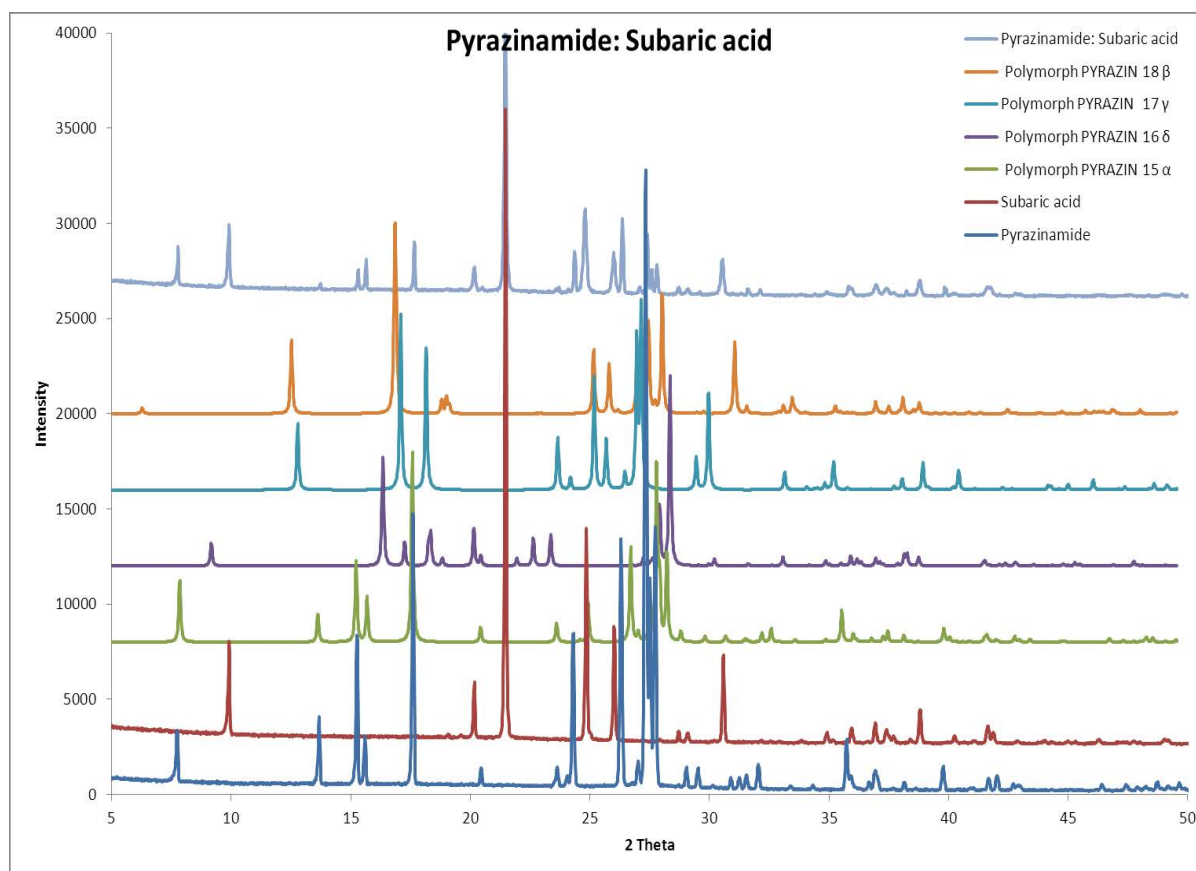
Figure 3.31: X-ray powder diffraction pattern of the product of pyrazinamide and subaric acid crystallisation from methanol, the starting materials (pyrazinamide, subaric acid) and common pyrazinamide polymorphs.

3.11   <u>Pyrazinamide and azelaic acid</u>

Pyrazinamide was crystallised with azelaic acid and methanol used as solvent for synthesis in a 1:1 starting stoichiometric ratio. A new product was obtained through the solvent evaporation method as a white solid. The X-ray powder diffraction pattern of this product (figure 3.32) shows the presence of both a new material and a significant amount of the pyrazinamide starting material (see peaks at 15º, 17º and 26 2-theta) or polymorph (α(PYRAZIN15))[97].
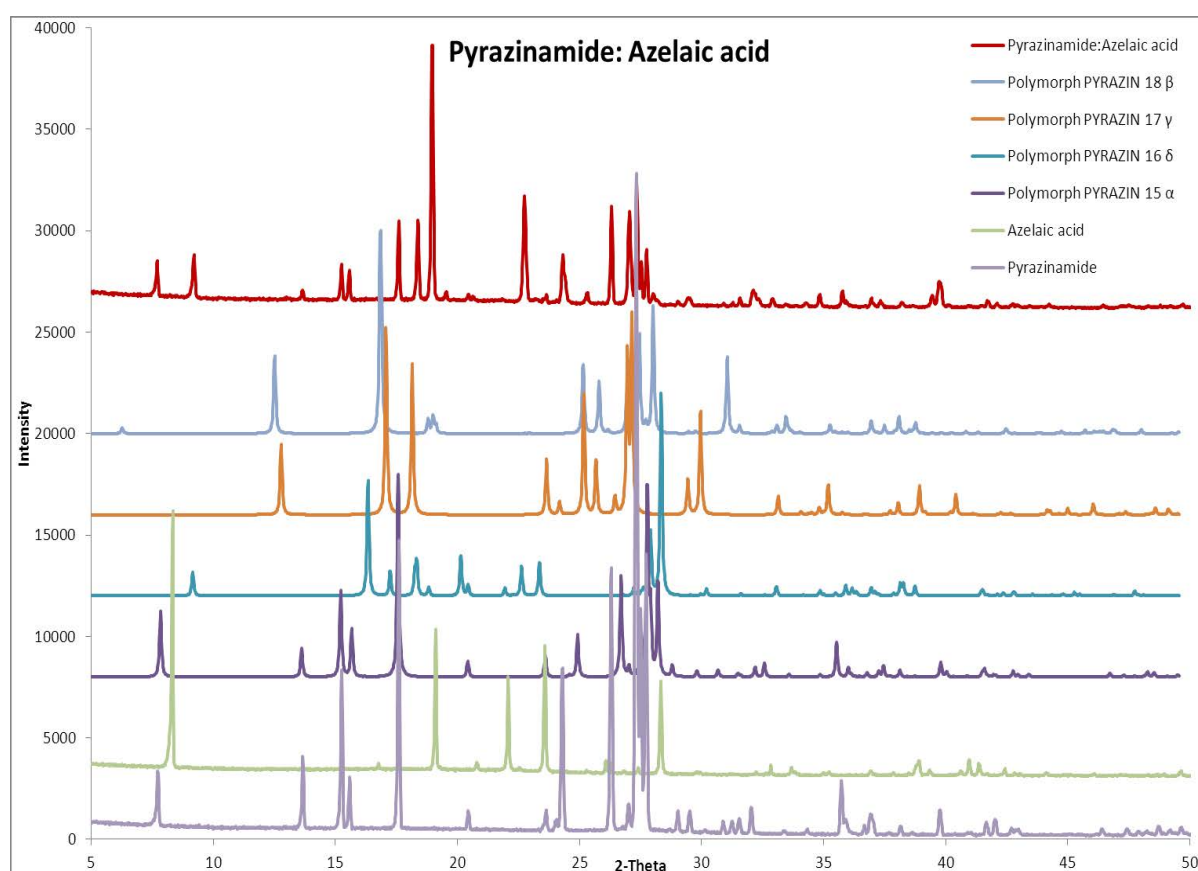
Figure 3.32: X-ray powder diffraction pattern of the product of pyrazinamide and azelaic acid crystallisation from methanol, the starting materials (pyrazinamide, azelaic acid) and other common pyrazinamide polymorphs.

The bulk product is a mixture, ^{1}H NMR indicate that the new material formed from crystallisation of 1:1 contains molecular coformers in a 1:1 stoichiometric ratio of starting materials of pyrazinamide and azelaic acid (figure 3.33).
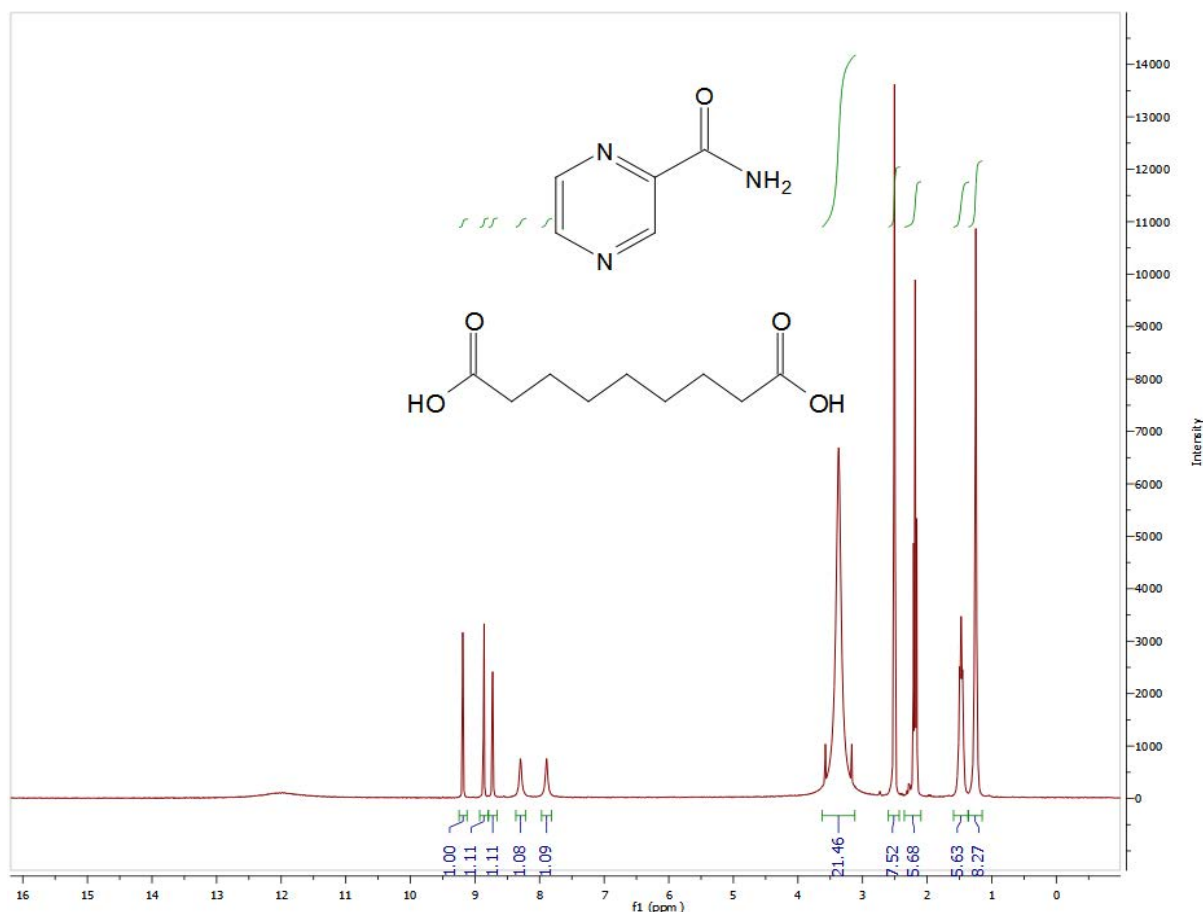
Figure 3.33: ^{1}H NMR of the product of pyrazinamide and azelaic acid (1:1) starting ratio using DMSO as a solvent. ^{1}H NMR 300MH$_z$ (DMS0-d$_6$): pyrazinamide 7.83 (1H, s), 8.29 (1H, s), 8.72 (1H, t), 8.92(1H, d), 9.19(1H, d) azelaic acid 1.23 (8H, s), 1.47 (5H, t), 2.21 (5H, t).
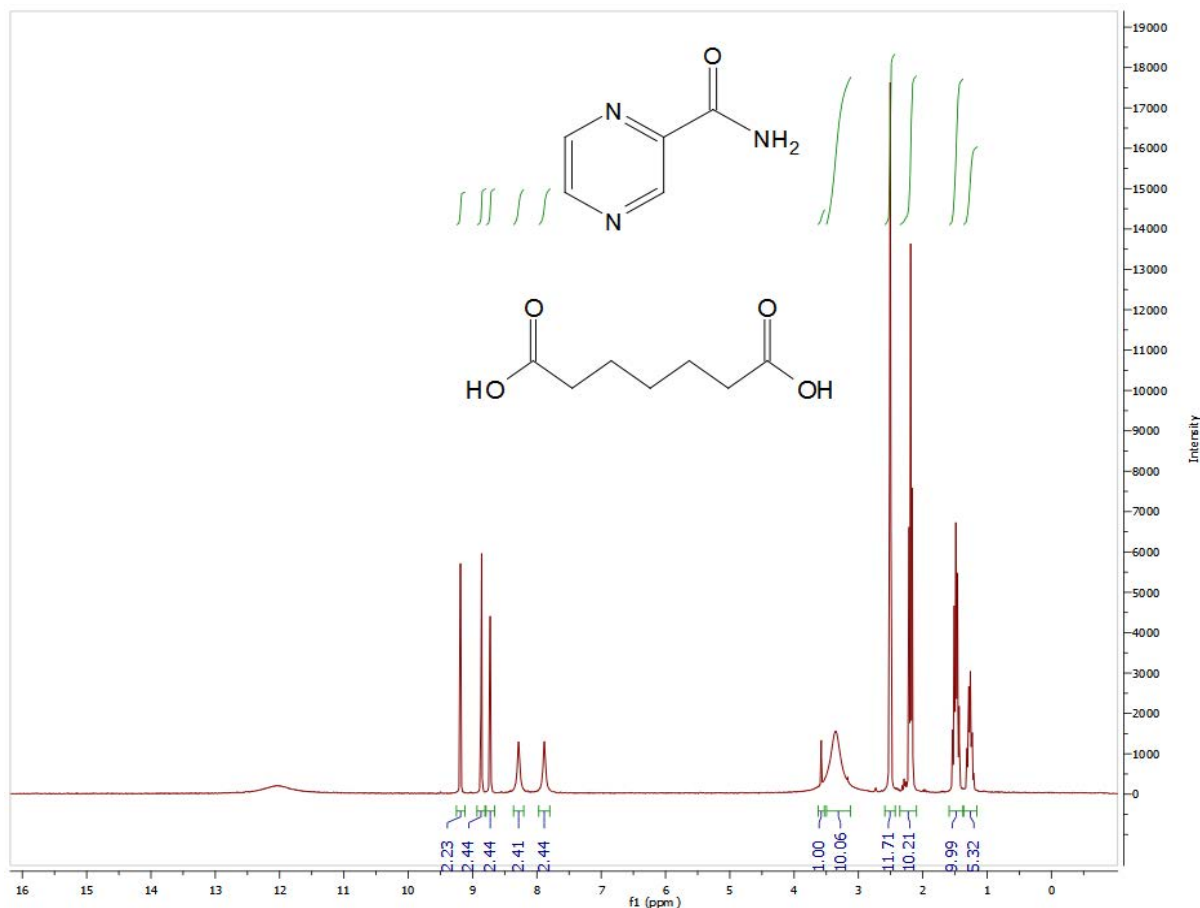
3.11.1 Crystal structure determination from single X-ray diffraction data

Once the bulk product was identified as containing a new material through X-ray powder diffraction, the sample was submitted for single crystal analysis. The crystal structure determination confirmed that the new material formed was not an adduct of the two components but was an unpublished polymorph of azelaic acid and hence the pyrazinamide detected in the NMR was starting material only. Further crystallographic details of this structure determination are given in Table 3.12.

Figure 3.34 shows the asymmetric unit and the atom labelling used in this crystal structure of azelaic acid. The crystal structure polymorph of azelaic acid was published from 1967 at room temperature (CDS: AZELAC10)[99].

Table 3.12. Crystal data and structure refinement of azelaic acid.

Identification code	Azelaic Acid	
Empirical formula	$C_9H_{16}O_4$	
Formula weight	188.22	
Temperature	100.00(10) K	
Wavelength	1.5418 Å	
Crystal system	Monoclinic	
Space group	$P\ 2_1/c$	
Unit cell dimensions	a = 5.4938(2) Å	α = 90°.
	b = 9.4418(3) Å	β = 95.673(3)°.
	c = 18.8258(6) Å	γ = 90°.
Volume	971.74(6) Å^3	
Z	4	
Density (calculated)	1.287 Mg/m^3	
Absorption coefficient	0.838 mm^{-1}	
F(000)	408	
Crystal size	0.140 x 0.130 x 0.030 mm^3	
Theta range for data collection	6.657 to 74.248°.	
Index ranges	-6<=h<=6, -10<=k<=11, -22<=l<=21	
Reflections collected	3622	
Independent reflections	1922 [R_{int} = 0.0182]	
Completeness to theta = 67.684°	99.7 %	
Absorption correction	Semi-empirical from equivalents	
Max. and min. transmission	1.00000 and 0.89788	
Refinement method	Full-matrix least-squares on F^2	
Data / restraints / parameters	1922 / 0 / 126	
Goodness-of-fit on F^2	1.171	
Final R indices [I>2sigma(I)]	R1 = 0.0430, wR2 = 0.1254	
R indices (all data)	R1 = 0.0480, wR2 = 0.1287	
Extinction coefficient	n/a	
Largest diff. peak and hole	0.288 and -0.224 e.Å^{-3}	

Note: The hydrogen atoms bonded to O(1) and O(9) were located in the electron density and freely refined. All other hydrogen atoms were fixed as riding models.

[This polymorph was originally published before in 1967[79] as a structure determined from data collected at room temperature with a final R factor (based on observed data) of 9 % (CSD AZELAC10)].
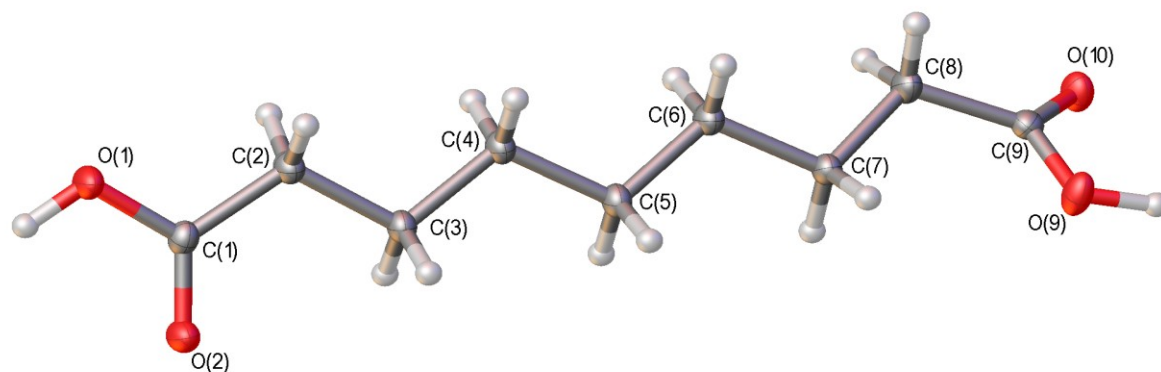
Figure 3.34: The asymmetric unit in the crystal structure polymorph of azelaic acid showing the atom numbering scheme.

The basic supramolecular structure motif within the asymmetric unit (figure 3.34) is formed by one molecule of azelaic acid.

Table 3.13: Intermolecular hydrogen bond distances (Å) and angles (°) within the azelaic acid

D-H-A	d(D-H)	d(H······A)	d(D······A)	<(DHA)
O(1)-H(1)···O(2)^i	0.89(3)	1.76(3)	2.656(18)	177(3)
O(9)-H(9)···O(10)^{ii}	0.94(3)	1.73(3)	2.667(17)	175(3)
C(8)-H(8B)···O(2)	0.990	2.67	3.338	124.64

Symmetry code: i) x-1,y+1,z ii) x+3,y+1,z+1

The asymmetric units are linked together into an infinite chain by hydrogen bonds (Table 3.13) O-H··O in which O(1) acts as a donor via H(1) and O(2) acts as an acceptor and the other hydrogen bond O-H···O in which O(9) acts as a donor via H(9) and O(10) acts as an acceptor. Together these hydrogen bonds form a $R_2^2(8)$ ring such that a supramolecular chain of alternating $R_2^2(8)$ rings are generated through acid-acid motifs (figure 3.35).

Within each of these chains the azelaic acid molecules adopt the same orientation and face the same direction. These hydrogen bonded chains are cross-linked to another neighbouring parallel chain via an additional two week hydrogen bonds; C-H···O in which C(8) in azelaic acid molecule acts as a donor via H(8B) to oxygen O(2) as acceptor in the neighbouring azelaic acid molecule and the other hydrogen bond in which O(1) in the azelaic acid act as a donor via H(1) to O(10) as acceptor in the other neighbouring azelaic acid molecule. The complementary hydrogen bond results in the formation of an $R_4^2(8)$ ring between the chains running in opposite but parallel directions (figure 3.36)
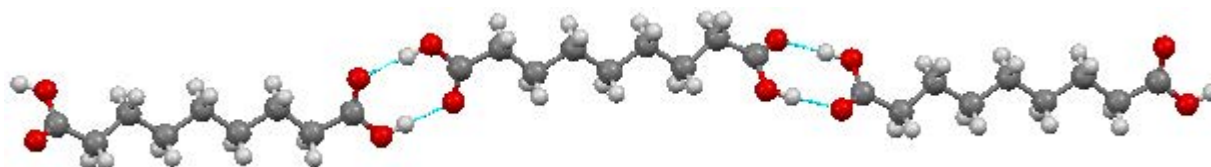
Figure 3.35: A view of the crystal structure polymorph of azelaic acid showing the alternating acid-acid rings through hydrogen bonds in the molecules.
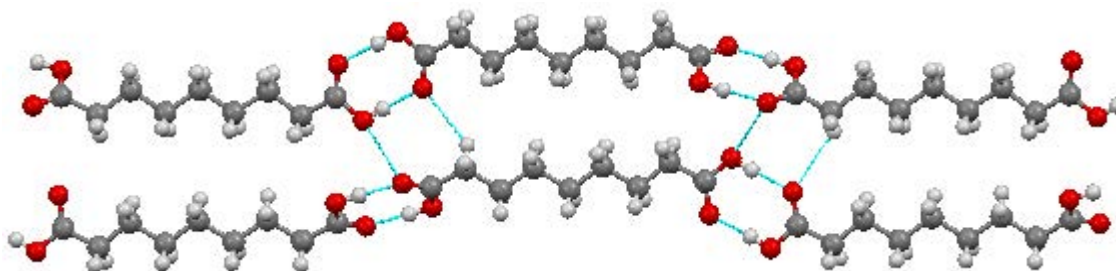
Figure 3.36: Diagram of the crystal structure polymorph of azelaic acid showing the intermolecular hydrogen bonds between the molecules in two chains.

Table 3.14: Hydrogen bonds (Å) and torsion angles (^{o}) in azelaic acid polymorph.

Bond Lengths	(Å)	Acid Angles	(^{o})
C(1)-O(2)	1.323(2)	C(1)-C(2)-C(3)-C(4)	174.32(14)
C(1)-O(2)	1.223(2)	C(3)-C(4)-C(5)-C(6)	174.41(14)
C(9)-O(9)	1.318(2)	C(2)-C(3)-C(4)-C(5)	179.48(14)
C(9)-O(10)	1.228(2)	C(6)-C(7)-C(8)-C(9)	177.87(14)
		O(1)-C(1)-C(2)-C(3)	179.34(14)
		O(1)-C(1)-C(9)-O(9)	133.70
		O(1)-C(1)-C(9)-O(10)	-67.98

The bond lengths within the azelaic acid are given in Table 3.14. The bond lengths of C(1)-O(1) and C(1)-O(2) are 1.323(2) and 1.223(2); C(9)-O(9) and C(9)-O(10) are 1.318(2) and 1.228(2) respectively showing a clear distinction between the C=O and C-O(H) components of the carboxylic acid functional group.

The torsion angles within the azelaic acid molecule of the carbon backbone C(1)-C(2)-C(3)-C(4) and C(3)-C(4)-C(5)-C(6); C(2)-C(3)-C(4)-C(5) and C(6)-C(7)-C(8)-C(9) are 174.32 and 174.41(14); 179.48(14) and 177.97(11) respectively, show that is close to planar. The other angles of carboxylic acid groups O(1)-C(1)-C(9)-O(9) and O(1)-C(1)-C(9)-O(10) are 133.70 and -67.98 respectively, show that carboxylic acid groups are significantly distorted. The

relationship between the acid groups and carbon backbone is differs from planarity, giving a 'bent' flexible linker within other azelaic acid molecules. This type of conformation is not unusual for diacids with odd chain length.

The X-ray powder diffraction pattern of pyrazinamide:azelaic acid formed was compared with single crystal simulated pattern of azelaic acid polymorph structure formed at 100 k and also compared with a number of simulated patterns of previously published azelaic acid polymorphs[79]. The simulated pattern of azelaic acid polymorph formed is matching the simulated pattern of previously published polymorph (α(AZELAC10))[99] and some peaks are shifted being generated at a low temperature (figure3.37). The bulk powder pattern shows a match to the simulated single crystal pattern of azelaic acid formed but there are also a number of differences in peaks that arise from the bulk sample being a mixture with pyrazinamide starting material. These different peaks are match the peaks of powder pattern of pyrazinamide starting material. The azelaic acid polymorph formed was high quality determined at low temperature (100 k). This figure confirms that the azelaic acid used as a starting material is matches azelaic acid polymorph (β(AZELAC10))[99].
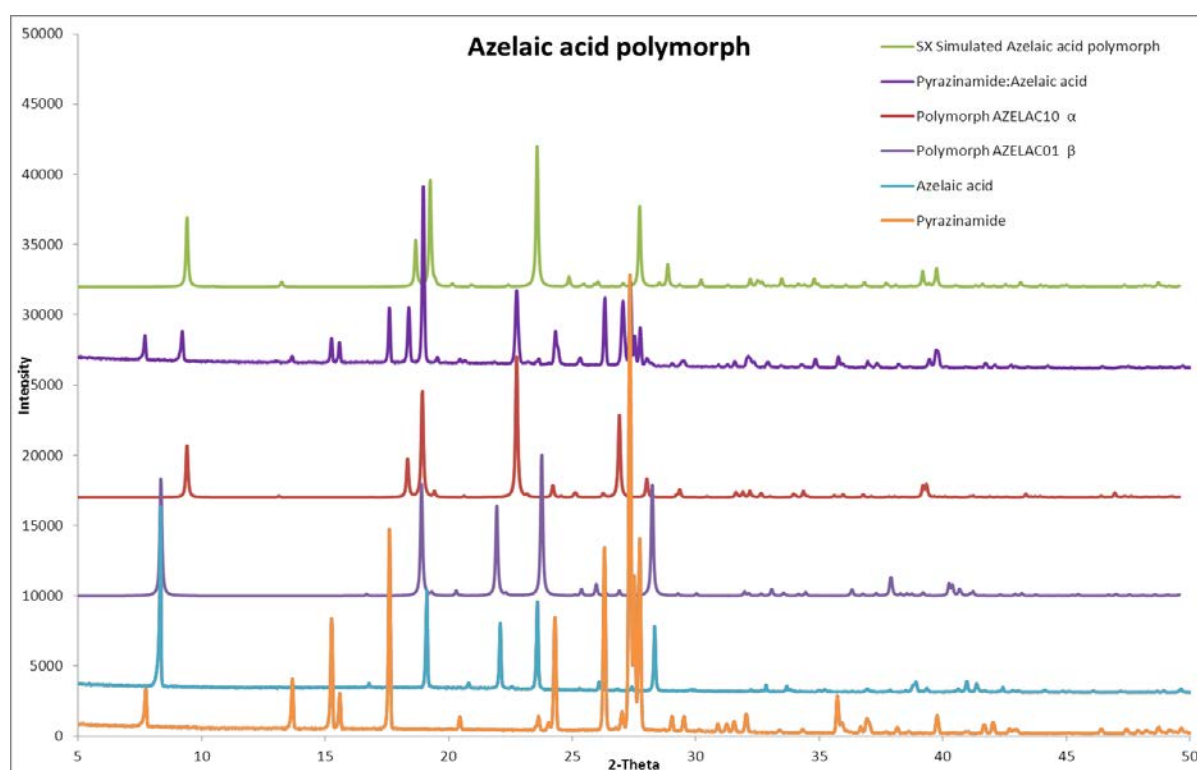
Figure 3.37: X-ray powder diffraction pattern of the product azelaic acid polymorph, the starting materials (pyrazinamide, azelaic acid), common azelaic acid polymorphs and the simulated pattern from the single crystal structure.

3.12 <u>**Pyrazinamide and sebacic acid**</u>

Pyrazinamide and sebacic acid were dissolved in methanol and combined for crystallisation in a 1:1 stoichiometric ratio. The solvent evaporation method was used for synthesis. The new product formed was a yellow solid crystal. The X-ray powder diffraction pattern of this product is different to those of the starting materials, confirming the formation of new material. The powder diffraction pattern of product formed was also compared with a number of simulated patterns from previously published pyrazinamide polymorphs[76,83,97,98]. It can be seen from the figure 3.38 that the product may contain small amount of sebacic acid starting material (see peaks 24º 2-theta) in a mixture with the new product.

Figure 3.38: X-ray powder diffraction pattern of the product of pyrazinamide and sebacic acid crystallisation from methanol, the starting materials (pyrazinamide, sebacic acid) and other common pyrazinamide polymorphs.

The bulk material looks like it is a mixture and this may effect interpretation of the NMR. ^{1}H NMR indicated that the new product formed from crystallisation of a 1:1 ratio of starting materials show a resulting 2:1 stoichiometric ratio of pyrazinamide and sebacic acid (figure 3.39).
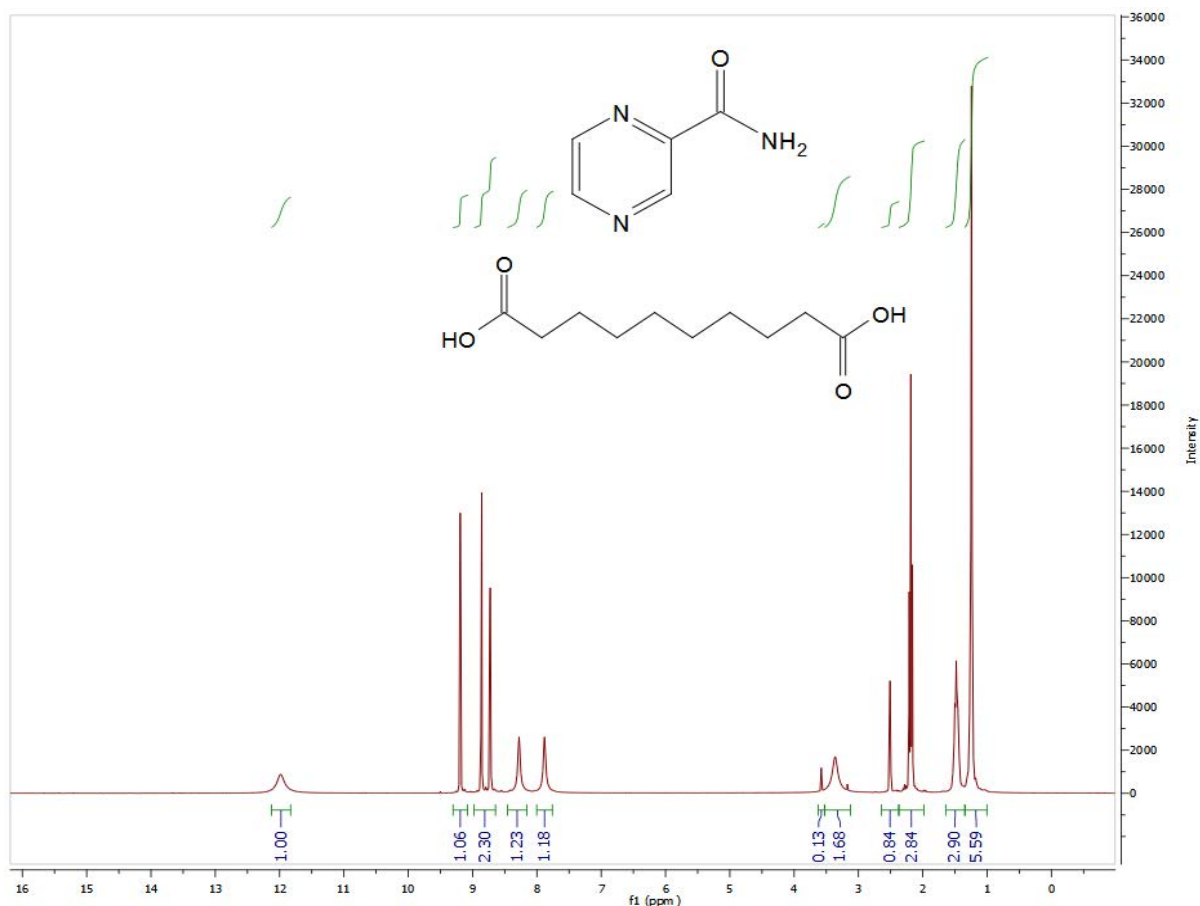
Figure 3.39: ^1H NMR of the product of pyrazinamide and sebacic acid (1:1) starting ratio using DMSO as a solvent. ^1H NMR 300MH$_z$ (DMS0-d$_6$): pyrazinamide 7.86 (1H, s), 8.27 (1H, s), 8.72 (1H, t), 8.85 (1H, d), 9.19 (1H, d): sebacic acid 1.25 (4 H, s), 1.56 (2H, q), 2.24 (2H, t).

3.12.1 Crystal structure determination from single crystal X-ray diffraction data

A small amount of yellow crystalline product was submitted for single crystal analysis and the crystal structure of a new pyrazinamide:sebacic acid cocrystal was determined. This established that the stoichiometric ratio of the pyrazinamide and sebacic acid in this material was 2:1. The crystal structure also confirmed that a neutral cocrystal has been formed in which no proton transfer had taken place between the two molecular components. The sample itself was found to contain both yellow crystals and a small amount of colourless crystalline material that was identified as sebacic acid. Further crystallographic details of this structure determination are given in Table 3.15.

Table 3.15. Crystal data and structure refinement for pyrazinamide:sebacic acid 2:1.

Identification code	Pyrazinamide_Sebacic Acid	
Empirical formula	$2(C_5 H_5 N_3 O)$, $C_{10} H_{18} O_4$	
Formula weight	448.48	
Temperature	100.00(10) K	
Wavelength	1.5418 Å	
Crystal system	Triclinic	
Space group	P -1	
Unit cell dimensions	a = 5.1790(2) Å	α= 94.342(3)°.
	b = 5.4406(2) Å	β= 93.910(3)°.
	c = 19.2691(7) Å	γ= 94.681(3)°.
Volume	538.07(3) Å^3	
Z	1	
Density (calculated)	1.384 Mg/m^3	
Absorption coefficient	0.869 mm^{-1}	
F(000)	238	
Crystal size	0.350 x 0.200 x 0.100 mm^3	
Theta range for data collection	6.933 to 70.058°.	
Index ranges	-6<=h<=6, -6<=k<=6, -23<=l<=23	
Reflections collected	5733	
Independent reflections	2026 [R(int) = 0.0159]	
Completeness to theta = 67.684°	98.9 %	
Absorption correction	Semi-empirical from equivalents	
Max. and min. transmission	1.00000 and 0.84544	
Refinement method	Full-matrix least-squares on F^2	
Data / restraints / parameters	2026 / 0 / 154	
Goodness-of-fit on F^2	1.073	
Final R indices [I>2sigma(I)]	R1 = 0.0339, wR2 = 0.0899	
R indices (all data)	R1 = 0.0355, wR2 = 0.0911	
Extinction coefficient	n/a	
Largest diff. peak and hole	0.290 and -0.169 e.Å^{-3}	

Notes: The hydrogen atoms bonded to N(7) and O(8) were located in the electron density and their positions refined freely, with their isotropic thermal parameters based on the equivalent isotropic thermal parameter of the parent atom ($U_{iso}(H) = 1.2(U_{eq}(N)$ and $U_{iso}(H) = 1.5(U_{eq}(O))$. All hydrogen atoms were fixed as riding models.

Figure 3.40 shows the atom labelling and the hydrogen bonds present in the asymmetric unit of this cocrystal structure; it contains one pyrazinamide molecule per one half sebacic acid molecule linked by a strong hydrogen bond.
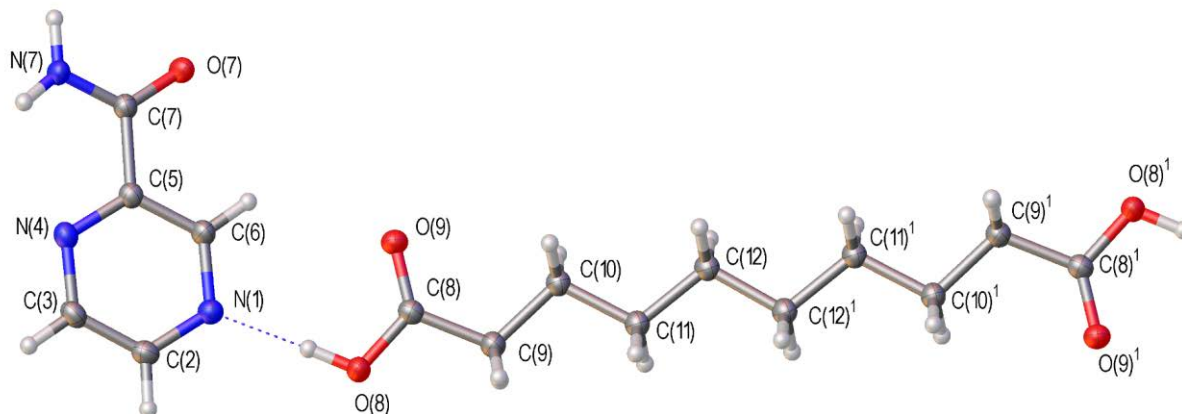
Figure 3.40: The asymmetric unit of the crystal structure of pyrazinamide:sebacic acid (2:1) showing the atom numbering scheme. Strong hydrogen bonds are shown as dotted lines. Atom labels with a superscript denote the crystallographically equivalent half sebacic acid molecule.

The basic supramolecular structure motif within the asymmetric unit (figure 3.40) is formed by one pyrazinamide molecule and one half sebacic acid molecule (that is located on an inversion centre to create the complete molecule). There is a strong acid-pyridine interaction O-H⋯N in which O(8) in the acid acts as a donor via H(8) to the pyridine nitrogen N(1); this is reinforced by a weak hydrogen bond C-H⋯O in which C(6) in the pyrazinamide acts as donor via H(6A) to O(9) in the sebacic acid. These combine to form a $R_2^2(7)$ hydrogen bond ring. There is an N-H⋯N intra molecular hydrogen bond in the pyrazinamide molecule N-H⋯N in which the amide nitrogen N(7A) acts as a donor via H(7A) to the pyridine nitrogen N(4) (as seen in the other structures) which influences the planarity of the pyrazinamide molecule (table 3.16).

Each pyrazinamide molecule is then linked to another through a complementary hydrogen bond N-H⋯O in which the amide nitrogen N(7) acts as a donor via H(7B) to the amide oxygen O(7) to form a complementary $R_2^2(8)$ pyrazinamide dimer rings. Finally, these units are linked together into an infinite chain through the sebacic acid lying on an inversion centre (figure 3.41).

Table 3.16: Intermolecular hydrogen bond distances (Å) and angles (°) within the pyrazinamide:sebacic acid.

D-H-A	d(D-H)	d(H⋯⋯A)	d(D⋯⋯A)	<(DHA)
N(7)-H(7A)⋯O(7)^{iii}	0.86	2.54	3.178(13)	130
N(7)-H(7B)⋯O(7)^{iv}	0.91	1.97	2.887(14)	177
N(7)-H(7A)⋯N(4)	0.86	2.36	2.738(13)	106
O(8)-H(8)⋯N(1)	0.92	1.79	2.714(13)	177
C(2)-H(2A)⋯O(9)^{ii}	0.95	2.36	3.247(15)	154
C(3)-H(3A)⋯O(7)^{ii}	0.95	2.54	3.383(14)	147
C(6)-H(6A)⋯O(9)	0.95	2.60	3.285(14)	129

Symmetry code: i) -x+3,-y+3,-z+1 ii) x-1,y-1,z iii) x-1,y,z iv) -x,-y+3,-z
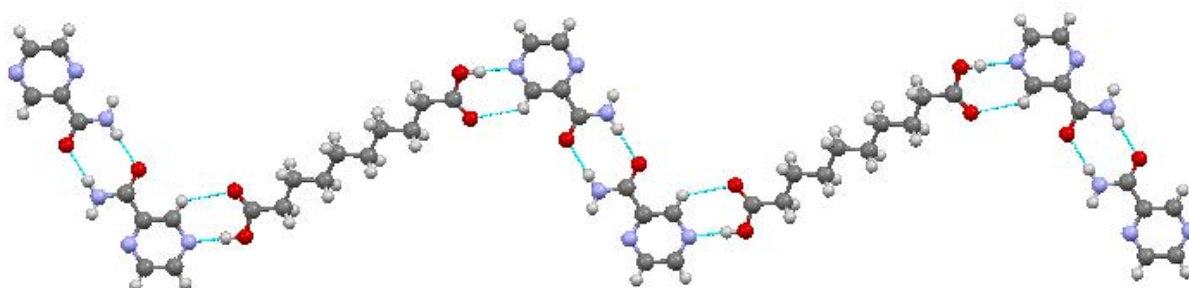
Figure 3.41: A view of the pyrazinamide:sebacic acid (2:1) cocrystal structure showing the acid-pyridine and pyrazinamide hydrogen bonded rings forming an infinite chain. Hydrogen bonds are shown as thin light blue lines.

These hydrogen bonded chains are then linked to a neighbouring parallel chains through two additional weak C-H⋯O hydrogen bonds in which C(2) in pyrazinamide acts as a donor via H(2A) to O(9) in sebacic acid and C(3) in pyrazinamide acts as a donor via H(3A) to O(7) in the neighbouring pyrazinamide molecule (figure 3.42). This network brings the chains together to form an infinite molecular sheet.

Finally these hydrogen bonded sheets interact with others above and below through a single strong N-H⋯O hydrogen bond in which N(7) in pyrazinamide acts as a donor via H(7A) to O(7) in the in the neighbouring pyrazinamide molecule (figure 3.43).

All strong hydrogen bonding donor and acceptor sites are involved in the hydrogen-bonding network in this structure.
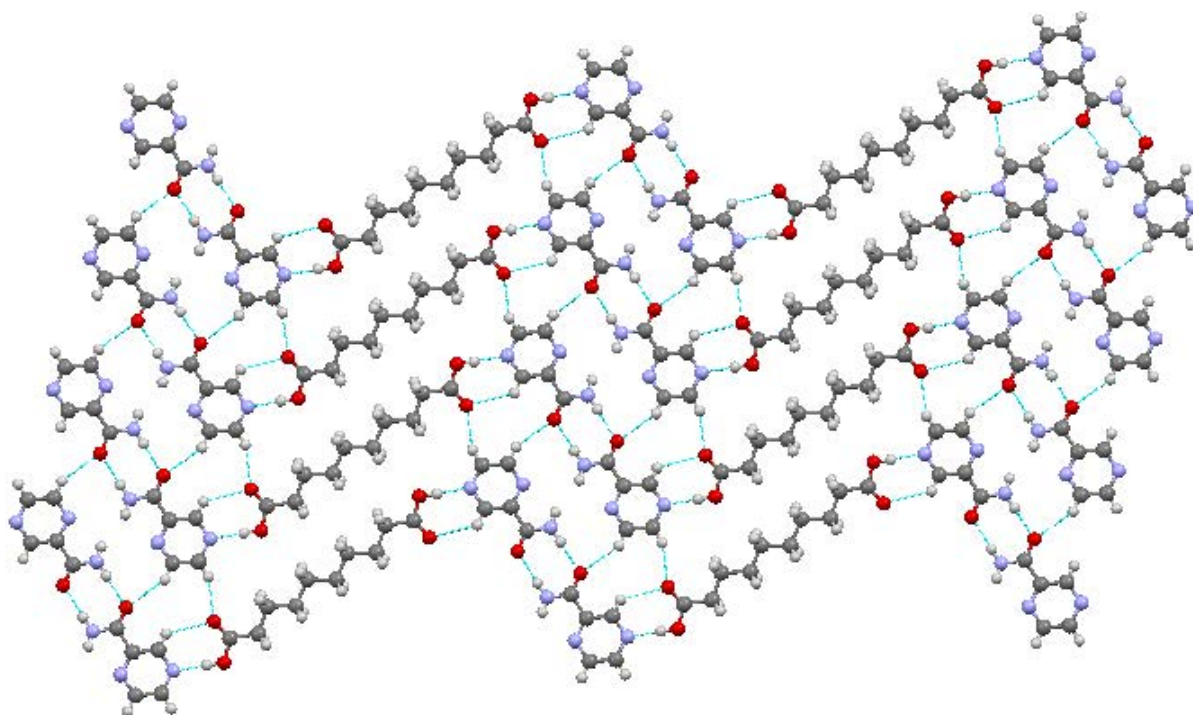
Figure 3.42: A view of the pyrazinamide:sebacic acid (2:1) cocrystal structure showing the infinite molecular sheet.
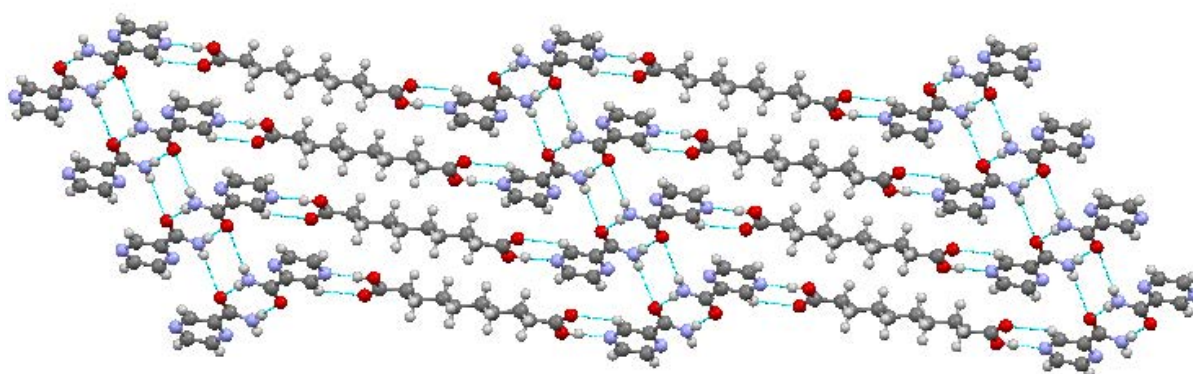
Figure 3.43: A view of the pyrazinamide:sebacic acid (2:1) cocrystal structure showing the hydrogen bonded sheets through a single strong hydrogen bond.

The bond lengths and torsion angles within the pyrazinamide:sebacic acid cocrystal are given in Table 3.17. The bond lengths C(7)-N(7) and C(7)-O(7) are 1.328(15) and 1.240(14) respectively and confirm the orientation of the amide group. In the acid, the bonds lengths C(8)-O(8) and C(8)-O(9) are 1.332(14) and 1.211(14) respectively, showing a clear distinction between the C=O and C-O(H) components of the carboxylic acid functional group, hence confirming that there is no proton transfer between the neutral components in this cocrystal structure.

The torsion angles within the pyrazinamide molecule N(4)-C(5)-C(7)-N(7) and C(6)-C(5)-C(7)-N(7) are 10.93(16) and -168.66(11) respectively and show a slight deviation from planarity. The molecule is partially stabilized by the intramolecular N-H⋯N interaction which would result in a planar conformation, but other intermolecular interactions also effect this conformation and those formed by the amide group are most likely to cause distortion of the expected conformation.

The torsion angles within the sebacic acid molecule O(8)-C(8)-C(9)-C(10) and O(9)-C(8)-C(9)-C(10) are -173.30(10) and 7.27(18) and show a slight deviation from planarity and arises from interactions formed by the acid to pyridine acceptor. The other torsion angles show that overall the molecule is approximately planar and adopts the conformation expected in this type of diacid with an even chain length.

Table 3.17: Selected intramolecular bond lengths and torsion angles within the pyrazinamide: sebacic acid (2:1) cocrystal.

Pyrazinamide Bond Lengths	(Å)	Acid Bond Lengths	(Å)
C(7)-N(7)	1.328(15)	C(8)-O(8)	1.332(14)
C(7)-O(7)	1.240(14)	C(8)-O(9)	1.211(14)
Pyrazinamide Torsion Angles	(º)	Acid Torsion Angles	(º)
N(4)-C(5)-C(7)-N(7)	10.93(16)	O(8)-C(8)-C(9)-C(10)	-173.30(10)
N(4)-C(5)-C(7)-O(7)	-168.86(10)	O(9)-C(8)-C(9)-C(10)	7.27(18)
C(6)-C(5)-C(7)-O(7)	11.54(17)	C(8)-C(9)-C(10)-C(11)	173.33(10)
C(6)-C(5)-C(7)-N(7)	-168.66(11)	C(9)-C(10)-C(11)-C(12)	-179.23(10)
		C(10)-(11)-C(12)-C(12)[1]	178.63(12)
		C(11)-C(12)-C(12)[1]-C(11)[1]	180.00

The synthesis of this pyrazinamide:sebacic acid (2:1) adduct was also attempted using different methods of synthesis and their X-ray powder diffraction patterns were compared with each other. The X-ray powder diffraction of the product obtained through solvent evaporation matches that obtained from solvent drop-grinding although there is more excess sebacic acid also present in the ground sample (figure 3.44). The crystal structure of pyrazinamide:sebacic acid (2:1) was determined at low temperature and hence some peak positions are shifted relative to the experimental room temperature data. The bulk powder patterns clearly show a match to the simulated single crystal pattern but there are also a number of differences that arise from the bulk sample being a mixture and the possible presence of preferred orientation.
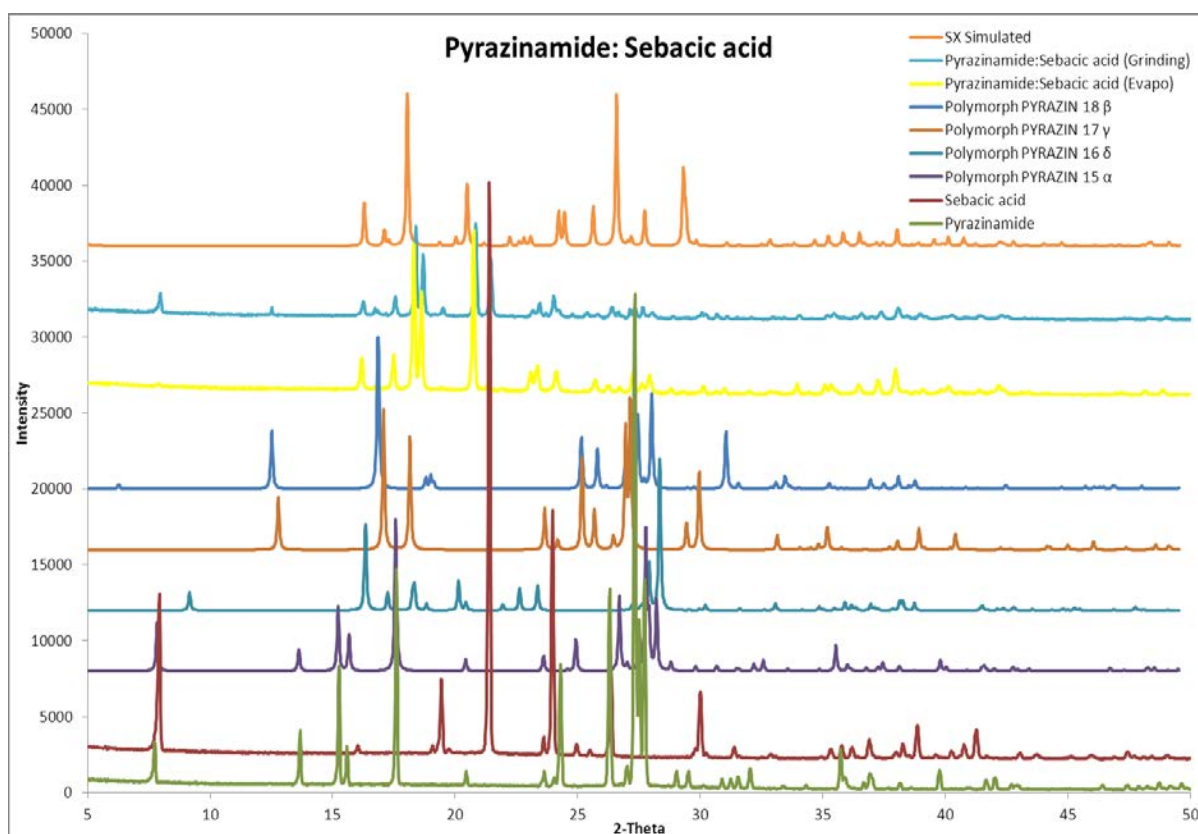
Figure 3.44: X-ray powder diffraction patterns of the products of pyrazinamide and sebacic acid crystallisation from methanol through different method of synthesis, the starting materials (pyrazinamide, sebacic acid), common pyrazinamide polymorphs and the simulated pattern from the single crystal structure.

3.13   **Pyrazinamide and isonicotinamide**

Pyrazinamide was crystallised with isonicotinamide using the solvent evaporation method with methanol used as the solvent to dissolve the starting materials in a 1:1 stoichiometric ratio. The new product formed was a white solid. The X-ray powder diffraction pattern of the product formed is different to that of the starting materials but when compared to the simulated patterns of previously published pyrazinamide polymorphs[76,83,97,98], It can be seen form the figure 3.45 that the product contains a mixture of a small amount of the starting materials with the formation of an additional pyrazinamide polymorph (δ (PYRAZIN16))[98].
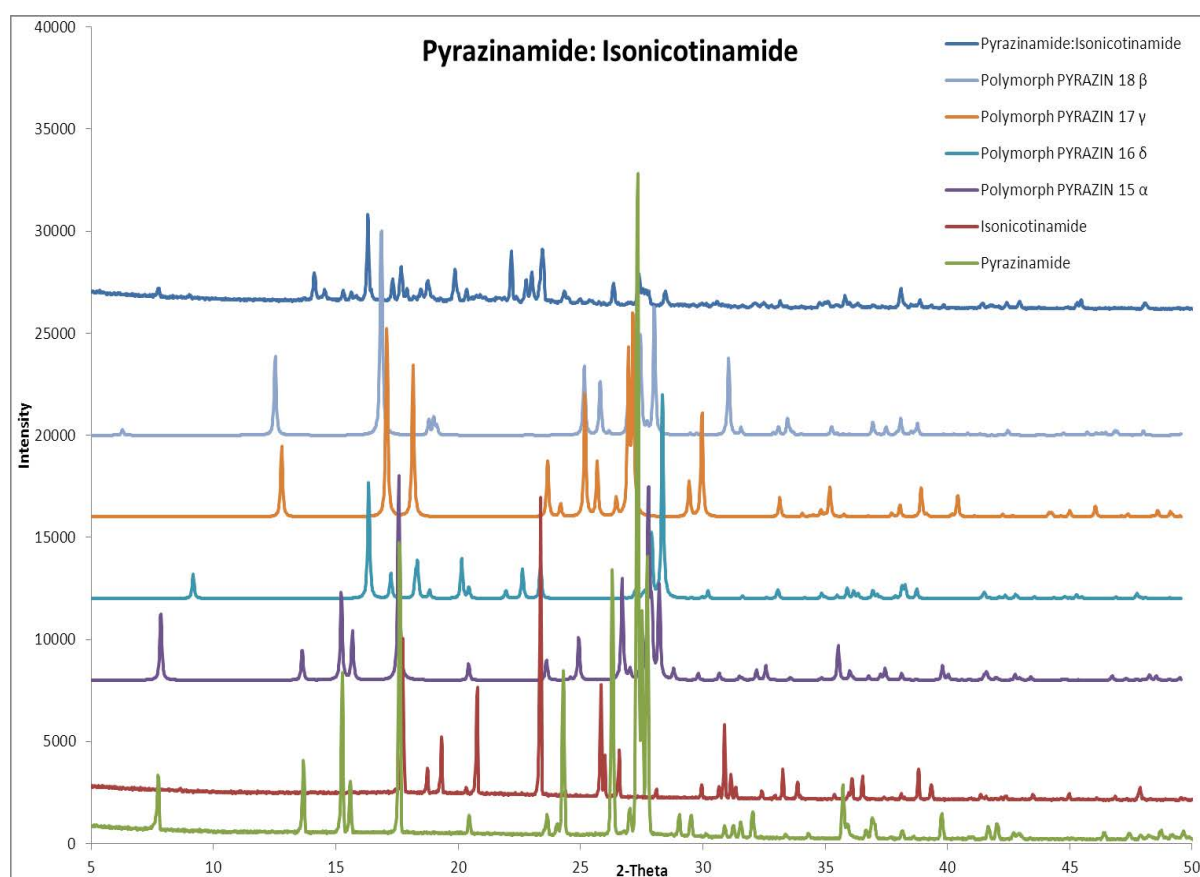
Figure 3.45: X-ray powder diffraction patterns of the product of pyrazinamide and isonicotinamide crystallisation from methanol, the starting materials (pyrazinamide, isonicotinamide) and common pyrazinamide polymorphs.

3.14 <u>Pyrazinamide and nicotinamide</u>

Pyrazinamide was dissolved with nicotinamide using methanol as the solvent in a 1:1 stoichiometric ratio and the solvent evaporation method used for crystallisation. The product formed was a white solid. The X-ray powder diffraction pattern of the product shows clearly that the product is a mixture of starting materials, predominantly nicotinamide. The figure 4.46 also shows that the product also contains a small amount of polymorph (β (PYRAZIN18))[76].
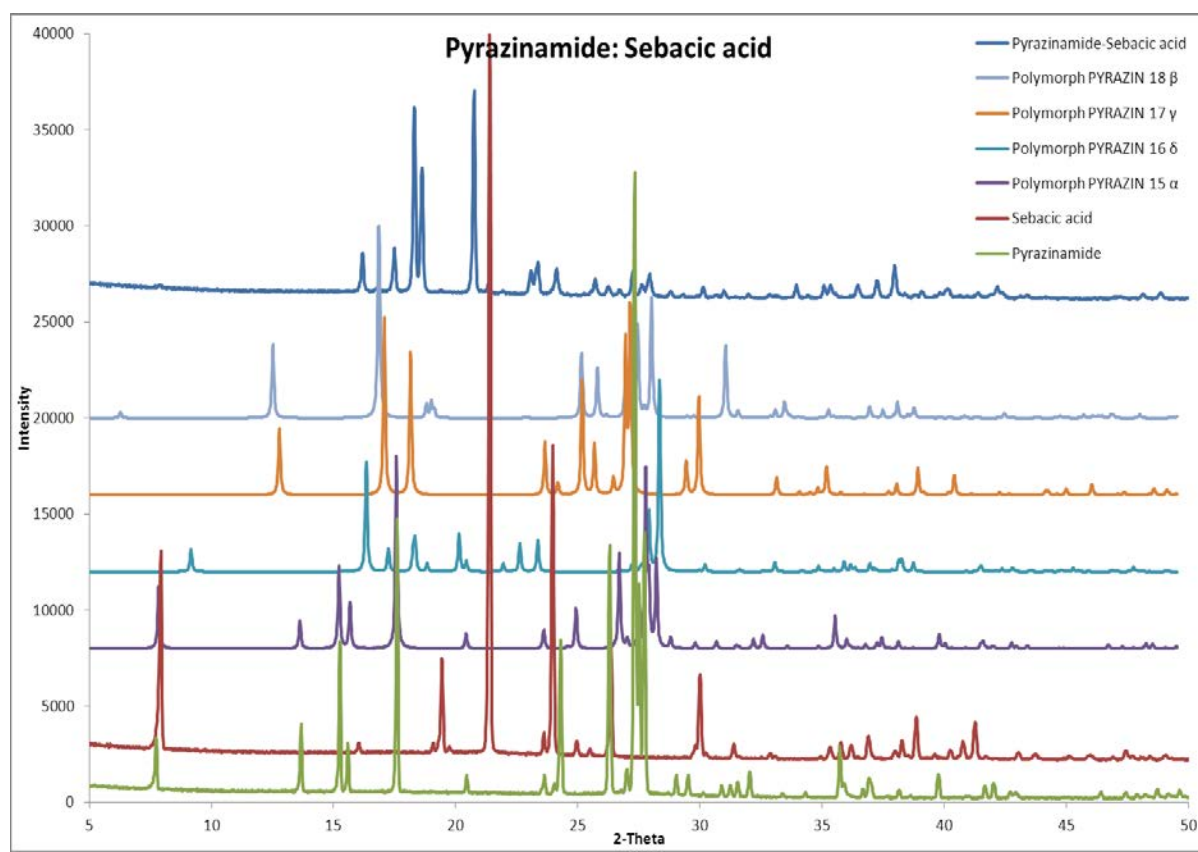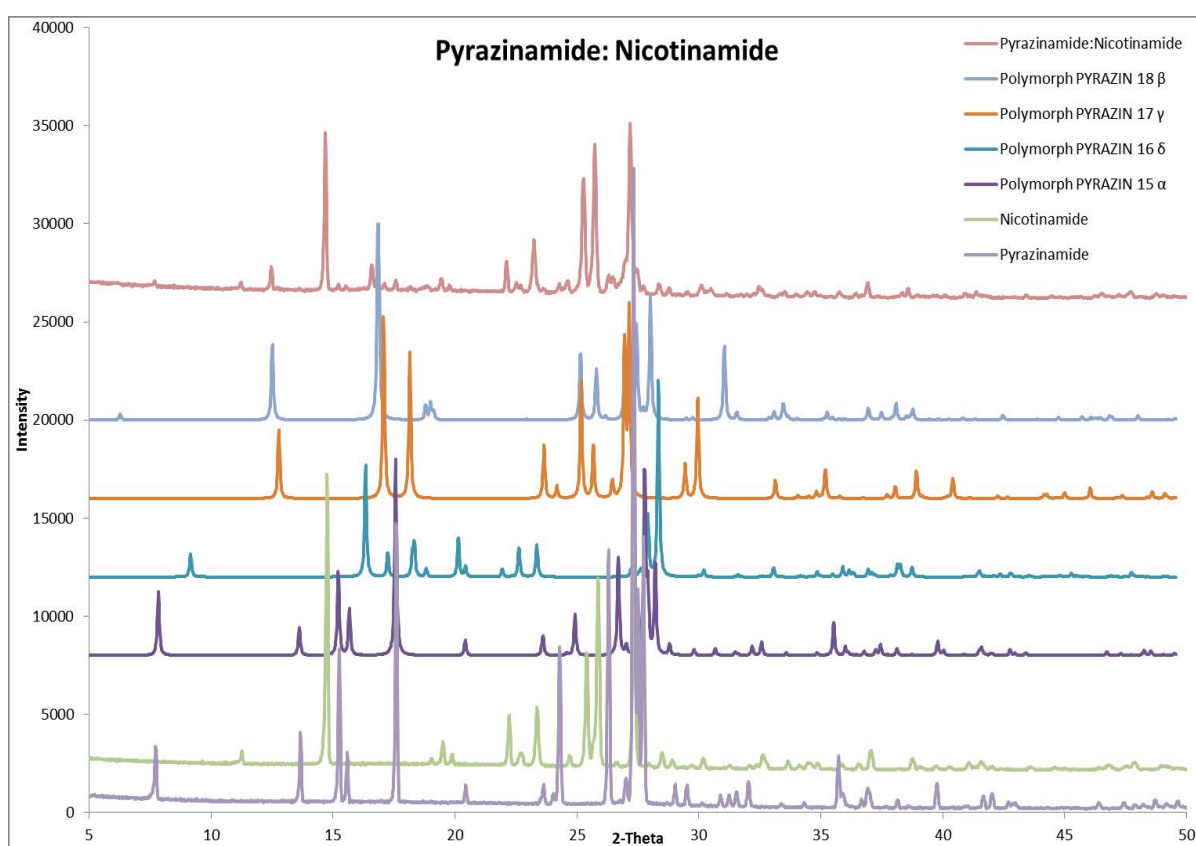

Figure 4.46: X-ray powder diffraction patterns of the product of pyrazinamide and nicotinamide crystallization from methanol, the starting materials (pyrazinamide, nicotinamide) and common pyrazinamide polymorphs.

3.15   <u>Pyrazinamide and histidine</u>

In this case, pyrazinamide was ground with histidine in a 1:1 starting stoichiometric ratio using the solvent drop grinding method for synthesis; some drops of methanol were used as the solvent for this process. Histidine is insoluble in alcohols and acids and therefore the solvent evaporation method was not used for synthesis here. The product formed was a white solid. The X-ray powder diffraction pattern of the product was compared with the powder patterns of the starting materials and confirmed that the product is a mixture of starting materials and that no new material has been formed (figure 4.47).
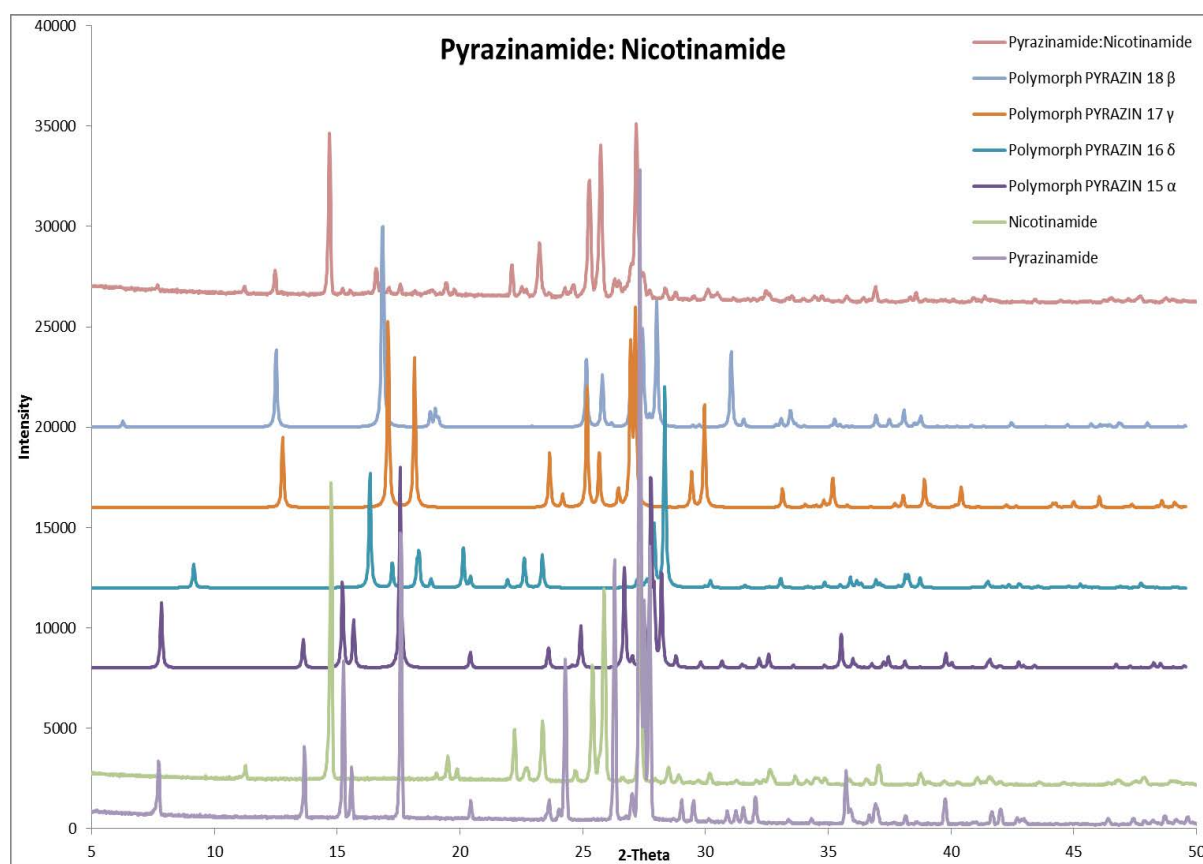
Figure 4.47: X-ray powder diffraction pattern of the product of pyrazinamide and histidine using the solvent drop grinding method, the starting materials (pyrazinamide, histidine) and common pyrazinamide polymorphs.

3.16 <u>Nicotinamide and isonicotinamide</u>

Nicotinamide was crystallised with isonicotinamide using methanol as the solvent with the components in a number of different stoichiometric ratios (1:1, 1:2 and 2:1). All new products were formed as white solids. The X-ray powder diffraction pattern of products formed confirms the formation of a new material in the 1:1 synthesis. This product is also formed in the 1:2 synthesis with excess isonicotinamide present (see peaks at 18º, 21º and 24º 2-theta) , whereas in the 2:1 synthesis, the same product was formed in a mixture with excess nicotinamide present (see peaks at 15º, 25º and 27º 2-theta) (figure 4.48).
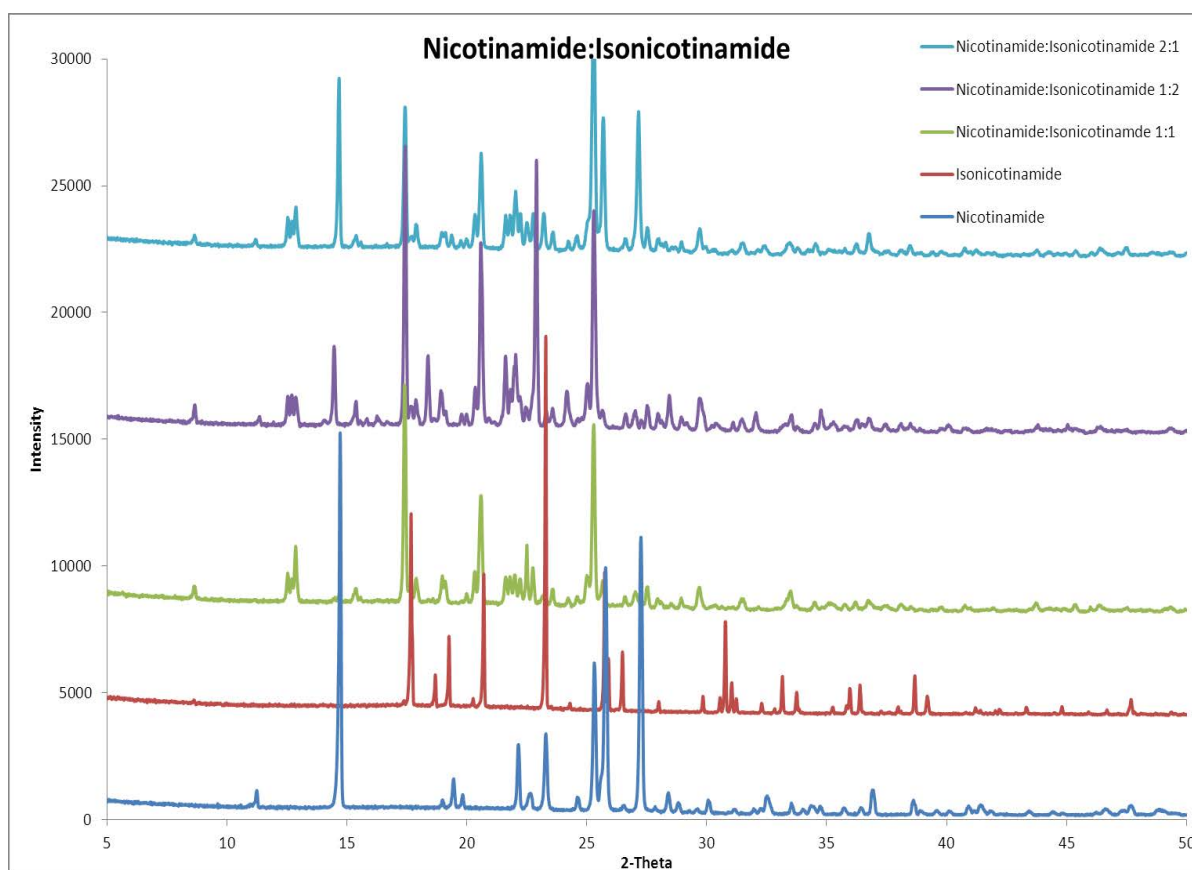
Figure 4.48: X-ray powder diffraction patterns of the products of nicotinamide and isonicotinamide crystallisation from methanol from different stoichiometric ratios (1:1, 1:2, and 2:1) and the starting materials (nicotinamide, isonicotinamide).

3.17 Isonicotinamide and fumaric acid

Isonicotinamide and fumaric acid were dissolved using methanol and crystallised from a 1:1 starting stoichiometric ratio with the solvent evaporation method used for synthesis. The new product formed was a white solid. The X-ray powder diffraction pattern of the material formed was different to that of the starting materials, confirming the formation of a new material. The pattern of this product was also compared with the simulated powder pattern of the previously published isonicotinamide:fumaric acid cocrystal[100]. It can be seen from figure 4.49 that the product matches the published cocrystal structure, demonstrating the success of the synthesis approach used here. Although there is some peak shift present due to the simulated pattern being generated from a low temperature structure, it is clear that product is phase pure.
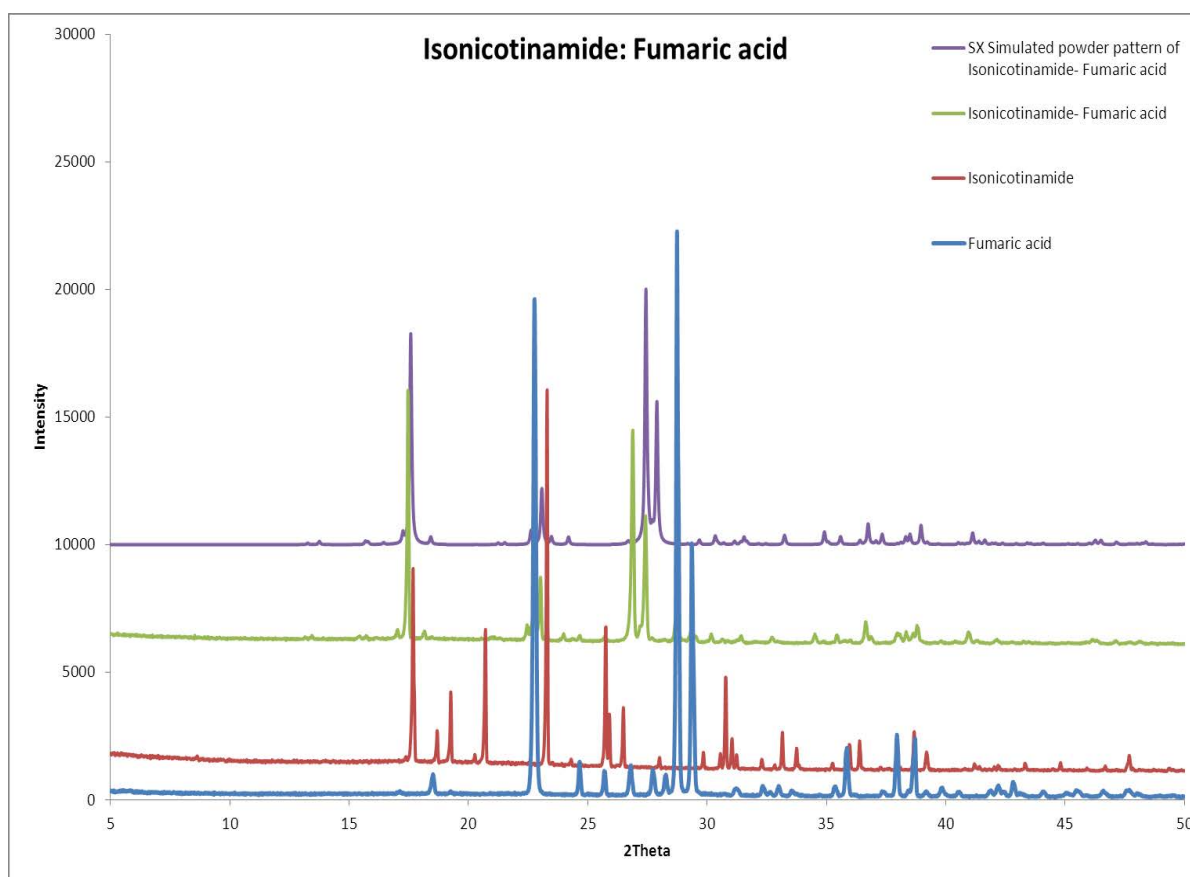
Figure 4.49: X-ray powder diffraction patterns of the product of isonicotinamide and fumaric acid crystallisation from methanol, the starting materials (isonicotinamide, fumaric acid), and the simulated powder pattern from the published isonicotinamide:fumaric acid cocrystal structure.

3.18   L-dopamine and succinic acid

L-dopamine was ground with succinic acid in a 1:1 starting stoichiometric ratio using the solvent drop grinding method for synthesis; some drops of methanol were used. L-dopamine is slightly soluble in water but insoluble in alcoholic slovents therefore the solvent evaporation method was not used for synthesis here. The product formed was a white solid. The X-ray powder diffraction pattern of product formed is clearly a match to a combination of the patterns of the starting materials, confirming that this is a mixture of the starting materials and there is no new material has been formed (figure 4.50).
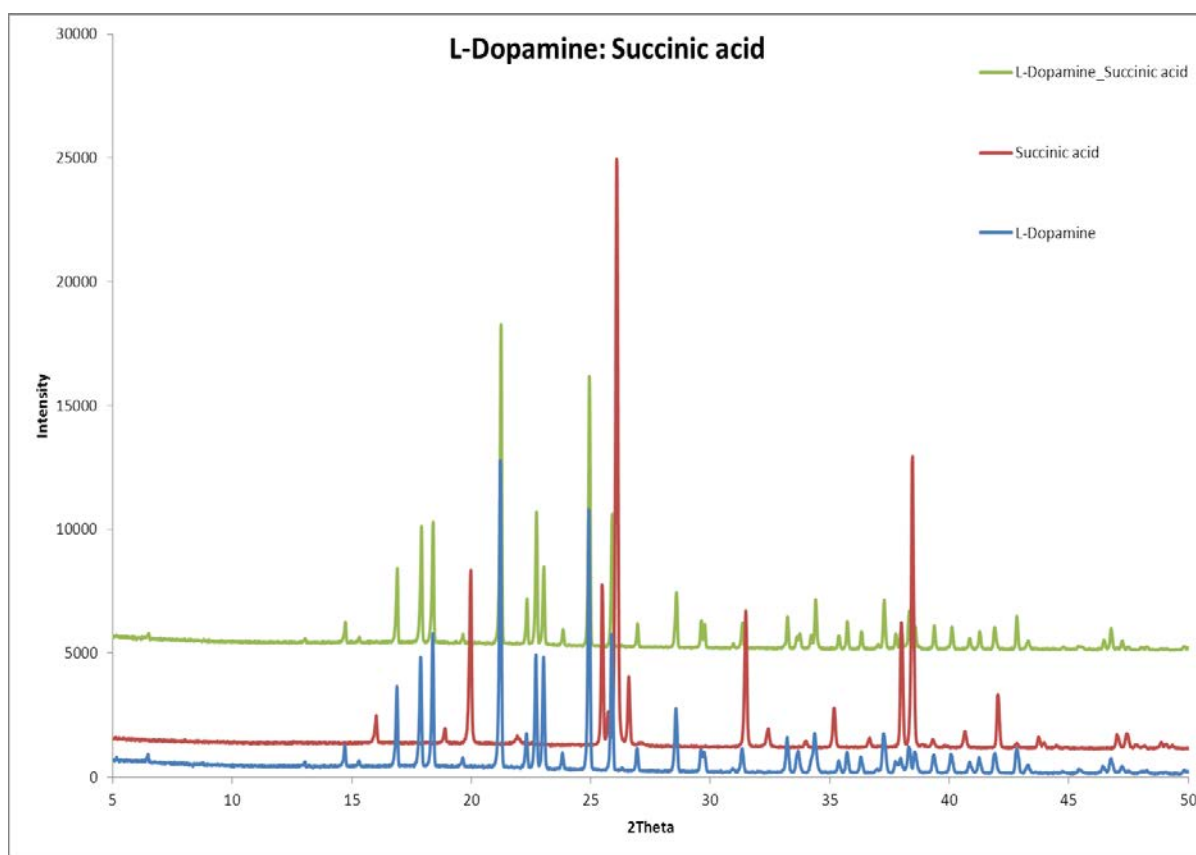
Figure 4.50: X-ray powder diffraction pattern of product of L-dopamine and succinic acid from grinding and the staring materials (l-dopamine, succinic acid).

Table 3.18: Summary of new cocrystals formed.

Combination	Product	Polymorph	Stoichiometric ratio	SX Structure
Pyrazinamid:oxalic acid	New product		1:1	
Pyrazinamide:oxamic acid	Mixture	γ(PYRAZIN17)	1:1	
Pyrazinamide:malonic acid	New product	δ(PYRAZIN16), γ(PYRAZIN17)	1:1	
Pyrazinamide:maleic acid	New product	γ(PYRAZIN17)	1:1	
Pyrazinamide:fumaric acid	New product		1:1	
Pyrazinamide:succinic acid	Mixture		1:1	
Pyrazinamide:glutaric acid	New product	γ(PYRAZIN17)	1:1	Cocrystal (1:1)
Pyrazinamide:adipic acid	New product	β (PYRAZIN18)	1:1	Cocrystal (4:1)
Pyrazinamide:pimelic acid	New product	α(PYRAZIN15, δ(PYRAZIN16	1:1,1:2, 2:1	Cocrystal (1:1)
Pyrazinamide:subaric acid	Mixture		1:1	
Pyrazinamide:azelaic acid	New product	α(PYRAZIN15)	1:1	Polymorph Cocrystal (2:1)
Pyrazinamide:sebacic acid	New product		1:1	
Pyrazinamide:isonicotinamide	New product	δ (PYRAZIN16)	1:1	
Pyrazinamide:nicotinamide	Mixture	β (PYRAZIN18)	1:1	
Pyrazinamide:histidine	Mixture		1:1	
Nicotinamide:Isonicotinamide	New product		1:1,1:2, 2:1	
Isonicotinamide:fumaric acid	New product		1:1	
L-dopamine:succinic acid	Mixture		1:1	

4. <u>Conclusion</u>

A number of cocrystals were synthesised from pyrazinamide with dicarboxylic acid (oxalic, oxamic, malonic, maleic, fumaric, succinic, glutaric, adipic, pimelic, subaric, azelaic and sebacic acid) using either slow solvent evaporation or solvent drop grinding methods and methanol, ethanol, propanol or ethyl acetate as a solvent in a different combination of stoichiometric ratios. Most of the products were formed employing methanol as the solvent while pyrazinamide:pimelic acid cocrystals were formed by using different solvents (methanol, ethanol, propanol or ethyl acetate) and all the products formed were of similar purity.

^{1}H NMR spectroscopy confirmed that the cocrystals formed had stoichiometric ratios of pyrazinamide:oxalic acid (1:1), pyrazinamide:oxamic acid (1:1), pyrazinamide:fumaric (2:1), pyrazinamide:succinic acid (3:2), pyrazinamide:maleic acid (1:1), pyrazinamide:glutaric acid (1:1), pyrazinamide:adipic acid (2:3), pyrazinamide:pimelic acid (1:1), pyrazinamide:subaric acid (1:1), pyrazinamide: azelaic acid (1:1), pyrazinamide:sebacic acid (2:1), pyrazinamide:isonicotinamide (1:1), nicotinamide:isonicotinamide (1:1, 1:2 and 2:1) and isonicotinamide:fumaric acid(1:1).

 X-ray powder diffraction confirmed the formation of new materials of pyrazinamide:oxalic acid, pyrazinamide:fumaric acid, pyrazinamide:maleic acid, pyrazinamie:malonic acid, pyrazinamide:glutaric acid, pyrazinamide:adipic acid, pyrazinamide:pimelic acid, pyrazinamide:azelaic acid, pyrazinamide:sebacic acid, pyrazinamide:isonicotinamide, isonicotinamide:nicotinamide and isonicotinamide:fumaric acid. X-ray powder diffraction indicated that pyrazinamide forms a mixture with oxamic acid, subaric acid, nicotinamide and histidine. It also indicated that the L-dopamine forms a mixture with succinic acid. The product was synthesised through the grinding method, probably due to L-dopamine being insoluble in most alcoholic solvents and therefore it was not possible to obtain a cocrystal of L-dopamine:succnic acid via the slow solvent evaporation method.

The crystal structures of pyrazinamide:glutaric acid (1:1), pyrazinamide:adipic acid (4:1) pyrazinamide:pimelic acid (1:1), pyrazinamide:sebacic acid (2:1) and a polymorph of azelaic acid were determined by single crystal X-ray diffraction analysis. The crystal structure of pyrazinamide:glutaric acid (1:1) includes one molecule of pyrazinamide linked to one molecule of glutaric acid through acid-amide and acid-pyridine hydrogen bonds between the

two molecules forming an infinite chain. The single crystal pattern of the cocrystal product formed matched the simulated single crystal pattern of the previously published structure of pyrazinamide:glutaric acid (1:1)[90]. The crystal structure of pyrazinamide:adipic acid (4:1) includes two molecules of pyrazinamide linked to half a molecule of adipic acid. Again, this structure forms through acid-pyridine and amide-amide hydrogen bonds, forming an infinite chain. The crystal structure of pyrazinamide:pimelic acid (1:1) includes one molecule of pyrazinamide linked with one molecule of pimelic acid through acid-pyridine and acid-amide hydrogen bonds, forming an infinite chain. The crystal structure of pyrazinamide:sebacic acid (2:1) includes one molecule of pyrazinamide linked to half a molecule of sebacic acid through acid-pyridine and amide-amide hydrogen bonds, forming a zigzag chain. The crystal structure of the polymorph of azelaic acid formed a chain through linked molecules of azelaic acid through acid-acid hydrogen bonds.

Future work will investigate other physical properties of pyrazinamide cocrystals such as melting point, solubility, dissolution and bioavailability. Pyrazinamide may form cocrystals with other molecules or indeed other active drug ingredients and through drug-drug cocrystals may increase the therapeutic activity and efficacy of the drugs under consideration.

5. <u>References</u>

1.   C. N. R. Rao, *Bull. Mater. Sci.*, 1993, **16**, 405.

2.   P. Vishweshwar, J. A. McMahon, J. A. Bis and M. J. Zaworotko, *J. Pharm. Sci.*, 2006, **95**, 499.

3.   N. Schulthesis and A. Newman, *Cryst. Growth Des*., 2009, **9**, 2950.

4.   R. Thakuria, A. Delori, W. Jones, M. P. Lipert, L. Roy and N. R. Hornedo, *Int. J. Pharm.*, 2013, **453**, 101.

5.   D. J. Good and N. R. Hornedo, *Cryst. Growth Des*., 2009, **9**, 2252.

6.   B. S. Sekhon, *Ars Pharm*., 2009, **50**, 99.

7.   N. Shan and M. Zaworotko, *Drug Discov. Today*, 2008, **13**, 440.

8.   B. G. Lakatos and B. Szilagy, *Cryst. Growth Des*., 2015, **15**, 5726.

9.   N. Blagden, D. Berry, A. Parkin, H. Javed, A, Ibrahim, P. T.Gavan, L. L. De Matos and C. C. Seaton, *New J. Chem.,* 2008, **32**, 1659.

10.   A. D. Bond, *CrystEngComm.,* 2007, **9**, 833.

11.   Z . H. Stachurski, *Materials*, 2011, **4**, 1564.

12.   M. I. Ojivan and W. E. Lee, *J. Non-Cryst. Solids*, 2010, **356**, 2534.

13.   S. Aitipamula, R. Banerjee, A. Bansal, K. Biradha, M. Cheney, A.Choudhury, G. Desiraju, A. Dikundwar, R. Dubey, N. Duggirala, P. Ghogale, S.Ghosh, P.Goswami, N. Goud, R. Jetti and P. Karpinski, *Cryst. Growth Des*., 2012, **12**, 2147.

14.   D. Braga, F. Grepioni, L. Maini and M. Polito, *Struct. Bond.*, 2009, **132**, 25.

15.   N. J. Badu, L. Reddy, S. Aitipamula and A. Nangia, *Chem. Asian J*., 2008, **3**, 1122.

16.   G. P. Stahly, *Cryst. Growth Des.,* 2007, **7**, 1007.

17.   A. Dahan, J. M. Miller and G. L. Amidon, *AAPS J.*, 2009, **11**, 740.

18.   S. Byrn, R. Pfeiffer and J. Stowell, *Solid State Chemistry of Drugs*, 2nd Edition, West Lafayette 1991.

19.   G. P. Stahly, *Cryst. Growth Des.,* 2009, **9**, 4212.

20.   C. B. Aakeroy and D. J. Salmon, *CrystEngComm.,* 2005, **7**, 439.

21. C. B. Aakeroy, M. Fasulo and J. Desper, *Mol. Pharma*., 2007, **4**, 317.

22. C. B. Aakeroy, I. Hussain and J. Desper, *Cryst. Growth Des*., 2006, **6**, 474.

23. S. Mohamed, D. A. Tocher, M. Vichers, P. G. karamertzanis and S. L. Price, *Cryst. Growth Des.*, 2009, **9**, 2881.

24. A. T. M. Serajuddin, *Adv. Drug Deliv. Rev.*, 2007, **59**, 603.

25. S. L. Childs, G. P. Stahly and A. Park, *Mol. Pharma.,* 2007, **4**, 323.

26. B. R. Bhogala, S. Basavoju and A. Nangia, *CrystEngComm.*, 2005, **7**, 551.

27. K. S. Huang, D. Britton, M. Etter and S. R. Byrn, *J. Mater. Chem*., 1997,**7**, 713.

28. H. N. Po and N. M. Senozan, *J. Chem. Educ*., 2001, **78**, 1499.

29. J. H. Clark and C. W. Jones, *ChemCommun.*, 1990, **24**, 1786.

30. D. A. Haynes, W. Jones and W.D. S. Motherwell, *CrystEngComm.*, 2006, **8**, 830.

31. A. O. Patil, W. T. Pennington, G. R. Desiraju, D. Y. Curtin and I. C. Paul, *Mol. Cryst. Liq. Cryst.*, 1986, **134**, 279.

32. K. Hoogsteen*, Acta Cryst*., 1963, **16**, 907.

33. S. L. Childs and M. J. Zaworotko, *Cryst. Growth Des.,* 2009, **9**, 4208.

34. CSD, Growth of the CSD since 1972 the red bar shows structures added annually, Available online from : http://www.ccdc.cam.ac.uk/solutions/csd-system/components/csd/ [accessed 20 September 2015].

35. R.D.B. Walsh, M.W. Bradner, S.G. Fleischman, L. A. Morales, B. Moulton, N, Rodriguez-Hornedob and M. J. Zaworotko, *Chem. Commun.*, 2003, 186.

36. L. Thompson, R. Voguri, L. Male and M. Tremayne, *CrystEngComm.*, 2011, **13**, 4188.

37. T. Friscic and W. Jones, *Cryst. Growth Des*., 2009, **9**, 1621.

38. C. Kulkarni, C. Wood, A. L. Kelly, Tim. Gough, N. Blagden and A. Paradkar, *Cryst. Growth Des.,* 2015, **15**, 5648.

39.   E. I. Korotkova and B. Kratochvil, *Procedia Chem.*, 2014, **10**, 473.

40.   K. Yamamoto, S. Tsutsumi and Y. Ikeda, *Int. J. Pharm.*, 2012, **437**, 162.

41.   S. Karki, T. Friscic, W. Jones and W. D. S Motherwell, *Mol. Pharmaceutics*, 2007, **4**, 347.

42.   E. Yonemochi, S. Kitahara, S. Maeda, S. Yamamura, T. Oquchi and K. Yamamoto, *Eur. J. Pharm. Sci.,* 1999, **7**, 331.

43.   S. A. Myz, T. P. Shakhtshneider , K. Fucke, A. P. Fedotov, E. V. Boldyreva, V. V. Boldyrev and N. l. Kuleshova, *Mendeleev Commun.,* 2009, **19**, 272.

44.   A. Lemmerer, C. Esterhuysen and J. Bernstein, *J. Pharm. Sci.*, 2010, **99**, 4054.

45.   Z. Rahman, C. Agarabi, A. Zidan, S. Khan and M. Khan, *AAPS. PharmSciTech.*, 2011, **12**, 693.

46.   L. Padrela, M. Rodrigues, S. Velage, A.C. Fernandes and E. G. Azevedo, *J. Supercrit Fluids*, 2010, **53**, 156.

47.   L. Padrela, M. A. Rodrigues, S. P. Velaga, H. A. Matos and E. G. Azevedo, *Eur. J. Pharm. Sci.,* 2009, **38**, 9.

48.   B. S. Sekhon, *Int. J. Pharmtech. Res.*, 2010, **2**, 810.

49.   B. Hargo and K. Ming Ng*, Ind. Eng. Chem. Res.,* 2005, **44**, 8248.

50.   N. Takata, K. Shiraki, R. Takano, Y. Hayashi and K. Terada, *Cryst. Growth Des.*, 2008, **8**, 3032.

51.   T. Kojima, S. Tsutsumi, K. Yamamoto, Y. Ikeda and T. Moriwaki, *Int. J. Pharm.*, 2010, **399**, 52.

52.   L. Padrela, G. E. De Azevedo and P. S. Velaga, *Drug Dev. Ind. Pharm.*, 2012, **38**, 923.

53.   M. A. Elbagerma, H. G. M. Edwards, T. Munshi, M. D. Hargreaves, P. Matousek and I. J. Scowen*, Cryst. Growth Des.,* 2010, **10**, 2360.

54.   K. Maruyoshi, D. Iuga, O. N. Antzutkin, A. Alhalaweh, S. P. Velaga and S.P Brown, *Chem. Commun.,* 2012, **48**, 10844.

55.   Y. Lin, H. Yang and C. Yang and J. wang, *Pharm. Res.,* 2014, **31**, 566.

56.   W. Jounes, W. D. Motherwell and A. V. Trask, *MRS Bulletin*, 2006, **31**, 875.

57.   N. Blagden, S. J. Coles and D. J. Berry, *CrystEngComm.*, 2014, **16**, 5753.

58.   FDA, GRAS list, Available online from :
       http://www.accessdata.fda.gov/scripts/fdcc/?set=SCOGS [accessed 6 May 2016].

59.   T. Higuchi and R. Kuramotor, *J. Am. Pharm. Assoc.,* 1954, **43**, 393.

60.   M. B. Hickey, M. L. Peterson, L. A. Scoppettuolo, S. L. Morrisette, A. Vetter, H.
       Guzman, J. F. Remenar, Z. Zhang. M. D. Tawa, S. Haley, M. J. Zaworotko and O.
       Almarsson, *Eur. J. Pharma. Biopharma*., 2007, **67**, 112.

61.   W. W. Porter, S. C. Elie, and A. J. Matzger, *Cryst. Growth Des.,* 2008, **8**, 14.

62.   S. L. Childs, L. J. Chyall, J. T. Dunlap, V. N. Smolenskaya, B. C. Stahly and G. P.
       Stahly, *J. Am. Chem. Soc*., 2004, **126**, 13335.

63.   M. L. Cheney, D. R. Weynet, N. Shan, M. Hanna, L. Wojtas and M. J. Zaworotko,
       Cryst. Growth Des., 2010, **10**, 4401.

64.   C. B. Aakeroy, A. B. Grommet and J. Desper, *Pharmaceutics*, 2011, **3**, 601.

65.   J. I. Arenas-García, D. Herrera-Ruiz, K. Mondragon-Vaskquez, H. Morales-Rojast
       and H. Hopfl, *Cryst. Growth Des*., 2010, **10**, 3732.

66.   I. Barsky, J. Bernstein, P. W. Stephens and K. H. Stone, *New J. Chem*., 2008, **32**,
       1747.

67.   Y. Ito and S. Arimoto, *J. Phys. Org. Chem*., 2003, **16**, 849.

68.   L. Orola, and M. V.Veidis, *CrystEngComm.*, 2009,**11**, 415.

69.   C. C. Seaton, A. Parkin, C. C. Wilson and N. Blagden, *Cryst. Growth Des.*, 2009, **9**,
       47.

70.   R. Purohit and P. Venugopalan, *Resonance,* 2009, **14**, 882.

71.   L. Borka and J. K Haleblian, *Acta Pharm*., 1990, **40**, 71.

72.   F. Wohler and J. Liebig, *Ann. Pharm*., 1832, **3**, 249.

73.   J. Thun, L. Seyfarth, J. Senker, R. E. Dinnebier and J. Breu, Angew. *Chem. Int. Ed.*, 2007, **46**, 6729.

74.   G. M. Day, A. V. Trask, W. D. Motherwell and W. Jones, *Chem. Commun.,* 2006, **1**, 54.

75.   B. Rodríguez-Spong, C. P. Price, A. Jayasankar, A. J. Matzger and N. Rodriguez-Hornedo, *Adv. Drug Deliv. Rev.*, 2004, **56**, 241.

76.   S. Cherukuvada, R. Thakuria and A. Nangia, *Cryst. Growth Des*., 2010, **10**, 3931.

77.   E. H. Lee, *Asian J. Pharm. Sci.,* 2014, **9**, 163.

78.   P. Espeau, R. Ceolin, J. L. Tamarit, M. A. Perrin, J. P. Gauchi and F. Leveiller, *J. Pharm. Sci.*, 2005, **94**, 524.

79.   P. Bashpa, K. Bijudas, A. M. Tom, P. K. Archana, K. P. Murshida, K. Noufala, K. R. Amritha and K. Vimisha, *Int. J. Chem. Stud*., 2014, **1**, 25.

80.   G. Nichols and C. S. Frampton, *J. Pharm. Sci*., 1998, **87**, 684.

81.   M. A. Steele and R. M Des Prez, *Chest*, 1988, **94**, 845.

82.   S. Cherukuvada and A. Nangia, *CrystEngComm.,* 2012, **14**, 2579.

83.   R. A. E. Castro, T. M. R. Mariat, A. O. L. Evorat, J. C. Feiteira, M. R. Silva, M. A. Beja, J. Canotilho and M. E. S. Eusebio, *Cryst. Growth Des.,* 2010, **10**, 274.

84.   X. Tan, K. Wang , S. Li, H. Yuan, T. Yan, J. Liu. K. Yang, B. Liu, G. Zou and S. Yuan, *J. Phys. Chem. B*., 2012, **116** , 14441.

85.   H. Abourahma, D. S. Coucuzza, J. Melendez and J. M. Urban, *CrystEngComm.*, 2011, **13**, 6442.

86.   Y. Takaki, Y. Sasada, T. Watanabe, *Acta Crystallogr*., 1960, **13**, 693.

87.   G. Ro and H. Sourm, *Acta Crystallogr*. Sect B, 1972, **B28**, 991.

88.   G. Ro and H. Sourm, *Acta Crystallogr*. Sect B, 1972, **B28**, 1677.

89.   C. Tamura, H. Huwano and Y. Sasada, *Acta Crystallogr*., 1961, **14**, 693 .

90.   Y. Luo and B. Sun, *Cryst. Growth Des.,* 2013, **13**, 2098.

91.   J. A. Mcmahon, J. A. Bis, P. Vishweshwar, T. R. Shattock, O. Mclaughlin and M. J. Zaworotko, *Z. Kristallogr.,* 2005, **220**, 340.

92.   S. J. Coles and P. A. Gale, *Chem. Sci.,* 2012, **3**, 683.

93.   Crystal Clear-SM Expert, *Rigaku*, 3.1 b26, 2012.

94.   CrysAlisPro, *Agilent Technologies*, Version 1.171.36.28, 2013.

95.   G. M. Sheldrick, *Acta Cryst.,* 2008, **A64**, 112-122.4.

96.   MestRenova software LITE, Mestrelab research, Version 5.2.5-4731, 2008.

97.   A. Nangia and A. Srinivasulu, *Private Communication CCDC-PYRAZIN15*, 2005.

98.   A. Nangia and A. Srinivasulu, *Private Communication CCDC-PYRAZIN16*, 2005.

99.   J. Housty and M. Hospital, *Acta Crystallogr.,* 1967, **22**, 288.

100.   C. B. Aakeroy, A. M. Beatty and B. A. Helfrich, *J. Am. Chem. Soc.,* 2002, **124**, 14425.

5. <u>Appendices</u>

Appendix A: ^{1}H NMR spectrum

A-1: ^{1}H NMR pyrazinamide:maleic acid
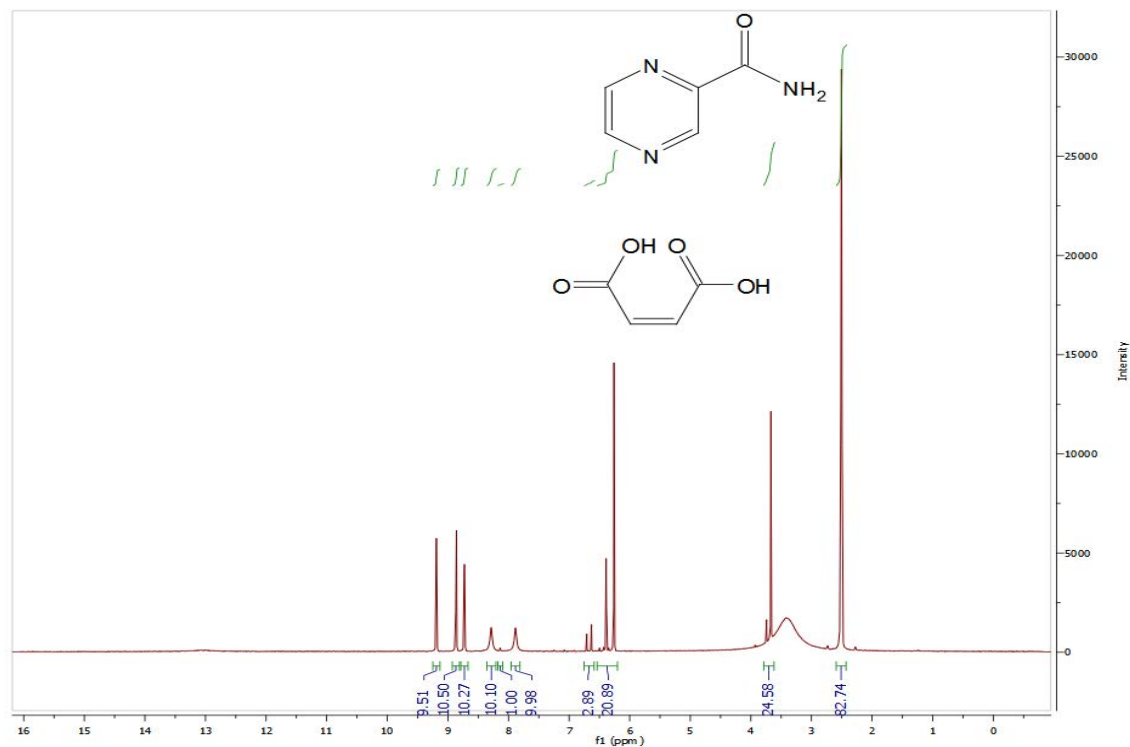
^{1}H NMR pyrazinamide: 7.84 (1H, s), 8.28 (1H, s), 8.73 (1H, t), 8.93(1H, d), 9.18(1H, d)
^{1}H NMR maleic acid: 6.38 (2H, s)

A-2: ^{1}H NMR pyrazinamide:isonicotinamide
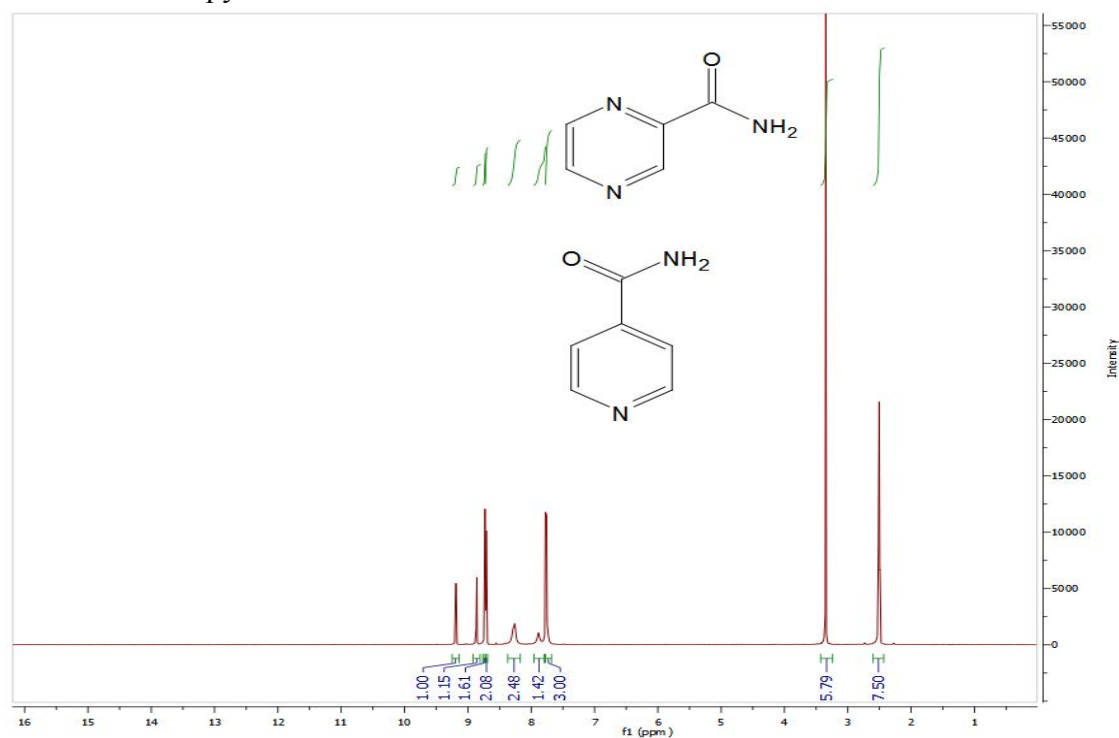
^{1}H NMR pyrazinamide: 7.84 (1H, s), 8.28 (1H, s), 8.73 (1H, t), 8.93(1H, d), 9.18(1H, d)
^{1}H NMR Isonicotinamide: 7.76 (3H, dd), 8.27 (1H, s), 8.74 (2H, dd)

A-3: ¹H NMR pyrazinamide:nicotinamide
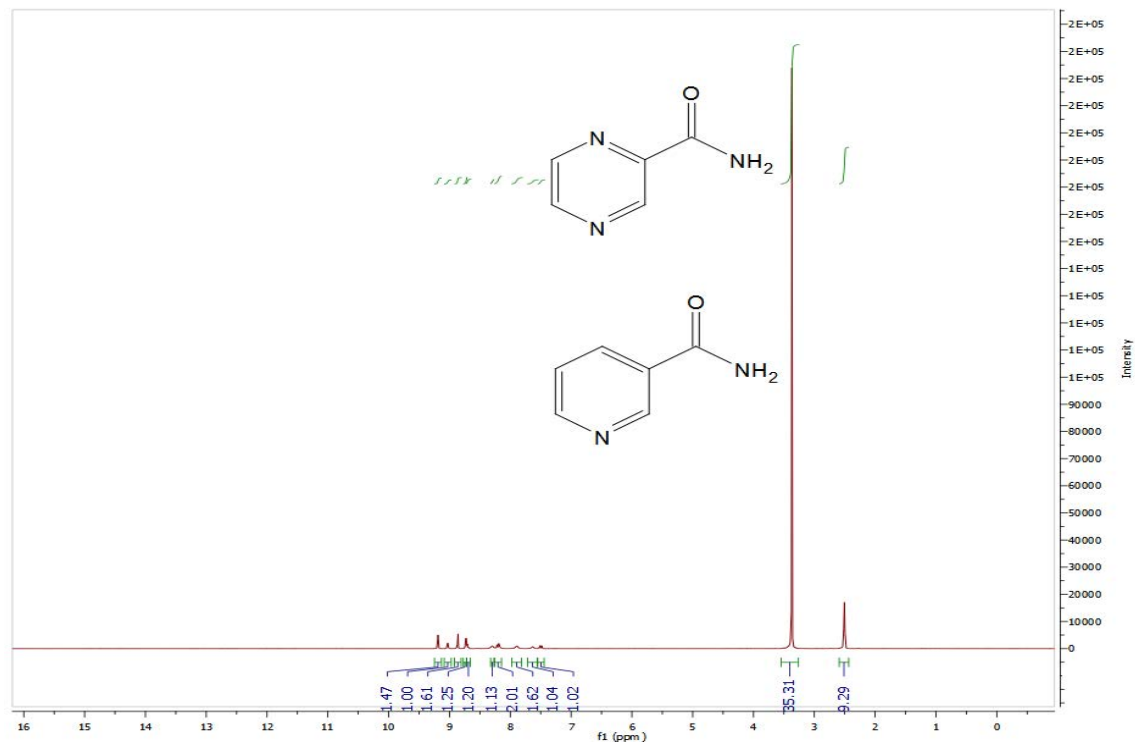
¹H NMR pyrazinamide: 7.89 (1H, s), 8.24 (1H, s), 8.72 (1H, t), 8.87 (1H, d), 9.02 (1H, d)
¹H NMR nicotinamide: 7.51 (1H, q), 7.63(1H, s), 8.18 (2H, dt), 8.70 (1H,dd) , 9.05(1H,d)

A-4: ¹H NMR isonicotinamide:nicotinamide (1:1)
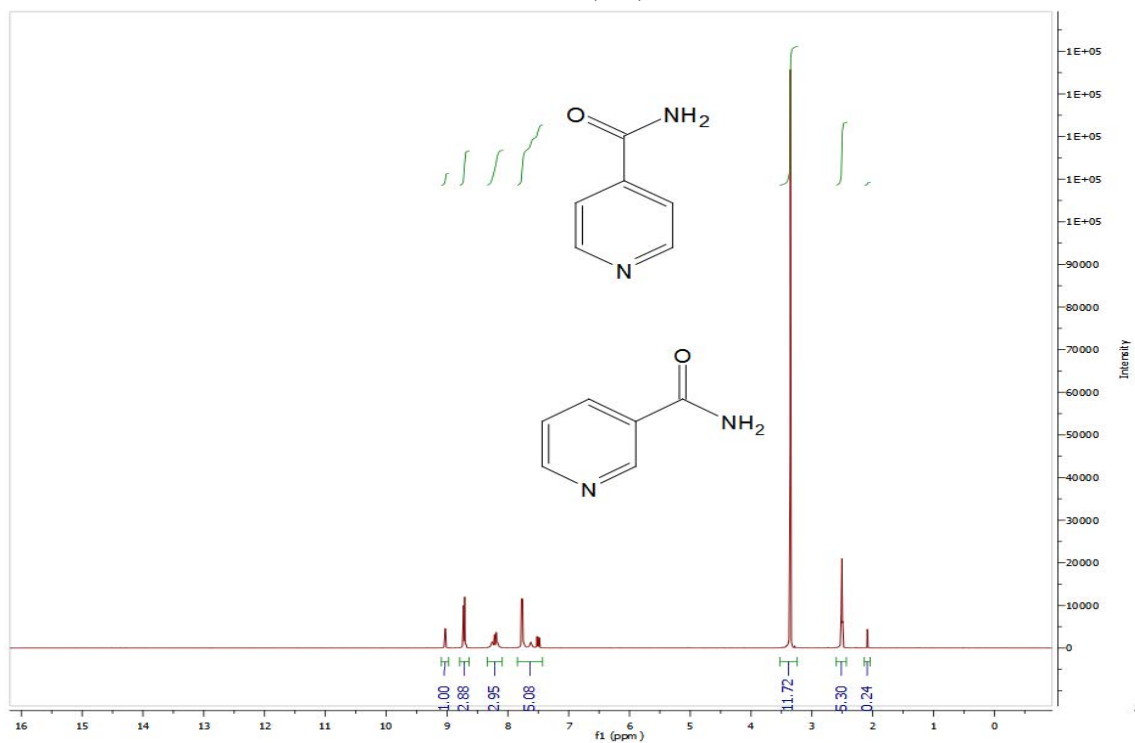
¹H NMR isonicotinamide: 7.76 (3H, dd), 8.27 (1H, s), 8.74 (2H, dd)
¹H NMR nicotinamide: 7.51 (1H, q), 7.63(1H, s), 8.18 (2H, dt), 8.70 (1H,dd) , 9.03(1H,d)

A-5: ^{1}H NMR isonicotinamide:nicotinamide (1:2)
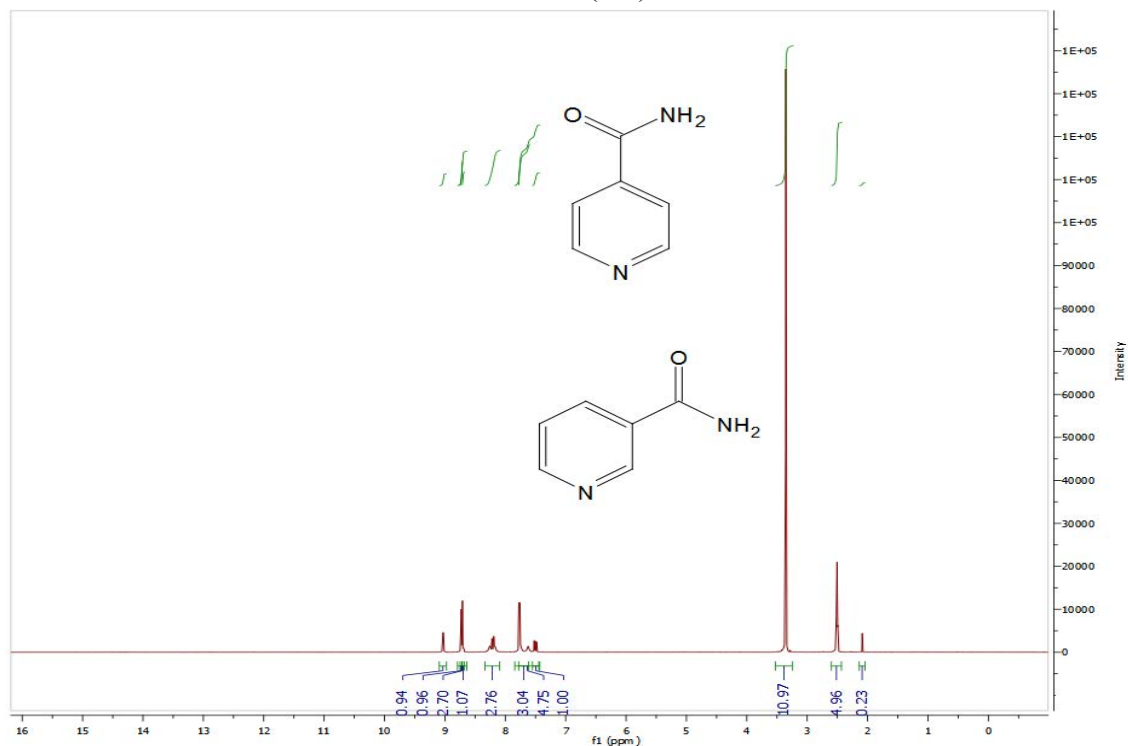
^{1}*H NMR isonicotinamide: 7.76 (3H, dd), 8.27 (1H, s), 8.74 (2H, dd)*
^{1}*H NMR nicotinamide: 7.48 (1H, q), 7.61(5H, s), 8.18 (1H, dt), 8.70 (1H,dd) , 9.03(2H,dd)*

A-6: ^{1}H NMR isonicotinamide:fumaric acid
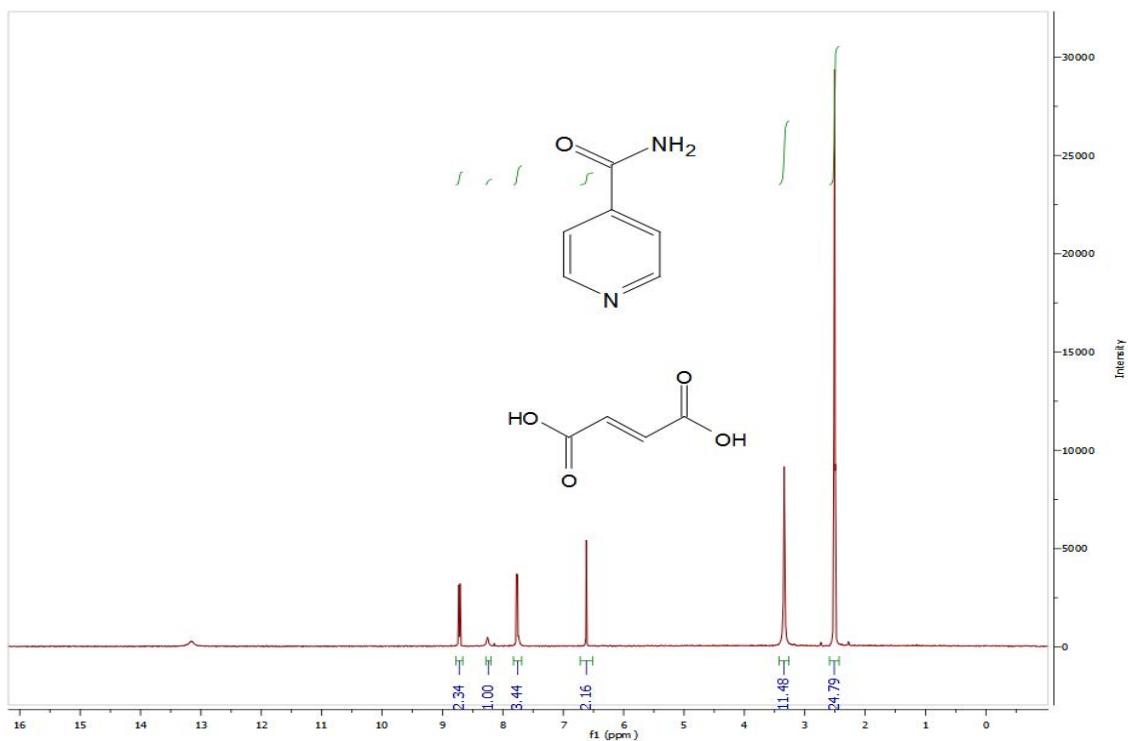
^{1}*H NMR isonicotinamide: 7.76 (3H, dd), 8.27 (1H, s), 8.74 (2H, dd)*
^{1}*H NMR nicotinamide: 6.65 (2H, s)*

Appendix B : CIF file data of crystal structures

B-1: Data_Pyrazinamide_Glutaric

_publ_section_comment
;
The crystal was a non-merohedral twin with the domains
related by 180 degrees about the direct axis [0 0 1]
and the refined percentage domain ratio being 64:36.
;
_audit_creation_method   SHELXL-97
_chemical_name_systematic
;
 ?
;
_chemical_name_common   ?
_chemical_melting_point   ?
_chemical_formula_moiety
 'C5 H5 N3 O1, C5 H8 O4'
_chemical_formula_sum
 'C10 H13 N3 O5'
_chemical_formula_weight   255.23
loop_
 _atom_type_symbol
 _atom_type_description
 _atom_type_scat_dispersion_real
 _atom_type_scat_dispersion_imag
 _atom_type_scat_source
 'C' 'C' 0.0181 0.0091
 'International Tables Vol C Tables 4.2.6.8 and 6.1.1.4'
 'H' 'H' 0.0000 0.0000
 'International Tables Vol C Tables 4.2.6.8 and 6.1.1.4'
 'N' 'N' 0.0311 0.0180
 'International Tables Vol C Tables 4.2.6.8 and 6.1.1.4'
 'O' 'O' 0.0492 0.0322
 'International Tables Vol C Tables 4.2.6.8 and 6.1.1.4'
_symmetry_cell_setting   Monoclinic
_symmetry_space_group_name_H-M   'P 2(1)/c'

loop_
 _symmetry_equiv_pos_as_xyz
 'x, y, z'
 '-x, y+1/2, -z+1/2'
 '-x, -y, -z'
 'x, -y-1/2, z-1/2'

_cell_length_a   11.3844(9)
_cell_length_b   4.8251(7)
_cell_length_c   21.9011(16)
_cell_angle_alpha   90.00
_cell_angle_beta   104.610(9)
_cell_angle_gamma   90.00
_cell_volume   1164.1(2)
_cell_formula_units_Z   4
_cell_measurement_temperature   100(2)

_cell_measurement_reflns_used   1614
_cell_measurement_theta_min   4.1540
_cell_measurement_theta_max   74.1980

_exptl_crystal_description   Plate
_exptl_crystal_colour   Colourless
_exptl_crystal_size_max   0.15
_exptl_crystal_size_mid   0.10
_exptl_crystal_size_min   0.03
_exptl_crystal_density_meas   ?
_exptl_crystal_density_diffrn   1.456
_exptl_crystal_density_method   'not measured'
_exptl_crystal_F_000   536
_exptl_absorpt_coefficient_mu   1.012
_exptl_absorpt_correction_type   Multi-scan
_exptl_absorpt_correction_T_min   0.77183
_exptl_absorpt_correction_T_max   1.00000
_exptl_absorpt_process_details
;
CrysAlisPro, Agilent Technologies,
Version 1.171.36.28 (release 01-02-2013 CrysAlis171 .NET)
(compiled Feb 1 2013,16:14:44)
Empirical absorption correction using spherical harmonics,
 implemented in SCALE3 ABSPACK scaling algorithm.
;
_exptl_special_details
;
 ?
;
_diffrn_ambient_temperature 100.00(10)
_diffrn_radiation_wavelength 1.5418
_diffrn_radiation_type 'Cu K\a'
_diffrn_radiation_source 'SuperNova (Cu) X-ray Source'
_diffrn_radiation_monochromator 'mirror'
_diffrn_measurement_device_type 'SuperNova, Dual, Cu at zero, Atlas'
_diffrn_detector_area_resol_mean 5.1768
_diffrn_standards_number   ?
_diffrn_standards_interval_count ?
_diffrn_standards_interval_time ?
_diffrn_standards_decay_%   ?
_diffrn_reflns_number   3397
_diffrn_reflns_av_R_equivalents 0.0000
_diffrn_reflns_av_sigmaI/netI   0.0256
_diffrn_reflns_limit_h_min   -13
_diffrn_reflns_limit_h_max   13
_diffrn_reflns_limit_k_min   -5
_diffrn_reflns_limit_k_max   5
_diffrn_reflns_limit_l_min   -22
_diffrn_reflns_limit_l_max   26
_diffrn_reflns_theta_min   6.49
_diffrn_reflns_theta_max   66.58
_reflns_number_total   3397
_reflns_number_gt   2837
_reflns_threshold_expression   >2\s(I)

_computing_data_collection
;

CrysAlisPro, Agilent Technologies,
Version 1.171.36.28 (release 01-02-2013 CrysAlis171 .NET)
(compiled Feb 1 2013,16:14:44)
;
_computing_cell_refinement
;
CrysAlisPro, Agilent Technologies,
Version 1.171.36.28 (release 01-02-2013 CrysAlis171 .NET)
(compiled Feb 1 2013,16:14:44)
;
_computing_data_reduction
;
CrysAlisPro, Agilent Technologies,
Version 1.171.36.28 (release 01-02-2013 CrysAlis171 .NET)
(compiled Feb 1 2013,16:14:44)
;
_computing_structure_solution   'SHELXS-97 (Sheldrick, 2008)'
_computing_structure_refinement   'SHELXL-97 (Sheldrick, 2008)'
_computing_molecular_graphics
;
OLEX2 (Dolomanov, O.V., Bourhis, L.J., Gildea, R.J., Howard, J.A.K,
& Puschmann, H., 2009)
;
_computing_publication_material 'WinGX (Farrugia, 1999)'

_refine_special_details
;
 Refinement of F^2^ against ALL reflections. The weighted R-factor wR and
 goodness of fit S are based on F^2^, conventional R-factors R are based
 on F, with F set to zero for negative F^2^. The threshold expression of
 F^2^ > 2\s(F^2^) is used only for calculating R-factors(gt) etc. and is
 not relevant to the choice of reflections for refinement. R-factors based
 on F^2^ are statistically about twice as large as those based on F, and R-
 factors based on ALL data will be even larger.
;
 _refine_ls_structure_factor_coef Fsqd
 _refine_ls_matrix_type   full
 _refine_ls_weighting_scheme   calc
 _refine_ls_weighting_details
 'calc w=1/[\s^2^(Fo^2^)+(0.0675P)^2^+0.0460P] where P=(Fo^2^+2Fc^2^)/3'
 _atom_sites_solution_primary   direct
 _atom_sites_solution_secondary   difmap
 _atom_sites_solution_hydrogens   geom
 _refine_ls_hydrogen_treatment   constr
 _refine_ls_extinction_method   none
 _refine_ls_extinction_coef   ?
 _refine_ls_number_reflns   3397
 _refine_ls_number_parameters   166
 _refine_ls_number_restraints   0
 _refine_ls_R_factor_all   0.0491
 _refine_ls_R_factor_gt   0.0397
 _refine_ls_wR_factor_ref   0.1076
 _refine_ls_wR_factor_gt   0.1037
 _refine_ls_goodness_of_fit_ref   1.049
 _refine_ls_restrained_S_all   1.049
 _refine_ls_shift/su_max   0.000
 _refine_ls_shift/su_mean   0.000

```
loop_
_atom_site_label
_atom_site_type_symbol
_atom_site_fract_x
_atom_site_fract_y
_atom_site_fract_z
_atom_site_U_iso_or_equiv
_atom_site_adp_type
_atom_site_occupancy
_atom_site_symmetry_multiplicity
_atom_site_calc_flag
_atom_site_refinement_flags
_atom_site_disorder_assembly
_atom_site_disorder_group
C2 C 0.89154(13) 2.0494(3) 0.05030(8) 0.0249(3) Uani 1 1 d . . .
H2 H 0.9410 2.1893 0.0391 0.030 Uiso 1 1 calc R . .
C3 C 0.82064(13) 1.8848(3) 0.00340(7) 0.0256(3) Uani 1 1 d . . .
H3 H 0.8242 1.9129 -0.0390 0.031 Uiso 1 1 calc R . .
C5 C 0.74684(13) 1.6590(3) 0.07678(7) 0.0194(3) Uani 1 1 d . . .
C6 C 0.81945(13) 1.8188(3) 0.12416(7) 0.0206(3) Uani 1 1 d . . .
H6 H 0.8176 1.7875 0.1667 0.025 Uiso 1 1 calc R . .
C7 C 0.66383(12) 1.4434(3) 0.09198(7) 0.0188(3) Uani 1 1 d . . .
N1 N 0.89194(11) 2.0156(3) 0.11122(6) 0.0226(3) Uani 1 1 d . . .
N4 N 0.74770(11) 1.6886(3) 0.01577(6) 0.0227(3) Uani 1 1 d . . .
N7 N 0.60145(11) 1.2946(2) 0.04418(6) 0.0205(3) Uani 1 1 d . . .
H7A H 0.5520 1.1640 0.0507 0.025 Uiso 1 1 calc R . .
H7B H 0.6093 1.3261 0.0058 0.025 Uiso 1 1 calc R . .
O7 O 0.65787(9) 1.4118(2) 0.14771(4) 0.0218(2) Uani 1 1 d . . .
C8 C 0.45077(12) 0.8820(3) 0.13900(6) 0.0190(3) Uani 1 1 d . . .
C9 C 0.36751(13) 0.6981(3) 0.16330(7) 0.0208(3) Uani 1 1 d . . .
H9A H 0.4158 0.5796 0.1974 0.025 Uiso 1 1 calc R . .
H9B H 0.3233 0.5755 0.1289 0.025 Uiso 1 1 calc R . .
C10 C 0.27577(13) 0.8666(3) 0.18878(7) 0.0217(3) Uani 1 1 d . . .
H10A H 0.3204 0.9961 0.2216 0.026 Uiso 1 1 calc R . .
H10B H 0.2252 0.9784 0.1540 0.026 Uiso 1 1 calc R . .
C11 C 0.19339(14) 0.6850(3) 0.21685(7) 0.0233(3) Uani 1 1 d . . .
H11A H 0.2447 0.5609 0.2486 0.028 Uiso 1 1 calc R . .
H11B H 0.1473 0.8055 0.2391 0.028 Uiso 1 1 calc R . .
C12 C 0.10484(13) 0.5108(3) 0.16998(7) 0.0213(3) Uani 1 1 d . . .
O8 O 0.51735(10) 1.0470(2) 0.18238(5) 0.0251(3) Uani 1 1 d . . .
H8 H 0.5595 1.1511 0.1656 0.038 Uiso 1 1 calc R . .
O9 O 0.45676(9) 0.8842(2) 0.08404(5) 0.0241(3) Uani 1 1 d . . .
O12 O 0.04475(9) 0.3386(2) 0.19860(5) 0.0264(3) Uani 1 1 d . . .
H12 H -0.0011 0.2373 0.1716 0.040 Uiso 1 1 calc R . .
O13 O 0.08886(9) 0.5219(2) 0.11311(5) 0.0271(3) Uani 1 1 d . . .

loop_
_atom_site_aniso_label
_atom_site_aniso_U_11
_atom_site_aniso_U_22
_atom_site_aniso_U_33
_atom_site_aniso_U_23
_atom_site_aniso_U_13
_atom_site_aniso_U_12
C2 0.0214(7) 0.0252(8) 0.0299(8) 0.0011(7) 0.0097(7) 0.0003(6)
C3 0.0262(7) 0.0299(9) 0.0233(8) 0.0009(7) 0.0107(6) -0.0003(7)
```

C5 0.0194(7) 0.0196(8) 0.0197(7) 0.0007(6) 0.0057(6) 0.0047(6)
C6 0.0207(7) 0.0213(8) 0.0207(7) -0.0018(6) 0.0065(6) 0.0024(6)
C7 0.0184(6) 0.0201(8) 0.0186(7) -0.0005(6) 0.0056(6) 0.0027(6)
N1 0.0198(6) 0.0232(7) 0.0258(7) -0.0029(5) 0.0074(5) 0.0006(5)
N4 0.0227(6) 0.0274(7) 0.0186(7) -0.0005(5) 0.0065(5) -0.0005(5)
N7 0.0234(6) 0.0236(7) 0.0149(6) -0.0022(5) 0.0055(5) -0.0041(5)
O7 0.0251(5) 0.0256(6) 0.0148(5) -0.0012(4) 0.0048(4) -0.0029(4)
C8 0.0190(7) 0.0204(8) 0.0166(7) -0.0008(6) 0.0026(6) 0.0027(6)
C9 0.0238(8) 0.0223(8) 0.0164(7) -0.0014(6) 0.0055(6) -0.0001(6)
C10 0.0247(7) 0.0213(8) 0.0204(7) -0.0024(6) 0.0081(6) -0.0038(6)
C11 0.0247(7) 0.0279(8) 0.0187(7) -0.0033(7) 0.0080(6) -0.0035(6)
C12 0.0175(7) 0.0244(8) 0.0234(8) 0.0003(6) 0.0077(6) 0.0016(6)
O8 0.0292(6) 0.0312(6) 0.0158(5) -0.0046(5) 0.0073(4) -0.0098(5)
O9 0.0293(6) 0.0285(6) 0.0151(5) -0.0036(4) 0.0067(4) -0.0067(5)
O12 0.0269(6) 0.0285(6) 0.0247(6) -0.0041(5) 0.0080(5) -0.0085(5)
O13 0.0252(5) 0.0362(7) 0.0192(6) -0.0034(5) 0.0041(4) -0.0047(5)

_geom_special_details
 All s.u.'s (except the s.u. in the dihedral angle between two l.s. planes)
 are estimated using the full covariance matrix. The cell s.u.'s are taken
 into account individually in the estimation of s.u.'s in distances, angles
 and torsion angles; correlations between s.u.'s in cell parameters are only
 used when they are defined by crystal symmetry. An approximate (isotropic)
 treatment of cell s.u.'s is used for estimating s.u.'s involving l.s. planes.
;

loop_
 _geom_bond_atom_site_label_1
 _geom_bond_atom_site_label_2
 _geom_bond_distance
 _geom_bond_site_symmetry_2
 _geom_bond_publ_flag
C2 N1 1.343(2) . ?
C2 C3 1.385(2) . ?
C2 H2 0.9500 . ?
C3 N4 1.332(2) . ?
C3 H3 0.9500 . ?
C5 N4 1.346(2) . ?
C5 C6 1.386(2) . ?
C5 C7 1.498(2) . ?
C6 N1 1.3345(19) . ?
C6 H6 0.9500 . ?
C7 O7 1.2488(17) . ?
C7 N7 1.3192(19) . ?
N7 H7A 0.8800 . ?
N7 H7B 0.8800 . ?
C8 O9 1.2227(18) . ?
C8 O8 1.3221(17) . ?
C8 C9 1.491(2) . ?
C9 C10 1.535(2) . ?
C9 H9A 0.9900 . ?
C9 H9B 0.9900 . ?
C10 C11 1.522(2) . ?
C10 H10A 0.9900 . ?
C10 H10B 0.9900 . ?
C11 C12 1.501(2) . ?
C11 H11A 0.9900 . ?

C11 H11B 0.9900 . ?
C12 O13 1.2137(18) . ?
C12 O12 1.3295(18) . ?
O8 H8 0.8400 . ?
O12 H12 0.8400 . ?

loop_
_geom_angle_atom_site_label_1
_geom_angle_atom_site_label_2
_geom_angle_atom_site_label_3
_geom_angle
_geom_angle_site_symmetry_1
_geom_angle_site_symmetry_3
_geom_angle_publ_flag
N1 C2 C3 121.50(14) . . ?
N1 C2 H2 119.3 . . ?
C3 C2 H2 119.3 . . ?
N4 C3 C2 122.23(14) . . ?
N4 C3 H3 118.9 . . ?
C2 C3 H3 118.9 . . ?
N4 C5 C6 122.13(14) . . ?
N4 C5 C7 117.19(13) . . ?
C6 C5 C7 120.68(13) . . ?
N1 C6 C5 121.38(14) . . ?
N1 C6 H6 119.3 . . ?
C5 C6 H6 119.3 . . ?
O7 C7 N7 123.91(14) . . ?
O7 C7 C5 119.66(13) . . ?
N7 C7 C5 116.43(13) . . ?
C6 N1 C2 116.74(13) . . ?
C3 N4 C5 116.01(13) . . ?
C7 N7 H7A 120.0 . . ?
C7 N7 H7B 120.0 . . ?
H7A N7 H7B 120.0 . . ?
O9 C8 O8 122.54(14) . . ?
O9 C8 C9 123.72(13) . . ?
O8 C8 C9 113.74(12) . . ?
C8 C9 C10 111.51(12) . . ?
C8 C9 H9A 109.3 . . ?
C10 C9 H9A 109.3 . . ?
C8 C9 H9B 109.3 . . ?
C10 C9 H9B 109.3 . . ?
H9A C9 H9B 108.0 . . ?
C11 C10 C9 112.76(12) . . ?
C11 C10 H10A 109.0 . . ?
C9 C10 H10A 109.0 . . ?
C11 C10 H10B 109.0 . . ?
C9 C10 H10B 109.0 . . ?
H10A C10 H10B 107.8 . . ?
C12 C11 C10 114.96(12) . . ?
C12 C11 H11A 108.5 . . ?
C10 C11 H11A 108.5 . . ?
C12 C11 H11B 108.5 . . ?
C10 C11 H11B 108.5 . . ?
H11A C11 H11B 107.5 . . ?
O13 C12 O12 123.34(14) . . ?
O13 C12 C11 125.31(14) . . ?

O12 C12 C11 111.35(13) . . ?
C8 O8 H8 109.5 . . ?
C12 O12 H12 109.5 . . ?
loop_
 _geom_torsion_atom_site_label_1
 _geom_torsion_atom_site_label_2
 _geom_torsion_atom_site_label_3
 _geom_torsion_atom_site_label_4
 _geom_torsion
 _geom_torsion_site_symmetry_1
 _geom_torsion_site_symmetry_2
 _geom_torsion_site_symmetry_3
 _geom_torsion_site_symmetry_4
 _geom_torsion_publ_flag
N1 C2 C3 N4 1.2(2) . . . . ?
N4 C5 C6 N1 1.7(2) . . . . ?
C7 C5 C6 N1 -178.57(13) . . . . ?
N4 C5 C7 O7 -178.55(13) . . . . ?
C6 C5 C7 O7 1.7(2) . . . . ?
N4 C5 C7 N7 2.1(2) . . . . ?
C6 C5 C7 N7 -177.63(13) . . . . ?
C5 C6 N1 C2 -0.4(2) . . . . ?
C3 C2 N1 C6 -1.0(2) . . . . ?
C2 C3 N4 C5 0.0(2) . . . . ?
C6 C5 N4 C3 -1.4(2) . . . . ?
C7 C5 N4 C3 178.87(13) . . . . ?
O9 C8 C9 C10 -117.84(16) . . . . ?
O8 C8 C9 C10 61.34(16) . . . . ?
C8 C9 C10 C11 -177.22(12) . . . . ?
C9 C10 C11 C12 -68.44(17) . . . . ?
C10 C11 C12 O13 -6.1(2) . . . . ?
C10 C11 C12 O12 173.80(12) . . . . ?

loop_
 _geom_hbond_atom_site_label_D
 _geom_hbond_atom_site_label_H
 _geom_hbond_atom_site_label_A
 _geom_hbond_distance_DH
 _geom_hbond_distance_HA
 _geom_hbond_distance_DA
 _geom_hbond_angle_DHA
 _geom_hbond_site_symmetry_A
N7 H7A O9 0.88 1.98 2.8499(16) 168.1 .
N7 H7B O9 0.88 2.17 2.8515(16) 133.6 3_675
O8 H8 O7 0.84 1.79 2.6167(15) 166.5 .
O12 H12 N1 0.84 1.89 2.7272(16) 178.3 1_435

_diffrn_measured_fraction_theta_max   0.999
_diffrn_reflns_theta_full   66.58
_diffrn_measured_fraction_theta_full   0.999
_refine_diff_density_max   0.179
_refine_diff_density_min -0.217
_refine_diff_density_rms   0.048

B-2: Data_Pyrazinamide_AdipicAcid

```
_audit_creation_method        SHELXL-97
_chemical_name_systematic
;
 ?
_chemical_name_common          ?
_chemical_melting_point        ?
_chemical_formula_moiety
 '4(C5 H5 N3 O), C6 H10 O4'
_chemical_formula_sum
 'C26 H30 N12 O8'
_chemical_formula_weight       638.62

loop_
 _atom_type_symbol
 _atom_type_description
 _atom_type_scat_dispersion_real
 _atom_type_scat_dispersion_imag
 _atom_type_scat_source
 'C' 'C'  0.0181  0.0091
 'International Tables Vol C Tables 4.2.6.8 and 6.1.1.4'
 'H' 'H'  0.0000  0.0000
 'International Tables Vol C Tables 4.2.6.8 and 6.1.1.4'
 'N' 'N'  0.0311  0.0180
 'International Tables Vol C Tables 4.2.6.8 and 6.1.1.4'
 'O' 'O'  0.0492  0.0322
 'International Tables Vol C Tables 4.2.6.8 and 6.1.1.4'

_space_group_crystal_system       triclinic
_space_group_IT_number            2
_space_group_name_H-M_alt         'P -1'
_space_group_name_Hall            '-P 1'

_shelx_space_group_comment
;
The symmetry employed for this shelxl refinement is uniquely defined
by the following loop, which should always be used as a source of
symmetry information in preference to the above space-group names.
They are only intended as comments.
;

loop_
 _space_group_symop_operation_xyz
 'x, y, z'
 '-x, -y, -z'
_cell_length_a                5.1814(8)
_cell_length_b                11.7163(16)
_cell_length_c                12.2250(14)
_cell_angle_alpha             74.708(11)
_cell_angle_beta              87.314(11)
_cell_angle_gamma             85.212(12)
_cell_volume                  713.13(17)
_cell_formula_units_Z         1
_cell_measurement_temperature    100.00(10)
```

_cell_measurement_reflns_used   1781
_cell_measurement_theta_min   3.8960
_cell_measurement_theta_max   74.4610

_exptl_crystal_description   Rod
_exptl_crystal_colour   Colourless
_exptl_crystal_density_meas   ?
_exptl_crystal_density_method   ?
_exptl_crystal_density_diffrn   1.487
_exptl_crystal_F_000   334
_exptl_transmission_factor_min   ?
_exptl_transmission_factor_max   ?
_exptl_crystal_size_max   0.200
_exptl_crystal_size_mid   0.090
_exptl_crystal_size_min   0.060
_exptl_absorpt_coefficient_mu   0.963
_shelx_estimated_absorpt_T_min   0.831
_shelx_estimated_absorpt_T_max   0.944
_exptl_absorpt_correction_type   Multi-scan
_exptl_absorpt_correction_T_min 0.8308
_exptl_absorpt_correction_T_max 0.9445
_exptl_absorpt_process_details
;
CrysAlisPro, Agilent Technologies,
Version 1.171.36.28 (release 01-02-2013 CrysAlis171 .NET)
(compiled Feb 1 2013,16:14:44)
Empirical absorption correction using spherical harmonics,
 implemented in SCALE3 ABSPACK scaling algorithm.
;

_exptl_special_details
;
 ?

_diffrn_ambient_temperature 100.00(10)
_diffrn_radiation_wavelength 1.5418
_diffrn_radiation_type 'Cu K\a'
_diffrn_radiation_source 'SuperNova (Cu) X-ray Source'
_diffrn_radiation_monochromator 'mirror'
_diffrn_measurement_device_type 'SuperNova, Dual, Cu at zero, Atlas'
_diffrn_detector_area_resol_mean 5.1768
_diffrn_reflns_number   4178
_diffrn_reflns_av_unetI/netI   0.0405
_diffrn_reflns_av_R_equivalents 0.0348
_diffrn_reflns_limit_h_min   -6
_diffrn_reflns_limit_h_max   5
_diffrn_reflns_limit_k_min   -13
_diffrn_reflns_limit_k_max   14
_diffrn_reflns_limit_l_min   -14
_diffrn_reflns_limit_l_max   10
_diffrn_reflns_theta_min   7.516
_diffrn_reflns_theta_max   70.053
_diffrn_reflns_theta_full   67.684
_diffrn_measured_fraction_theta_max 0.982
_diffrn_measured_fraction_theta_full 0.990
_diffrn_reflns_Laue_measured_fraction_max 0.982
_diffrn_reflns_Laue_measured_fraction_full 0.990

_diffrn_reflns_point_group_measured_fraction_max 0.982
_diffrn_reflns_point_group_measured_fraction_full 0.990
_reflns_number_total   2666
_reflns_number_gt   2197
_reflns_threshold_expression   'I > 2\s(I)'
_reflns_Friedel_coverage   0.000
_reflns_Friedel_fraction_max   .
_reflns_Friedel_fraction_full   .

_reflns_special_details
;
 Reflections were merged by SHELXL according to the crystal
 class for the calculation of statistics and refinement.

 _reflns_Friedel_fraction is defined as the number of unique
 Friedel pairs measured divided by the number that would be
 possible theoretically, ignoring centric projections and
 systematic absences.
;

_computing_data_collection
;
CrysAlisPro, Agilent Technologies,
Version 1.171.36.28 (release 01-02-2013 CrysAlis171 .NET)
(compiled Feb 1 2013,16:14:44)
;
_computing_cell_refinement
;
CrysAlisPro, Agilent Technologies,
Version 1.171.36.28 (release 01-02-2013 CrysAlis171 .NET)
(compiled Feb 1 2013,16:14:44)
;
_computing_data_reduction
;
CrysAlisPro, Agilent Technologies,
Version 1.171.36.28 (release 01-02-2013 CrysAlis171 .NET)
(compiled Feb 1 2013,16:14:44)
;
_computing_structure_solution   'SHELXS-97 (Sheldrick, 2008)'
_computing_structure_refinement   'SHELXL-2013 (Sheldrick, 2013)'
_computing_molecular_graphics
;
OLEX2 (Dolomanov, O.V., Bourhis, L.J., Gildea, R.J., Howard, J.A.K,
& Puschmann, H., 2009)
;
_computing_publication_material   'WinGX (Farrugia, 1999)'
_refine_special_details
;
 ?
;
_refine_ls_structure_factor_coef Fsqd
_refine_ls_matrix_type   full
_refine_ls_weighting_scheme   calc
_refine_ls_weighting_details
'w=1/[\s^2^(Fo^2^)+(0.1155P)^2^+0.1109P] where P=(Fo^2^+2Fc^2^)/3'
_atom_sites_solution_primary   ?
_atom_sites_solution_secondary   ?

_atom_sites_solution_hydrogens   mixed
_refine_ls_hydrogen_treatment   mixed
_refine_ls_extinction_method   none
_refine_ls_extinction_coef   .
_refine_ls_number_reflns   2666
_refine_ls_number_parameters   223
_refine_ls_number_restraints   0
_refine_ls_R_factor_all   0.0731
_refine_ls_R_factor_gt   0.0623
_refine_ls_wR_factor_ref   0.1780
_refine_ls_wR_factor_gt   0.1642
_refine_ls_goodness_of_fit_ref   1.050
_refine_ls_restrained_S_all   1.050
_refine_ls_shift/su_max   0.000
_refine_ls_shift/su_mean   0.000

loop_
 _atom_site_label
 _atom_site_type_symbol
 _atom_site_fract_x
 _atom_site_fract_y
 _atom_site_fract_z
 _atom_site_U_iso_or_equiv
 _atom_site_adp_type
 _atom_site_occupancy
 _atom_site_site_symmetry_order
 _atom_site_calc_flag
 _atom_site_refinement_flags_posn
 _atom_site_refinement_flags_adp
 _atom_site_refinement_flags_occupancy
 _atom_site_disorder_assembly
 _atom_site_disorder_group
C2A C 0.4085(4) 0.35859(19) -0.07386(19) 0.0263(5) Uani 1 1 d . . . . .
H2A H 0.2676 0.4053 -0.1144 0.032 Uiso 1 1 calc R U . . .
C3A C 0.5801(4) 0.29094(19) -0.12799(19) 0.0270(5) Uani 1 1 d . . . . .
H3A H 0.5523 0.2923 -0.2046 0.032 Uiso 1 1 calc R U . . .
C5A C 0.8115(4) 0.22510(18) 0.03340(18) 0.0235(5) Uani 1 1 d . . . . .
C6A C 0.6400(4) 0.29184(18) 0.08805(18) 0.0245(5) Uani 1 1 d . . . . .
H6A H 0.6662 0.2897 0.1650 0.029 Uiso 1 1 calc R U . . .
C7A C 1.0351(4) 0.15261(18) 0.09798(18) 0.0239(5) Uani 1 1 d . . . . .
N1A N 0.4400(4) 0.35846(15) 0.03390(16) 0.0251(4) Uani 1 1 d . . . . .
N4A N 0.7817(3) 0.22463(16) -0.07480(15) 0.0250(4) Uani 1 1 d . . . . .
N7A N 1.1931(4) 0.08911(16) 0.04328(16) 0.0249(4) Uani 1 1 d . . . . .
H7A1 H 1.163(5) 0.093(2) -0.030(2) 0.034 Uiso 1 1 d . U . . .
H7A2 H 1.327(6) 0.046(2) 0.087(2) 0.034 Uiso 1 1 d . U . . .
O7A O 1.0634(3) 0.15611(14) 0.19676(13) 0.0284(4) Uani 1 1 d . . . . .
C2B C 2.2314(4) -0.22531(19) 0.49135(19) 0.0263(5) Uani 1 1 d . . . . .
H2B H 2.3622 -0.2679 0.5413 0.032 Uiso 1 1 calc R U . . .
C3B C 2.0239(4) -0.16545(19) 0.53444(19) 0.0269(5) Uani 1 1 d . . . . .
H3B H 2.0174 -0.1688 0.6130 0.032 Uiso 1 1 calc R U . . .
C5B C 1.8543(4) -0.10190(18) 0.35921(18) 0.0233(5) Uani 1 1 d . . . . .
C6B C 2.0611(4) -0.16248(19) 0.31587(18) 0.0260(5) Uani 1 1 d . . . . .
H6B H 2.0670 -0.1597 0.2374 0.031 Uiso 1 1 calc R U . . .
C7B C 1.6513(4) -0.02988(19) 0.27996(18) 0.0243(5) Uani 1 1 d . . . . .
N1B N 2.2514(4) -0.22450(17) 0.38192(16) 0.0277(4) Uani 1 1 d . . . . .
N4B N 1.8333(3) -0.10325(16) 0.46885(15) 0.0248(4) Uani 1 1 d . . . . .

N7B N 1.4875(4) 0.04159(17) 0.32306(17) 0.0287(5) Uani 1 1 d . . . . .
H7B1 H 1.510(5) 0.042(2) 0.396(2) 0.033 Uiso 1 1 d . U . . .
H7B2 H 1.355(6) 0.080(2) 0.279(2) 0.033 Uiso 1 1 d . U . . .
O7B O 1.6442(3) -0.03823(13) 0.18110(12) 0.0271(4) Uani 1 1 d . . . . .
C8 C 0.1943(4) 0.44251(18) 0.26678(18) 0.0244(5) Uani 1 1 d . . . . .
C9 C 0.0075(4) 0.4960(2) 0.34221(18) 0.0261(5) Uani 1 1 d . . . . .
H9A H -0.1603 0.4601 0.3468 0.031 Uiso 1 1 calc R U . . .
H9B H -0.0231 0.5821 0.3069 0.031 Uiso 1 1 calc R U . . .
C10 C 0.1036(4) 0.47780(19) 0.46206(18) 0.0260(5) Uani 1 1 d . . . . .
H10A H 0.2611 0.5211 0.4588 0.031 Uiso 1 1 calc R U . . .
H10B H 0.1506 0.3924 0.4953 0.031 Uiso 1 1 calc R U . . .
O8 O 0.1055(3) 0.46106(14) 0.16325(13) 0.0288(4) Uani 1 1 d . . . . .
O9 O 0.3997(3) 0.38959(15) 0.29721(14) 0.0341(4) Uani 1 1 d . . . . .
H8 H 0.211(6) 0.432(3) 0.116(3) 0.051 Uiso 1 1 d . U . . .

loop_
 _atom_site_aniso_label
 _atom_site_aniso_U_11
 _atom_site_aniso_U_22
 _atom_site_aniso_U_33
 _atom_site_aniso_U_23
 _atom_site_aniso_U_13
 _atom_site_aniso_U_12
C2A 0.0287(11) 0.0235(11) 0.0269(11) -0.0092(9) -0.0045(9) 0.0075(9)
C3A 0.0305(11) 0.0289(11) 0.0230(10) -0.0115(9) -0.0050(9) 0.0073(9)
C5A 0.0285(11) 0.0200(10) 0.0236(11) -0.0100(8) -0.0020(8) 0.0029(8)
C6A 0.0291(10) 0.0228(11) 0.0228(10) -0.0100(8) -0.0023(8) 0.0053(8)
C7A 0.0266(11) 0.0228(11) 0.0240(11) -0.0107(9) -0.0027(8) 0.0049(8)
N1A 0.0264(9) 0.0224(9) 0.0270(10) -0.0096(7) -0.0002(7) 0.0061(7)
N4A 0.0291(9) 0.0244(9) 0.0227(9) -0.0106(7) -0.0021(7) 0.0061(7)
N7A 0.0277(9) 0.0262(9) 0.0216(9) -0.0107(7) -0.0045(7) 0.0096(7)
O7A 0.0299(8) 0.0320(9) 0.0245(8) -0.0128(7) -0.0049(6) 0.0114(6)
C2B 0.0289(11) 0.0237(11) 0.0270(11) -0.0091(9) -0.0046(9) 0.0044(8)
C3B 0.0300(11) 0.0268(11) 0.0251(11) -0.0109(9) -0.0044(9) 0.0057(9)
C5B 0.0286(11) 0.0204(10) 0.0228(11) -0.0103(8) -0.0016(8) 0.0026(8)
C6B 0.0309(11) 0.0251(11) 0.0223(11) -0.0089(8) -0.0019(9) 0.0059(9)
C7B 0.0280(11) 0.0235(11) 0.0230(10) -0.0103(8) -0.0028(8) 0.0034(8)
N1B 0.0295(10) 0.0279(10) 0.0261(10) -0.0106(8) -0.0013(7) 0.0067(7)
N4B 0.0294(9) 0.0238(9) 0.0232(9) -0.0111(7) -0.0031(7) 0.0047(7)
N7B 0.0314(10) 0.0312(10) 0.0254(10) -0.0142(8) -0.0047(8) 0.0121(8)
O7B 0.0305(8) 0.0305(8) 0.0216(8) -0.0116(6) -0.0036(6) 0.0084(6)
C8 0.0270(10) 0.0243(11) 0.0227(11) -0.0097(8) -0.0024(8) 0.0066(8)
C9 0.0278(11) 0.0276(11) 0.0249(11) -0.0131(9) -0.0032(8) 0.0081(9)
C10 0.0272(11) 0.0255(11) 0.0271(11) -0.0128(9) -0.0016(9) 0.0071(9)
O8 0.0303(8) 0.0332(9) 0.0251(8) -0.0158(7) -0.0042(6) 0.0147(7)
O9 0.0297(8) 0.0421(10) 0.0324(9) -0.0182(7) -0.0048(7) 0.0156(7)

_geom_special_details
;
 All esds (except the esd in the dihedral angle between two l.s. planes)
 are estimated using the full covariance matrix. The cell esds are taken
 into account individually in the estimation of esds in distances, angles
 and torsion angles; correlations between esds in cell parameters are only
 used when they are defined by crystal symmetry. An approximate (isotropic)
 treatment of cell esds is used for estimating esds involving l.s. planes.
;
loop_

_geom_bond_atom_site_label_1
_geom_bond_atom_site_label_2
_geom_bond_distance
_geom_bond_site_symmetry_2
_geom_bond_publ_flag
C2A N1A 1.335(3) . ?
C2A C3A 1.400(3) . ?
C2A H2A 0.9500 . ?
C3A N4A 1.334(3) . ?
C3A H3A 0.9500 . ?
C5A N4A 1.340(3) . ?
C5A C6A 1.397(3) . ?
C5A C7A 1.502(3) . ?
C6A N1A 1.333(3) . ?
C6A H6A 0.9500 . ?
C7A O7A 1.235(2) . ?
C7A N7A 1.334(3) . ?
N7A H7A1 0.90(3) . ?
N7A H7A2 0.92(3) . ?
C2B N1B 1.335(3) . ?
C2B C3B 1.393(3) . ?
C2B H2B 0.9500 . ?
C3B N4B 1.340(3) . ?
C3B H3B 0.9500 . ?
C5B N4B 1.336(3) . ?
C5B C6B 1.397(3) . ?
C5B C7B 1.508(3) . ?
C6B N1B 1.341(3) . ?
C6B H6B 0.9500 . ?
C7B O7B 1.240(2) . ?
C7B N7B 1.331(3) . ?
N7B H7B1 0.91(3) . ?
N7B H7B2 0.91(3) . ?
C8 O9 1.209(3) . ?
C8 O8 1.324(3) . ?
C8 C9 1.516(3) . ?
C9 C10 1.525(3) . ?
C9 H9A 0.9900 . ?
C9 H9B 0.9900 . ?
C10 C10 1.534(4) 2_566 ?
C10 H10A 0.9900 . ?
C10 H10B 0.9900 . ?
O8 H8 0.89(3) . ?

loop_
_geom_angle_atom_site_label_1
_geom_angle_atom_site_label_2
_geom_angle_atom_site_label_3
_geom_angle
_geom_angle_site_symmetry_1
_geom_angle_site_symmetry_3
_geom_angle_publ_flag
N1A C2A C3A 120.97(19) . . ?
N1A C2A H2A 119.5 . . ?
C3A C2A H2A 119.5 . . ?
N4A C3A C2A 121.71(19) . . ?
N4A C3A H3A 119.1 . . ?

C2A C3A H3A 119.1 . . ?
N4A C5A C6A 121.71(19) . . ?
N4A C5A C7A 119.48(17) . . ?
C6A C5A C7A 118.81(18) . . ?
N1A C6A C5A 121.00(19) . . ?
N1A C6A H6A 119.5 . . ?
C5A C6A H6A 119.5 . . ?
O7A C7A N7A 124.22(19) . . ?
O7A C7A C5A 118.73(17) . . ?
N7A C7A C5A 117.05(18) . . ?
C6A N1A C2A 117.78(17) . . ?
C3A N4A C5A 116.84(17) . . ?
C7A N7A H7A1 119.0(18) . . ?
C7A N7A H7A2 113.7(17) . . ?
H7A1 N7A H7A2 127(2) . . ?
N1B C2B C3B 121.8(2) . . ?
N1B C2B H2B 119.1 . . ?
C3B C2B H2B 119.1 . . ?
N4B C3B C2B 122.3(2) . . ?
N4B C3B H3B 118.9 . . ?
C2B C3B H3B 118.9 . . ?
N4B C5B C6B 122.02(19) . . ?
N4B C5B C7B 118.55(18) . . ?
C6B C5B C7B 119.41(18) . . ?
N1B C6B C5B 121.83(19) . . ?
N1B C6B H6B 119.1 . . ?
C5B C6B H6B 119.1 . . ?
O7B C7B N7B 123.74(19) . . ?
O7B C7B C5B 120.52(18) . . ?
N7B C7B C5B 115.73(18) . . ?
C2B N1B C6B 116.19(18) . . ?
C5B N4B C3B 115.88(18) . . ?
C7B N7B H7B1 117.0(17) . . ?
C7B N7B H7B2 117.2(17) . . ?
H7B1 N7B H7B2 126(2) . . ?
O9 C8 O8 123.99(18) . . ?
O9 C8 C9 124.2(2) . . ?
O8 C8 C9 111.82(17) . . ?
C8 C9 C10 113.57(17) . . ?
C8 C9 H9A 108.9 . . ?
C10 C9 H9A 108.9 . . ?
C8 C9 H9B 108.9 . . ?
C10 C9 H9B 108.9 . . ?
H9A C9 H9B 107.7 . . ?
C9 C10 C10 111.3(2) . 2_566 ?
C9 C10 H10A 109.4 . . ?
C10 C10 H10A 109.4 2_566 . ?
C9 C10 H10B 109.4 . . ?
C10 C10 H10B 109.4 2_566 . ?
H10A C10 H10B 108.0 . . ?
C8 O8 H8 115(2) . . ?

loop_
 _geom_torsion_atom_site_label_1
 _geom_torsion_atom_site_label_2
 _geom_torsion_atom_site_label_3
 _geom_torsion_atom_site_label_4

_geom_torsion
_geom_torsion_site_symmetry_1
_geom_torsion_site_symmetry_2
_geom_torsion_site_symmetry_3
_geom_torsion_site_symmetry_4
_geom_torsion_publ_flag
N1A C2A C3A N4A -0.4(4) . . . . ?
N4A C5A C6A N1A -0.4(3) . . . . ?
C7A C5A C6A N1A 179.36(19) . . . . ?
N4A C5A C7A O7A 178.3(2) . . . . ?
C6A C5A C7A O7A -1.4(3) . . . . ?
N4A C5A C7A N7A -0.9(3) . . . . ?
C6A C5A C7A N7A 179.3(2) . . . . ?
C5A C6A N1A C2A 0.4(3) . . . . ?
C3A C2A N1A C6A 0.0(3) . . . . ?
C2A C3A N4A C5A 0.4(3) . . . . ?
C6A C5A N4A C3A 0.0(3) . . . . ?
C7A C5A N4A C3A -179.8(2) . . . . ?
N1B C2B C3B N4B -0.3(4) . . . . ?
N4B C5B C6B N1B -0.6(4) . . . . ?
C7B C5B C6B N1B 177.7(2) . . . . ?
N4B C5B C7B O7B -170.6(2) . . . . ?
C6B C5B C7B O7B 11.0(3) . . . . ?
N4B C5B C7B N7B 9.9(3) . . . . ?
C6B C5B C7B N7B -168.5(2) . . . . ?
C3B C2B N1B C6B 0.2(3) . . . . ?
C5B C6B N1B C2B 0.2(3) . . . . ?
C6B C5B N4B C3B 0.5(3) . . . . ?
C7B C5B N4B C3B -177.81(19) . . . . ?
C2B C3B N4B C5B -0.1(3) . . . . ?
O9 C8 C9 C10 0.5(3) . . . . ?
O8 C8 C9 C10 -179.37(19) . . . . ?
C8 C9 C10 C10 -174.2(2) . . . 2_566 ?

loop_
 _geom_hbond_atom_site_label_D
 _geom_hbond_atom_site_label_H
 _geom_hbond_atom_site_label_A
 _geom_hbond_distance_DH
 _geom_hbond_distance_HA
 _geom_hbond_distance_DA
 _geom_hbond_angle_DHA
 _geom_hbond_site_symmetry_A
N7A H7A1 O7B 0.90(3) 2.28(3) 3.025(2) 140(2) 2_855
N7A H7A2 O7B 0.92(3) 2.08(3) 2.998(2) 175(2) .
N7B H7B2 O7A 0.91(3) 1.88(3) 2.783(2) 176(2) .
N7B H7B1 N4B 0.91(3) 2.56(3) 3.183(3) 127(2) 2_856
O8 H8 N1A 0.89(3) 1.82(3) 2.711(2) 173(3) .

_refine_diff_density_max   0.353
_refine_diff_density_min   -0.368
_refine_diff_density_rms   0.091

_shelxl_version_number 2013-4

_shelx_res_file
;

TITL Pyrazinamide_AdipicAcid_(1)1_1 in P-1 #2
CELL 1.54184 5.1814 11.7163 12.2250 74.708 87.314 85.212
ZERR   1.00 0.0008 0.0016 0.0014 0.011 0.011 0.012

TITL Pyrazinamide_AdipicAcid_(1)1_1 in P-1
REM P-1 (#2 in standard setting)
CELL 1.54184 5.181357 11.716258 12.225045 74.7082 87.3141 85.2121
ZERR 2.00 0.000790 0.001554 0.001360 0.0106 0.0110 0.0117
LATT 1
SFAC C H N O
UNIT 22.00 30.00 6.00 10.00
TREF
HKLF 4
END

B-3: Data_Pyrazinamide_PimelicAcid

_audit_creation_method   SHELXL-97
_chemical_name_systematic
;
 ?
;
_chemical_name_common   ?
_chemical_melting_point   ?
_chemical_formula_moiety   ?
_chemical_formula_sum
 'C12 H17 N3 O5'
_chemical_formula_weight   283.29

loop_
 _atom_type_symbol
 _atom_type_description
 _atom_type_scat_dispersion_real
 _atom_type_scat_dispersion_imag
 _atom_type_scat_source
 'C' 'C' 0.0033 0.0016
 'International Tables Vol C Tables 4.2.6.8 and 6.1.1.4'
 'H' 'H' 0.0000 0.0000
 'International Tables Vol C Tables 4.2.6.8 and 6.1.1.4'
 'N' 'N' 0.0061 0.0033
 'International Tables Vol C Tables 4.2.6.8 and 6.1.1.4'
 'O' 'O' 0.0106 0.0060
 'International Tables Vol C Tables 4.2.6.8 and 6.1.1.4'

_symmetry_cell_setting   Triclinic
_symmetry_space_group_name_H-M   'P -1'

loop_
 _symmetry_equiv_pos_as_xyz
 'x, y, z'
 '-x, -y, -z'

_cell_length_a   5.3302(4)
_cell_length_b   8.4201(6)

```
_cell_length_c            15.5321(11)
_cell_angle_alpha          89.478(7)
_cell_angle_beta           82.760(7)
_cell_angle_gamma          71.840(6)
_cell_volume              656.75(9)
_cell_formula_units_Z       2
_cell_measurement_temperature    100(2)
_cell_measurement_reflns_used    0
_cell_measurement_theta_min     2.5
_cell_measurement_theta_max     27.5

_exptl_crystal_description      Plate
_exptl_crystal_colour          Colourless
_exptl_crystal_size_max        0.42
_exptl_crystal_size_mid        0.16
_exptl_crystal_size_min        0.02
_exptl_crystal_density_meas      ?
_exptl_crystal_density_diffrn   1.433
_exptl_crystal_density_method    'not measured'
_exptl_crystal_F_000          300
_exptl_absorpt_coefficient_mu    0.113
_exptl_absorpt_correction_type      'Multi-scan'
_exptl_absorpt_correction_T_max     1.000
_exptl_absorpt_correction_T_min     0.791
_exptl_absorpt_process_details
;
CrystalClear-SM Expert 3.1 b26 (Rigaku, 2012)
;

_exptl_special_details
;
 ?
;

_diffrn_ambient_temperature     100(2)
_diffrn_radiation_wavelength    0.71075
_diffrn_radiation_type         MoK\a
_diffrn_source                'Rotating Anode'
_diffrn_radiation_monochromator      'Graphite Monochromator'
_diffrn_measurement_specimen_support   'MiTeGen'
_diffrn_detector              'CCD'
_diffrn_measurement_device
;
AFC12 (Right): Kappa 3 circle
;
_diffrn_measurement_device_type
;
Rigaku Saturn724+ (2x2 bin mode)
;
_diffrn_detector_area_resol_mean      28.5714
_diffrn_measurement_method         'profile data from \w-scans'
_diffrn_standards_number       ?
_diffrn_standards_interval_count  ?
_diffrn_standards_interval_time   ?
_diffrn_standards_decay_%        ?
_diffrn_reflns_number          7308
_diffrn_reflns_av_R_equivalents   0.0290
```

_diffrn_reflns_av_sigmaI/netI   0.0228
_diffrn_reflns_limit_h_min   -6
_diffrn_reflns_limit_h_max   6
_diffrn_reflns_limit_k_min   -10
_diffrn_reflns_limit_k_max   10
_diffrn_reflns_limit_l_min   -20
_diffrn_reflns_limit_l_max   20
_diffrn_reflns_theta_min   3.73
_diffrn_reflns_theta_max   27.48
_reflns_number_total   2979
_reflns_number_gt   2697
_reflns_threshold_expression   >2\s(I)

_computing_data_collection
;
CrystalClear-SM Expert 3.1 b26 (Rigaku, 2012)
;
_computing_cell_refinement
;
CrystalClear-SM Expert 3.1 b26 (Rigaku, 2012)
;
_computing_data_reduction
;
CrystalClear-SM Expert 3.1 b26 (Rigaku, 2012)
;
_computing_structure_solution   'SHELXS-97 (Sheldrick, 2008)'
_computing_structure_refinement   'SHELXL-97 (Sheldrick, 2008)'
_computing_molecular_graphics
;
OLEX2 (Dolomanov, O.V., Bourhis, L.J., Gildea, R.J., Howard, J.A.K,
& Puschmann, H., 2009)
;
_computing_publication_material   'WinGX (Farrugia, 1999)'

_refine_special_details
;
 Refinement of F^2^ against ALL reflections. The weighted R-factor wR and
 goodness of fit S are based on F^2^, conventional R-factors R are based
 on F, with F set to zero for negative F^2^. The threshold expression of
 F^2^ > 2\s(F^2^) is used only for calculating R-factors(gt) etc. and is
 not relevant to the choice of reflections for refinement. R-factors based
 on F^2^ are statistically about twice as large as those based on F, and R-
 factors based on ALL data will be even larger.
;

_refine_ls_structure_factor_coef Fsqd
_refine_ls_matrix_type   full
_refine_ls_weighting_scheme   calc
_refine_ls_weighting_details
 'calc w=1/[\s^2^(Fo^2^)+(0.0572P)^2^+0.1477P] where P=(Fo^2^+2Fc^2^)/3'
_atom_sites_solution_primary   direct
_atom_sites_solution_secondary   difmap
_atom_sites_solution_hydrogens   geom
_refine_ls_hydrogen_treatment   constr
_refine_ls_extinction_method   none
_refine_ls_extinction_coef   ?
_refine_ls_number_reflns   2979

_refine_ls_number_parameters   183
_refine_ls_number_restraints   0
_refine_ls_R_factor_all   0.0381
_refine_ls_R_factor_gt   0.0350
_refine_ls_wR_factor_ref   0.1010
_refine_ls_wR_factor_gt   0.0984
_refine_ls_goodness_of_fit_ref   1.062
_refine_ls_restrained_S_all   1.062
_refine_ls_shift/su_max   0.000
_refine_ls_shift/su_mean   0.000

loop_
 _atom_site_label
 _atom_site_type_symbol
 _atom_site_fract_x
 _atom_site_fract_y
 _atom_site_fract_z
 _atom_site_U_iso_or_equiv
 _atom_site_adp_type
 _atom_site_occupancy
 _atom_site_symmetry_multiplicity
 _atom_site_calc_flag
 _atom_site_refinement_flags
 _atom_site_disorder_assembly
 _atom_site_disorder_group
C2 C 0.1996(2) 0.74419(13) 0.06798(7) 0.0191(2) Uani 1 1 d . . .
H2 H 0.1590 0.8029 0.0164 0.023 Uiso 1 1 calc R . .
C3 C -0.0048(2) 0.75477(13) 0.13515(7) 0.0190(2) Uani 1 1 d . . .
H3 H -0.1818 0.8185 0.1277 0.023 Uiso 1 1 calc R . .
C5 C 0.29496(19) 0.59084(11) 0.21663(6) 0.0151(2) Uani 1 1 d . . .
C6 C 0.5000(2) 0.57605(12) 0.14905(7) 0.0166(2) Uani 1 1 d . . .
H6 H 0.6764 0.5103 0.1561 0.020 Uiso 1 1 calc R . .
C7 C 0.3575(2) 0.51222(12) 0.30214(6) 0.0160(2) Uani 1 1 d . . .
N1 N 0.45164(17) 0.65344(11) 0.07417(6) 0.01757(19) Uani 1 1 d . . .
N4 N 0.04111(17) 0.67780(11) 0.20971(6) 0.01756(19) Uani 1 1 d . . .
N7 N 0.15084(18) 0.52093(11) 0.36128(6) 0.0211(2) Uani 1 1 d . . .
H7A H 0.1766 0.4781 0.4125 0.025 Uiso 1 1 calc R . .
H7B H -0.0121 0.5695 0.3493 0.025 Uiso 1 1 calc R . .
O7 O 0.59382(14) 0.44627(10) 0.31319(5) 0.02045(18) Uani 1 1 d . . .
C8 C 0.7003(2) 0.79984(13) -0.11307(6) 0.0170(2) Uani 1 1 d . . .
C9 C 0.8954(2) 0.82530(13) -0.18699(7) 0.0185(2) Uani 1 1 d . . .
H9A H 0.9673 0.7211 -0.2233 0.022 Uiso 1 1 calc R . .
H9B H 1.0461 0.8454 -0.1626 0.022 Uiso 1 1 calc R . .
C10 C 0.7777(2) 0.96990(13) -0.24476(6) 0.0173(2) Uani 1 1 d . . .
H10A H 0.9253 0.9949 -0.2818 0.021 Uiso 1 1 calc R . .
H10B H 0.6809 1.0704 -0.2074 0.021 Uiso 1 1 calc R . .
C11 C 0.5880(2) 0.93678(12) -0.30307(6) 0.0175(2) Uani 1 1 d . . .
H11A H 0.4393 0.9125 -0.2664 0.021 Uiso 1 1 calc R . .
H11B H 0.6841 0.8366 -0.3408 0.021 Uiso 1 1 calc R . .
C12 C 0.4742(2) 1.08466(13) -0.36022(6) 0.0176(2) Uani 1 1 d . . .
H12A H 0.3269 1.0661 -0.3874 0.021 Uiso 1 1 calc R . .
H12B H 0.3999 1.1881 -0.3233 0.021 Uiso 1 1 calc R . .
C13 C 0.6836(2) 1.10813(13) -0.43110(6) 0.0180(2) Uani 1 1 d . . .
H13A H 0.8219 1.1369 -0.4034 0.022 Uiso 1 1 calc R . .
H13B H 0.7704 1.0006 -0.4638 0.022 Uiso 1 1 calc R . .
C14 C 0.5754(2) 1.24171(13) -0.49419(6) 0.0169(2) Uani 1 1 d . . .
O8 O 0.81265(15) 0.66873(9) -0.06626(5) 0.02025(18) Uani 1 1 d . . .

H8 H 0.7033 0.6622 -0.0235 0.030 Uiso 1 1 calc R . .
O9 O 0.47061(15) 0.88701(10) -0.09651(5) 0.0265(2) Uani 1 1 d . . .
O14 O 0.75951(15) 1.24772(10) -0.55884(5) 0.02310(19) Uani 1 1 d . . .
H14 H 0.6895 1.3171 -0.5949 0.035 Uiso 1 1 calc R . .
O15 O 0.34542(15) 1.33214(10) -0.48753(5) 0.02399(19) Uani 1 1 d . . .

loop_
 _atom_site_aniso_label
 _atom_site_aniso_U_11
 _atom_site_aniso_U_22
 _atom_site_aniso_U_33
 _atom_site_aniso_U_23
 _atom_site_aniso_U_13
 _atom_site_aniso_U_12
C2 0.0210(5) 0.0204(5) 0.0180(5) 0.0050(4) -0.0053(4) -0.0082(4)
C3 0.0158(5) 0.0191(5) 0.0227(5) 0.0039(4) -0.0049(4) -0.0054(4)
C5 0.0163(5) 0.0124(4) 0.0168(5) 0.0015(3) -0.0015(4) -0.0052(4)
C6 0.0164(5) 0.0151(5) 0.0179(5) 0.0013(4) -0.0014(4) -0.0046(4)
C7 0.0179(5) 0.0124(4) 0.0164(5) 0.0013(3) -0.0004(4) -0.0037(4)
N1 0.0187(4) 0.0181(4) 0.0165(4) 0.0023(3) -0.0018(3) -0.0069(3)
N4 0.0165(4) 0.0166(4) 0.0195(4) 0.0023(3) -0.0011(3) -0.0054(3)
N7 0.0171(4) 0.0225(4) 0.0188(4) 0.0068(3) 0.0017(3) -0.0008(3)
O7 0.0168(4) 0.0237(4) 0.0191(4) 0.0067(3) -0.0014(3) -0.0044(3)
C8 0.0183(5) 0.0177(5) 0.0155(5) 0.0027(4) -0.0035(4) -0.0059(4)
C9 0.0152(5) 0.0210(5) 0.0179(5) 0.0050(4) -0.0016(4) -0.0039(4)
C10 0.0174(5) 0.0182(5) 0.0169(5) 0.0046(4) -0.0020(4) -0.0066(4)
C11 0.0193(5) 0.0178(5) 0.0163(5) 0.0040(4) -0.0027(4) -0.0072(4)
C12 0.0147(5) 0.0198(5) 0.0164(5) 0.0036(4) -0.0008(4) -0.0034(4)
C13 0.0166(5) 0.0185(5) 0.0167(5) 0.0049(4) -0.0010(4) -0.0028(4)
C14 0.0171(5) 0.0174(5) 0.0160(5) 0.0015(4) -0.0014(4) -0.0054(4)
O8 0.0198(4) 0.0207(4) 0.0180(4) 0.0067(3) -0.0007(3) -0.0038(3)
O9 0.0188(4) 0.0308(4) 0.0233(4) 0.0096(3) 0.0024(3) -0.0003(3)
O14 0.0179(4) 0.0269(4) 0.0203(4) 0.0108(3) 0.0008(3) -0.0025(3)
O15 0.0187(4) 0.0255(4) 0.0208(4) 0.0075(3) 0.0011(3) 0.0015(3)

_geom_special_details
;
 All s.u.'s (except the s.u. in the dihedral angle between two l.s. planes)
 are estimated using the full covariance matrix. The cell s.u.'s are taken
 into account individually in the estimation of s.u.'s in distances, angles
 and torsion angles; correlations between s.u.'s in cell parameters are only
 used when they are defined by crystal symmetry. An approximate (isotropic)
 treatment of cell s.u.'s is used for estimating s.u.'s involving l.s. planes.
;

loop_
 _geom_bond_atom_site_label_1
 _geom_bond_atom_site_label_2
 _geom_bond_distance
 _geom_bond_site_symmetry_2
 _geom_bond_publ_flag
C2 N1 1.3377(13) . ?
C2 C3 1.3922(14) . ?
C2 H2 0.9500 . ?
C3 N4 1.3342(13) . ?
C3 H3 0.9500 . ?
C5 N4 1.3402(13) . ?

C5 C6 1.3928(14) . ?
C5 C7 1.5070(13) . ?
C6 N1 1.3419(13) . ?
C6 H6 0.9500 . ?
C7 O7 1.2414(12) . ?
C7 N7 1.3261(13) . ?
N7 H7A 0.8800 . ?
N7 H7B 0.8800 . ?
C8 O9 1.2116(13) . ?
C8 O8 1.3375(12) . ?
C8 C9 1.5095(14) . ?
C9 C10 1.5255(13) . ?
C9 H9A 0.9900 . ?
C9 H9B 0.9900 . ?
C10 C11 1.5269(14) . ?
C10 H10A 0.9900 . ?
C10 H10B 0.9900 . ?
C11 C12 1.5333(13) . ?
C11 H11A 0.9900 . ?
C11 H11B 0.9900 . ?
C12 C13 1.5234(14) . ?
C12 H12A 0.9900 . ?
C12 H12B 0.9900 . ?
C13 C14 1.5086(13) . ?
C13 H13A 0.9900 . ?
C13 H13B 0.9900 . ?
C14 O15 1.2167(13) . ?
C14 O14 1.3251(12) . ?
O8 H8 0.8400 . ?
O14 H14 0.8400 . ?

loop_
_geom_angle_atom_site_label_1
_geom_angle_atom_site_label_2
_geom_angle_atom_site_label_3
_geom_angle
_geom_angle_site_symmetry_1
_geom_angle_site_symmetry_3
_geom_angle_publ_flag
N1 C2 C3 121.69(9) . . ?
N1 C2 H2 119.2 . . ?
C3 C2 H2 119.2 . . ?
N4 C3 C2 121.80(9) . . ?
N4 C3 H3 119.1 . . ?
C2 C3 H3 119.1 . . ?
N4 C5 C6 122.31(9) . . ?
N4 C5 C7 117.89(9) . . ?
C6 C5 C7 119.76(9) . . ?
N1 C6 C5 120.87(9) . . ?
N1 C6 H6 119.6 . . ?
C5 C6 H6 119.6 . . ?
O7 C7 N7 124.55(9) . . ?
O7 C7 C5 119.04(9) . . ?
N7 C7 C5 116.40(9) . . ?
C2 N1 C6 116.94(9) . . ?
C3 N4 C5 116.35(9) . . ?
C7 N7 H7A 120.0 . . ?

C7 N7 H7B 120.0 . . ?
H7A N7 H7B 120.0 . . ?
O9 C8 O8 123.25(9) . . ?
O9 C8 C9 125.09(9) . . ?
O8 C8 C9 111.66(8) . . ?
C8 C9 C10 114.37(8) . . ?
C8 C9 H9A 108.7 . . ?
C10 C9 H9A 108.7 . . ?
C8 C9 H9B 108.7 . . ?
C10 C9 H9B 108.7 . . ?
H9A C9 H9B 107.6 . . ?
C9 C10 C11 114.24(8) . . ?
C9 C10 H10A 108.7 . . ?
C11 C10 H10A 108.7 . . ?
C9 C10 H10B 108.7 . . ?
C11 C10 H10B 108.7 . . ?
H10A C10 H10B 107.6 . . ?
C10 C11 C12 112.74(8) . . ?
C10 C11 H11A 109.0 . . ?
C12 C11 H11A 109.0 . . ?
C10 C11 H11B 109.0 . . ?
C12 C11 H11B 109.0 . . ?
H11A C11 H11B 107.8 . . ?
C13 C12 C11 112.32(8) . . ?
C13 C12 H12A 109.1 . . ?
C11 C12 H12A 109.1 . . ?
C13 C12 H12B 109.1 . . ?
C11 C12 H12B 109.1 . . ?
H12A C12 H12B 107.9 . . ?
C14 C13 C12 114.21(8) . . ?
C14 C13 H13A 108.7 . . ?
C12 C13 H13A 108.7 . . ?
C14 C13 H13B 108.7 . . ?
C12 C13 H13B 108.7 . . ?
H13A C13 H13B 107.6 . . ?
O15 C14 O14 123.66(9) . . ?
O15 C14 C13 124.27(9) . . ?
O14 C14 C13 112.06(8) . . ?
C8 O8 H8 109.5 . . ?
C14 O14 H14 109.5 . . ?

loop_
 _geom_torsion_atom_site_label_1
 _geom_torsion_atom_site_label_2
 _geom_torsion_atom_site_label_3
 _geom_torsion_atom_site_label_4
 _geom_torsion
 _geom_torsion_site_symmetry_1
 _geom_torsion_site_symmetry_2
 _geom_torsion_site_symmetry_3
 _geom_torsion_site_symmetry_4
 _geom_torsion_publ_flag
N1 C2 C3 N4 1.39(16) . . . . ?
N4 C5 C6 N1 1.96(15) . . . . ?
C7 C5 C6 N1 -175.91(9) . . . . ?
N4 C5 C7 O7 -172.48(9) . . . . ?
C6 C5 C7 O7 5.48(14) . . . . ?

N4 C5 C7 N7 6.76(13) . . . . ?
C6 C5 C7 N7 -175.28(9) . . . . ?
C3 C2 N1 C6 -1.56(15) . . . . ?
C5 C6 N1 C2 -0.03(14) . . . . ?
C2 C3 N4 C5 0.49(14) . . . . ?
C6 C5 N4 C3 -2.11(14) . . . . ?
C7 C5 N4 C3 175.79(9) . . . . ?
O9 C8 C9 C10 -2.54(15) . . . . ?
O8 C8 C9 C10 178.24(8) . . . . ?
C8 C9 C10 C11 -72.02(11) . . . . ?
C9 C10 C11 C12 -179.92(8) . . . . ?
C10 C11 C12 C13 70.18(11) . . . . ?
C11 C12 C13 C14 174.49(8) . . . . ?
C12 C13 C14 O15 4.55(15) . . . . ?
C12 C13 C14 O14 -174.50(9) . . . . ?

loop_
 _geom_hbond_atom_site_label_D
 _geom_hbond_atom_site_label_H
 _geom_hbond_atom_site_label_A
 _geom_hbond_distance_DH
 _geom_hbond_distance_HA
 _geom_hbond_distance_DA
 _geom_hbond_angle_DHA
 _geom_hbond_site_symmetry_A
N7 H7A O15 0.88 2.09 2.9385(12) 162.5 1_546
N7 H7B O15 0.88 2.57 3.0116(12) 111.9 2_575
O8 H8 N1 0.84 1.91 2.7510(12) 178.6 .
O14 H14 O7 0.84 1.81 2.6433(11) 169.2 1_564

_diffrn_measured_fraction_theta_max   0.993
_diffrn_reflns_theta_full   27.48
_diffrn_measured_fraction_theta_full   0.993
_refine_diff_density_max   0.404
_refine_diff_density_min   -0.207
_refine_diff_density_rms   0.046

B-4: Data_Azelaic_Acid

_audit_creation_method   SHELXL-2013
_chemical_name_systematic
;
 ?
;
_chemical_name_common   ?
_chemical_melting_point   ?
_chemical_formula_moiety
 'C9 H16 O4'
_chemical_formula_sum
 'C9 H16 O4'
_chemical_formula_weight   188.22

loop_
 _atom_type_symbol

_atom_type_description
_atom_type_scat_dispersion_real
_atom_type_scat_dispersion_imag
_atom_type_scat_source
'C' 'C' 0.0181 0.0091
'International Tables Vol C Tables 4.2.6.8 and 6.1.1.4'
'H' 'H' 0.0000 0.0000
'International Tables Vol C Tables 4.2.6.8 and 6.1.1.4'
'O' 'O' 0.0492 0.0322
'International Tables Vol C Tables 4.2.6.8 and 6.1.1.4'

_space_group_crystal_system   monoclinic
_space_group_IT_number   14
_space_group_name_H-M_alt   'P 21/c'
_space_group_name_Hall   '-P 2ybc'

_shelx_space_group_comment
;
The symmetry employed for this shelxl refinement is uniquely defined
by the following loop, which should always be used as a source of
symmetry information in preference to the above space-group names.
They are only intended as comments.
;

loop_
 _space_group_symop_operation_xyz
 'x, y, z'
 '-x, y+1/2, -z+1/2'
 '-x, -y, -z'
 'x, -y-1/2, z-1/2'

_cell_length_a   5.4938(2)
_cell_length_b   9.4418(3)
_cell_length_c   18.8258(6)
_cell_angle_alpha   90
_cell_angle_beta   95.673(3)
_cell_angle_gamma   90
_cell_volume   971.74(6)
_cell_formula_units_Z   4
_cell_measurement_temperature 100.00(10)
_cell_measurement_reflns_used 2039
_cell_measurement_theta_min   4.7030
_cell_measurement_theta_max   74.1230

_exptl_crystal_description   Slab
_exptl_crystal_colour   Colourless
_exptl_crystal_density_meas   ?
_exptl_crystal_density_method   ?
_exptl_crystal_density_diffrn   1.287
_exptl_crystal_F_000   408
_exptl_transmission_factor_min   ?
_exptl_transmission_factor_max   ?
_exptl_crystal_size_max   0.140
_exptl_crystal_size_mid   0.130
_exptl_crystal_size_min   0.030
_exptl_absorpt_coefficient_mu   0.838
_shelx_estimated_absorpt_T_min   0.892

_shelx_estimated_absorpt_T_max   0.975
_exptl_absorpt_correction_T_min   0.89788
_exptl_absorpt_correction_T_max   1.00000
_exptl_absorpt_correction_type   'multi-scan'
_exptl_absorpt_process_details
;
CrysAlisPro, Agilent Technologies,
Version 1.171.36.28 (release 01-02-2013 CrysAlis171 .NET)
(compiled Feb 1 2013,16:14:44)
Empirical absorption correction using spherical harmonics,
 implemented in SCALE3 ABSPACK scaling algorithm.
;

_exptl_special_details
;
 ?
;

_diffrn_ambient_temperature 100.00(10)
_diffrn_radiation_wavelength 1.5418
_diffrn_radiation_type 'Cu K\a'
_diffrn_radiation_source 'SuperNova (Cu) X-ray Source'
_diffrn_radiation_monochromator 'mirror'
_diffrn_measurement_device_type 'SuperNova, Dual, Cu at zero, Atlas'
_diffrn_detector_area_resol_mean 5.1768
_diffrn_reflns_number   3622
_diffrn_reflns_av_unetI/netI   0.0257
_diffrn_reflns_av_R_equivalents   0.0182
_diffrn_reflns_limit_h_min   -6
_diffrn_reflns_limit_h_max   6
_diffrn_reflns_limit_k_min   -10
_diffrn_reflns_limit_k_max   11
_diffrn_reflns_limit_l_min   -22
_diffrn_reflns_limit_l_max   21
_diffrn_reflns_theta_min   6.657
_diffrn_reflns_theta_max   74.248
_diffrn_reflns_theta_full   67.684
_diffrn_measured_fraction_theta_max   0.969
_diffrn_measured_fraction_theta_full 0.997
_diffrn_reflns_Laue_measured_fraction_max   0.969
_diffrn_reflns_Laue_measured_fraction_full 0.997
_diffrn_reflns_point_group_measured_fraction_max   0.969
_diffrn_reflns_point_group_measured_fraction_full 0.997
_reflns_number_total   1922
_reflns_number_gt   1726
_reflns_threshold_expression   'I > 2\s(I)'
_reflns_Friedel_coverage   0.000
_reflns_Friedel_fraction_max   .
_reflns_Friedel_fraction_full   .

_reflns_special_details
;
 Reflections were merged by SHELXL according to the crystal
 class for the calculation of statistics and refinement.

 _reflns_Friedel_fraction is defined as the number of unique
 Friedel pairs measured divided by the number that would be

 possible theoretically, ignoring centric projections and
 systematic absences.
;

_computing_data_collection
;
CrysAlisPro, Agilent Technologies,
Version 1.171.36.28 (release 01-02-2013 CrysAlis171 .NET)
(compiled Feb 1 2013,16:14:44)
;
_computing_cell_refinement
;
CrysAlisPro, Agilent Technologies,
Version 1.171.36.28 (release 01-02-2013 CrysAlis171 .NET)
(compiled Feb 1 2013,16:14:44)
;
_computing_data_reduction
;
CrysAlisPro, Agilent Technologies,
Version 1.171.36.28 (release 01-02-2013 CrysAlis171 .NET)
(compiled Feb 1 2013,16:14:44)
;
_computing_structure_solution   'SHELXS-2013 (Sheldrick, 2013)'
_computing_structure_refinement   'SHELXL-2013 (Sheldrick, 2013)'
_computing_molecular_graphics
;
OLEX2 (Dolomanov, O.V., Bourhis, L.J., Gildea, R.J., Howard, J.A.K,
& Puschmann, H., 2009)
;
_computing_publication_material   'WinGX (Farrugia, 1999)'

_refine_special_details
;
 ?
;
_refine_ls_structure_factor_coef Fsqd
_refine_ls_matrix_type   full
_refine_ls_weighting_scheme   calc
_refine_ls_weighting_details
'w=1/[\s^2^(Fo^2^)+(0.0458P)^2^+0.7566P] where P=(Fo^2^+2Fc^2^)/3'
_atom_sites_solution_primary   ?
_atom_sites_solution_secondary   ?
_atom_sites_solution_hydrogens   mixed
_refine_ls_hydrogen_treatment   mixed
_refine_ls_extinction_method   none
_refine_ls_extinction_coef   .
_refine_ls_number_reflns   1922
_refine_ls_number_parameters   126
_refine_ls_number_restraints   0
_refine_ls_R_factor_all   0.0480
_refine_ls_R_factor_gt   0.0430
_refine_ls_wR_factor_ref   0.1287
_refine_ls_wR_factor_gt   0.1254
_refine_ls_goodness_of_fit_ref   1.171
_refine_ls_restrained_S_all   1.171
_refine_ls_shift/su_max   0.000
_refine_ls_shift/su_mean   0.000

```
loop_
 _atom_site_label
 _atom_site_type_symbol
 _atom_site_fract_x
 _atom_site_fract_y
 _atom_site_fract_z
 _atom_site_U_iso_or_equiv
 _atom_site_adp_type
 _atom_site_occupancy
 _atom_site_site_symmetry_order
 _atom_site_calc_flag
 _atom_site_refinement_flags_posn
 _atom_site_refinement_flags_adp
 _atom_site_refinement_flags_occupancy
 _atom_site_disorder_assembly
 _atom_site_disorder_group
C1 C -0.2214(3) 0.4162(2) 0.05512(9) 0.0174(4) Uani 1 1 d . . . . .
C2 C -0.0183(3) 0.3432(2) 0.09975(9) 0.0182(4) Uani 1 1 d . . . . .
H2A H 0.0734 0.2841 0.0681 0.022 Uiso 1 1 calc R U . . .
H2B H -0.0909 0.2789 0.1334 0.022 Uiso 1 1 calc R U . . .
C3 C 0.1616(3) 0.44099(19) 0.14230(9) 0.0174(4) Uani 1 1 d . . . . .
H3A H 0.0709 0.5066 0.1711 0.021 Uiso 1 1 calc R U . . .
H3B H 0.2501 0.4983 0.1091 0.021 Uiso 1 1 calc R U . . .
C4 C 0.3453(3) 0.3563(2) 0.19155(9) 0.0183(4) Uani 1 1 d . . . . .
H4A H 0.2549 0.2994 0.2244 0.022 Uiso 1 1 calc R U . . .
H4B H 0.4324 0.2897 0.1623 0.022 Uiso 1 1 calc R U . . .
C5 C 0.5336(3) 0.4472(2) 0.23560(9) 0.0181(4) Uani 1 1 d . . . . .
H5A H 0.4476 0.5200 0.2616 0.022 Uiso 1 1 calc R U . . .
H5B H 0.6365 0.4967 0.2031 0.022 Uiso 1 1 calc R U . . .
C6 C 0.6976(3) 0.35978(19) 0.28923(9) 0.0188(4) Uani 1 1 d . . . . .
H6A H 0.5937 0.3104 0.3215 0.023 Uiso 1 1 calc R U . . .
H6B H 0.7818 0.2866 0.2630 0.023 Uiso 1 1 calc R U . . .
C7 C 0.8895(3) 0.44712(19) 0.33420(9) 0.0173(4) Uani 1 1 d . . . . .
H7A H 0.8099 0.5298 0.3545 0.021 Uiso 1 1 calc R U . . .
H7B H 1.0123 0.4828 0.3035 0.021 Uiso 1 1 calc R U . . .
C8 C 1.0170(3) 0.3582(2) 0.39464(10) 0.0213(4) Uani 1 1 d . . . . .
H8A H 0.8917 0.3250 0.4252 0.026 Uiso 1 1 calc R U . . .
H8B H 1.0870 0.2733 0.3734 0.026 Uiso 1 1 calc R U . . .
C9 C 1.2166(3) 0.42989(19) 0.44144(9) 0.0172(4) Uani 1 1 d . . . . .
O1 O -0.3709(2) 0.32655(14) 0.01868(7) 0.0239(3) Uani 1 1 d . . . . .
H1 H -0.496(6) 0.372(4) -0.0052(16) 0.059(9) Uiso 1 1 d . . . . .
O2 O -0.2510(2) 0.54463(14) 0.05291(7) 0.0238(3) Uani 1 1 d . . . . .
O9 O 1.3510(2) 0.51934(15) 0.40831(7) 0.0242(3) Uani 1 1 d . . . . .
H9 H 1.483(6) 0.548(3) 0.4406(15) 0.053(8) Uiso 1 1 d . . . . .
O10 O 1.2566(2) 0.40404(15) 0.50543(6) 0.0226(3) Uani 1 1 d . . . . .


loop_
 _atom_site_aniso_label
 _atom_site_aniso_U_11
 _atom_site_aniso_U_22
 _atom_site_aniso_U_33
 _atom_site_aniso_U_23
 _atom_site_aniso_U_13
 _atom_site_aniso_U_12
C1 0.0159(8) 0.0196(9) 0.0160(8) -0.0005(7) -0.0012(6) -0.0023(7)
```

C2 0.0170(8) 0.0183(9) 0.0184(8) -0.0010(7) -0.0034(6) 0.0009(7)
C3 0.0146(8) 0.0185(9) 0.0183(8) -0.0004(7) -0.0028(6) 0.0001(7)
C4 0.0157(8) 0.0193(9) 0.0189(8) -0.0005(7) -0.0036(6) 0.0010(7)
C5 0.0154(8) 0.0196(9) 0.0185(8) -0.0007(7) -0.0033(6) 0.0002(7)
C6 0.0178(8) 0.0179(9) 0.0195(8) -0.0008(7) -0.0045(7) 0.0000(7)
C7 0.0160(8) 0.0169(8) 0.0181(8) 0.0007(7) -0.0034(6) -0.0007(7)
C8 0.0200(9) 0.0192(9) 0.0228(9) 0.0018(7) -0.0072(7) -0.0024(7)
C9 0.0157(8) 0.0150(8) 0.0203(8) -0.0001(7) -0.0008(6) 0.0012(6)
O1 0.0210(7) 0.0187(7) 0.0295(7) -0.0014(5) -0.0109(5) -0.0004(5)
O2 0.0220(7) 0.0181(7) 0.0289(7) 0.0000(5) -0.0091(5) 0.0004(5)
O9 0.0212(7) 0.0309(8) 0.0191(6) 0.0019(5) -0.0044(5) -0.0096(6)
O10 0.0206(6) 0.0272(7) 0.0185(6) 0.0036(5) -0.0057(5) -0.0035(6)

_geom_special_details
;
 All esds (except the esd in the dihedral angle between two l.s. planes)
 are estimated using the full covariance matrix. The cell esds are taken
 into account individually in the estimation of esds in distances, angles
 and torsion angles; correlations between esds in cell parameters are only
 used when they are defined by crystal symmetry. An approximate (isotropic)
 treatment of cell esds is used for estimating esds involving l.s. planes.
;

loop_
 _geom_bond_atom_site_label_1
 _geom_bond_atom_site_label_2
 _geom_bond_distance
 _geom_bond_site_symmetry_2
 _geom_bond_publ_flag
C1 O2 1.223(2) . ?
C1 O1 1.323(2) . ?
C1 C2 1.497(2) . ?
C2 C3 1.521(2) . ?
C2 H2A 0.9900 . ?
C2 H2B 0.9900 . ?
C3 C4 1.527(2) . ?
C3 H3A 0.9900 . ?
C3 H3B 0.9900 . ?
C4 C5 1.525(2) . ?
C4 H4A 0.9900 . ?
C4 H4B 0.9900 . ?
C5 C6 1.527(2) . ?
C5 H5A 0.9900 . ?
C5 H5B 0.9900 . ?
C6 C7 1.527(2) . ?
C6 H6A 0.9900 . ?
C6 H6B 0.9900 . ?
C7 C8 1.527(2) . ?
C7 H7A 0.9900 . ?
C7 H7B 0.9900 . ?
C8 C9 1.499(2) . ?
C8 H8A 0.9900 . ?
C8 H8B 0.9900 . ?
C9 O10 1.228(2) . ?
C9 O9 1.318(2) . ?
O1 H1 0.89(3) . ?
O9 H9 0.94(3) . ?

loop_
_geom_angle_atom_site_label_1
_geom_angle_atom_site_label_2
_geom_angle_atom_site_label_3
_geom_angle
_geom_angle_site_symmetry_1
_geom_angle_site_symmetry_3
_geom_angle_publ_flag
O2 C1 O1 122.90(16) . . ?
O2 C1 C2 124.36(16) . . ?
O1 C1 C2 112.72(15) . . ?
C1 C2 C3 115.18(15) . . ?
C1 C2 H2A 108.5 . . ?
C3 C2 H2A 108.5 . . ?
C1 C2 H2B 108.5 . . ?
C3 C2 H2B 108.5 . . ?
H2A C2 H2B 107.5 . . ?
C2 C3 C4 110.98(15) . . ?
C2 C3 H3A 109.4 . . ?
C4 C3 H3A 109.4 . . ?
C2 C3 H3B 109.4 . . ?
C4 C3 H3B 109.4 . . ?
H3A C3 H3B 108.0 . . ?
C5 C4 C3 114.07(15) . . ?
C5 C4 H4A 108.7 . . ?
C3 C4 H4A 108.7 . . ?
C5 C4 H4B 108.7 . . ?
C3 C4 H4B 108.7 . . ?
H4A C4 H4B 107.6 . . ?
C4 C5 C6 112.31(15) . . ?
C4 C5 H5A 109.1 . . ?
C6 C5 H5A 109.1 . . ?
C4 C5 H5B 109.1 . . ?
C6 C5 H5B 109.1 . . ?
H5A C5 H5B 107.9 . . ?
C7 C6 C5 113.86(15) . . ?
C7 C6 H6A 108.8 . . ?
C5 C6 H6A 108.8 . . ?
C7 C6 H6B 108.8 . . ?
C5 C6 H6B 108.8 . . ?
H6A C6 H6B 107.7 . . ?
C6 C7 C8 110.91(14) . . ?
C6 C7 H7A 109.5 . . ?
C8 C7 H7A 109.5 . . ?
C6 C7 H7B 109.5 . . ?
C8 C7 H7B 109.5 . . ?
H7A C7 H7B 108.0 . . ?
C9 C8 C7 116.41(15) . . ?
C9 C8 H8A 108.2 . . ?
C7 C8 H8A 108.2 . . ?
C9 C8 H8B 108.2 . . ?
C7 C8 H8B 108.2 . . ?
H8A C8 H8B 107.3 . . ?
O10 C9 O9 122.51(16) . . ?
O10 C9 C8 122.46(16) . . ?
O9 C9 C8 115.00(15) . . ?

C1 O1 H1 111(2) . . ?
C9 O9 H9 108.3(18) . . ?

loop_
 _geom_torsion_atom_site_label_1
 _geom_torsion_atom_site_label_2
 _geom_torsion_atom_site_label_3
 _geom_torsion_atom_site_label_4
 _geom_torsion
 _geom_torsion_site_symmetry_1
 _geom_torsion_site_symmetry_2
 _geom_torsion_site_symmetry_3
 _geom_torsion_site_symmetry_4
 _geom_torsion_publ_flag
O2 C1 C2 C3 -1.8(3) . . . . ?
O1 C1 C2 C3 179.34(14) . . . . ?
C1 C2 C3 C4 174.23(14) . . . . ?
C2 C3 C4 C5 179.47(14) . . . . ?
C3 C4 C5 C6 174.38(14) . . . . ?
C4 C5 C6 C7 179.76(15) . . . . ?
C5 C6 C7 C8 170.42(15) . . . . ?
C6 C7 C8 C9 177.87(15) . . . . ?
C7 C8 C9 O10 145.95(18) . . . . ?
C7 C8 C9 O9 -36.1(2) . . . . ?

loop_
 _geom_hbond_atom_site_label_D
 _geom_hbond_atom_site_label_H
 _geom_hbond_atom_site_label_A
 _geom_hbond_distance_DH
 _geom_hbond_distance_HA
 _geom_hbond_distance_DA
 _geom_hbond_angle_DHA
 _geom_hbond_site_symmetry_A
O1 H1 O2 0.89(3) 1.76(3) 2.6566(18) 177(3) 3_465
O9 H9 O10 0.94(3) 1.73(3) 2.6673(17) 175(3) 3_866

_refine_diff_density_max   0.288
_refine_diff_density_min -0.224
_refine_diff_density_rms   0.050

_shelxl_version_number 2013-4

_shelx_res_file
;
TITL AzelaicAcid in P21/c #14
CELL 1.54184 5.4938 9.4418 18.8258 90.000 95.673 90.000
ZERR   4.00 0.0002 0.0003 0.0006 0.000 0.003 0.000
LATT 1
SYMM - X, 1/2 + Y, 1/2 - Z
SFAC C   H   O
UNIT 36 64 16
MERG 2
SHEL 7 0.80
EQIV $1 -x-1, -y+1, -z
HTAB O1 O2_$1
EQIV $2 -x+3, -y+1, -z+1

HTAB O9 O10_$2
FMAP 2
PLAN 5
SIZE   0.030 0.130 0.140
ACTA
BOND $H
CONF
L.S. 20
TEMP -173.00
WGHT 0.045800 0.756600
FVAR   7.64177
C1 1 -0.221437 0.416236 0.055116 11.00000 0.01589 0.01962 =
      0.01601 -0.00047 -0.00121 -0.00225
C2 1 -0.018275 0.343218 0.099748 11.00000 0.01695 0.01828 =
      0.01843 -0.00101 -0.00342 0.00091
AFIX 23
H2A 2 0.073374 0.284093 0.068072 11.00000 -1.20000
H2B 2 -0.090851 0.278866 0.133426 11.00000 -1.20000
AFIX 0
C3 1 0.161566 0.440991 0.142304 11.00000 0.01456 0.01852 =
      0.01832 -0.00039 -0.00284 0.00012
AFIX 23
H3A 2 0.070912 0.506610 0.171142 11.00000 -1.20000
H3B 2 0.250077 0.498269 0.109086 11.00000 -1.20000
AFIX 0
C4 1 0.345325 0.356325 0.191547 11.00000 0.01567 0.01928 =
      0.01888 -0.00053 -0.00358 0.00103
AFIX 23
H4A 2 0.254855 0.299370 0.224424 11.00000 -1.20000
H4B 2 0.432369 0.289720 0.162268 11.00000 -1.20000
AFIX 0
C5 1 0.533615 0.447189 0.235596 11.00000 0.01535 0.01958 =
      0.01851 -0.00072 -0.00331 0.00017
AFIX 23
H5A 2 0.447605 0.519979 0.261555 11.00000 -1.20000
H5B 2 0.636520 0.496678 0.203119 11.00000 -1.20000
AFIX 0
C6 1 0.697588 0.359777 0.289235 11.00000 0.01777 0.01786 =
      0.01955 -0.00078 -0.00449 0.00003
AFIX 23
H6A 2 0.593746 0.310445 0.321509 11.00000 -1.20000
H6B 2 0.781825 0.286588 0.263035 11.00000 -1.20000
AFIX 0
C7 1 0.889494 0.447115 0.334201 11.00000 0.01602 0.01689 =
      0.01811 0.00072 -0.00340 -0.00066
AFIX 23
H7A 2 0.809930 0.529810 0.354522 11.00000 -1.20000
H7B 2 1.012321 0.482788 0.303493 11.00000 -1.20000
AFIX 0
C8 1 1.017014 0.358205 0.394644 11.00000 0.01998 0.01917 =
      0.02280 0.00182 -0.00718 -0.00239
AFIX 23
H8A 2 0.891715 0.325044 0.425160 11.00000 -1.20000
H8B 2 1.086978 0.273317 0.373422 11.00000 -1.20000
AFIX 0
C9 1 1.216646 0.429893 0.441442 11.00000 0.01571 0.01504 =
      0.02027 -0.00013 -0.00078 0.00124

O1   3 -0.370911   0.326549   0.018681   11.00000   0.02099   0.01867 =
     0.02947 -0.00136 -0.01094 -0.00038
O2   3 -0.250979   0.544627   0.052907   11.00000   0.02201   0.01814 =
     0.02894   0.00001 -0.00912   0.00043
O9   3   1.350991   0.519341   0.408314   11.00000   0.02118   0.03095 =
     0.01907   0.00190 -0.00444 -0.00957
O10 3   1.256631   0.404039   0.505435   11.00000   0.02062   0.02717 =
     0.01849   0.00365 -0.00571 -0.00349
H1   2 -0.495599   0.372344 -0.005179   11.00000   0.05883
H9   2   1.482825   0.548358   0.440562   11.00000   0.05280
HKLF   4

REM AzelaicAcid in P21/c #14
REM R1 = 0.0430 for   1726 Fo > 4sig(Fo) and 0.0480 for all   1922 data
REM   126 parameters refined using   0 restraints

END

B-5: Data_Pyrazinamide_SebacicAcid

_audit_creation_method   SHELXL-97
_chemical_name_systematic
;
 ?
;
_chemical_name_common   ?
_chemical_melting_point   ?
_chemical_formula_moiety
 '2(C5 H5 N3 O), C10 H18 O4'
_chemical_formula_sum
 'C20 H28 N6 O6'
_chemical_formula_weight   448.48

loop_
 _atom_type_symbol
 _atom_type_description
 _atom_type_scat_dispersion_real
 _atom_type_scat_dispersion_imag
 _atom_type_scat_source
 'C' 'C' 0.0181 0.0091
 'International Tables Vol C Tables 4.2.6.8 and 6.1.1.4'
 'H' 'H' 0.0000 0.0000
 'International Tables Vol C Tables 4.2.6.8 and 6.1.1.4'
 'N' 'N' 0.0311 0.0180
 'International Tables Vol C Tables 4.2.6.8 and 6.1.1.4'
 'O' 'O' 0.0492 0.0322
 'International Tables Vol C Tables 4.2.6.8 and 6.1.1.4'

_space_group_crystal_system   triclinic
_space_group_IT_number   2
_space_group_name_H-M_alt   'P -1'
_space_group_name_Hall   '-P 1'

_shelx_space_group_comment

;
The symmetry employed for this shelxl refinement is uniquely defined
by the following loop, which should always be used as a source of
symmetry information in preference to the above space-group names.
They are only intended as comments.
;

loop_
 _space_group_symop_operation_xyz
 'x, y, z'
 '-x, -y, -z'

 _cell_length_a   5.1790(2)
 _cell_length_b   5.4406(2)
 _cell_length_c   19.2691(7)
 _cell_angle_alpha   94.342(3)
 _cell_angle_beta   93.910(3)
 _cell_angle_gamma   94.681(3)
 _cell_volume   538.07(3)
 _cell_formula_units_Z   1
 _cell_measurement_temperature 100.00(10)
 _cell_measurement_reflns_used 4287
 _cell_measurement_theta_min   4.6040
 _cell_measurement_theta_max   73.7000

 _exptl_crystal_description   Block
 _exptl_crystal_colour   'Pale Yellow'
 _exptl_crystal_density_meas   ?
 _exptl_crystal_density_method   ?
 _exptl_crystal_density_diffrn   1.384
 _exptl_crystal_F_000   238
 _exptl_transmission_factor_min ?
 _exptl_transmission_factor_max ?
 _exptl_crystal_size_max   0.350
 _exptl_crystal_size_mid   0.200
 _exptl_crystal_size_min   0.100
 _exptl_absorpt_coefficient_mu   0.869
 _shelx_estimated_absorpt_T_min 0.751
 _shelx_estimated_absorpt_T_max 0.918
 _exptl_absorpt_correction_T_min   0.84544
 _exptl_absorpt_correction_T_max   1.00000
 _exptl_absorpt_correction_type   'multi-scan'
 _exptl_absorpt_process_details
;
CrysAlisPro, Agilent Technologies,
Version 1.171.36.28 (release 01-02-2013 CrysAlis171 .NET)
(compiled Feb 1 2013,16:14:44)
Empirical absorption correction using spherical harmonics,
 implemented in SCALE3 ABSPACK scaling algorithm.
;

_exptl_special_details
;
 ?
;

_diffrn_ambient_temperature 100.00(10)

_diffrn_radiation_wavelength 1.5418
_diffrn_radiation_type 'Cu K\a'
_diffrn_radiation_source 'SuperNova (Cu) X-ray Source'
_diffrn_radiation_monochromator 'mirror'
_diffrn_measurement_device_type 'SuperNova, Dual, Cu at zero, Atlas'
_diffrn_detector_area_resol_mean 5.1768
_diffrn_reflns_number   5733
_diffrn_reflns_av_unetI/netI   0.0159
_diffrn_reflns_av_R_equivalents 0.0159
_diffrn_reflns_limit_h_min   -6
_diffrn_reflns_limit_h_max   6
_diffrn_reflns_limit_k_min   -6
_diffrn_reflns_limit_k_max   6
_diffrn_reflns_limit_l_min   -23
_diffrn_reflns_limit_l_max   23
_diffrn_reflns_theta_min   6.933
_diffrn_reflns_theta_max   70.058
_diffrn_reflns_theta_full   67.684
_diffrn_measured_fraction_theta_max 0.984
_diffrn_measured_fraction_theta_full 0.989
_diffrn_reflns_Laue_measured_fraction_max   0.984
_diffrn_reflns_Laue_measured_fraction_full   0.989
_diffrn_reflns_point_group_measured_fraction_max 0.984
_diffrn_reflns_point_group_measured_fraction_full 0.989
_reflns_number_total   2026
_reflns_number_gt   1902
_reflns_threshold_expression   'I > 2\s(I)'
_reflns_Friedel_coverage   0.000
_reflns_Friedel_fraction_max   .
_reflns_Friedel_fraction_full   .

_reflns_special_details
;
 Reflections were merged by SHELXL according to the crystal
 class for the calculation of statistics and refinement.

 _reflns_Friedel_fraction is defined as the number of unique
 Friedel pairs measured divided by the number that would be
 possible theoretically, ignoring centric projections and
 systematic absences.
;

_computing_data_collection
;
CrysAlisPro, Agilent Technologies,
Version 1.171.36.28 (release 01-02-2013 CrysAlis171 .NET)
(compiled Feb 1 2013,16:14:44)
;
_computing_cell_refinement
;
CrysAlisPro, Agilent Technologies,
Version 1.171.36.28 (release 01-02-2013 CrysAlis171 .NET)
(compiled Feb 1 2013,16:14:44)
;
_computing_data_reduction
;
CrysAlisPro, Agilent Technologies,

Version 1.171.36.28 (release 01-02-2013 CrysAlis171 .NET)
(compiled Feb 1 2013,16:14:44)
;
_computing_structure_solution   'SHELXS-2013 (Sheldrick, 2013)'
_computing_structure_refinement   'SHELXL-2013 (Sheldrick, 2013)'
_computing_molecular_graphics
;
OLEX2 (Dolomanov, O.V., Bourhis, L.J., Gildea, R.J., Howard, J.A.K,
& Puschmann, H., 2009)
;
_computing_publication_material   'WinGX (Farrugia, 1999)'

_refine_special_details
;
 ?
;
_refine_ls_structure_factor_coef Fsqd
_refine_ls_matrix_type   full
_refine_ls_weighting_scheme   calc
_refine_ls_weighting_details
'w=1/[\s^2^(Fo^2^)+(0.0448P)^2^+0.1746P] where P=(Fo^2^+2Fc^2^)/3'
_atom_sites_solution_primary   ?
_atom_sites_solution_secondary   ?
_atom_sites_solution_hydrogens   mixed
_refine_ls_hydrogen_treatment   mixed
_refine_ls_extinction_method   none
_refine_ls_extinction_coef   .
_refine_ls_number_reflns   2026
_refine_ls_number_parameters   154
_refine_ls_number_restraints   0
_refine_ls_R_factor_all   0.0355
_refine_ls_R_factor_gt   0.0339
_refine_ls_wR_factor_ref   0.0911
_refine_ls_wR_factor_gt   0.0899
_refine_ls_goodness_of_fit_ref   1.073
_refine_ls_restrained_S_all   1.073
_refine_ls_shift/su_max   0.000
_refine_ls_shift/su_mean   0.000

loop_
 _atom_site_label
 _atom_site_type_symbol
 _atom_site_fract_x
 _atom_site_fract_y
 _atom_site_fract_z
 _atom_site_U_iso_or_equiv
 _atom_site_adp_type
 _atom_site_occupancy
 _atom_site_site_symmetry_order
 _atom_site_calc_flag
 _atom_site_refinement_flags_posn
 _atom_site_refinement_flags_adp
 _atom_site_refinement_flags_occupancy
 _atom_site_disorder_assembly
 _atom_site_disorder_group
C2 C -0.1144(2) 0.6643(2) 0.20111(6) 0.0238(3) Uani 1 1 d . . . . .
H2A H -0.1355 0.5330 0.2306 0.029 Uiso 1 1 calc R U . . .

C3 C -0.3091(2) 0.6919(2) 0.14948(6) 0.0241(3) Uani 1 1 d . . . . .
H3A H -0.4607 0.5795 0.1451 0.029 Uiso 1 1 calc R U . . .
C5 C -0.0699(2) 1.0212(2) 0.11408(6) 0.0208(3) Uani 1 1 d . . . . .
C6 C 0.1245(2) 0.9977(2) 0.16610(6) 0.0228(3) Uani 1 1 d . . . . .
H6A H 0.2759 1.1104 0.1705 0.027 Uiso 1 1 calc R U . . .
C7 C -0.0348(2) 1.2224(2) 0.06542(6) 0.0210(3) Uani 1 1 d . . . . .
N1 N 0.10188(19) 0.81926(19) 0.21000(5) 0.0237(2) Uani 1 1 d . . . . .
N4 N -0.28994(19) 0.87068(19) 0.10596(5) 0.0230(2) Uani 1 1 d . . . . .
N7 N -0.2433(2) 1.2627(2) 0.02522(5) 0.0243(2) Uani 1 1 d . . . . .
H7A H -0.390(3) 1.182(3) 0.0321(8) 0.029 Uiso 1 1 d . U . . .
H7B H -0.228(3) 1.387(3) -0.0036(8) 0.029 Uiso 1 1 d . U . . .
O7 O 0.18104(15) 1.33865(16) 0.06464(4) 0.0265(2) Uani 1 1 d . . . . .
C8 C 0.6488(2) 1.0352(2) 0.31551(6) 0.0224(3) Uani 1 1 d . . . . .
C9 C 0.8526(2) 1.0475(2) 0.37557(6) 0.0246(3) Uani 1 1 d . . . . .
H9A H 0.9513 0.8998 0.3700 0.029 Uiso 1 1 calc R U . . .
H9B H 0.7635 1.0377 0.4193 0.029 Uiso 1 1 calc R U . . .
C10 C 1.0450(2) 1.2761(2) 0.38383(6) 0.0233(3) Uani 1 1 d . . . . .
H10A H 0.9496 1.4266 0.3848 0.028 Uiso 1 1 calc R U . . .
H10B H 1.1536 1.2770 0.3435 0.028 Uiso 1 1 calc R U . . .
C11 C 1.2187(2) 1.2783(2) 0.45125(6) 0.0233(3) Uani 1 1 d . . . . .
H11A H 1.1070 1.2722 0.4909 0.028 Uiso 1 1 calc R U . . .
H11B H 1.3122 1.1266 0.4495 0.028 Uiso 1 1 calc R U . . .
C12 C 1.4175(2) 1.5017(2) 0.46547(6) 0.0240(3) Uani 1 1 d . . . . .
H12A H 1.3257 1.6544 0.4665 0.029 Uiso 1 1 calc R U . . .
H12B H 1.5336 1.5061 0.4268 0.029 Uiso 1 1 calc R U . . .
O8 O 0.47398(17) 0.84256(16) 0.31714(4) 0.0271(2) Uani 1 1 d . . . . .
H8 H 0.351(3) 0.836(3) 0.2796(9) 0.041 Uiso 1 1 d . U . . .
O9 O 0.64349(17) 1.17980(16) 0.27073(4) 0.0282(2) Uani 1 1 d . . . . .

loop_
 _atom_site_aniso_label
 _atom_site_aniso_U_11
 _atom_site_aniso_U_22
 _atom_site_aniso_U_33
 _atom_site_aniso_U_23
 _atom_site_aniso_U_13
 _atom_site_aniso_U_12
C2 0.0255(6) 0.0215(6) 0.0245(6) 0.0053(5) 0.0029(5) -0.0019(5)
C3 0.0224(6) 0.0220(6) 0.0272(6) 0.0024(5) 0.0030(5) -0.0048(5)
C5 0.0196(5) 0.0219(6) 0.0207(5) 0.0026(4) 0.0013(4) -0.0005(4)
C6 0.0193(6) 0.0246(6) 0.0240(6) 0.0061(5) -0.0002(4) -0.0032(4)
C7 0.0203(6) 0.0222(6) 0.0200(5) 0.0028(5) 0.0000(4) -0.0013(4)
N1 0.0230(5) 0.0241(5) 0.0237(5) 0.0069(4) -0.0007(4) -0.0016(4)
N4 0.0207(5) 0.0236(5) 0.0238(5) 0.0025(4) -0.0004(4) -0.0028(4)
N7 0.0205(5) 0.0264(5) 0.0251(5) 0.0088(4) -0.0042(4) -0.0040(4)
O7 0.0198(4) 0.0309(5) 0.0286(4) 0.0125(4) -0.0021(3) -0.0043(3)
C8 0.0223(6) 0.0213(6) 0.0234(6) 0.0043(5) 0.0017(4) -0.0014(4)
C9 0.0236(6) 0.0244(6) 0.0250(6) 0.0058(5) -0.0017(5) -0.0025(5)
C10 0.0214(6) 0.0241(6) 0.0239(6) 0.0048(5) -0.0013(4) -0.0013(5)
C11 0.0209(6) 0.0236(6) 0.0249(6) 0.0049(5) -0.0012(5) -0.0009(5)
C12 0.0209(6) 0.0237(6) 0.0270(6) 0.0055(5) -0.0014(5) -0.0008(5)
O8 0.0257(5) 0.0287(5) 0.0253(4) 0.0101(4) -0.0057(3) -0.0077(3)
O9 0.0293(5) 0.0271(5) 0.0275(5) 0.0106(4) -0.0041(3) -0.0048(4)

_geom_special_details
;
 All esds (except the esd in the dihedral angle between two l.s. planes)

are estimated using the full covariance matrix. The cell esds are taken
into account individually in the estimation of esds in distances, angles
and torsion angles; correlations between esds in cell parameters are only
used when they are defined by crystal symmetry. An approximate (isotropic)
treatment of cell esds is used for estimating esds involving l.s. planes.
;

loop_
_geom_bond_atom_site_label_1
_geom_bond_atom_site_label_2
_geom_bond_distance
_geom_bond_site_symmetry_2
_geom_bond_publ_flag
C2 N1 1.3387(15) . ?
C2 C3 1.3925(17) . ?
C2 H2A 0.9500 . ?
C3 N4 1.3336(16) . ?
C3 H3A 0.9500 . ?
C5 N4 1.3408(15) . ?
C5 C6 1.3919(16) . ?
C5 C7 1.5020(16) . ?
C6 N1 1.3385(15) . ?
C6 H6A 0.9500 . ?
C7 O7 1.2403(14) . ?
C7 N7 1.3283(15) . ?
N7 H7A 0.869(16) . ?
N7 H7B 0.912(16) . ?
C8 O9 1.2114(14) . ?
C8 O8 1.3317(14) . ?
C8 C9 1.5058(16) . ?
C9 C10 1.5203(16) . ?
C9 H9A 0.9900 . ?
C9 H9B 0.9900 . ?
C10 C11 1.5275(15) . ?
C10 H10A 0.9900 . ?
C10 H10B 0.9900 . ?
C11 C12 1.5227(16) . ?
C11 H11A 0.9900 . ?
C11 H11B 0.9900 . ?
C12 C12 1.534(2) 2_886 ?
C12 H12A 0.9900 . ?
C12 H12B 0.9900 . ?
O8 H8 0.926(18) . ?

loop_
_geom_angle_atom_site_label_1
_geom_angle_atom_site_label_2
_geom_angle_atom_site_label_3
_geom_angle
_geom_angle_site_symmetry_1
_geom_angle_site_symmetry_3
_geom_angle_publ_flag
N1 C2 C3 121.30(11) . . ?
N1 C2 H2A 119.4 . . ?
C3 C2 H2A 119.4 . . ?
N4 C3 C2 122.25(11) . . ?
N4 C3 H3A 118.9 . . ?

C2 C3 H3A 118.9 . . ?
N4 C5 C6 122.21(11) . . ?
N4 C5 C7 118.44(10) . . ?
C6 C5 C7 119.35(10) . . ?
N1 C6 C5 121.18(11) . . ?
N1 C6 H6A 119.4 . . ?
C5 C6 H6A 119.4 . . ?
O7 C7 N7 124.17(11) . . ?
O7 C7 C5 119.54(10) . . ?
N7 C7 C5 116.28(10) . . ?
C2 N1 C6 116.96(10) . . ?
C3 N4 C5 116.07(10) . . ?
C7 N7 H7A 117.7(10) . . ?
C7 N7 H7B 117.8(9) . . ?
H7A N7 H7B 124.0(14) . . ?
O9 C8 O8 123.66(11) . . ?
O9 C8 C9 124.88(11) . . ?
O8 C8 C9 111.46(10) . . ?
C8 C9 C10 116.09(10) . . ?
C8 C9 H9A 108.3 . . ?
C10 C9 H9A 108.3 . . ?
C8 C9 H9B 108.3 . . ?
C10 C9 H9B 108.3 . . ?
H9A C9 H9B 107.4 . . ?
C9 C10 C11 110.31(9) . . ?
C9 C10 H10A 109.6 . . ?
C11 C10 H10A 109.6 . . ?
C9 C10 H10B 109.6 . . ?
C11 C10 H10B 109.6 . . ?
H10A C10 H10B 108.1 . . ?
C12 C11 C10 114.89(10) . . ?
C12 C11 H11A 108.5 . . ?
C10 C11 H11A 108.5 . . ?
C12 C11 H11B 108.5 . . ?
C10 C11 H11B 108.5 . . ?
H11A C11 H11B 107.5 . . ?
C11 C12 C12 112.86(12) . 2_886 ?
C11 C12 H12A 109.0 . . ?
C12 C12 H12A 109.0 2_886 . ?
C11 C12 H12B 109.0 . . ?
C12 C12 H12B 109.0 2_886 . ?
H12A C12 H12B 107.8 . . ?
C8 O8 H8 110.5(10) . . ?

loop_
_geom_torsion_atom_site_label_1
_geom_torsion_atom_site_label_2
_geom_torsion_atom_site_label_3
_geom_torsion_atom_site_label_4
_geom_torsion
_geom_torsion_site_symmetry_1
_geom_torsion_site_symmetry_2
_geom_torsion_site_symmetry_3
_geom_torsion_site_symmetry_4
_geom_torsion_publ_flag
N1 C2 C3 N4 0.73(19) . . . . ?
N4 C5 C6 N1 1.16(18) . . . . ?

C7 C5 C6 N1 -179.25(10) . . . . ?
N4 C5 C7 O7 -168.86(10) . . . . ?
C6 C5 C7 O7 11.54(17) . . . . ?
N4 C5 C7 N7 10.94(16) . . . . ?
C6 C5 C7 N7 -168.66(11) . . . . ?
C3 C2 N1 C6 -1.43(17) . . . . ?
C5 C6 N1 C2 0.53(17) . . . . ?
C2 C3 N4 C5 0.92(17) . . . . ?
C6 C5 N4 C3 -1.83(17) . . . . ?
C7 C5 N4 C3 178.58(10) . . . . ?
O9 C8 C9 C10 7.25(18) . . . . ?
O8 C8 C9 C10 -173.30(10) . . . . ?
C8 C9 C10 C11 173.33(10) . . . . ?
C9 C10 C11 C12 -179.22(10) . . . . ?
C10 C11 C12 C12 178.63(12) . . . 2_886 ?

loop_
 _geom_hbond_atom_site_label_D
 _geom_hbond_atom_site_label_H
 _geom_hbond_atom_site_label_A
 _geom_hbond_distance_DH
 _geom_hbond_distance_HA
 _geom_hbond_distance_DA
 _geom_hbond_angle_DHA
 _geom_hbond_site_symmetry_A
C2 H2A O9 0.95 2.36 3.2476(15) 154.6 1_445
C3 H3A O7 0.95 2.54 3.3833(14) 147.5 1_445
C6 H6A O9 0.95 2.60 3.2855(14) 129.2 .
N7 H7A O7 0.869(16) 2.546(15) 3.1780(13) 130.4(12) 1_455
N7 H7B O7 0.912(16) 1.976(17) 2.8874(14) 177.8(14) 2_585
O8 H8 N1 0.926(18) 1.790(18) 2.7147(13) 177.1(15) .

_refine_diff_density_max   0.290
_refine_diff_density_min   -0.169
_refine_diff_density_rms   0.035

_shelxl_version_number 2013-4

_shelx_res_file
;
TITL Pyrazinamide_SebacicAcid_(1)1_1 in P-1 #2
CELL 1.54184 5.1790 5.4406 19.2691 94.342 93.910 94.681
ZERR   1.00 0.0002 0.0002 0.0007 0.003 0.003 0.003
LATT   1
SFAC C   H   N   O
UNIT 20 28 6   6
MERG   2
SHEL 7 0.82
EQIV $1 x-1, y-1, z
HTAB C2 O9_$1
HTAB C3 O7_$1
HTAB C6 O9
EQIV $2 x-1, y, z
HTAB N7 O7_$2
EQIV $3 -x, -y+3, -z
HTAB N7 O7_$3
HTAB O8 N1

FMAP 2
PLAN 5
SIZE   0.100 0.200 0.350
ACTA
HTAB 2.00000
BOND $H
CONF
L.S. 10
TEMP -173.00
WGHT 0.044800 0.174600
FVAR   20.93984
MOLE   1
C2   1 -0.114387 0.664334 0.201111 11.00000 0.02550 0.02149 =
     0.02449 0.00530 0.00288 -0.00187
AFIX 43
H2A 2 -0.135463 0.533021 0.230604 11.00000 -1.20000
AFIX 0
C3   1 -0.309058 0.691879 0.149481 11.00000 0.02235 0.02196 =
     0.02716 0.00241 0.00296 -0.00478
AFIX 43
H3A 2 -0.460669 0.579461 0.145113 11.00000 -1.20000
AFIX 0
C5   1 -0.069916 1.021221 0.114083 11.00000 0.01963 0.02193 =
     0.02067 0.00259 0.00128 -0.00050
C6   1   0.124482 0.997739 0.166102 11.00000 0.01925 0.02462 =
     0.02401 0.00612 -0.00024 -0.00323
AFIX 43
H6A 2   0.275906 1.110401 0.170526 11.00000 -1.20000
AFIX 0
C7   1 -0.034791 1.222371 0.065423 11.00000 0.02035 0.02224 =
     0.01996 0.00282 -0.00001 -0.00132
N1   3   0.101881 0.819262 0.210002 11.00000 0.02304 0.02407 =
     0.02370 0.00689 -0.00073 -0.00160
N4   3 -0.289940 0.870678 0.105958 11.00000 0.02068 0.02362 =
     0.02381 0.00249 -0.00037 -0.00279
N7   3 -0.243266 1.262682 0.025220 11.00000 0.02052 0.02640 =
     0.02510 0.00883 -0.00416 -0.00398
H7A 2 -0.389798 1.181818 0.032096 11.00000 -1.20000
H7B 2 -0.227910 1.387486 -0.003633 11.00000 -1.20000
O7   4   0.181041 1.338650 0.064636 11.00000 0.01979 0.03086 =
     0.02864 0.01254 -0.00211 -0.00430
MOLE   2
C8   1   0.648838 1.035200 0.315513 11.00000 0.02230 0.02129 =
     0.02343 0.00425 0.00171 -0.00141
C9   1   0.852592 1.047508 0.375569 11.00000 0.02365 0.02438 =
     0.02499 0.00579 -0.00168 -0.00253
AFIX 23
H9A 2   0.951338 0.899816 0.370036 11.00000 -1.20000
H9B 2   0.763516 1.037717 0.419257 11.00000 -1.20000
AFIX 0
C10 1   1.045045 1.276088 0.383834 11.00000 0.02136 0.02406 =
     0.02389 0.00482 -0.00129 -0.00127
AFIX 23
H10A 2   0.949618 1.426595 0.384833 11.00000 -1.20000
H10B 2   1.153560 1.276966 0.343484 11.00000 -1.20000
AFIX 0
C11 1   1.218741 1.278346 0.451246 11.00000 0.02089 0.02358 =

```
   0.02487   0.00492  -0.00123  -0.00088
AFIX  23
H11A 2   1.106997   1.272174   0.490874   11.00000  -1.20000
H11B 2   1.312182   1.126605   0.449454   11.00000  -1.20000
AFIX  0
C12  1   1.417521   1.501704   0.465470   11.00000   0.02091   0.02371 =
   0.02703   0.00546  -0.00139  -0.00083
AFIX  23
H12A 2   1.325676   1.654401   0.466538   11.00000  -1.20000
H12B 2   1.533620   1.506091   0.426756   11.00000  -1.20000
AFIX  0
O8   4   0.473981   0.842556   0.317137   11.00000   0.02570   0.02872 =
   0.02526   0.01014  -0.00567  -0.00773
H8   2   0.351258   0.836381   0.279643   11.00000  -1.50000
O9   4   0.643488   1.179803   0.270729   11.00000   0.02926   0.02709 =
   0.02755   0.01056  -0.00409  -0.00483
HKLF   4

REM  Pyrazinamide_SebacicAcid_(1)1_1 in P-1 #2
REM R1 =  0.0339 for   1902 Fo > 4sig(Fo)  and  0.0355 for all   2026 data
REM   154 parameters refined using     0 restraints

END
```